Springer Theses
Recognizing Outstanding Ph.D. Research

Ali Saeedi

Experimental Study of Multiphase Flow in Porous Media during CO_2 Geo-Sequestration Processes

Springer

Springer Theses

Recognizing Outstanding Ph.D. Research

For further volumes:
http://www.springer.com/series/8790

Aims and Scope

The series "Springer Theses" brings together a selection of the very best Ph.D. theses from around the world and across the physical sciences. Nominated and endorsed by two recognized specialists, each published volume has been selected for its scientific excellence and the high impact of its contents for the pertinent field of research. For greater accessibility to non-specialists, the published versions include an extended introduction, as well as a foreword by the student's supervisor explaining the special relevance of the work for the field. As a whole, the series will provide a valuable resource both for newcomers to the research fields described, and for other scientists seeking detailed background information on special questions. Finally, it provides an accredited documentation of the valuable contributions made by today's younger generation of scientists.

Theses are accepted into the series by invited nomination only and must fulfill all of the following criteria

- They must be written in good English.
- The topic should fall within the confines of Chemistry, Physics and related interdisciplinary fields such as Materials, Nanoscience, Chemical Engineering, Complex Systems and Biophysics.
- The work reported in the thesis must represent a significant scientific advance.
- If the thesis includes previously published material, permission to reproduce this must be gained from the respective copyright holder.
- They must have been examined and passed during the 12 months prior to nomination.
- Each thesis should include a foreword by the supervisor outlining the significance of its content.
- The theses should have a clearly defined structure including an introduction accessible to scientists not expert in that particular field.

Ali Saeedi

Experimental Study of Multiphase Flow in Porous Media during CO_2 Geo-Sequestration Processes

Doctoral Thesis accepted by
the Curtin University of Technology,
Perth, Western Australia

Springer

Author
Dr. Ali Saeedi
Department of Petroleum Engineering
Curtin University
Dick Perry Avenue 26
Kensington, WA 6151
Australia
e-mail: Ali.Saeedi@Curtin.edu.au

Supervisor
Assoc. Prof. Reza Rezaee
Department of Petroleum Engineering
Curtin University
ARRC Building
26 Dick Perry Avenue
Kensington, WA 6151
Australia
e-mail: R.Rezaee@exchange.curtin.edu.au

ISSN 2190-5053
ISBN 978-3-642-25040-8
DOI 10.1007/978-3-642-25041-5
Springer Heidelberg Dordrecht London New York

e-ISSN 2190-5061
e-ISBN 978-3-642-25041-5

Library of Congress Control Number: 2011941706

Printed on acid-free paper

Springer is part of Springer Science+Business Media (www.springer.com)

Parts of this thesis have been published in the following journal articles:

- Saeedi, A., R. Rezaee, B. Evans, and B. Clennell, 2011, "Multiphase flow behaviour during CO_2 geo-sequestration: Emphasis on the effect of cyclic CO_2-brine flooding", Journal of Petroleum Science and Engineering, In Press, Accepted Manuscript, doi: 10.1016/j.petrol.2011.07.007.

- Saeedi, A., R. Rezaee, and B. Evans, 2011, "Effect of Residual Natural Gas Saturation on Multiphase Flow Behaviour during CO_2 Geo-sequestration", [Journal of Petroleum Science and Engineering, under review]

- Saeedi, A., and R. Rezaee, 2011, "Effect of Flow Direction on Multiphase Flow Behaviour during CO_2 Geo-sequestration in Sandstone Reservoirs", [Journal of Transport in Porous Media, under review]

- Saeedi, A., Rezaee, R., and Evans, B., 2011, "Experimental Study of the Effect of Variation in In-situ Stress on Capillary Residual Trapping during CO_2 Geo-sequestration in Sandstone Reservoirs", [Geofluids, accepted for publication]

To my wife Elham and our parents

Supervisor's Foreword

Carbon dioxide emissions account for 64% of the total global greenhouse gas effect. The recorded data at the Mauna Loa observatory site in Hawaii shows that over the last 50 years, the atmospheric concentration of carbon dioxide has risen by 23%, equal to an increase of 0.45% per year. A large portion of these CO_2 emissions are released by stationary sources—such as power plants, which consume fossil fuels as their main source of energy. It is inarguably accepted that humans have to try to eventually reduce their dependence on fossil fuels which not only creates excessive CO_2 volumes but also is not renewable. However, it also goes without saying that, considering the degree of human dependence on fossil fuels, such a goal may not be easily achievable at least for the century or so. Therefore, there needs to be practical techniques developed, which while allow humans to continue burning fossil fuels, offer adequate measures for eliminating or at least reducing the extent of the CO_2 emissions released to the atmosphere towards slowing down the global warming phenomenon.

During the past two decades carbon capture and storage (CCS) has emerged as a promising methodology to reduce the amount of anthropogenic CO_2 emissions into the atmosphere. CCS involves capturing the CO_2 at its emitting source and injecting it underground into geological formations where it will be sequestered for perpetuity. For successful implementation, monitoring and verification of any CO_2 geo-sequestration project, there are a number of issues related to the target geological reservoir which need to be investigated before the commencement of the CO_2 injection, including storage capacity, confinement and integrity and multiphase flow characteristics of the fluids-rock system.

This research evaluates the significance of the effects that a number of important factors—such as cyclic CO_2-brine flooding, flow direction (horizontal versus vertical), change in the reservoir stress field, and residual natural gas saturation, can have on the multiphase flow during CO_2 geo-sequestration in sandstone reservoirs. To the best of our knowledge, to date there has been no experimental data produced in the literature on the potential effects of such parameters on the multiphase flow characteristics of the rock-fluids system during

underground CO_2 sequestration. A number of these factors have not been even discussed in the literature from the theoretical point of view.

We believe that the experimental results achieved by Dr. Saeedi during this research and the extensive discussions presented in the dissertation on the subject of multiphase flow behaviour during CO_2 geo-sequestration could have significant implications to many proposed CO_2 geo-sequestration projects around the world. We hope that the technical community both in academia and the industry would benefit from reading this outstanding theses.

Perth, October 2011 Assoc. Prof. Reza Rezaee

Acknowledgments

I would like to express my deepest gratitude and sincere appreciation to Associate Professor Reza Rezaee and Professor Brian Evans for all their support, guidance and encouragement throughout the course of this study. Without you, especially during some difficult times that I have had during this journey, accomplishment of this work would not be possible.

I would also like to give special thanks to Dr. Ben Clennell and Dr. Lincoln Paterson for all their advice, support and help during the development of this dissertation and for serving as members of my supervisory panel. Needless to say, I am especially grateful to Dr. Ben Clennell for granting me free and flexible access to his laboratories at CSIRO Petroleum.

I am debited to many others at Curtin Department of Petroleum Engineering, CSIRO Petroleum and CO2CRC for providing me with all the support I needed. Special thanks go to CO2CRC management who provided financial support during the course of development of this study.

Thanks to my wife and our families for their love, understanding and encouragement which made me work harder every day, without it I would not be where I am now.

Contents

Symbols

2D	2 dimensional
3D	3 dimensional
A	Area
API	American Petroleum Institute (Unit of gravity)
AWCT	Anti-Water Coning Treatment
BPR	Back pressure regulator
BT	Breakthrough
CCS	Carbon capture and storage
CO2CRC	Cooperative Research Centre for Greenhouse gas Technologies
CO2-EOR	Enhanced oil recovery using CO_2 injection
cP	Centipoise
CPMG	Carr–Purcell–Meiboom–Gill
d	Diameter
Drain.	Drainage
EOR	Enhanced oil recovery
EOS	Equation of state
F	Degree of freedom
FID	Free Induction Decay
g	Gravity acceleration constant
Gr	Pressure gradient
Gt	Gigatonnes
IFC	International Formulation Committee
IFT	Interfacial tension
Imb.	Imbibition
k	Permeability
K	Degrees Kelvin
k_h	Horizontal permeability
kJ	Kilojoule
km	Kilometre
k_r	Relative permeability
k_v	Vertical permeability

L	Length
LNG	Liquefied natural gas
M	Mobility ratio
mD	Milli-Darcy
MHz	Megahertz
mmt	Million metric tonnes
mmtpa	Million metric tonnes per annum
mol	Mole
MPa	Megapascal
n	Number of components
N_{BO}	Bond number
N_{ca}	Capillary number
NIST	National Institute of Standards and Technology (US)
NMR	Nuclear Magnetic Resonance
N_s	Stability number
NS	Number of scans
N_w	Wettability constant
OBP	Otway Basin Project
P	Pressure
P_c	Critical pressure
P_{ca}	Capillary pressure
PID	Proportional–Integral–Derivative controller
ppm	Parts per million
ppmv	Parts per million by volume
psi	Pound per square inch
psig	psi-gauge
P_t	Triple point pressure
P-T	Pressure-temperature
P-T-x	Pressure–temperature-composition
PV	Pore volume
PVT	Pressure–volume–temperature
PVTx	Pressure–volume–temperature-composition
P-x	Pressure-composition
q	Volumetric flow-rate
r	Number of phases
RD	Relaxation delay
RF	Recovery factor
R_m	Molar gas constant
R_p	Pore radius
R_{th}	Pore-throat radius
S	Saturation
SEM	Scanning Electron Microscopy
SS	Steady-state
T	Temperature
T_c	Critical temperature

T_t	Triple point temperature
TVD	Total vertical depth
u	Superficial displacement velocity
u_c	Critical superficial displacement velocity
USS	Unsteady-state
WAG	Water-alternating-gas
μ	Viscosity
φ	Porosity
ρ	Density
ρ_t	Triple point density
ρ_c	Critical point density
θ	Contact angle
Δp	Differential pressure
σ	Interfacial tension

Chapter 1
Introduction

In this research the effect of a number of factors which are considered as greatly influencing the CO_2-brine flow characteristics during carbon dioxide geo-sequestration have been evaluated. The main focus of the research has been on the factors which change the multiphase flow behaviour of the involved fluids in the underground porous media over time in short and long terms. The first part of this chapter focuses on the importance of carbon capture and storage (CCS) as a means of reducing the level of the atmospheric CO_2. The second part presents an outline of the research objectives and the chapter ends with a brief overview of the contents of this dissertation.

1.1 Background and Problem Description

Carbon dioxide along with other greenhouse gases such as methane, water vapour, nitrous oxide and ozone, effectively trap infra-red radiation emitted from the Earth's surface [1]. This phenomenon traps the heat inside the atmosphere surrounding the Earth and is vital for the survival of life on the Earth. Without the existence of such a naturally occurring phenomenon, the average temperature on the Earth would be −18°C instead of the current +15°C [2]. However, high concentrations of such gases in the atmosphere can cause an abnormal increase in the Earth's surface temperature. Excessive emissions of carbon dioxide from anthropogenic sources—such as power plants and car exhausts, into the Earth's atmosphere, has been identified as the main cause for the ongoing global warming phenomenon [3] occurring since the industrial revolution back in the eighteenth century. Carbon dioxide accounts for 64% of the total global greenhouse effect.

During the twentieth century, especially because of the developments made in the fossil fuel hungry industries, the amount of CO_2 emissions has increased dramatically. Data recorded at the Mauna Loa observatory site in Hawaii shows that over the last 50 years, the atmospheric concentration of carbon dioxide has

A. Saeedi, *Experimental Study of Multiphase Flow in Porous Media during CO_2 Geo-Sequestration Processes*, Springer Theses, DOI: 10.1007/978-3-642-25041-5_1,

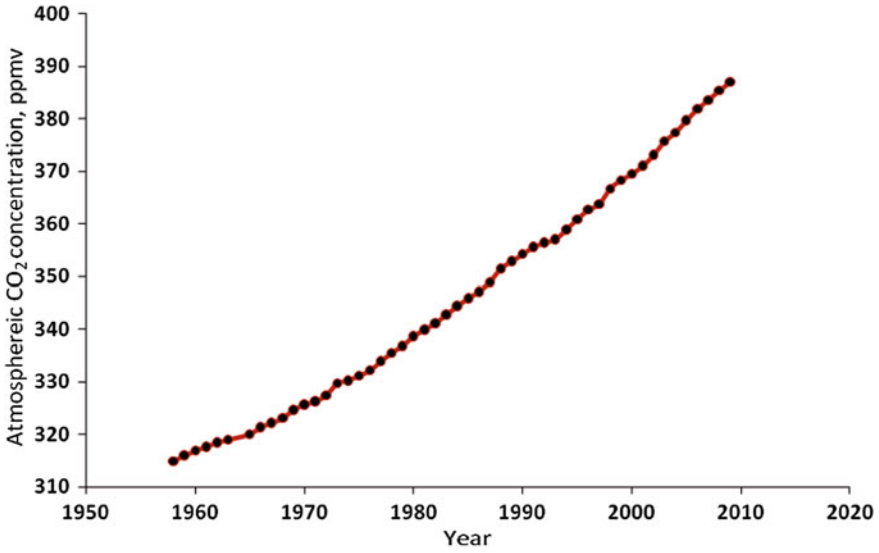

Fig. 1.1 Increase in atmospheric concentration of CO_2 over time since 1958 (data taken from [4])

risen from less than 315 ppmv in 1958 to almost 387 ppmv in 2009 (Fig. 1.1), which is an increase of 23% in total, equal to an increase of 0.45% per year [4].

With an ever increasing demand for fossil fuels, it is predicted that the current trends will even become steeper. This can be avoided, or at least the rate of global warming can be reduced, in two ways. One option is by reducing the dependence of humans on fossil fuels as their main source of energy. However, the fact that currently burning fossil fuels accounts for 85% of total global energy demands makes this first option out of reach, at least for several decades or so [5]. The second option, which seems to be more pragmatic, is finding a way to prevent or significantly reduce the amount of carbon dioxide emissions released into the atmosphere while humans continue to burn fossil fuels. During the past two decades carbon capture and storage has emerged as a promising technology to bring the second option closer to reality. CCS means capturing the carbon dioxide at its large stationary source such as power plants and then transporting it through pipelines to geological sites having large enough underground storage capacity and injecting it into such secure storage reservoirs. CCS is considered to be compatible with the continued large-scale use of fossil fuels, while providing the necessary means to reduce the emissions of carbon dioxide to the atmosphere [6].

Apart from underground geological structures, oceans are also considered to have large storage capacity for CCS projects. In fact, the capacity of oceans for the purpose of CCS is considerably larger than underground structures (Table 1.1).

Despite the fact that oceans represent the largest potential storage media for anthropogenic CO_2 emissions, CO_2 storage on the ocean floor may not be feasible at least for the time being for various reasons [2, 6, 8] listed below:

Table 1.1 Capacity of potential carbon reservoirs (after [7])

Storage medium	Capacity (Gt)
Oceans	$1{,}400-2\times10^7$
Underground geological structures	300−3,200

- Since potential physiochemical processes involved are complex and not well understood, long-term effectiveness and potential side effects of using the oceans in this way are unknown.
- Could have major environmental impacts and any attempt to implement such plans would face, not easy to overcome, challenges by the public and especially environmental activists.
- The technology is still immature and the cost could be high.
- Natural ocean circulation currents impose legal, political and international limitations on any large scale CO_2 storage in the oceans.

Even if all of the above-mentioned issues are resolved, the fact that marine storage sites are not available in the vicinity of many large heavily industrialised landlocked regions or countries makes CO_2 storage in underground geological structures (geo-sequestration) more attractive. Over the past 100 years, the required knowledge and technology for the deep injection of CO_2 into underground geological reservoirs has been well developed mainly by the energy, chemical and petrochemical industries. In addition, CO_2 injection for enhanced oil recovery (EOR), acid gas (CO_2 and H_2S) disposal, and disposal of liquid wastes through underground deep injection have been in practice for several decades [9–12].

There is a variety of underground storage media available for geo-sequestration which includes: deep saline aquifers, active and depleted oil and gas reservoirs, unminable deep coal seams and mined salt domes. Table 1.2 presents an overview of the main advantages and disadvantages of these various geological media.

Of the various proposed underground geological structures suitable for carbon storage, deep saline aquifers are considered to be the best option. Injection of carbon dioxide in such structures may not have the added value of injecting it in hydrocarbon reservoirs for enhanced oil or gas recovery but in return, deep saline aquifers provide the largest capacity of underground geological storage for carbon sequestration. Saline aquifers are also abundant in sedimentary basins all around the world and finding one in the vicinity of an existing large point source of CO_2 emissions would not be very difficult. From a technical point of view, the following issues need to be addressed before the implementation of any aquifer disposal of CO_2 can commence [2, 9, 10, 14]:

- *Storage capacity*: the storage capacity of the target formation needs to be adequate.
- *Confinement and integrity*: the aquifer needs to have an overlaying seal or caprock to prevent the leakage of CO_2 into the formations above. Any leakage could have adverse environmental impacts such as the release of the injected

Table 1.2 Comparison of various types of geological carbon storage sites (in part after [13])

• Geological medium	• Advantage	• Disadvantage
• Unminable coal seams	• Large capacity	• High cost
	• Enhanced methane production	• Not available in all regions
• Mined salt domes	• Custom design	• High cost
	• Storage integrity	• Not available in all regions
• Deep saline aquifers	• Large capacity	• Unproven storage integrity
	• Widespread availability	
• Active or depleted oil and gas reservoirs	• Proven storage integrity	• Not available in all regions
	• Enhanced hydrocarbon recovery	• May not be available for immediate injection
	• Established infrastructure	• Uncertainties associated with existence of residual hydrocarbon

CO_2 back into the atmosphere again and/or contamination of the potable water aquifers.

- *Monitoring system*: implementation of adequate monitoring and verification system is vital for any CCS project to determine the fate of the injected CO_2.
- *Use of compatible transport and well completion material*: CO_2 especially in the aqueous phase, when coupled with brine containing concentrations of various salts, dictates the use of corrosion resistant material for transport and onsite compression and injection of CO_2. This influences the material selection for pipelines, compressors and well completion material (e.g. cement, casing, completion tubing, etc.).
- *Multiphase flow characteristics of the CO_2-brine-rock system*: the issues related to multiphase flow behaviour of the CO_2-brine-rock system for each individual storage reservoir must be thoroughly investigated before the implementation of any CCS project. The interaction between the three elements of this system would greatly influence many important factors—such as injectivity, storage capacity, integrity, plume migration etc., determining the success or failure of any underground CO_2 storage project.

The other candidate storage media for underground CO_2 disposal are active or depleted hydrocarbon reservoirs. As pointed out in Table 1.2, hydrocarbon reservoirs have the disadvantage that they may not be necessarily located close to the large sources of CO_2 emissions and even if they are, they may not be available for immediate injection due to ongoing production operations. On the other hand, they have several important advantages such as added value through enhanced hydrocarbon recovery, proven storage integrity as the reservoirs have held the hydrocarbon confined in place for millions of years. The hydrocarbon reservoirs also have the advantage that they already have the majority of the required expensive injection infrastructure ready in place.

In comparing a depleted gas reservoir to a depleted oil reservoir, with presumably the same hydrocarbon pore volume, in terms of the storage capacity, the depleted gas reservoir can accommodate significantly higher volumes of CO_2 for two main reasons [13, 15]. Firstly, the recovery factor for a gas reservoir is generally much higher than an oil reservoir. Furthermore, the gas density is significantly less than the crude oil density, which means at complete depletion of the reservoir, the mass of the bypassed hydrocarbon left behind, would be significantly less for the gas reservoir, which leaves more space for the injected CO_2 to occupy. Secondly, the compressibility of the gas is on average 30 times greater than crude oil, which means the injected CO_2 even can take over more space in a depleted gas reservoir due to compression of the easily compressible residual gas. This reasoning assumes that there is no hydrocarbon recovery while storing the CO_2. If this is not the case, since the incremental hydrocarbon recovery due to CO_2 injection is generally higher for gas reservoirs compared to oil reservoirs, there could become more space available for the injected CO_2, if it is injected into a depleted gas reservoir. One main issue associated with injection of CO_2 into oil reservoirs is the more pronounced complications with the multiphase flow behaviour of the CO_2-crude-brine system which would be different from the brine-CO_2-natural gas system encountered in depleted gas reservoirs.

It is generally accepted within the technical community that CO_2 needs to be in its supercritical state while being stored in the underground geological structures. There are various reasons stated for this [10, 14] including:

- Avoiding the negative impacts of CO_2 separation into gas and liquid phases in the injection line and complications associated with multiphase flow making it much easier to physically handle
- CO_2 has relatively high density in its supercritical state, which provides efficient utilisation of the available pore space
- Due to its higher density, supercritical CO_2 is less buoyant than its gas phase. This reduces the upward migration tendency of the injected fluid and thus decreases the risk of the seal integrity breach.

In order to achieve the required pressure–temperature (P–T) conditions, the target geological structure for CO_2 storage should be located below a certain depth to make sure that CO_2 would be stored and remain in its supercritical state. Based on the data published by Span and Wagner [16], the critical point of CO_2 is at $P_c = 1069.989\,psi$ and $T_c = 31.95^{o}\text{C}$. With an average hydrostatic pressure gradient of $0.43\,(psi.ft^{-1})$, average surface temperature of 15°C and an average geothermal gradient of 27°C per km, it is easily calculated that the minimum depth for CO_2 to be injected and remain in its supercritical state is 800 m.

The first large commercial scale CO_2 injection project for the purpose of enhanced oil recovery (EOR) began operation in 1972 at the SACROC field in West Texas. Since then many more projects have utilised CO2-EOR technique and by 2008 their number had reached a total of 126 cases globally out of which 119 or 89% were active in the US and Canada [17]. Around 30 million metric tonnes (mmt)

of CO_2 is presently being injected into the above mentioned CO2-EOR projects annually. Much, if not all, of the injected CO_2 is being recovered from naturally occurring underground CO_2 reservoirs and reinjected into those projects while little or no monitoring is carried out to verify the CO_2 storage integrity of the underground structures [18].

Currently there are four active large scale commercial CCS projects globally, which sequester anthropogenic CO_2 into underground structures: Sleipner and Snøhvit in Norway, In-Salah in Algeria and Weyburn-Midale in Canada. The Sleipner CCS project is located offshore Norway and has been in operation for 14 years. The CO_2 is separated from the produced natural gas and reinjected for disposal at a depth of 800–1,000 m into the Utsira sandstone formation. So far nearly 11 mmt of CO_2 has been successfully stored at the Sleipner project. Since its commencement 6 years ago, the In-Salah project has been reinjecting about 1.2 mmt per annum of CO_2 separated from the produced natural gas, into Carboniferous Sandstone in the heart of the Sahara desert [18].

The Weyburn-Midale is not a pure CO_2 storage project. It involves 2 mmt per annum of CO_2 injection for CO_2-EOR purposes and the injected CO_2 will be recycled several times and eventually could be exported and used in other injection projects. The Snøhvit project started in 2008 and operationally is similar to the Sleipner and In-Salah projects as it involves separation of CO_2 onshore from an LNG plant. The separated CO_2 is piped 150 km offshore Norway in the Barents Sea and injected into the Tubåen sandstone formation at a depth of 2,600 m below sea level [18].

Geo-sequestration of supercritical CO_2 in either depleted hydrocarbon reservoirs or deep saline aquifers is accompanied by a wide range of hydrological, chemical and physical/mechanical processes. These processes, which could greatly influence the mechanisms, which are active in permanent entrapment of CO_2, include the following:

- *Change in the reservoir stress field*: unlike fluid injections involved in conventional pressure maintenance and EOR operations associated with hydrocarbon production, there is no fluid production occurring during underground CO_2 disposal. As a result, CO_2 injection causes an increase in reservoir pore pressure, which in turn decreases the reservoir net effective pressure. Any changes in net effective stress can change all the reservoir and cap-rock properties, which are dependent on the stress field, such as the absolute and relative permeabilities, capillary pressure, rock porosity, residual saturations, etc. Therefore any change in the stress field can ultimately alter a number of the trapping mechanisms active during CO_2 storage.
- *Solute transport in porous media*: as it will be discussed in Chap. 2, it has been shown experimentally that considerable quantities of CO_2 could be dissolved in brine at elevated P–T conditions. Once CO_2 is dissolved in brine, carbon acid and subsequently bicarbonate ion, HCO_3^- and H^+ would form. The convection mixing phenomenon [19] and other forces such as natural aquifer currents or induced displacements due to continuous injection would transport the solute created within the porous medium.

- *Fluid-rock chemical interactions*: the solute created and transported in the previous step can react with certain minerals present in the matrix or cement of the host reservoir rock and cause precipitation of secondary carbonate minerals. Both dissolution and precipitation of minerals can alter the permeability and porosity of the rock, which in turn influences the flow characteristics and in some instances the mechanical properties of the reservoir [20–23].
- *Multiphase flow behaviour*: injection of CO_2 into deep underground structures is initially in the free supercritical state, which will form a plume around the wellbore and then, due to gravity and buoyancy forces, it will move upwards towards the top of the geological structure. This whole process could be classified as immiscible displacement of the higher density and higher viscosity brine, which becomes partially or fully saturated with CO_2, by supercritical CO_2. Due to an unfavourable mobility ratio, this displacement is greatly influenced by strong instabilities, even in a homogeneous medium. Cyclic flooding and subsequent hysteresis effect is also frequently experienced by the porous medium [24, 25] due to the above-mentioned flow instabilities, intermittent or seasonal injection of CO_2, or coupled injection of brine and CO_2 (i.e. water alternating gas (WAG)). As mentioned above, multiphase flow characteristics could also be influenced by other chemical and physical processes occurring during underground CO_2 disposal.

Compared to the petroleum and other geoscience fields of engineering, the technical and engineering aspects of CO_2 geo-sequestration are still in their early stages of development. Consequently, there are many issues in this field that need to be explored; out of which multiphase flow characteristics of the CO_2-brine-rock system and how they are influenced by different factors and changed over time, both over the short and long terms, are those which require further thorough experimental investigation to shed light on the many remaining uncertainties.

1.2 Research Objectives

The general aim of this research is to have a better understanding of the multiphase fluid flow characteristics of the brine-rock-CO_2 system during the geo-sequestration process. There have been numerous computer-based simulation studies carried out on the subject of CO_2 geo-sequestration. The results of a number of published experimental studies are also available in the literature but still there are various aspects of the multiphase flow behaviour of the CO_2-brine-rock system which require further investigation. The ultimate goal of this research is to experimentally evaluate the change in the above mentioned multiphase flow characteristics over time caused by the potential chemical and physical/mechanical processes occurring during deep CO_2 disposal with the following specific objectives:

- Investigating the effect of cyclic/alternating CO_2-brine flooding on the fluid flow characteristics during the CO_2 sequestration processes.

- Investigating the effect of flow direction (i.e. horizontal vs. vertical) on the CO_2-brine-rock multiphase flow characteristics.
- Investigating the effect of residual hydrocarbon (natural gas) on the fluid flow behaviour during CO_2 sequestration in a depleted hydrocarbon reservoir.
- Investigating the effect of change in the reservoir stress field on the fluid flow characteristics over the long term.

1.3 Organisation of Theses

This theses is organised in six chapters. The Chap. 2 presents a detailed description of the aspects of multiphase flow in porous medium pertaining specifically to the CO_2 geo-sequestration process. After giving an overview of the thermophysical fluid properties of CO_2, brine and their mixtures under conditions encountered during deep CO_2 disposal, those factors affecting the CO_2-brine flow characteristics, especially those which are investigate experimentally in this research program, are discussed. Then the chapter ends with a comprehensive review of the experimental work conducted to date on evaluating the multiphase flow behaviour pertaining to the underground CO_2 disposal.

The Chap. 3 is divided into two parts. The first part gives a detailed description of the experimental setup used to carry out the laboratory work, while the second part discusses the details of the experimental procedure adopted in performing the various experimental work.

Chapter 4 presents the results of the experiments. In Chap. 5, the experimental results presented in Chap. 4 are analysed and discussed in detail and conclusions are drawn.

Finally, Chap. 6 summarises the research findings and presents recommendations on possible new research directions to be further investigated.

References

1. IPCC (2007) Climate change 2007: syntheses report. Contribution of working groups I, II and III to the fourth assessment report of the intergovernmental panel on climate change, Intergovernmental Panel on Climate Change
2. García JE (2003) Fluid dynamics of carbon dioxide disposal into saline aquifers. PhD theses, University of California, Berkeley
3. UNFCCC (2002) Climate change information kit. Technical report, United Nations Framework Convention on Climate Change
4. Scripps Institution of Oceanography (2010) Mauna Loa observatory, Hawaii. http://scrippsco2.ucsd.edu/data/flask_co2_and_isotopic/monthly_co2/monthly_mlf.csv. La Jolla, CA. Accessed 23/5/2010
5. Orr FM Jr (2004) Storage of carbon dioxide in geologic formations. J Pet Tech 56:90–97
6. DOE's Office of Fossil Energy and Office of Science (1999) Carbon sequestration research and development. The U.S. Department of Energy

7. Rudins G, Bajura (1999) Carbon sequestration R and D program plan. http://www.fossil.energy.gov/programs/sequestration/publications/programplans/1999/Program_Plan_-_1999.html. The U.S. Department of Energy. Accessed 1 June 2010
8. Bachu S (2000) Sequestration of CO_2 in geological media: criteria and approach for site selection in response to climate change. Energy Conserv Manag 41:953–970
9. Bachu S, Haug K (2005) In situ characteristics of acid-gas injection operations in the Alberta basin, western Canada: demonstration of CO_2 geological storage. In: Benson SM (ed) Geological storage of carbon dioxide with monitoring and verification, vol 2. Elsevier, London, pp 867–876
10. Bennion B, Bachu S (2005) Relative permeability characteristics for supercritical CO2 displacing water in a veriety of potential sequestration zones in the Western Canada sedimentary basin. SPE 95547, The SPE annual technical conference and exhibition, Society of Petroleum Engineers, Dallas, Texas, USA
11. Braiser FM, Kobelski BJ (1996) Deep injection disposal of hazardous and industrial waste: scientific and engineering aspects. Academic, San Diego
12. Moritis G (2002) Special report: enhanced oil recovery-2002 worldwide EOR survey. Oil Gas J 100:43–47
13. Seo JG (2004) Experimental and simulation studies of sequestration of supercritical carbon dioxide in depleted gas reservoirs. PhD theses, Texas A and M University, Texas, p 132
14. Pruess K, Tianfu X, Apps J, Garcia J (2003) Numerical modeling of aquifer disposal of CO_2: SPE 83695. SPE J 8:49–60
15. Seo JG, Mamora DD (2003) Experimental and simulation studies of sequestration of supercritical carbon dioxide in depleted gas reservoirs. SPE 81200, SPE 81200, SPE/EPA/DOE Exploration and production environmental conference, Society of Petroleum Engineers, San Antonio, Texas
16. Span R, Wagner W (1996) A new equation of state for carbon dioxide covering the fluid region from triple-point temperature to 1,100 K at pressures up to 800 MPa. J Phys Chem Ref Data 25:1509–1597
17. Sweatman RE, Parker ME, Crookshank SL (2009) Industry experience with CO_2-enhanced oil recovery technology, SPE 126446, SPE international conference on CO_2 capture, storage, and utilization, Society of Petroleum Engineers, San Diego, California, USA
18. Wright I, Ringrose P, Mathieson A, Eiken O (2009) An overview of active large-scale CO_2 storage projects. SPE 127096, SPE international conference on CO_2 capture, storage and utilization, Society of Petroleum Engineers, San Diego, California
19. Ennis-King J, Paterson L (2007) Coupling of geochemical reactions and convective mixing in the long-term geological storage of carbon dioxide. Int J Greenh Gas Control 1:86–93
20. Izgec O, Demiral B, Bertin H, Akin S (2008) CO_2 injection into saline carbonate aquifer formations: laboratory investigation. Transp Porous Media 72:1–24
21. Nogueira M (2005) Effect of flue gas impurities on the process of injection and storage of carbon dioxide in depleted gas reservoirs. MSc theses, Texas A and M University, Texas
22. Ross GD, Todd AC, Tweedie JA, Will AG (1982) The dissolution effects of CO_2-brine systems on the permeability of U.K. and North Sea calcareous sandstones. SPE 10685, SPE/DOE third joint symposium on enhanced oil recovery of the Society of Petroleum Engineers, Society of Petroleum Engineers, Tulsa, OK
23. Wellman TP, Grigg RB, McPherson BJ, Svec RK, Lichtner PC (2003) Evaluation of CO_2-brine-reservoir rock interaction with laboratory flow tests and reactive transport modeling. In: International symposium on oilfield chemistry. Society of Petroleum Engineers, Houston
24. Juanes R, Spiteri EJ, Orr FM Jr, Blunt MJ (2006) Impact of relative permeability hysteresis on geological CO_2 storage. Water Resour Res 42:W12418
25. Spiteri EJ, Juanes R (2006) Impact of relative permeability hysteresis on the numerical simulation of WAG injection. J Pet Sci Eng 50:115–139

Chapter 2
Multiphase Flow during CO_2 Geo-Sequestration

2.1 Introduction

Both quantitative and qualitative evaluations of multiphase flow in porous medium is necessary in order to understand the processes involved and optimum management of the underground reservoirs subjected to either production or injection of fluids. The flow of fluids through pipes and conduits is relatively easy to model. However, due to the complex nature of the geological porous medium, analysing multiphase flow through them involves complex formulation and cannot be described explicitly.

The simplest case of fluid flow through porous media is the linear flow of a single-phase fluid under a constant pressure gradient, which is known as linear steady-state flow [1]. Darcy's Law, which is an empirical relationship derived by Henry Darcy in 1856 (Fig. 2.1 and Eq. 2.1) can be used to describe the above mentioned fluid flow type. However, below are three basic assumptions necessary in order to apply Darcy's Law in the form presented in Eq. 2.1:

- The fluids exhibit laminar flow (i.e. fixed flow paths).
- There are no chemical reactions between the fluid and the rock.
- Only one fluid is present, occupying 100% of the pore space.

$$q = -\left(\frac{k}{\mu}\right)\left(\frac{A}{L}\right)\Delta p \tag{2.1}$$

Where: $q =$ rate of fluid flow (cm^3/s)
$A =$ cross-sectional area open to flow (cm^2)
$\mu =$ dynamic viscosity of flowing fluid (cp)
$\Delta p =$ pressure drop across porous medium (atm)

A. Saeedi, *Experimental Study of Multiphase Flow in Porous Media during CO_2 Geo-Sequestration Processes*, Springer Theses, DOI: 10.1007/978-3-642-25041-5_2,

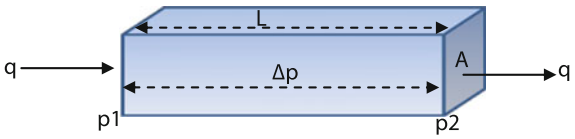

Fig. 2.1 Single-phase fluid flow through porous medium

$L =$ length of porous medium (cm)
$k =$ permeability $(Darcy)$

In the early Twentieth century it was demonstrated by Muskat and Meres [2], [3] that the flow of two or more fluids through porous rocks could be described using alternative derivatives of Darcy's Law incorporating the concept of relative permeability. By the use of this additional empirically determined term, a better understanding of the complex behaviour of immiscible multiphase flow through porous medium can be achieved. Each individual phase has its own experimentally measureable relative permeability which itself is a function of a number of factors. Using the concept of relative permeability, a new set of Darcy's Law formulations can be constructed for each fluid flowing through the porous medium (Eq. 2.2).

$$q_f = -\left(\frac{kk_{rf}}{\mu_f}\right)\left(\frac{A}{L}\right)\Delta p_f \tag{2.2}$$

In Eq. 2.2 subscript f refers to each individual fluid, among the fluids flowing through the porous medium simultaneously, and k_r refers to the fluid's relative permeability (i.e. the ratio of the fluid's effective permeability to absolute permeability of the porous medium).

Although originally it was assumed that relative permeabilities, or broadly speaking multiphase flow characteristics of a fluids-rock system, were unique functions of fluid saturations, later conclusive theoretical and experimental evidence emerged showing that, apart from fluid saturations, they also depend on a number of other rock and fluid characteristics, including the wetting tendency of the rock, various physical rock properties, fluid viscosity, interfacial tension (IFT), displacement flow-rate, saturation history (hysteresis effect), existence and magnitude of an immobile third phase saturation, magnitude of capillary end effect, clay and fines content, temperature, overburden pressure and in situ stress field [4–6], and flow direction [7, 8].

The aim of this chapter is to give a detailed insight into the multiphase flow characteristics of the supercritical CO_2-brine-rock system with special emphasis on the rationale and motivation behind this research. Section 2.2 will review the existing models and available data for thermophysical properties of pure CO_2 and H_2O and aqueous solutions of CO_2 and NaCl, as these are the main fluids involved in deep geological CO_2 disposal. The second and main part of this chapter presents a detailed description of the factors influencing the flow characteristics of supercritical CO_2 and brine in the porous medium. Finally, the chapter ends with a review of the experimental studies conducted to date to evaluate the multiphase flow behaviour during subsurface CO_2 disposal.

2.2 Thermophysical Properties of Fluids during CO_2 Geo-Sequestration

As mentioned earlier, multiphase flow behaviour of fluids through porous medium, among others, depends on the thermophysical properties of the in situ fluids and fluid mixtures. Therefore, a detailed knowledge of the thermophysical properties of the fluids involved in deep CO_2 disposal [i.e. pure CO_2, brine and aqueous solutions of CO_2 and NaCl (binary CO_2–H_2O and ternary CO_2–H_2O–NaCl systems)] is necessary for successful implementation of such projects. The phase behaviour of these chemical species and their aqueous solutions in a system depends on the system's intensive properties of pressure and temperature, which for the case of a potential underground storage structure depend on its depth and regional geothermal and hydrostatic pressure gradients. In general, the P–T ranges of interest for CO_2 disposal extend from low temperature (hydrate formation and ocean carbon sequestration) and low pressure (atmospheric) to intermediate temperatures and pressures (deep geological sequestration) [9]. For underground CO_2 geo-sequestration however, the medium P–T range only is applicable.

2.2.1 Pure Carbon Dioxide

CO_2 or carbon dioxide at atmospheric conditions is a colourless, odourless, faintly acidic-tasting and non-flammable gas. Apart from research conducted during the early Twentieth century for the refrigeration industry into the CO_2 thermophysical properties at low temperatures, the mid Twentieth century saw the interest diverted to the use of CO_2 in its supercritical state as an efficient coolant in nuclear power plants. Later, the interest in CO_2 properties grew as it was found to be an efficient tool for EOR purposes and its supercritical state could be used as a powerful industrial dry solvent.

Research on the thermophysical properties of CO_2 in the high P–T ranges was initiated when the role of the naturally occurring CO_2 in various areas of geosciences and geothermal engineering became evident. Since the early 1990s, with the introduction of geo-sequestration as a means for reducing CO_2 emissions into the atmosphere, the measurement and development of tools for accurate prediction of such properties has received special attention.

Tables 2.1 and 2.2 present CO_2 and the available wide-range equations of state to predict the thermophysical properties of pure CO_2, respectively. Figure 2.2 also illustrates the P–T phase diagram for pure CO_2.

Since 1960, numerous correlation equations for predicting the thermophysical properties of pure CO_2, applicable to conditions encountered during CO_2 geo-sequestration, have been developed (Table 2.2), among which those proposed by Altunin, Angus et al., Span and Wagner and Mäder and Berman are the most commonly accepted and used [9]. Vargaftik et al. [11] in their handbook, which is

Table 2.1 Physical constants for pure CO_2 (after [10])

Property	Value
Molar mass, M (gr/mol)	44.009
Molar gas constant, R_m $(J/(molK))$	8.314510
Critical temperature, T_c (K)	304.128
Critical pressure, P_c (MPa)	7.377
Critical density, ρ_c (kg/m^3)	467.6
Triple point temperature, T_t (K)	216.592
Triple point pressure, P_t (MPa)	0.51795

Table 2.2 Available wide-range equations of state for pure CO_2

Authors	Year	Temperature range (°C)	Pressure range (psi)
Render	1970	−56.2–803.9	0–7,252.0
Altunin and Gadetskii	1971	−57.2–1,027.9	0–43,512.0
Starling et al.	1972	−29.2–140.9	0–6,961.9
Meyer-Pittroff	1973	−72.2–1,000.9	0–8,702.4
Angus et al. (IUPAC)	1976	−52.2–827.9	0–14,504.0
Huang et al.	1985	−56.2–150.9	0–44,962.4
Ely	1986	−56.2–750.9	0–43,512.0
Ely et al.	1987	−56.2–750.9	0–43,512.0
Pitzer and Schreiber	1988	−42.2–757.9	0–14,504.0
Ely et al.	1989	−56.2–750.9	0–45,832.6
Mäder and Berman	1991	127.9–1,527.9	0–609,168.0
Pitzer and Sterner	1994	−52.2–1,727.9	0–1,450,400.0
Span and Wagner	1996	up to 827.9	Up to 116,032.0

an updated version of their older book published in 1983 (Vargaftik and Vinogradov), have also presented extensive PVT tables on thermophysical properties of various pure substances and mixtures including carbon dioxide. US National Institute of Standards and Technology (NIST) also has an excellent databank of thermophysical properties of fluid systems including CO_2 and various other pure and mixed substances [12], which is freely accessible by public through their website. Furthermore, the published correlations developed by Fenghour et al. [13] and Rah and Eu [14] can be used to calculate viscosity of CO_2. Figure 2.3 shows the change in the viscosity of pure CO_2 against pressure for a number of different temperatures.

2.2.2 Pure H_2O

The thermophysical properties of pure H_2O are well defined in the literature. The first comprehensive database on properties of ordinary water was published by the International Formulation Committee (IFC) [15]. Since then, there have been

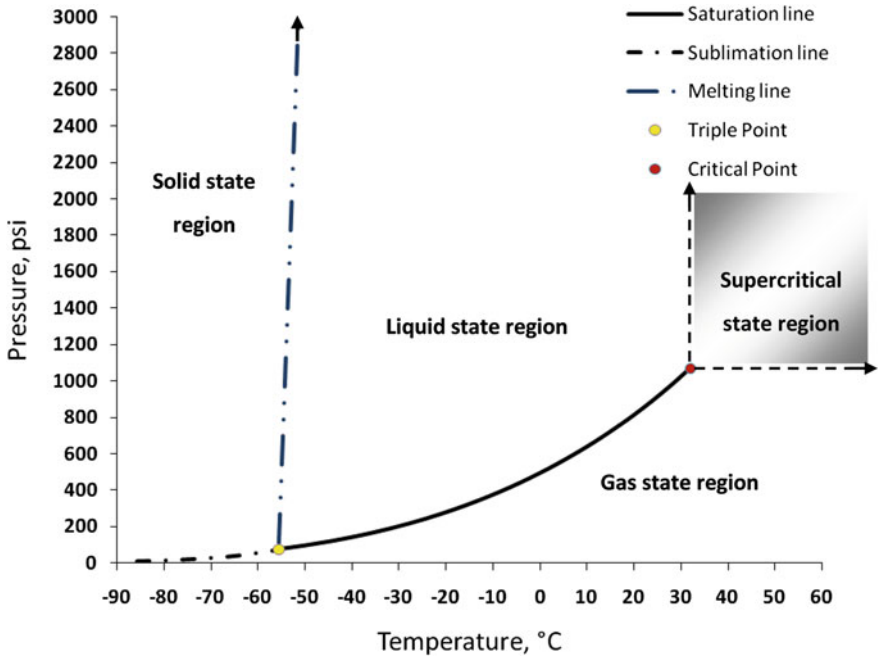

Fig. 2.2 P–T phase diagram for pure CO_2 (data taken from [10])

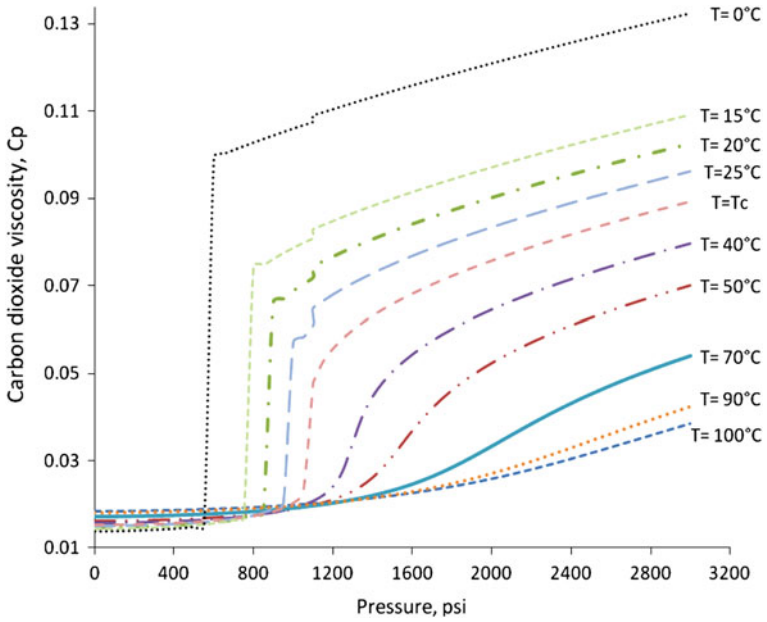

Fig. 2.3 Carbon dioxide viscosity at various P–T conditions (data taken from [12])

Table 2.3 Physical constants of pure H_2O (after [16])

Property	Value
Molar mass, M (gr/mol)	18.015
Critical temperature, T_c (K)	647.096
Critical pressure, P_c (MPa)	22.064
Critical density, ρ_c (kg/m^3)	322
Triple point temperature, T_t (K)	273.16
Triple point pressure, P_t (Pa)	611.655
Triple point liquid density, ρ_t' (kg/m^3)	999.793
Triple point vapour density, ρ_t'' (kg/m^3)	0.597657

numerous publications covering various properties of H_2O from very low to very high pressures and temperatures. The most widely used equation of state to predict the thermophysical properties of H_2O is due to Wagner and Pruss [16] which is valid for temperatures from the melting line (lowest temperature 251.2 K at 209.9 Mpa) to 1,273 K and pressures up to 1,000 MPa. In addition, Saul and Wagner have developed a separate model to predict the properties of water at pressures and temperatures of up to 25,000 MPa and 1,273 K respectively [17]. Furthermore, there are a number of other publications [18–21], which are dedicated to individual thermophysical properties of water (e.g. thermal conductivity, viscosity, surface tension and dielectric constant). Table 2.3 presents a number of physical constant of pure H_2O.

2.2.3 Aqueous Solutions of CO_2 and NaCl

Aqueous solutions of CO_2 and NaCl are the most common fluid mixtures encountered in various geological environments around the globe. Therefore, the knowledge of the pressure–volume–temperature-composition (PVTx) and phase equilibrium properties of these fluid systems is essential in understanding various geochemical processes which are of great interest to different fields of geoscience and geothermal engineering, including subsurface CO_2 sequestration.

2.2.3.1 Phase Behaviour of the Binary CO_2–H_2O System

In the 1870s, Gibbs' Phase Rule [22] was presented in the form of Eq. 2.3. This equation proposed that if a system in equilibrium contains r number of phases and n number of components then the number of the degrees of freedom is equal to F. The number of degrees of freedom for a system is the number of intensive variables of the system that may be arbitrarily specified without changing the number of phases [23].

$$F = n - r + 2 \tag{2.3}$$

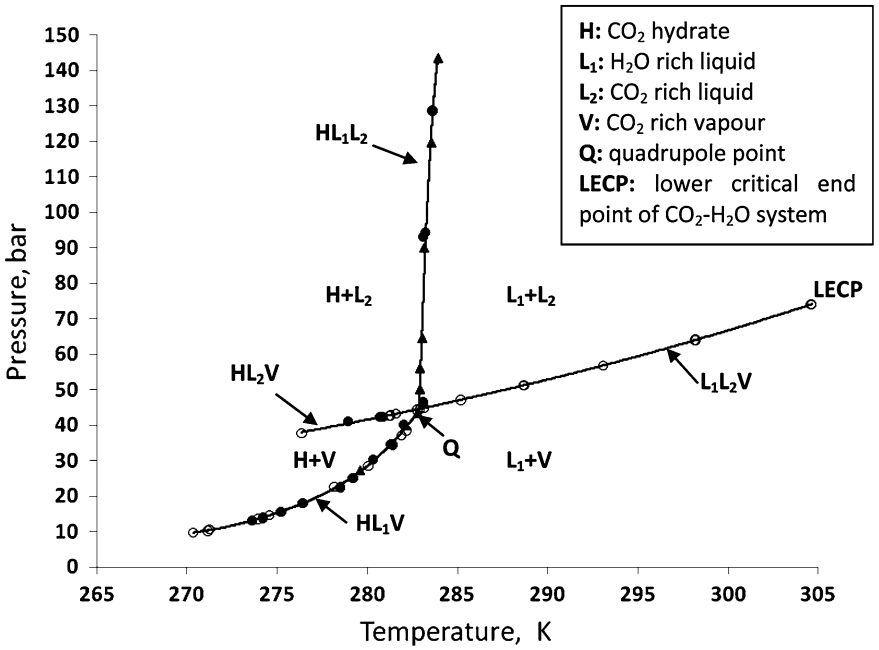

Fig. 2.4 P–T slice of the CO_2–H_2O phase diagram showing the two and three phase coexistence curves and the critical points (data taken from [24–26])

In a binary system with two chemically independent species (e.g. CO_2–H_2O system) n = 2, therefore $F = 4 - r$ and because at least one phase needs to exist, the minimum value of r is 1. As a result, the maximum number of degrees of freedom or maximum number of phase rule variables which need to be specified to fix the state of the system is equal to 3. Those three variables, as mentioned earlier, are pressure, temperature and composition (P–T–x). Two 2D P–T and P–x slices of the 3D P–T–x diagram of the CO_2–H_2O system are shown in Figs. 2.4 and 2.5, respectively. From Figs. 2.4, 2.5, and 2.6 it can be concluded that for the underground conditions encountered during deep CO_2 storage the main phases expected to exist are CO_2-rich gas and H_2O-rich liquid.

2.2.3.2 Thermophysical Properties of H_2O–CO_2 and H_2O–CO_2–NaCl Systems

Dissolution of CO_2 directly affects two (i.e. dissolution trapping and mineral trapping) of four possible CO_2 trapping mechanisms active during deep CO_2 disposal. It also influences the thermophysical properties of the fluids used in carrying out related experimental work. Therefore predicting the mutual solubility of CO_2 and H_2O/brine and its effect on the phase behaviour of these systems is of

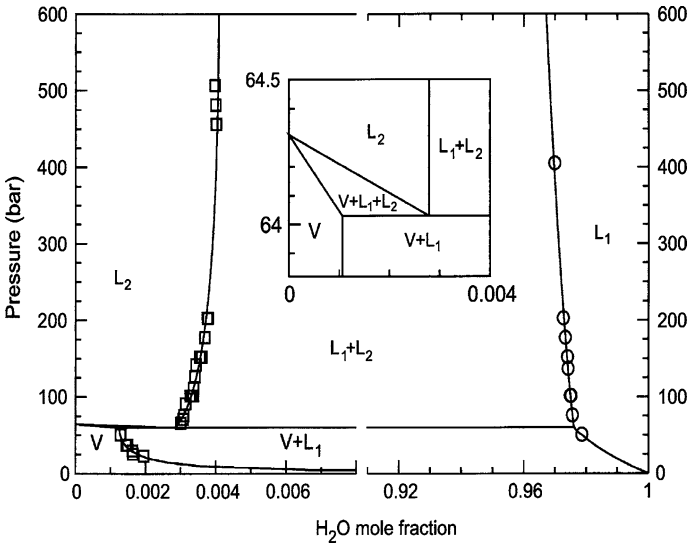

Fig. 2.5 P–x slice of the CO_2–H_2O phase diagram at T = 25°C. Square data points show H_2O solubility in CO_2 and circle data points show CO_2 solubility in H_2O (after [27])

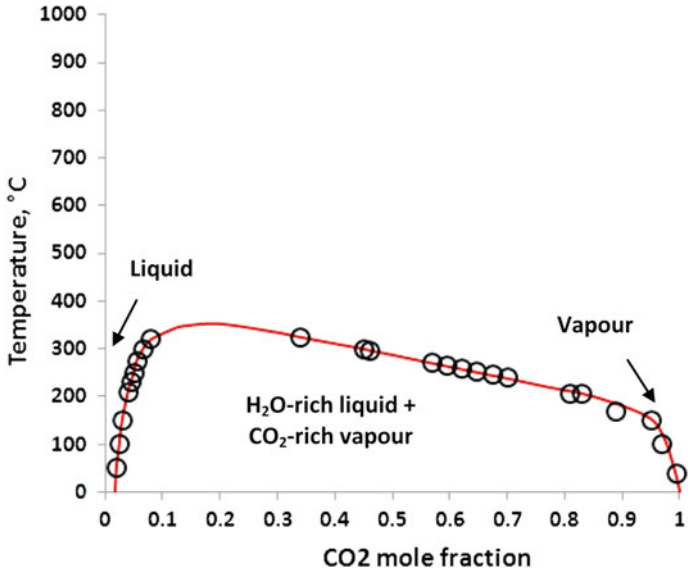

Fig. 2.6 Temperature-composition diagram for the CO_2–H_2O system at P = 350 bar-circles show experimental data (after [9])

great importance for the implementation of any such projects. Since the water, which exists in the underground aquifer or as residual water saturation inside the hydrocarbon reservoirs, is rarely pure, the effect of salt, most commonly sodium chloride (NaCl) concentrations on such processes also needs to be evaluated. This data is essential for both reservoir simulation tasks and accurate interpretation of the experimental work. Along with various experimental studies, there have been a number of models proposed in the literature which can be used to predict the mutual solubility of carbon dioxide and water/brine which then allows calculation of the thermophysical properties of the fluid mixtures.

The first publicly published experimental data for mutual solubility of CO_2 and H_2O was presented by Wiebe and Gaddy [28–30] but this data does not cover the full range of P–T conditions expected to be encountered during CO_2 geo-sequestration. After Wiebe et al. various other researchers have published their experimental results of which full reviews have been presented recently in a number of publications by Carroll et al. [31], Crovetto [32], Duan et al. [33], Diamond and Akinfiev [34], Duan et al. [35], Duan and Sun [36], Spycher et al. [27] and Hu et al. [37].

Tables 2.4 and 2.5 are comprehensive lists of the experimental data for thermophysical properties of the CO_2–H_2O and CO_2–H_2O–NaCl systems respectively. As can be seen, there are far less experimental data available for the CO_2–H_2O–NaCl system than those for the CO_2–H_2O system.

In addition to these experimental data, since the 1970s, there have been various correlations developed [38–43] to predict the thermophysical properties of CO_2–H_2O at low to medium pressures. The data generated using these correlations, however, deviate from experimental results rapidly with pressure. Therefore, they are not regarded as adequate prediction tools when it comes to the P–T conditions encountered in the geoscience related underground activities including CO_2 geo-sequestration. To overcome this issue a number of EOS's (Equation of state) have been developed to predict the thermophysical properties of the CO_2–H_2O mixtures covering a wider range of P–T conditions [44–50]. Furthermore, there are a number of density models of aqueous CO_2 solutions available in the literature which can be regarded as another type of EOS for the CO_2–H_2O system [51–54]. With regards to the available models on solubility and PVTx of CO_2–H_2O–NaCl system, the most widely used models, applicable to P–T conditions encountered in deep CO_2 disposal, are due to Duan, Møller and Weare [33, 35], Duan and Sun [36], Duan et al. [55], Bachu and Adams [51], Ji et al. [47], Bando et al. [56] and Chang et al. [44]. In addition to all the publications and databases mentioned before for predicting the thermophysical properties of CO_2–H_2O and CO_2–H_2O–NaCl systems, the Zhenhao Duan Research Group [57] has an interactive online database which integrates the most accurate and widely used models to calculate the thermophysical properties of various pure, binary, ternary and multi-component systems including binary CO_2–H_2O and ternary CO_2–H_2O–NaCl systems.

One other parameter of the CO_2–H_2O and CO_2–H_2O–NaCl systems which is of great importance for prediction and interpretation of the multiphase flow behaviour during CO_2 geo-sequestration is the interfacial tension (IFT) between the aqueous

Table 2.4 Available experimental data for the thermophysical properties of the CO_2–H_2O system (after [37])

Authors	Year	Temperature, K	Pressure, MPa	Concentration range	Number of data
Ohsumi et al.	1992	276.15	34.754	$x(CO_2)\% = 0.1798–0.6294$	5
Song et al.	2003a, b	273.25–284.15	5–12.5	$x(CO_2)\% = 0–0.61$	33
Teng et al.	1997	278–293	6.44–29.49	$x(CO_2)\% = 2.5–3.49$	24
Parkinson and De Nevers	1969	278.1–313.7	1.0342–34.4744	$x(CO_2)\% = 0.1–2.2$	28
Hebach et al.	2004	283.8–333.19	1.09–30.66	$x(CO_2)\%$ = saturated values	201
King et al.	1992	288.15–298.15	6.08–24.32	$x(CO_2)\% = 2.445–3.070$	27
Hnedkovsky et al.	1996	298.15–633.41	1–35	$x(CO_2)\% = 0.279–0.332$	18
Zhang et al.	2002	308.15	7.752–12.484	$x(CO_2)\% = 99.7$	16
Patel et al.	1987	323.15–498.15	0.1–10	$x(CO_2) = 0.5–0.98$	423
Patel and Eubank	1988	323.15–498.15	0.0855–10.0237	$x(CO_2) = 0.02–0.5$	297
Nighswander et al.	1989	352.85–471.25	2.04–10.21	$x(CO_2)\% = 0.22–1.66$	33
Zawisza and Malesińska	1981	373.15–473.15	0.385–3.35	$y(H_2O) = 0.1210–0.9347$	142
Ellis	1959	387.15–621.15	0.5–16.4	$y(CO_2)\% = 3.90–6.27–84.02$	36
Fenghour et al.	1996	415.36–644.78	5.884–27.964	$x(CO_2) = 0.0612–0.7913$	104
Wormald et al.	1986	473.2–623.2	1–12	$x(CO_2) = 0.5$	57
Sterner and Bodnar	1991	494.15–608.15	48.7–310	$x(CO_2) = 0.1234–0.7473$	84
Ellis and Golding	1963	504.15–643.15	4.791–25.443	Not directly reported	9
Singh et al.	2000	573.15	7.44–99.93	$x(CO_2) = 0.05–0.9$	58
Seitz and Blencoe	1997	573.15–623.15	99.93	$x(CO_2) = 0.1–0.9$	18
Blencoe et al.	2001b	573.15	7.44–99.93	$x(CO_2) = 0–0.9$	148
Zakirov	1984	573.15	5–180	$x(CO_2) = 0.3–0.77$	55
Zhang and Frantz	1992	519.95–634.45	Not reported	$x(CO_2)\% = 5.5–16.5$	29
Crovetto and Wood	1992	622.75–642.70	19.64–28.13	$x(CO_2)\% = 0.48–0.8745$	72

x, y = mole fraction

Table 2.5 Available experimental data for the thermophysical properties of the CO_2–H_2O-NaCl system (after [37])

Authors	Year	T, K	P, MPa	Concentration range	Number of data
Song et al.	2005	276.15–283.15	4–13	wt.(CO_2)% = 0–7.7, Sr% = 3.5%	64[a]
Teng and Yamasaki	1998	278–293	6.44–29.49	x(CO_2)% = 1.96–3.27, m(NaCl) = 0.99–4.99	24[b]
Song et al.	(2003a,b)	303.15–323.15	10–20	wt.(CO_2)% = 1–4, Sr = underground brine	99[b]
Li et al.	2004	332.15	0.24–28.93	c(CO_2) = 0–0.958 × 10 − 3 mol·cm − 3, Sr% = Weyburn brine	37[c]
Nighswander et al.	1989	353.15–473.65	2.11–10.03	x(CO_2)% = 0.28–1.54, wt.(NaCl)% = 1.0	34
Gehrig et al.	1986	408–647	3–281.2	x(CO_2)% = 0.18–84.9, Sr% = 6.0–20.0	52
Schmidt et al.	1995	623.15	400	x(CO_2)% = 5 (relative to H2O), Sr% = 40	1
Krüger and Diamond	(2001b)	540–TC(H_2O)	65–350	x(CO_2)% = 9.69, x(NaCl)% = 1.74	Not reported

[a] a specific underground saline water within a Japanese city
[b] artificial seawater
[c] Weyburn brine
Sr relative salinity, *wt.* weight, *m* molality, *x* mole fraction, *c* concentration

solutions and the CO_2. There are a number of publications [58–67] presenting experimental data and correlations, mainly empirically derived, which can be used to predict the IFT values for the P–T conditions of interest for such systems.

2.3 Factors Influencing the Multiphase Flow behaviour during CO_2 Geo-Sequestration

As was pointed out earlier in this chapter, multiphase flow through porous medium (e.g. CO_2-brine flow through reservoir rock during CO_2 geo-sequestration) apart from fluid saturations, is controlled by a number of rock and fluid characteristics. In this section of the theses the importance of a number of these factors, which are known to influence the multiphase flow characteristics of the CO_2-brine-rock system during deep CO_2 storage, is discussed. Since the importance of these factors is mainly due to the way they influence the effectiveness of the potential trapping mechanisms active during deep CO_2 disposal (Fig. 2.7), prior to any further discussion on this topic, a short discussion on these trapping mechanisms is necessary.

Injected CO_2 can be permanently trapped in the subsurface geological structures through four different trapping mechanisms [68–73]:

- *Structural trapping*: once CO_2 is injected into the deep underground porous medium, as it moves away from the injection well, it starts to flow upwards, due to buoyancy forces, and moves towards the top of the structure. Depending on the multiphase phase flow characteristics of the fluids-rock system, most or some of the CO_2, which exists as mobile liquid or in its supercritical state, would eventually reach the top of the geological structure and is trapped just below the caprock. This trapping mechanism is called structural trapping which falls into the hydrodynamic trapping category. The potential of an underground structure to securely contain a certain amount of CO_2 depends on the degree of integrity of the seal above it. The presence of any fractures, activated faults or poorly completed wells could potentially result in leakage and escape of the CO_2 into the formations above the reservoir. This could not only undermine the main purpose of the CO_2 injection being sequestered, it can also contaminate other regional resources such as the potable water reservoirs. One other risk associated with structural trapping is the possible change in the properties of the caprock layer as it comes in contact with the mobile CO_2 phase. These possible alterations will be explained in more detail in the following sections of this chapter.
- *Solubility trapping*: as it was pointed out earlier, relatively considerable quantities of the injected CO_2 could be dissolved into the brine contained in the pore space of the porous medium. The dissolution process is considered to be slow, however, it could be slightly enhanced by the convection mixing, which is expected to occur due to the fact that CO_2 saturated brine is slightly denser than

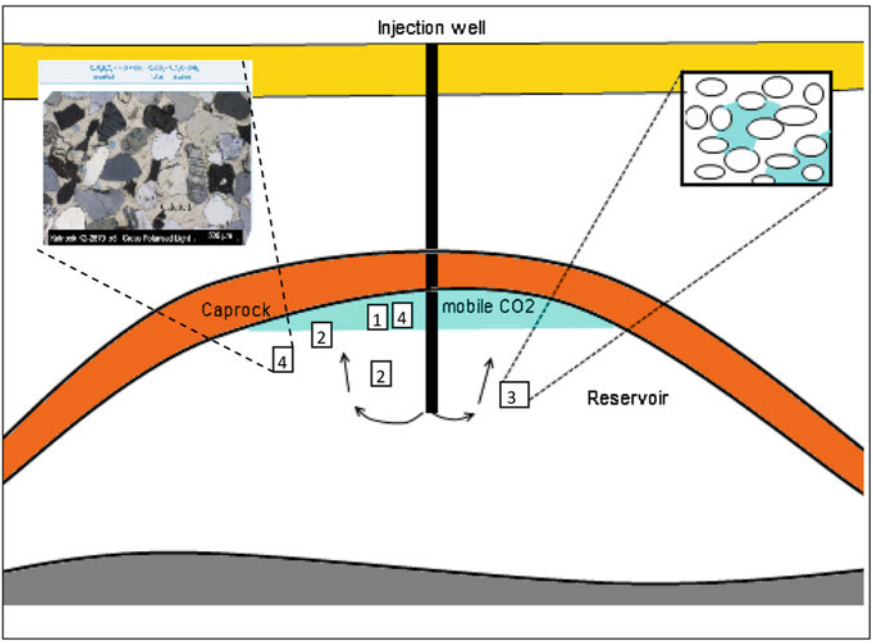

Fig. 2.7 Schematic of the main four trapping mechanisms: *1*. Structural trapping, *2*. Solubility trapping, *3*. Capillary trapping and *4*. In mineral trapping

the unsaturated brine [70]. There are a number of factors which could influence the speed and significance of the dissolution trapping such as the reservoir P–T conditions, properties of the formation brine, etc.

- *Capillary trapping*: capillary residual trapping is the disconnection of the mobile CO_2 phase into an immobile trapped fraction. During post CO_2 injection or water injection in the case of a WAG type process, the mobile CO_2 phase is displaced away from the well and upwards. Since the majority of reservoir rocks are water-wet, the CO_2 will be the non-wetting phase, therefore various trapping mechanisms (e.g. snap-off, pore doublet, etc.) would lead to disconnection and bypassing of the CO_2. The disconnected CO_2 becomes immobile and trapped permanently within the pores. The capillary residual trapping is a function of various fluids and rock properties, reservoir P–T conditions and the actual type of the injection procedure.
- *Mineral trapping*: mineral trapping involves the formation of stable carbonate minerals. This mineralisation process, however, is very slow and is expected to take hundreds if not thousands of years from the onset of the CO_2 injection to reach its full trapping potential. Furthermore, many underground reservoirs have low mineralisation potential. The mineral trapping mechanism relies on a series of consecutive chemical reactions to occur (Eqs. 2.4–2.8).

$$CO_2 + H_2O_{(l)} \leftrightarrow H_2CO_{3(aq)} \leftrightarrow H^+_{(aq)} + HCO^-_{3(aq)} \tag{2.4}$$

$$\text{Silicates} + 2H^+ \leftrightarrow M^{2+} + \text{silica} \tag{2.5}$$

$$Mg^{2+}_{(aq)} + HCO^-_{3(aq)} \leftrightarrow H^+_{(aq)} + MgCO_{3(s)}\,(magnesite) \tag{2.6}$$

$$Ca^{2+}_{(aq)} + HCO^-_{3(aq)} \leftrightarrow H^+_{(aq)} + CaCO_{3(s)}\,(calcite) \tag{2.7}$$

$$Fe^{2+}_{(aq)} + HCO^-_{3(aq)} \leftrightarrow H^+_{(aq)} + FeCO_{3(s)}\,(siderite) \tag{2.8}$$

Where: M^{2+} = generic cation
l = liquid
aq = aqueous
s = solid

The focus of the rest of this chapter is on presenting a detailed discussion on the factors affecting multiphase flow characteristics of the fluids-rock system during CO_2 geo-sequestration, and the effects of these factors on different trapping mechanisms are also discussed.

2.3.1 Wetting Tendency of Porous Media

As defined, wettability is the measure of the preferential tendency of a fluid to wet the interstitial surfaces of the porous media in the presence of other immiscible fluids [74]. Wettability is a major factor controlling the location, flow and distribution of individual fluids within an underground reservoir [75]. For instance, the wetting tendency of porous media controls the distribution of the immiscible fluids within the reservoir by influencing the relative permeabilities. In an underground oil reservoir the oil relative permeability increases, causing a decrease in water relative permeability, as the wettability changes from water-wet to oil-wet. Furthermore, this change in wettability causes the crossover point of the relative permeability curves to move from lower to higher water saturations [74].

Before the implementation of any CO_2 geo-sequestration project, two critical issues of post-injection distribution of the injected CO_2 and the effectiveness of the storage site to contain the injected CO_2 need to be addressed in order to demonstrate the effectiveness of the process to trap the injected fluids permanently. Similar to underground hydrocarbon reservoirs, multiphase flow behaviour during CO_2 geo-sequestration is greatly influenced by the wetting tendency of the target storage formation [76]. In addition, the capillary-sealing potential of the caprock overlaying a potential underground CO_2 storage reservoir is vital for efficient entrapment of the injected CO_2 while the capillary pressure–saturation relationship

in turn, similar to relative permeability, is directly influenced by the wettability of the porous medium. In a CO_2 storage site, the capillary leakage through the caprock occurs when the net pressure exerted by the CO_2 phase from beneath (P_{CO_2}) exceeds the threshold or capillary entry pressure (P_{c,CO_2}), which is defined as the minimum pressure required to initiate the displacement of brine contained in the rock layer acting as the seal (Eq. 2.9).

$$P_{ca,CO_2} = P_{CO_2} - P_w = \frac{2\sigma_{w,CO_2} COS(\theta)}{R} \tag{2.9}$$

Where: P_{CO_2} = net pressure exerted by the CO_2 phase from beneath
P_{ca,CO_2} = threshold or capillary entry pressure of the caprock
P_w = hydrostatic water pressure inside the pore space of the caprock
σ_{w,CO_2} = brine-CO_2 interfacial tension (IFT)
R = effective pore radius of the caprock
θ = contact angle measured in the brine phase

Furthermore, it has been shown experimentally [77] that carbon dioxide can potentially alter the original wetting tendency of the porous medium which it comes in contact with, which in turn could cause alteration of the originally predicted fluid distribution within and containment effectiveness of the underground geological structure.

2.3.2 Saturation History

In a multiphase immiscible displacement process depending on the wetting tendency of the porous medium and whether the wetting fluid is displacing or being displaced, the process is called imbibition or drainage respectively. In other words, drainage is defined as the change in saturation towards reduction in the wetting phase saturation (e.g. water-flooding in an oil-wet reservoir) and imbibition is defined as the change in the saturation towards increase in the wetting phase saturation (e.g. water-flooding in a water-wet reservoir). Saturation history dependence of multiphase flow or the hysteresis effect (i.e. irreversibility or path dependence) is evident whenever the porous medium undergoes a cyclic flooding process. In other words, the multiphase flow through porous medium depends on the saturation history and saturation path. Therefore multiphase flow characteristics of a fluids-rock system (e.g. capillary pressure, relative permeability, etc.) during an imbibition process are different from those of a consecutive drainage process and vice versa. From a pore-scale processes point of view hysteresis has at least two main sources [6, 71, 78]:

- *Contact angle hysteresis*: the advancing contact angle which is measured at the immiscible interface when the wetting phase displaces the non-wetting phase

(i.e. imbibition) is larger than the receding contact angle which is measured at immiscible interface when the non-wetting phase displaces the wetting phase (i.e. drainage). These two angles are different due to chemical heterogeneities and/or surface roughness and tortuosity of the pores and pore throats.

- *Trapping of the non-wetting phase:* during an imbibition process due to various trapping mechanisms (e.g. snap-off, pore doublet, etc.) part of the non-wetting phase becomes disconnected in the form of blobs and ganglia. The disconnected non-wetting phase becomes immobile and trapped within the pores. Due to the presence of this immobile phase, a subsequent drainage process results in different multiphase flow behaviour in comparison to the equivalent imbibition process.

As mentioned before, the hysteresis effect during multiphase flow in a porous medium is more pronounced in processes involving a strong flow reversal which is for instance experienced in the case of alternating water and gas injection (WAG) in which a fraction of the non-wetting gas phase is trapped during water injection which follows an initial gas flooding stage. Therefore it would be expected to experience the hysteresis phenomenon during deep CO_2 disposal at least when the WAG type or periodic CO_2 injection scenarios are followed. This could possibly cause the multiphase flow characteristics of the fluids-rock system to be different from one injection cycle to the other. The necessity of having a thorough understanding of the fate of the injected CO_2, how the CO_2 plume evolves and migrates through the porous medium and potential change in CO_2 injectivity into the target formation, demands a detailed investigation of the effect of the hysteresis phenomenon, using representative rock and fluid samples under in situ reservoir P–T conditions, before the commencement of any CO_2 geo-sequestration project.

2.3.3 *Existence and Magnitude of a Third Phase Saturation in the Porous Medium*

The existence of mobile or immobile third phase saturation can potentially alter the multiphase behaviour characteristics of the fluids-rock system. There has been considerable research done on evaluating the effect of immobile connate water and trapped residual gas saturation on the performance of gas-oil or oil–water displacements. In the research carried out by Schneider and Owens [79], for instance, the effect of trapped gas in both sandstone and carbonate samples was investigated. They concluded that both water and oil relative permeabilities were affected by the trapped gas saturation. Water phase relative permeabilities, however, were more significantly reduced compared to the oil phase relative permeabilities. The Anti-Water Coning Treatment (AWCT), which involves injection of non-condensable gas into the well to minimise the water coning problem, is in fact putting the above-mentioned relative permeability reduction phenomenon, due to the presence of trapped gas saturation, into work as a remedy for the water-coning problems.

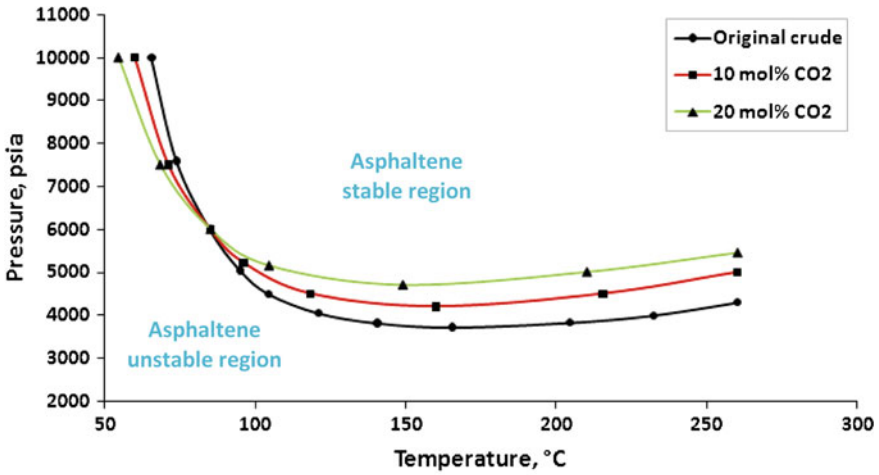

Fig. 2.8 Change in the asphaltene precipitation onsets of a 32° API gravity crude oil sample with addition of various concentrations of CO_2 (after [80])

As was mentioned in Chap. 1, active or depleted hydrocarbon reservoirs are considered as candidate storage mediums for CO_2 geo-sequestration, where CO_2 may be injected not only for CO_2 storage purposes but also for enhanced hydrocarbon recovery purposes. In this type of storage medium, either depleted or active, in addition to formation brine and, newly introduced CO_2 phases, there exists a third trapped residual hydrocarbon phase. Therefore, the multiphase flow behaviour of this system is expected to be different from a pure CO_2-brine system. The present residual gas or oil saturation may potentially increase or decrease the storage capacity of the underground structure. Moreover, the CO_2 injectivity into the target formation would be different from when CO_2 is injected into a subsurface saline aquifer with no hydrocarbon residues.

It has been some time since the problem of CO_2-induced asphaltene precipitation in the porous medium containing intermediate to heavy crude oils has been realised [80–85], (Fig. 2.8).

Once CO_2 is injected into an oil reservoir, either depleted or active, as it comes in contact with the oil, the displacement of the oil by CO_2 could become a miscible-type displacement. Furthermore, the phase behaviour of the fluids and in situ equilibrium conditions can change which in turn, depending on the asphaltene and heavy component content of the crude, favour flocculation and deposition of asphaltenes and other heavy organic particles. Precipitation of such solid particles can cause not only pore and pore-throat plugging and formation damage but also alteration of the reservoir rock wettability. Both of these effects can have serious adverse effects on the multiphase flow behaviour during deep CO_2 disposal.

In conclusion, the trapped residual hydrocarbon saturation in the form of gas or oil phases can alter the performance of the subsurface CO_2 disposal. Since gas is highly compressible or can be displaced efficiently by the injected CO_2, in situ

residual gas saturation may increase the storage capacity of the subsurface structure, compared to when the pores are filled with the liquid phase only, but at the same time it can have an adverse effect on the fluid flow performance during CO_2 injection. Since the involved physical and chemical interactions between the oil and CO_2 are much more complex, these adverse effects are expected to be more common and pronounced for the case of CO_2 injection into oil reservoirs.

2.3.4 Directional Dependence of Absolute and Relative Permeabilities

Unlike porosity, absolute permeability of a porous medium is a tensor and therefore can be different in different directions. In a Cartesian coordinate system the permeability tensor can be expressed by the following equation [86].

$$k = \begin{bmatrix} k_{11} & k_{12} & k_{13} \\ k_{21} & k_{22} & k_{23} \\ k_{31} & k_{32} & k_{33} \end{bmatrix} \tag{2.10}$$

Generally, horizontal permeability of sedimentary rocks tends to be higher than the vertical permeability in the absence of vertical fractures, fissures or channels. This is mainly for two reasons: firstly the natural vertical heterogeneity caused by the natural layering of sedimentary rocks. Secondly, because of the platy nature of some of the mineral fragments, when deposited, they tend to settle with their shortest axis aligned vertically, which provides the most stable position and least resistance against any current. This reduces the number of pore openings per unit of area available to flow fluids in the vertical direction compared to the horizontal direction (Fig. 2.9). This arrangement also can make the pore channels in vertical direction more tortuous.

It is commonly observed that the permeability is isotropic in the direction of the natural layering (i.e. horizontal direction) but anisotropic in the direction of perpendicular to the natural layering (i.e. vertical direction). Therefore, in a Cartesian coordinate system, if two out of three coordinates are placed in the horizontal plane, which makes them equal, and denoted as k_h and subsequently the third placed in the vertical direction and denoted as k_v, the Eq. 2.10 can be rewritten as follows [86]:

$$k = \begin{bmatrix} k_h & 0 & 0 \\ 0 & k_h & 0 \\ 0 & 0 & k_v \end{bmatrix} \tag{2.11}$$

It is believed and demonstrated experimentally that directional dependence is not only a feature of absolute permeability and, for even individual homogeneous rock samples, relative permeabilities are also different in different directions [7, 8]. Thus, when comparing curves obtained from the same core-sample subjected to displacement tests in horizontal and vertical directions, they show different values

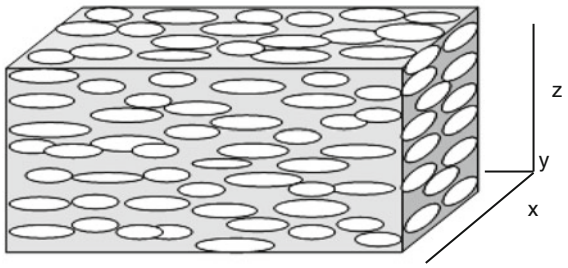

Fig. 2.9 A portion of a sedimentary rock showing the horizontal alignment of the flat grains

of residual saturations and overall displacement performances. There are numerous situations where vertical flooding and displacement occurs during deep underground processes—such as cross flow between layers of different absolute permeabilities, gravity segregation dominant flow, an expanding gas cap or formation of a secondary gas cap and, of course, vertical CO_2 or natural gas flow due to buoyancy forces during subsurface CO_2 or natural gas storage operations respectively. Therefore, despite the fact that according to the convention, horizontal relative permeabilities only receive adequate attention, evaluation of multiphase displacement performance of the porous medium in both directions are important and in fact in certain cases (e.g. CO_2 geo-sequestration) vertical displacement becomes the matter of primary importance.

2.3.5 Fines Migration and Mineral Dissolution and Precipitation

Mobilisation of fines or micro particles can severely impair the displacement performance of the porous medium when subjected to flooding procedures. Fines mobilisation is a costly source of formation damage especially in a porous medium around a wellbore. Fines migration has also been identified as a source of serious error during lab-scale flooding experiments [87–90]. Mobilisation of fines is a complex phenomenon but largely depends on mineralogy, permeability and pore network of the porous medium, changes in the pH, drag forces created by fluid currents, turbulence and fluid viscosity [91]. Fines migration in a porous medium occurs when the loosely attached naturally occurring particles present in a porous medium are detached from their stationary positions, due to one or several of the above-mentioned causes, and transported to pore-throat locations where they can potentially plug or bridge and subsequently cause permeability impairment in the porous medium (Fig. 2.10).

Based on the mineralogy, fines susceptible to mobilisation can be classified into two categories [89]:

- Clays—such as kaolinite, illite, montmorillonite etc.
- Non-clays—such as quartz, feldspars, carbonates, muscovite, amorphous material, salts, etc., which are normally present in the sandstones.

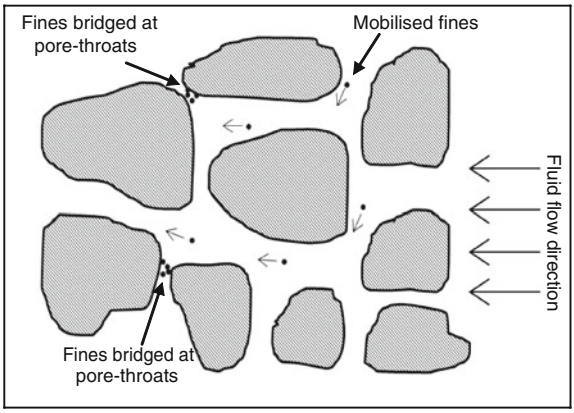

Fig. 2.10 Mobilised fines bridged the pore-throats

With regards to multiphase flow through a porous a medium during deep CO_2 disposal, like any other cases of fluid flow through a porous medium, fines migration could occur due to the potential existence of several of the causing factors mentioned earlier. In addition, during such processes, due to favourable conditions, mineral dissolution and precipitation can also contribute to either impairment or enhancement of the displacement performance of the porous medium. Moreover, mineral dissolution can enhance the dislodgement of the potentially damaging particulates and can intensify the fines migration and formation damage phenomenon. The chemical reactions which could occur and lead to dissolution and precipitation of minerals during the flow of CO_2 and its aqueous solutions through a porous medium have already been discussed in Sect. 2.3 of this chapter. Precipitates can cause permeability reduction through a number of mechanisms including [88, 92]:

- Precipitation of the minerals on the walls of the pores due to attractive forces between the particles and pore surfaces.
- Blockage of the pore-throats by individual particles.
- Several particles bridging across a pore-throat.
- In addition to mineral reactions and fines migration, salt precipitation due to evaporation of water and rock dry-out [93], which could occur near the wellbore region or during lab-scale flooding experiments, could cause permeability reduction and formation damage around the wellbore or serious error during interpretation of the lab experiments.

2.3.6 Change in In-Situ Stress Field

It has long been understood that physical properties of porous sedimentary layers change with change in the burial depth and subsequent change in the subsurface 3D stress field. The rock properties of porosity and permeability decrease with

burial depth and the resulting increase in the overburden pressure. With regards to relative permeabilities, however, since the early 1950s there has been an ongoing debate over the effect of the net overburden pressure. Fatt [94] and Thomas and Ward [95], after performing a number of experiments, concluded that although absolute permeability is reduced significantly with increase in the overburden pressure, effective permeabilities of each immiscible phase are also reduced by the same amounts, meaning that relative permeabilities do not change substantially with change in overburden pressure. A few other old and recently published work [96–98], however, has resulted in a different conclusion that, due to the fact that pore and pore-throat geometry changes, multiphase flow behaviour (e.g. relative permeabilities, end point saturations, etc.) of a porous medium can be altered significantly with a change in the overburden or more accurately the net effective pressure.

Generally, a change in the net effective pressure in underground reservoirs occurs when pore pressure changes due to withdrawal or injection of fluids from or into a reservoir. During subsurface disposal of CO_2, since there is no underground withdrawal, the reservoir pore pressure keeps increasing as the CO_2 injection continues, resulting in a reduction of the net effective pressure. Therefore, as time goes by, multiphase flow characteristics of the fluids-rock system change as well as the rock physical properties. Furthermore, with change in the system's multiphase flow behaviour, CO_2 entrapment due to the capillary trapping mechanism can be affected considerably. In other words, the ongoing change in the subsurface stress field not only alters the original multiphase flow behaviour (i.e. plume evolution, CO_2 injectivity, etc.) predictions which are generally done with the assumption of constant effective stress, but it also affects the storage capacity of the underground structure in the long term.

2.3.7 Change in Thermophysical Properties of Fluids

The effects of change in the reservoir pore pressure are not limited to the rock and the rock-fluid interactions, but also it influences the phase behaviour and thermophysical properties of the fluids inside the pore space. The isothermal depletion process is a well-known process occurring during production of hydrocarbon from subsurface geological structures. That is one reason behind running extensive lab experiments to produce PVT tables which are used in simulation software to predict the phase behaviour of the reservoir fluids as they undergo such isothermal pressure reduction processes. During subsurface CO_2 disposal a similar process occurs but instead of reduction, pore pressure increases. This isothermal increase in pressure changes the phase behaviour of fluids involved over time and subsequently, as it will be discussed shortly, it alters all four CO_2 trapping mechanisms.

Interfacial tension of the CO_2-brine system decreases with increase in the pore pressure of the CO_2 storage medium [58, 62, 64]. This change in the IFT values would alter the capillary trapping mechanism which relies on the capillary

pressure character of the rock-fluids system, which in turn is an IFT dependant property. In addition, increase in the reservoir pressure increases the solubility of the CO_2 in the formation brine of the host porous medium [27, 36] and therefore enhances the solubility trapping mechanism. Subsequently, the mineral trapping mechanism is altered by further dissolution of CO_2 in the formation brine. Furthermore, increase in the pore pressure, by increasing the differential pressure across the caprock and decreasing the IFT, can alter the containment characteristics of the caprock, which overlays the storage medium. Thus, leakage of the structurally trapped CO_2 into layers above the reservoir may occur, which could cause contamination of the potable water reservoirs or potentially CO_2 could reach the surface and be released to the atmosphere again.

2.4 Previous Experimental Work

Since Van Der Meer [99] published one of the first papers on the computer based simulation of CO_2 aquifer disposal, there have been numerous simulation studies carried out in order to understand the multiphase flow behaviour occurring during CO_2 geo-sequestration from a dynamic simulation modelling perspective. But by contrast, there has been a limited number of experimental studies carried out on this topic, of which a review is presented in this final section of this chapter. It is worth noting that there have been a large number of experimental studies carried out investigating the multiphase flow behaviour during CO_2 flooding as a means of enhanced hydrocarbon recovery and the results of some of these studies, to some degree, could be applicable to underground CO_2 storage.

One of the first core-flooding studies, which produced results of direct application to CO_2 geo-sequestration, was carried out by Ross et al. [100]. They investigated the effect of mineral dissolution, which is expected to occur during CO_2 injection, on the permeability of a number of North Sea calcareous sandstone samples. They carried out their experiments by injecting carbonated brine into sandstone samples. The results of their work showed that mineral dissolution could occur during the flooding process causing increase in the permeability of the samples. However, as shown in Fig. 2.11, in the majority of the experiments conducted, the rate of increase in permeability would gradually decline close to the end of each experiment with eventually a constant permeability value being attained.

Similar experimental work carried out by a few other researchers confirm the findings of Ross et al. [100]. Omole and Osoba [101] investigated the effect of the amount of CO_2 injection, the injection pressure and the differential pressure across the core on the permeability of the samples. After conducting 3 sets of experiments displacing NaCl solution by CO_2 at 27°C, they observed a maximum 64% increase in permeability after 3.28 pore volumes of CO_2 injection, and an increase in permeability from 5 to 22% by increasing the injection pressure from 1,050 to 2,500 psi. But they found that increasing the differential pressure across the

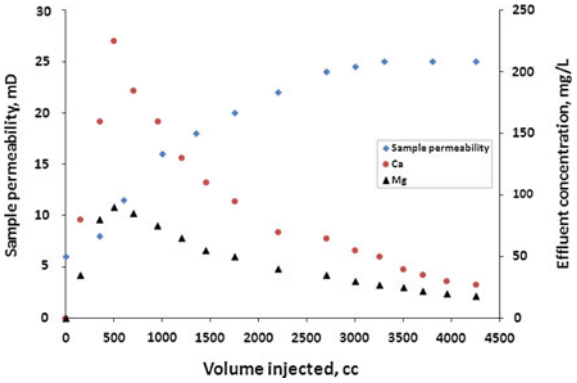

Fig. 2.11 Permeability and effluent Ca and Mg concentration profiles during a core-flooding test on a Rotliegende sandstone sample (carbonated brine injection at 2,000 psi and 80°C) (after [100])

sample would have adverse effect on the samples by decreasing their permeability In other words, the general trend showed that the greater the differential pressure, the greater the permeability reduction. Contrary to the results of the previous studies, the experimental work carried out by Sayegh et al. [102] at 45°C and 2,000 psi showed an overall reduction in the permeability of the samples tested. During their experiments they first observed a rapid decrease in permeability of the samples. However, extending the durations of the experiments resulted in a gradual increase in permeability, although the original permeability values were never regained. Sayegh et al. attributed the steep permeability reduction, observed at the beginning of each experiment, to migration of fines and blockage of the pore throats and the subsequent gradual increase of the permeability to the dissolution of carbonate minerals during the extended injection. In the flooding experiments conducted by Bowker and Shuler [103] no substantial change in permeability was observed. This was despite the fact that the rock samples they used contained about 10% by volume carbonate cement and effluent fluid analysis confirmed the dissolution of minerals inside the samples. Since the samples also contained about 5% by volume clay minerals, Bowker and Shuler [103] concluded that any increase in permeability due to the dissolution of carbonate minerals should have been offset by migration of clay fines to the pore throats.

Shiraki and Dunn [104] conducted an experimental study on the brine-rock interactions during CO_2 flooding. They conducted the experiments at 2,407 psi and 80°C using a number of sandstone samples taken from the Tensleep Formation in Wyoming, USA, which were cemented by dolomite and anhydrite. They reported three major reactions taking place during the flooding experiments, including dissolution of dolomite, alteration of K-feldspar to form kaolinite and precipitation or dissolution of anhydrite. The results published by Shiraki and Dunn [104] (Table 2.6) show that for the samples they used the core porosities increased when both dolomite and anhydrite dissolved into the solution, while no significant changes in porosities were observed when anhydrite precipitation took place along with the dissolution of dolomite. Except for one core-plug (Run 2, middle core), the permeability of the samples decreased even when the porosity enhancement

Table 2.6 Comparison of the physical properties of Tensleep sandstone samples before and after the CO_2 flooding experiments (after [104])

Run	Core	Pore volume (cc)			Porosity (%)			Air permeability (md)		
		Before (b)	After (a)	a − b	Before (b)	After (a)	a/b	Before (b)	After (a)	a/b
1	Upstream middle	12.6	12.6	0.0	14.8	14.6	0.99	76.0	64.2	0.84
	downstream total	12.0	12.1	0.1	14.2	14.3	1.01	64.6	53.7	0.83
	in pore volume	12.5	12.5	0.0	14.6	14.9	1.02	61.8	48.6	0.79
		37.1	37.2	0.1						
2	Upstream middle	7.8	8.5	0.7	9.2	10.0	1.09	6.62	4.54	0.69
	downstream total	12.1	12.3	0.2	14.4	14.7	1.02	99.7	126.9	1.27
	in pore volume	8.5	8.5	0.0	11.9	11.9	1.00	27.2	15.1	0.56
		28.4	29.3	0.9						

took place. After SEM examination of the core samples they concluded that the permeability reductions were due to the growth of kaolinite crystals in the samples' pore spaces putting restriction on the fluid flow.

In the research conducted by Wellman et al. [105] CO_2-brine-rock interactions were evaluated using laboratory flooding tests conducted on a dolomite-anhydrite San Andres core taken from Seminole field in west Texas and another sample taken from a quarried limestone. During their extended flooding tests they observed continuous enhancements of porosity and permeability which were due to excessive dissolution. This type of dissolution was also observed in the experimental work carried out by Grigg and Svec [106] and Izgec et al. [88]. However, after extensive experimental work on carbonate core samples, Izgec et al. [88] concluded that both reduction and increase in the sample permeabilities could be obtained and the trend of change in rock properties was case dependant. They pointed out that this behaviour was due to the fact that the change in the rock properties, when subjected to CO_2 flooding, depended on various factors of pore distribution, brine composition and thermodynamic conditions. For example it was observed that reducing the salt concentration would make the porosity and permeability reductions less pronounced. They also indicated that, during the laboratory flooding experiments, the extent of the calcite precipitation depended on the flow direction with vertical flooding resulting in less calcite precipitation compared to the horizontal flooding.

The focus of the literature reviewed so far has been mainly on the reactions between the rock and the fluids and how these reactions alter the rock properties. During the past few years there have been also a limited number of experimental studies carried out assessing the multiphase flow characteristics associated with the subsurface storage of CO_2 mainly in the supercritical state. A large portion of the published work on the CO_2-brine multiphase flow behaviour in the porous medium, applicable specifically to CO_2 geo-sequestration, has been carried out by Bennion and Bachu [58–61, 69, 107–109]. In their first paper [69] in the series, they investigated the drainage relative permeability characteristics of the

Table 2.7 Sample data, endpoint relative permeabilities, endpoint saturations and brine-to-CO_2 viscosity ratios (after [69])

Formation	Lithology	Porosity, fraction	In situ K, mD	K_{rCO2}	$S_{CO2,MAX}$, %	S_{wr}	Brine/CO_2 visc ratio
Cambrian	Sandstone	0.117	0.0808	0.5446	70.6	29.4	11.82
Cooking Lake	Carbonate	0.099	65.3	0.0685	52.4	47.6	15.43
Nisku	Carbonate	0.097	45.92	0.1768	67	33	11.8
Wabamun, low perm	Carbonate	0.079	0.0182	0.5289	40.5	59.5	15.41
Ellerslie	Sandstone	0.126	0.376	0.1156	34.1	65.9	14.52
Viking	Sandstone	0.125	2.7	0.3319	44.2	55.8	13.98
Wabamun, high perm	Carbonate	0.148	66.98	0.1883	43.1	56.9	15.41
Wabamun, high perm and low T	Carbonate	0.148	61.16	0.086	31.8	68.2	75
Wabamun, high perm and fresh water	Carbonate	0.148	60.64	0.1993	44.8	55.2	11.32

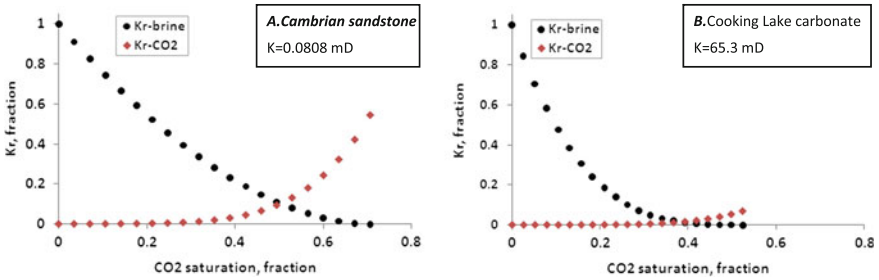

Fig. 2.12 The endpoint relative permeabilities and the maximum endpoint saturations of CO_2 are higher in a low permeability sample (**A**), compared to a high permeability sample (**B**), (after [69])

CO_2-brine-rock system using a series of core samples representing a variety of potential sequestration zones in the western Canada sedimentary basin. These rock samples included both sandstone and carbonate core-plugs taken from various formations (Table 2.7). They conducted their core-flooding experiments under reservoir in situ conditions with temperatures ranging from 40 to 75°C and pressures from 1,249 to 3,916 psi. Except for one experiment where fresh water was used, the brine used was of various salinities from 28,286 to 248,000 ppm. The sample properties along with some experimental results, including end-point relative permeability to CO_2 and the end-point saturations, are presented in Table 2.7.

During their experimental work, Bennion and Bachu [69] observed that there was a very good correlation between the CO_2 permeability (and hence relative permeability) and the samples' in situ absolute permeabilities. Their results also showed higher end-point relative permeability and in general higher maximum endpoint CO_2 saturation for the case of lower permeability but more homogeneous samples (Fig. 2.12). This was believed to be the result of the more effective sweep by CO_2 of the more homogenous lower permeability samples used compared to the

higher permeability samples with more heterogeneous pore network systems. Furthermore, Bennion and Bachu [69] concluded that the CO_2 end-point relative permeability and maximum end-point saturation levels were greatly influenced by the brine-to-CO_2 viscosity ratio and phase condition of the injected CO_2 (dense supercritical state versus gas phase), with the dense supercritical state showing a more effective displacement and sequestration character.

In a subsequent publication Bennion and Bachu [59] presented their experimental results on the effect of interfacial tension (IFT) and pore-size distribution on the relative permeability of CO_2 under in situ reservoir conditions. The samples used, except one new shale sample from the Calmar Formation, were similar to those used in their previous work [69]. They combined their new air-mercury capillary pressure (characteristic of the samples pore-size distribution) and drop-pendant IFT data with their previously published in situ relative permeability data for the CO_2-brine system to investigate the effect of the IFT and pore network on the relative permeability character of the samples used. During their experiments Bennion and Bachu [59] noticed that the end-point relative permeabilities to CO_2 appeared to be dependent on the IFT with end-point relative permeability values decreased as the IFT values increased. It is worth noting that the CO_2-brine IFT was increased by decreasing the pressure. They also found that the maximum end-point CO_2 saturation increased as IFT was decreased, although this dependence was not as strong as the dependence of endpoint relative permeability on IFT. No trend was found in the maximum end-point CO_2 saturation with the pore-size distribution. However, their results showed that the samples with higher fractions of micro-porosity resulted in higher CO_2 end-point relative permeability. This dependence was attributed to the more uniform displacement character of such samples. Overall, based on the results of the experimental work conducted, it is expected that deeper, higher pressure formations that have a more uniform porosity distribution are more likely to have more storage capacity. This conclusion was based on the maximum CO_2 saturation and relative permeability levels achievable under such conditions.

Further relative permeability data for the CO_2-brine system covering consecutive drainage and imbibition processes were published in later publications by Bennion and Bachu [60, 108]. Within the same publications the authors also presented the same data for the H_2S-brine system. Similar to their previous works on this topic, they carried out the experiments on both carbonate and sandstone samples. The main focus of this paper was on comparing the displacement performance of the CO_2-brine system with the H_2S-brine system. For both the CO_2-brine and H_2S-brine systems, this was the first relative permeability data published for consecutive drainage-imbibition processes in an attempt to cover the data gap existing at the time.

In the same year but in a separate paper, Bennion and Bachu [58], using their previously published data, presented further analysis on the dependence of the CO_2-brine displacement characteristics (e.g. IFT, end-point relative permeabilities and end-point saturations) on a number of reservoir in situ variables (e.g. pressure, temperature and salinity). As it was partly reported before, IFT was found to be

Table 2.8 Lithology, depth and reservoir P–T conditions for the carbonate samples tested (after [109])

Unit and Sample	Lithology	Depth, ft	Pressure, psi	Temperature, °C
Wabamun #3	Limestone	2,168.2	1,726	41
Nisku #3	Dolomite	3,869.7	2,524	56
Grosmont	Dolomite	1,647.1	1,726	41
Morinville Leduc	Dolomite	3,888.1	1,653	40
Redwater Leduc	Limestone	3,140.6	1,334	36
Cooking Lake #3	Dolomite	3,894.1	2,248	55
Slave Point	Dolomite	4,507.5	2,727	43
Winnipegosis	Dolomite	3,739.1	1,266	36

dependent on the pressure, temperature and brine salinity with IFT decreasing with increase in pressure while increasing temperature and brine salinity had an opposite effect. In addition to the analysis presented previously on the CO_2-brine displacement characteristics during the drainage process, the authors this time presented a review of the data which had become available for the subsequent imbibition process. They reported that the value of the trapped gas saturation at the end of the secondary imbibition decreased as IFT decreased. During the imbibition process following an earlier drainage process, the classical hysteresis behaviour was apparent but despite the expectations, in the data reported by Bennion and Bachu [58], the wetting brine phase showed a more pronounced hysteresis effect compared to the non-wetting CO_2 phase. The authors also reported less multiphase interference effects with decrease in the IFT values. This conclusion was based on the reduction in the curvature of the relative permeability curves towards becoming more linear with reducing IFT values. As pointed out by the authors, the effect of variation in IFT on the displacement characteristics shows similar trends to the effect of variation in the brine-to-CO_2 viscosity ratio. As mentioned by Bennion and Bachu [58], because the variations of IFT and brine-to-CO_2 viscosity ratio with change in pressure almost followed the same trend it made it even more difficult to quantify the extent to which each of these two parameters is responsible for the observed changes in the displacement characteristics. Based on the further analysis carried out by the authors, it was concluded that the observed trends in the displacement characteristics of the CO_2-brine system could be more strongly attributed to changes in the IFT rather than the changes in the viscosity ratio. Based on the experimental results gathered to date, Bennion and Bachu [58] concluded that the displacement performance during the CO_2-brine flooding processes is more influenced by the in situ reservoir conditions in lower permeability porous media, which generally have high fractions of micro-porosity, compared to higher permeability media where their larger pore sizes are easier to be accessed at even high IFT conditions.

In their most recent published paper, Bennion and Bachu [109] have presented the results of several drainage and imbibition core-flooding experiments conducted on a series of samples taken from a number of carbonate formations in the Alberta

Table 2.9 Average displacement characteristics of the drainage cycles for low, medium and high permeability groups of the carbonate samples tested (after [109])

Rock Group	In situ brine k, mD	Endpoint k_{rCO2}	S_{wr}, %	Corey exponent for brine	Corey exponent for CO_2
Low k	2.05	0.4346	48.7	1.8	4.18
Mid k	54.65	0.1238	51.9	2.22	3.69
High k	293.13	0.0774	57.2	1.71	4.55

Basin in Canada (Table 2.8). As was mentioned before, there has been similar data published on the carbonate samples by the authors in a number of previous publications. However, the new data sets are the result of the experiments conducted on carbonate rocks (calcite and dolomite) of higher absolute permeability values. As pointed out by the authors, the significance of the generated data for these higher permeability samples is in the fact that such samples are more likely to represent formations which will be chosen as candidates for subsurface CO_2 disposal.

At the conclusion of their experimental work, the authors found that the Corey exponents for the drainage relative permeability curves were much higher for the CO_2 phase compared to those for the brine, but there was no trend with the rock absolute permeabilities was evident among the data. However, there was an apparent trend among the same data for the secondary imbibition cycles with the lower permeability samples having higher Corey exponent values for both the brine and CO_2 phases. It was also noticed that the Corey exponents for a phase (either brine or CO_2) were greater when its saturation was being decreased than when it was being increased. It needs to be mentioned that Corey exponents are the two variables (N_w and N_o) used in the Corey relative permeability correlation as shown in Eqs. 2.12 and 2.13 for an oil–water system. As can be seen in Table 2.9 similar to their previous experimental works, Bennion and Bachu [109] reported that displacing the low permeability brine saturated samples with CO_2 resulted in lower irreducible water saturations compared to high permeability samples. This trend, which is somewhat contrary to the expectations, has been attributed by the authors to the more heterogeneous nature of the pore systems in the high permeability samples, which promotes channelling through the more permeable portions of the pore system and subsequent bypassing of the tighter portions. As expected from the trend observed in the endpoint irreducible brine saturations, the average CO_2 endpoint relative permeability in lower permeability samples was found to be higher compared to that of high permeability samples (Table 2.9).

$$k_{rw} = k_{rw}^{o}\left(\frac{S_w - S_{wr}}{1 - S_{wr} - S_{or}}\right)^{N_w} \tag{2.12}$$

$$k_{ro} = k_{ro}^{o}\left(\frac{1 - S_w - S_{or}}{1 - S_{wr} - S_{or}}\right)^{N_o} \tag{2.13}$$

Table 2.10 Average displacement characteristics of the secondary imbibition cycles for low, medium and high permeability groups of the carbonate samples tested (after [109])

Rock Group	Endpoint $k_{r-brine}$	$S_{CO2,r}$, %	Corey exponent for brine	Corey exponent for CO_2
Low k	0.1074	33.5	3.67	2.92
Mid k	0.6162	15.7	3.12	2.89
High k	0.3621	23.2	1.98	2.41

Table 2.11 Ultralow permeability samples used during the flooding experiments (after [107])

Formation unit	Lithology	k to brine
Colorado Group	Shale	0.0000788
Calmar Formation	Shale	0.00000294
Muskeg Formation	Anhydrite	0.000354

Where: k_{rw} = relative permeability of the water phase, fraction
k_{ro} = relative permeability of the oil phase, fraction
S_w = water saturation, fraction
S_{wr} = residual water saturation, fraction
S_{or} = residual oil saturation, fraction
k^o_{rw} = water end point relative permeability, fraction
k^o_{ro} = oil end point relative permeability, fraction
N_w and N_o = Corey exponents, dimensionless

Unlike the displacement characteristics during the drainage cycles, whose data followed the above-described distinctive trends, as can be seen in Table 2.10, there were no such trends evident among the data for the secondary imbibition cycles.

As can be seen in Tables 2.9 and 2.10, during the imbibition cycles, the brine phase consistently exhibited lower Corey exponent values than the CO_2 phase, while, during the imbibition cycles, the exponent values were comparable for the two phases. As also concluded by Bennion and Bachu [109], this confirmed the more effective displacement process, due to favourable mobility/viscosity ratios, during the imbibition cycles (i.e. brine displacing the more mobile, less viscous CO_2) compared to the drainage cycles dominated by unfavourable mobility/viscosity ratios.

Bennion and Bachu [107] also conducted a number of flooding experiments on three well-compacted, low permeability shale and anhydrite samples (Table 2.11), which often constitute the confining cap-rock for potential CO_2 storage sites.

The displacement experiments were carried out in a sequence of a drainage process followed by an imbibition process. The main results of the experiments are presented in Table 2.12. As pointed out by the authors, the experimental data showed the CO_2 effective permeability values during the primary drainage to be in the range of 1–100 picoDarcy. Such low permeability values guarantee the

Table 2.12 Relative permeability and saturation data for the experiments carried out on the ultralow permeability samples (after [107])

Core sample	k to brine, mD	k_{rCO2} at S_{wr}	$S_{CO2,max}$, %	k_{rw} at $S_{CO2,r}$	$S_{CO2,r}$, %
Colorado shale	0.0000788	0.0148	39.5	0.024	34.9
Calmar shale	0.00000294	0.1875	36.2	0.2823	25.6
Muskeg anhydrite	0.000354	0.0000828	18.5	–	18.0

effectiveness of the tested rock samples and similar formations as the cap-rock for a CO_2 geo-sequestration site. In other words, unless the cap-rock layer is very thin or extremely high differential pressure is applied across it, the volume of the lost CO_2 through the seal to the layers above it over non-geological time scale would be negligible if not zero. The tested samples also showed more endpoint residual brine saturation and more pronounced hysteresis behaviour between the drainage and imbibition processes, compared to the previously tested samples of higher permeability ranges. As concluded also by Bennion and Bachu [107], such characteristics are favourable when it comes to the effectiveness of the cap-rock to contain the injected CO_2.

In addition to the research conducted by Bennion and Bachu [58–60, 69, 107–110] on the multiphase flow behaviour of the CO_2-brine system in the porous media, there are a few other researchers who have also carried out experimental work on this subject. The effect of pore scale and sub-core heterogeneity on the CO_2 distribution in core-samples subjected to flooding experiments has been evaluated by a number of researchers [111–115]. After conducting a number of core-flooding experiments on sandstone core samples and evaluating the fluid distribution in the samples using X-ray CT imaging, Benson et al. [111] concluded that maximum end-point CO_2 saturation at the end of the drainage experiments varied from 25 to 40% and small scale heterogeneities limited the displacement efficiency at the core-scale. Furthermore, Okabe et al. [112] investigated the effect of the sub-core heterogeneities on capillary residual trapping of the injected CO_2 into a carbonate sample taken from a hydrocarbon reservoir in the Middle East. They also used the X-ray CT technique to quantify the fluid distribution along the length of the sample during both drainage and imbibition and compared it with the porosity distribution in the sample tested. At the conclusion of their experimental work, Okabe et al. [112] reported that the X-ray CT images clearly showed that there was a relation between the rock porosity heterogeneity and the residual CO_2 saturation along the length of the sample. The results showed that much of the CO_2 was displaced by the injected brine from the high porosity regions in the sample while the CO_2 residual saturation remained high within the low porosity regions. This behaviour was despite the fact that CO_2 saturation during the primary drainage process reached higher values in higher porosity regions.

The results of the experiments conducted by Perrin et al. [114] and Perrin and Benson [113] also confirmed the behaviour reported by Okabe et al. [112]. In the papers published by Perrin et al. [114] and Perrin and Benson [113], they reported the results of two steady state drainage experiments conducted on two sandstone

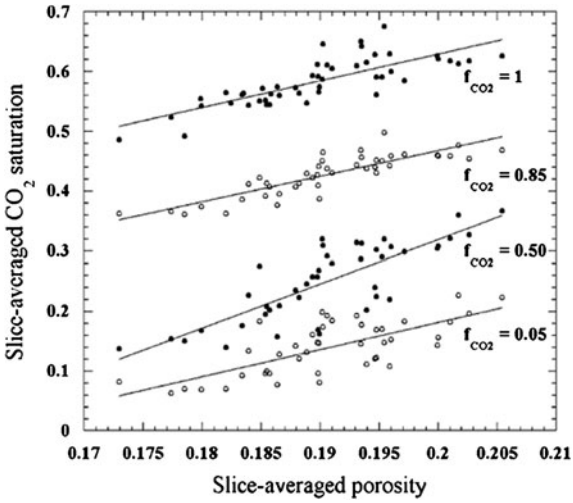

Fig. 2.13 Correlation between the CO_2 saturation and porosity for different fractional flows of CO_2 during a steady state flooding experiment (after [113])

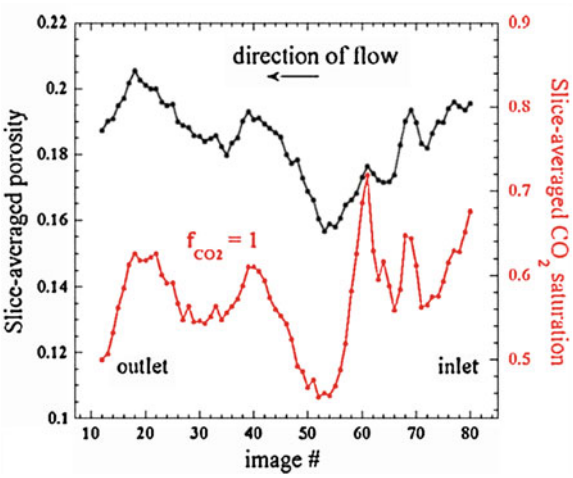

Fig. 2.14 The CO_2 saturation and porosity distribution profiles along the sample at the end of a steady state flooding experiment ($f_{CO2} = 1$) (after [113])

samples. Their experiments demonstrated that the CO_2 saturation distribution correlated well with the spatial porosity distribution within the samples at all stages of the experiments (Fig. 2.13). In other words, the higher porosity regions within the samples correlated with the high saturations and similarly, lower porosity regions with the lower saturations (Fig. 2.14).

The experimental results reported by Shi et al. [115] again showed that similar trends and correlations existed between the CO_2 saturation distribution and spatial porosity distribution within the Tako sandstone sample tested. It is worth noting that the complimentary computer-based core-flooding simulation results reported in the same publication showed that the effect of the porosity heterogeneity on the fluid distribution within the sample diminished as the injection flow-rate was increased. This effect was attributed by the authors to the diminishing effect of the

Table 2.13 Recovery factor (RF) at CO_2 breakthrough (BT) and dispersion coefficient for CO_2 displacing methane (after [116])

Run No.	Temp., °C	Press., psia	Methane RF at CO_2 BT, fraction	Disspers. coeff., cm^2/min
9	20	1,041.7	0.851	0.1
10	20	2,014.7	0.73	0.025
14	20	1,014.7	0.77	0.1
15	20	1,015.7	0.731	0.1
16	20	2,014.7	0.77	0.028
17	20	2,014.7	0.729	0.032
18	20	3,014.7	0.799	0.01
19	20	3,014.7	0.804	0.011
28	20	514.7	0.824	0.15
20	40	2,714.7	0.845	0.021
22	40	2,214.7	0.829	0.03
24	40	1,714.7	0.862	0.07
26	40	1,214.7	0.845	0.12
21	60	2,714.7	0.858	0.04
23	60	2,214.7	0.872	0.06
25	60	1,714.7	0.868	0.12
27	60	1,214.7	0.868	0.2
29	80	2,714.7	0.82	0.07
30	80	2,214.7	0.827	0.11
31	80	1,714.7	0.839	0.17
32	80	1,214.7	0.846	0.3
33	80	1,714.7	0.618	0.15

sub-core capillary heterogeneity on the displacement behaviour as the flow-rate was increased.

In addition to the experimental core-flooding studies carried out to date on the CO_2-brine system, there have been also a number of experimental studies carried out to determine the displacement performance of the CO_2-natural gas and flue gas-natural gas systems with the main focus of evaluating the effectiveness of storage of the pure and impure CO_2 in depleted natural gas reservoirs. Seo [116] investigated the displacement efficiency of storing CO_2 in depleted gas reservoirs. For his experimental work he displaced carbonate samples pre-saturated with methane using pure CO_2. In total he ran 22 experiments covering pressures ranging from 500 to 3,000 psi and temperatures varying between 20 and 80°C (Table 2.13). The experimental work carried out by Seo [116] showed that displacement of methane by CO_2, in all three possible phases of gas, liquid and supercritical, was very efficient resulting in methane recovery factors as high as 87% at CO_2 breakthrough (Table 2.13). The dispersion coefficient of CO_2 into methane was also calculated to be as low as 0.01 cm^2/min.

As can be seen in Figs. 2.15 and 2.16 and also reported by Seo [116], for constant temperature the coefficient of longitudinal dispersion of CO_2 decreases

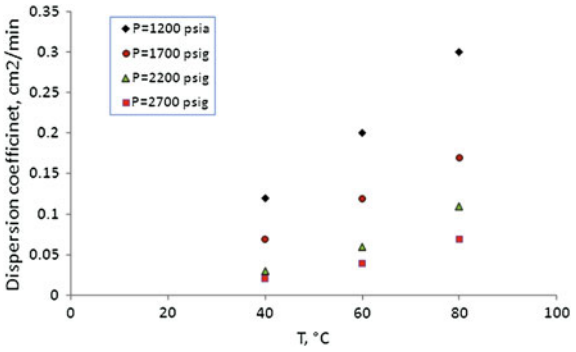

Fig. 2.15 Dispersion coefficient of CO_2 into methane versus temperature at various pressures (after [116])

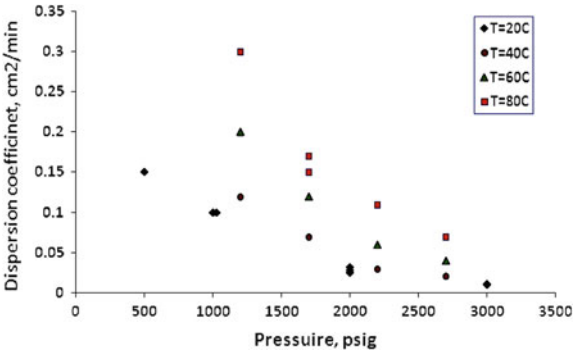

Fig. 2.16 Dispersion coefficient of CO_2 into methane versus pressure at various temperatures (after [116])

Table 2.14 Concentration (mole fraction) of various impurities in the two gas samples used to displace methane compared to a typical flue gas from power plant (after [117])

Component	Flue gas	Gas A, %	Gas B, %
H_2O	0.12	–	–
CO_2	0.11945	0.13574	0.99433
O_2	0.5258	0.5975	–
SO_2	0.00045	0.00051	0.00368
NO_2	0.00016	0.00018	0.00129
CO	0.0001	0.00012	0.0007

with increasing pressure while it increases at constant pressure when temperature is increased.

Furthermore Nogueira and Mamora [117], using similar carbonate samples, repeated the experiments conducted by Seo [116], but this time they used two different types of flue gases, namely Gas A and Gas B (Table 2.14), instead of the pure CO_2 as the displacing fluid in the flooding experiments.

As can be seen in Table 2.15 and also pointed out by the authors, lowering the concentration of CO_2 had a negative impact on the displacement efficiency with Gas A (13.574% CO_2) exhibited larger dispersion coefficients into the displaced methane compared to Gas B (99.433% CO_2), which showed dispersion coefficients close to those for pure CO_2 reported earlier. Furthermore, recovery factors of

Table 2.15 Recovery factor (RF) at CO_2 breakthrough (BT) and dispersion coefficient for flue gases displacing methane at 1,500 psig and 70°C (after [117])

Inj Gas	S_{wi}, %	Methane RF at CO_2 BT, fraction	Disspers. coeff., cm^2/min
Gas A	0.00	0.8066	0.18
	0.00	0.7946	0.19
	20	0.7436	0.25
Gas B	0.00	0.899	0.15
	0	0.8816	0.13

methane at CO_2 breakthrough are higher for Gas B (88–90%) and pure CO_2 compared to those for Gas A (79–81%).

In addition to the results reported by Nogueira and Mamora [117], elsewhere Nogueira [118] presented her findings on the effect of the core-flooding experiments conducted on the unconfined compressive strength of carbonate samples tested. She reported a reduction of approximately 30% in the unconfined compressive strength of the samples after undergoing an extended flooding process designed to be equivalent to 30 days of continuous CO_2 injection in the field.

References

1. Tiab D, Donaldson EC (2004) Petrophysics. Gulf Professional Publishing, Burlington
2. Muskat M, Meres MW (1936) The flow of gas-liquid mixtures through unconsolidated sands. Physics 7:346
3. Muskat M, Wyckoff RD, Botset HG, Meres MW (1937) Flow of gas-liquid mixtures through sands. Pet Trans AIME 123:69–96 SPE 937069
4. Avraam DG, Payatakes AC (1995) Flow regimes and relative permeabilities during steady-state two-phase flow in porous media. J Fluid Mech 293:207–236
5. Bennion B, Thomas FB, Bietz RF (1996) The effect of trapped critical fluid saturations on reservoir permeability and conformance. Hycal Energy Research Laboratories Ltd, Calgary
6. Bennion DB, Sarioglu G, Chan MYS, Hirata T, Courtnage D, Wansleeben J (1993) Steady-state bitumen-water relative permeability measurements at elevated temperatures in unconsolidated porous media, SPE 25803. In: SPE International thermal operations symposium, Bakersfield, California, Society of Petroleum Engineers
7. Crotti MA, Rosbaco JA (1998) Relative permeability curves: the influence of flow direction and heterogeneities. In: Dependence of end point saturations on displacement mechanisms, SPE 39657, SPE/DOE improved oil recovery symposium, Tulsa, Oklahoma, Society of Petroleum Engineers
8. Prats M, Lake LW (2008) The anisotropy of relative permeability: technical note. J Petrol Technol 60:99
9. García JE (2003) Fluid dynamics of carbon dioxide disposal into saline aquifers. PhD theses, University of California, Berkeley
10. Span R, Wagner W (1996) A new equation of state for carbon dioxide covering the fluid region from triple-point temperature to 1100 K at pressures up to 800 MPa. J Phys Chem Ref Data 25:1509–1597
11. Vargaftik NB, Vinogradov YK, Yargin VS (1996) Handbook of physical properties of liquids and gases: pure substances and mixtures. Begell House Publishers, New York

12. NIST (2010) Thermophysical properties of fluid systems. US National Institute of Standards and Technology http://webbook.nist.gov/chemistry/fluid/. Accessed 17 June 2010
13. Fenghour A, Wakeham WA, Vesovic WA (1998) The viscosity of carbon dioxide. J Phys Chem Ref Data 27:31–44
14. Rah K, Eu BC (2001) Density and temperature dependence of the bulk viscosity of molecular liquids: carbon dioxide and nitrogen. J Chem Phys 114:10436–10447
15. IFC (1967) A formaulation of the thermophysic properties of ordinary water substance. International formulation committee secretariat, Düsseldorf, Germany
16. Wagner W, Pruss A (2002) The IAPWS formulation 1995 for the thermodynamic properties of ordinary water substance for general and scientific use. J Phys Chem Ref Data 31:387–535
17. Saul A, Wagner W (1989) A fundamental equation for water covering the range from the melting line to 1273 K at pressures up to 25000 MPa. J Phys Chem Ref Data 18:1537–1564
18. Fernandez DP, Goodwin ARH, Lemmon EW, Levelt Sengers JM, Williams RC (1997) A formulation for the static permittivity of water and steam at temperatures from 238 K to 873 K at pressures up to 1200 MPa, including derivatives and Debye-Huckel coefficients. J Phys B: Atomic Mol Opt Phys 26:1125–1165
19. IAPWS (2008) Release on the IAPWS formulation 2008 for the viscosity of ordinary water substance. The international association for the properties of water and steam, Berlin, Germany
20. Kestin J, Sengers JV, Kamgar-Parsi B, Levelt Sengers JMH (1984) Thermophysical properties of fluid H_2O. J Phys Chem Ref Data 13:175–183
21. Wagner W, Saul A, Pruss A (1994) International equations for the pressure along the melting and along the sublimation curve of ordinary water substance. J Phys Chem Ref Data 23:515–527
22. Gibbs JW (1961) The scientific papers of J.W. Gibbs. Dover, New York, pp 1–55 Vol 1
23. Moore WJ (1972) Physical chemistry. Longman, London
24. Fan S-S, Guo T-M (1999) Hydrate formation of CO_2-rich binary and quaternary gas mixtures in aqueous sodium chloride solutions. J Chem Eng Data 44:829–832
25. Ng H-J, Robinson DB (1985) Hydrate formation in systems containing methane, ethane, propane, carbon dioxide or hydrogen sulfide in the presence of methanol. Fluid Phase Equilib 21:145–155
26. Wendland M, Hasse H, Maurer G (1999) Experimental pressure-temperature data on three- and four-phase equilibria of fluid, hydrate, and ice phases in the system carbon dioxide-water. J Chem Eng Data 44:901–906
27. Spycher N, Pruess K, Ennis-King J (2003) CO_2–H_2O mixtures in the geological sequestration of CO_2. I. Assessment and calculation of mutual solubilities from 12 to 100 °C and up to 600 bar. Geochim Cosmochim Acta 67:3015–3031
28. Wiebe R, Gaddy VL (1939) The solubility in water of carbon dioxide at 50, 75, and 100° C, at pressures to 700 atmospheres. J Am Chem Soc 61:315–318
29. Wiebe R, Gaddy VL (1940) The solubility of carbon dioxide in water at various temperatures from 12 to 40 and at pressures to 500 atmospheres: critical phenomena. J Am Chem Soc 62:815–817
30. Wiebe R, Gaddy VL (1941) Vapor phase composition of carbon dioxide-water mixtures at various temperatures and at pressures to 700 atmospheres. J Am Chem Soc 63:475–477
31. Carroll JJ, Slupsky JD, Mather AE (1991) The solubility of carbon dioxide in water at low pressure. J Phys Chem Ref Data 20:1201–1209
32. Crovetto R (1991) Evaluation of solubility data of the system CO_2–H_2O from 273 K to the critical point of water. J Phys Chem Ref Data 20:575–589
33. Duan Z, Møller N, Weare JH (1995) Equation of state for the NaCl-H_2O-CO_2 system: prediction of phase equilibria and volumetric properties. Geochim Cosmochim Acta 59: 2869–2882

34. Diamond LW, Akinfiev NN (2003) Solubility of CO_2 in water from 1.5 to 100 °C and from 0.1 to 100 MPa: evaluation of literature data and thermodynamic modelling. Fluid Phase Equilibria 208:265–290
35. Duan Z, Møller N, Weare JH (2003) Equations of state for the NaCl-H_2O-CH_4 system and the NaCl-H_2O-CO_2-CH_4 system: Phase equilibria and volumetric properties above 573 k. Geochim Cosmochim Acta 67:671–680
36. Duan Z, Sun R (2003) An improved model calculating CO_2 solubility in pure water and aqueous NaCl solutions from 273 to 533 K and from 0 to 2000 bar. Chem Geol 193:257–271
37. Hu J, Duan Z, Zhu C, Chou IM (2007) PVTx properties of the CO_2–H_2O and CO_2–H_2O-NaCl systems below 647 K: assessment of experimental data and thermodynamic models. Chem Geol 238:249–267
38. Abdulagatov AI, Kaplun AB, Meshalkin AB, Abdulagatov IM, Stepanov GV (2002) Second caloric virial coefficients for real gases and combined spherical symmetric potential for simple molecular interactions. J Chem Thermodyn 34:2049–2072
39. Harvey AH, Lemmon EW (2004) Correlation for the second virial coefficient of water. J Phys Chem Ref Data 33:369–376
40. Hendl H, Bich E, Vogel E (1997) A new evaluation of (p, ρ, T) measurements on steam with corrections for the effects of physical and chemical adsorption. J Chem Thermodyn 29:765–784
41. Holste JC, Hall KR, Eubank PT, Esper G, Watson MQ, Warowny W, Bailey DM, Young JG, Bellomy MT (1987) Experimental (p, Vm, T) for pure CO_2 between 220 and 450 K. J Chem Thermodyn 19:1233–1250
42. Plyasunov AV, Shock EL (2003) Second cross virial coefficients for interactions involving water critical data compilation. J Chem Eng Data 48:808–821
43. Tsonopouplos C (1974) An empirical correlation of second virial coefficient. AIChE J 20:263–272
44. Chang Y-B, Coats BK, Nolen JS (1998) A compositional model for CO2 floods including CO2 solubility in water. SPE Reservoir Eval Eng 1:155–160 SPE 35164
45. Churakov SV, Gottschalk M (2003) Perturbation theory based equation of state for polar molecular fluids: II. Fluid mixtures. Geochim Cosmochim Acta 67:2415–2425
46. Duan Z, Møller N, Weare JH (1992) An equation of state for the CH_4-CO_2–H_2O system: II. Mixtures from 50 to 1000 °C and 0 to 1000 bar. Geochim Cosmochim Acta 56:2619–2631
47. Ji X, Tan SP, Adidharma H, Radosz M (2005) SAFT1-RPM approximation extended to phase equilibria and densities of CO_2–H_2O and CO_2–H_2O-NaCl systems. Ind Eng Chem Res 44:8419–8427
48. Kerrick DM, Jacobs GK (1981) A modified Redlich-Kwong equation for H_2O, CO_2, and H_2O–CO_2 mixtures at elevated pressures and temperatures. Am J Sci 281:735–767
49. Nitsche JM, Teletzke GF, Scriven LE, Davis HT (1984) Phase behavior of binary mixtures of water, carbon dioxide and decane predicted with a lattice-gas model. Fluid Phase Equilib 17:243–264
50. Spycher NF, Reed MH (1988) Fugacity coefficients of H_2, CO_2, CH_4, H_2O and of H_2O-CO_2-CH_4 mixtures: a virial equation treatment for moderate pressures and temperatures applicable to calculations of hydrothermal boiling. Geochim Cosmochim Acta 52:739–749
51. Bachu S, Adams JJ (2003) Sequestration of CO_2 in geological media in response to climate change: capacity of deep saline aquifers to sequester CO_2 in solution. Energy Convers Manag 44:3151–3175
52. García JE (2001) Density of aqueous solutions of CO_2. Lawrence Berkeley National Laboratory, University of California, California
53. Song Y, Nishio M, Chen B, Someya S, Ohsumi T (2003) Measurement on CO_2 solution density by optical technology. J Visual 6:41–51
54. Teng H, Yamasaki A, Chun MK, Lee H (1997) Solubility of liquid CO_2 in water at temperatures from 278 to 293 K and pressures from 6.44 to 29.49 MPa and densities of the corresponding aqueous solutions. J Chem Thermodyn 29:1301–1310

55. Duan Z, Sun R, Zhu C, Chou IM (2006) An improved model for the calculation of CO_2 solubility in aqueous solutions containing Na^+, K^+, Ca^{2+}, Mg^{2+}, Cl^-, and SO_4^{2-}. Mar Chem 98:131–139
56. Bando S, Takemura F, Nishio M, Hihara E, Akai M (2004) Viscosity of aqueous NaCl solutions with dissolved CO_2 at (30–60) °C and (10–20) MPa. J Chem Eng Data 49:1328–1332
57. Zhenhao Duan Research Group (2010) Interactive online models. Institute of geology and geophysics, Chinese Academy of Sciences http://www.geochem-model.org/models.htm. Accessed 25 June 2010
58. Bennion B, Bachu S (2006) Dependence on temperature, pressure, and salinity of the IFT and relative permeability displacement characteristics of CO_2 injected in deep saline aquifers, SPE 102138. In: SPE Annual technical conference and exhibition, San Antonio, Texas, USA, Society of Petroleum Engineers
59. Bennion B, Bachu S (2006) The impact of interfacial tension and pore size distribution/capillary pressure character on CO_2 relative permeability at reservoir conditions in CO_2-brine systems, SPE 99325. In: SPE/DOE symposium on improved oil recovery, Tulsa, Oklahoma, USA, Society of Petroleum Engineers
60. Bennion B, Bachu S (2006) Supercritical CO_2 and H_2S-brine drainage and imbibition relative permeability relationships for intergranular sandstone and carbonate formations, SPE 99326. In: SPE Europec/EAGE annual conference and exhibition, Vienna, Austria, Society of Petroleum Engineers
61. Bennion B, Bachu S (2008) A correlation of the interfacial tension between supercritical phase CO_2 and equilibrium brines as a function of salinity, temperature and pressure, SPE 114479. In: SPE Annual technical conference and exhibition, Denver, Colorado, USA, Society of Petroleum Engineers
62. Chalbaud C, Robin M, Egermann P (2006) Interfacial tension data and correlations of brine-CO_2 systems under reservoir conditions, SPE 102918. In: SPE Annual technical conference and exhibition, San Antonio, Texas, USA, Society of Petroleum Engineers
63. Chun B-S, Wilkinson GT (1995) Interfacial tension in high-pressure carbon dioxide mixtures. Ind Eng Chem Res 34:4371–4377
64. Hebach A, Oberhof A, Dahmen N, Kögel A, Ederer H, Dinjus E (2002) Interfacial tension at elevated pressures measurements and correlations in the water + carbon dioxide system. J Chem Eng Data 47:1540–1546
65. Yan W, Zhao G-Y, Chen G-J, Guo T-M (2001) Interfacial tension of (methane + nitrogen) + water and (carbon dioxide + nitrogen) + water systems. J Chem Eng Data 46:1544–1548
66. Yang D, Gu Y (2004) Interfacial interactions of crude oil-brine-CO_2 systems under reservoir conditions, SPE 90198. In: SPE Annual technical conference and exhibition, Houston, Texas, Society of Petroleum Engineers
67. Harrison K (1996) Interfacial tension measurement of CO_2-polymer and CO_2-water systems and formation of water-in-CO_2 microemulsions. PhD theses, The University of Texas at Austin
68. Baines SJ, Worden RH (2004) Geological storage of carbon dioxide: Special Publications. Geological Society, vol 233. London, pp 1–6
69. Bennion B, Bachu S (2005) Relative permeability characteristics for supercritical CO2 displacing water in a veriety of potential sequestration zones in the Western Canada sedimentary basin, SPE 95547. In: The SPE annual technical conference and exhibition, Dallas, Texas, USA, Society of Petroleum Engineers
70. Ennis-King J, Paterson L, Gale J, Kaya Y (2003) Rate of dissolution due to convective mixing in the underground storage of carbon dioxide, In: 6th international conference, Greenhouse Gas Control Technologies. Kyoto, Japan
71. Juanes R, Spiteri EJ, Orr FM Jr, Blunt MJ (2006) Impact of relative permeability hysteresis on geological CO_2 storage. Water Resour Res 42:13

72. Kumar A, Ozah R, Noh M, Pope GA, Bryant S, Sepehrnoori K, Lake LW (2005) Reservoir simulation of CO_2 storage in deep saline aquifers. SPE J 10:336–348 SPE 89343
73. Hangx SJT (2009) Geological storage of CO_2: mechanical and chemical effects on host and seal formations. PhD theses, Utrecht University, Utrecht, The Netherlands
74. Donaldson EC, Alam W (2008) Wettability. Gulf Publishing Company, Houston
75. Anderson WG (1986) Wettability literature survey-part 1: rock/oil/brine interactions, the effects of core handling on wettability. SPE J Petrol Technol 38:1125–1144 SPE 13932
76. Chalbaud C, Robin M, Bekri S, Egermann P (2007) Wettability impact on CO2 storage in aquifers: visualisation and quantification using micromodel tests, pore network model and reservoir simulations. In: International symposium of the society of core analysts, Calgary, Canada
77. Chiquet P, Broseta D, Thibeau S (2007) Wettability alteration of caprock minerals by carbon dioxide. Geofluids 7:112–122
78. Larsen JA, Skauge A (1995) Comparing hysteresis models for relative permeability in WAG studies, SCA Conference, Paper number 9506
79. Schneider FN, Owens WW (1970) Sandstone and carbonate two- and three-phase relative permeability characteristics. SPE J 10:75–84 SPE 2445
80. Gonzalez DL, Vargas FM, Hirasaki GJ, Chapman WG (2007) Modeling study of CO_2-induced asphaltene precipitation. Energy Fuels 22:757–762
81. Idem RO, Ibrahim HH (2002) Kinetics of CO_2-induced asphaltene precipitation from various Saskatchewan crude oils during CO_2 miscible flooding. J Petrol Sci Eng 35:233–246
82. Kokal SL, Sayegh SG (1995) Asphaltenes: the cholesterol of petroleum. SPE 29787, middle east oil show, Bahrain, Society of Petroleum Engineers
83. Novosad Z, Costain TG (1990) Experimental and modeling studies of asphaltene equilibria for a reservoir under CO_2 injection, SPE 20530. In: SPE Annual technical conference and exhibition, New Orleans, Louisiana, Society of Petroleum Engineers
84. Srivastava RK, Huang SS (1997) Asphaltene deposition during CO_2 flooding: a laboratory assessment, SPE 37468. In: SPE Production operations symposium, Oklahoma City, Oklahoma, Society of Petroleum Engineers
85. Tavakkoli M, Kharrat R, Masihi M, Ghazanfari MH (2010) Prediction of asphaltene precipitation during pressure depletion and CO_2 injection for heavy crude. Pet Sci Technol 28:892–902
86. Peng S, Zhang J (2007) Engineering geology for underground rocks. Springer, Berlin
87. Gruesbeck C, Collins RE (1982) Entrainment and deposition of fine particles in porous media. SPE J 22:847–856 SPE 8430
88. Izgec O, Demiral B, Bertin H, Akin S (2008) CO_2 injection into saline carbonate aquifer formations I laboratory investigation. Trans porous media 72:1–24
89. Muecke TW (1979) Formation fines and factors controlling their movement in porous media. SPE J Petrol Technol 31:144–150 SPE 7007
90. Sarkar AK, Sharma MM (1990) Fines migration in two-phase flow. SPE J Petrol Technol 42:646–652 SPE 17437
91. Hibbeler J, Garcia T, Chavez N (2003) An integrated long-term solution for migratory fines damage, SPE 81017. In: SPE Latin American and Caribbean petroleum engineering conference, Port-of-Spain, Trinidad and Tobago, Society of Petroleum Engineers
92. Pruess K, Tianfu X, Apps J, Garcia J (2003) Numerical modeling of aquifer disposal of CO_2. SPE J 8:49–60 SPE 83695
93. Burton M, Kumar N, Bryant SL (2009) CO_2 injectivity into brine aquifers: Why relative permeability matters as much as absolute permeability. Energy Procedia 1:3091–3098
94. Fatt I (1953) The effect of overburden pressure on relative permeability. AIME 198:325–326 Petroleum Transactions
95. Thomas RD, Ward DC (1972) Effect of overburden pressure and water saturation on gas permeability of tight sandstone cores. SPE J Petrol Tech 24:120–124 SPE 3634
96. Al-Quraishi A, Khairy M (2005) Pore pressure versus confining pressure and their effect on oil-water relative permeability curves. J Petrol Sci Eng 48:120–126

97. Chierici GL, Ciucci GM, Long G, Eva F (1967) Effect of the overburden pressure on some petrophysical parameters of reservoir rocks, 7th World petroleum congress. Mexico City, Mexico, World Petroleum Congress
98. Jones A, Al-Quraishi A, Somerville JM, Hamilton SA (2001) Stress sensitivity of saturation and end-point relative permeabilities, Society of core analysts, Edinburgh, Scotland
99. van der Meer LGH (1993) The conditions limiting CO_2 storage in aquifers. Energy Convers Manag 34:959–966
100. Ross GD, Todd AC, Tweedie JA, Will AG (1982) The dissolution effects of CO_2-brine systems on the permeability of U.K. and North Sea calcareous sandstones, SPE 10685. In: SPE/DOE third joint symposium on enhanced oil recovery of the Society of Petroleum Engineers, Tulsa, OK, Society of Petroleum Engineers
101. Omole O, Osoba JS (1983) Carbon dioxide—dolomite rock interaction during CO_2 flooding process. Annual technical meeting, Banff, Petroleum Society of Canada
102. Sayegh SG, Krause FF, Girard M, Debree C (1987) Rock-carbonated brine interactions: part I cardium formation cores. Annual technical meeting, Calgary, Alberta, Petroleum Society of Canada
103. Bowker KA, Shuler PJ (1991) Carbon dioxide injection and resultant alteration of the weber sandstone, rangely field, colorado. AAPG Bulletin 75:1489–1499
104. Shiraki R, Dunn TL (2000) Experimental study on water-rock interactions during CO_2 flooding in the Tensleep Formation, Wyoming, USA. Appl Geochem 15:265–279
105. Wellman TP, Grigg RB, McPherson BJ, Svec RK, Lichtner PC (2003) Evaluation of CO_2-brine-reservoir rock interaction with laboratory flow tests and reactive transport modeling. In: International symposium on oilfield chemistry, Houston, Texas, Society of Petroleum Engineers
106. Grigg RB, Svec RK (2006) CO_2 transport mechanisms in CO_2/brine coreflooding, SPE 103228. In: SPE annual technical conference and exhibition, San Antonio, Texas, USA, Society of Petroleum Engineers
107. Bennion B, Bachu S (2007) Permeability and relative permeability measurements at reservoir conditions for CO_2-water systems in ultra low permeability confining caprocks, SPE 106995. In: EUROPEC/EAGE conference and exhibition, London, U.K., Society of Petroleum Engineers
108. Bennion B, Bachu S (2008) Drainage and imbibition relative permeability relationships for supercritical CO_2/brine and H_2S/brine systems in intergranular sandstone, carbonate, shale, and anhydrite rocks. SPE Reservoir Eval Eng 11:487–496 SPE 99326
109. Bennion B, Bachu S (2010) Drainage and imbibition CO_2/brine relative permeability curves at reservoir conditions for carbonate formations, SPE 134028. In: SPE Annual technical conference and exhibition, Florence, Italy, Society of Petroleum Engineers
110. Bennion B, Bachu S (2008) Effects of in situ conditions on relative permeability characteristics of CO_2-brine systems. Env Geol 54:1707–1722
111. Benson SM, Tomutsa L, Silin D, Kneafsey T, Miljkovic L (2005) Core scale and pore scale studies of carbon dioxide migration in saline formations. Lawrence Berkeley National Laboratory, USA
112. Okabe H, Tsuchiya Y, Mihama-ku H, Shinjyuku-ku O (2008) Experimental investigation of residual CO_2 saturation distribution in carbonate rock. International symposium of the society of core analysts, Abu Dhabi, UAE
113. Perrin J-C, Benson SM (2010) An experimental study on the influence of sub-core scale heterogeneities on CO_2 distribution in reservoir rocks. Transp Porous Med 82:93–109
114. Perrin J-C, Krause M, Kuo C-W, Miljkovic L, Charoba E, Benson SM (2009) Core-scale experimental study of relative permeability properties of CO_2 and brine in reservoir rocks. Energy Procedia 1:3515–3522
115. Shi J-Q, Xue Z, Durucan S (2010) Supercritical CO_2 core flooding and imbibition in Tako sandstone–Influence of sub-core scale heterogeneity: International Journal of Greenhouse Gas Control, v. In Press, Corrected Proof

116. Seo JG (2004) Experimental and simulation studies of sequestration of supercritical carbon dioxide in depleted gas reservoirs. PhD theses, Texas A&M University, Texas, p 132
117. Nogueira M, Mamora DD (2008) Effect of flue-gas impurities on the process of injection and storage of CO_2 in depleted gas reservoirs. J Energy Res Technol 1:013301–1–013301–5
118. Nogueira M (2005) Effect of flue gas impurities on the process of injection and storage of carbon dioxide in depleted gas reservoirs. MSc theses, Texas A&M University, Texas

Chapter 3
Experimental Setup, Material and Procedure

3.1 Introduction

A major part of the experimental work related to this research, consisting of a number of different types of core-flooding experiments, was carried out using the state-of-the-art, high pressure-high temperature, three-phase steady-state core-flooding apparatus located within the Department of Petroleum Engineering at Curtin University. To be able to achieve the objectives of this research program, various types of flooding experiments were designed and carried out using the above-mentioned core-flooding rig. In the first part of this chapter a detailed description of the experimental apparatus and its various components is presented. The second part starts with detailed description of the material (fluids and core samples) used during the experiments and then discussed afterwards are the experimental procedures followed, in performing various laboratory work, before, during and after carrying out the main core-flooding experiments. While describing the experimental procedures, the specifications of a number of other laboratory instruments, which were used on the side, to conduct various other complementary measurements are also presented.

3.2 Experimental Apparatus

The three-phase, steady-state core-flooding apparatus used in carrying out the displacement experiments, is capable of handling pressures up to 15,000 psi ($\sim$1,000 bar) and temperatures up to 200°C. The equipment is designed and constructed in a way to provide the capability to perform a wide range of core-flooding related research within one stand-alone integrated system. The system can be used for carrying out all main multiphase fluid-flow experimental analysis including, but not limited to, two and three phase relative permeability measure-

A. Saeedi, *Experimental Study of Multiphase Flow in Porous Media during CO_2 Geo-Sequestration Processes*, Springer Theses, DOI: 10.1007/978-3-642-25041-5_3,

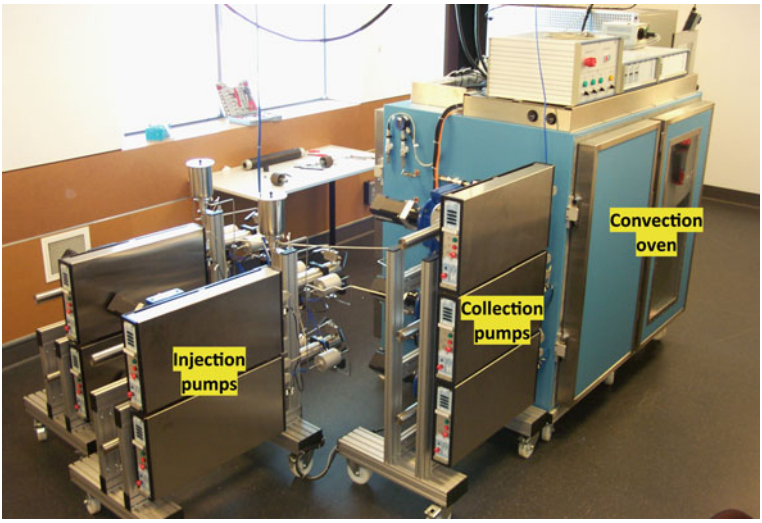

Fig. 3.1 The core-flooding system used in carrying out the flooding experiments

ments, most areas of enhanced hydrocarbon recovery related research, formation damage analysis, and of course CO_2 sequestration displacement performance analysis. Figures 3.1 and 3.2 show a photo and the schematic diagram of the core-flooding apparatus respectively.

The critical wetted metal parts of the apparatus are made of highly corrosion resistant material (e.g. hastelloy, titanium or duplex and super duplex stainless steel) which make the equipment rust free and corrosion resistant even under high temperature environments with high chloride concentrations. All the components carrying fluids during experiments are placed inside a large constant temperature convection oven. The temperature inside the oven is controlled using a PID (proportional–integral–derivative) controller module which can regulate the temperature with an accuracy of 0.2°C. The oven is also equipped with three fans, which help to circulate the hot air inside. Overall the apparatus comprises of four main parts, the injection system, the core-holder, the separation and collection system and the data logging and monitoring/controlling system. Presented below is a detailed description of each of these parts.

3.2.1 The Injection System

As shown in Fig. 3.2, the injection system consists of two main components, the injection pumps with their electronically controlled pneumatic valves (Fig. 3.3) and three fluid sample bottles (Fig. 3.4). While running the flooding experiments, all the fluid injections and pressurisations are carried out using four injection pumps, which

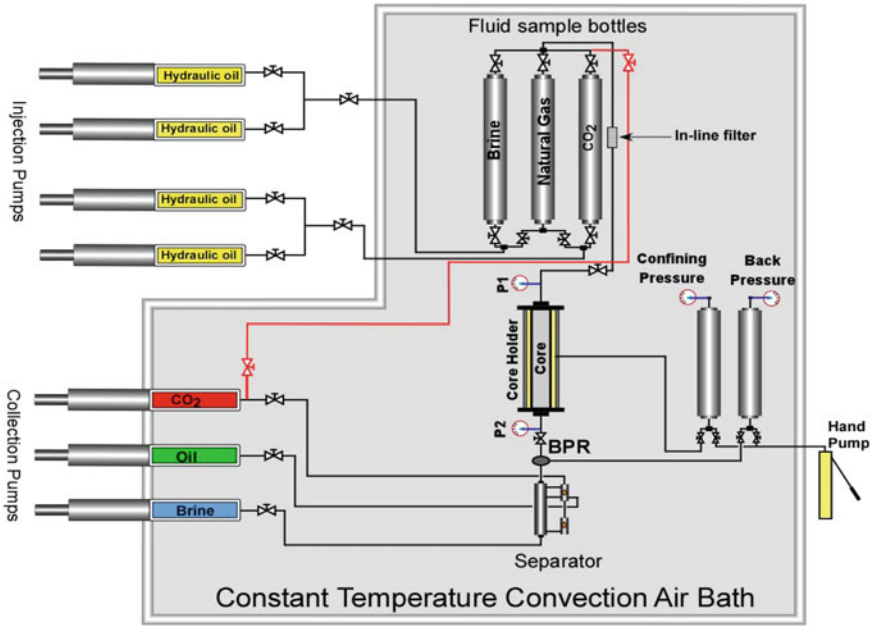

Fig. 3.2 The schematic diagram of the experimental apparatus used to run the core-flooding experiments, *black lines*: injection or collection lines, *red lines*: CO_2 recycling line

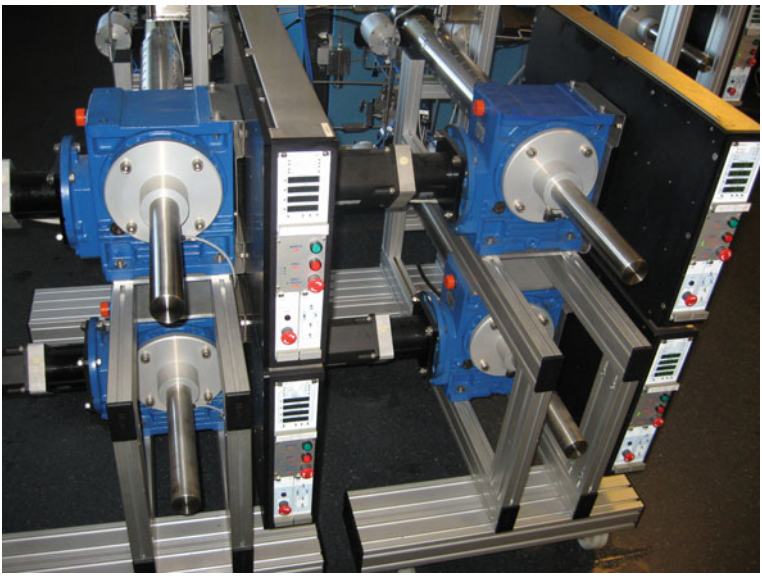

Fig. 3.3 Four injection pumps and their associated electronics

Fig. 3.4 Three fluid sample bottles containing the pressurised injection fluids

could be run either independently or in synchronised pairs. All four pumps are of pulsation-free, positive-displacement pump type and have an injection capacity of 300 cc in one cycle. They can inject the fluids under various injection scenarios of constant flow-rate, constant pressure, constant pressure with adjustable pressure ramp and reaching a target injection volume. All four pumps have a number of PID controllers integrated into their electronic interfaces which are required for pressure or volume regulations and could be operated directly using the keypads placed in front of the pumps or using the software installed on the computers.

Each of three fluid bottles has a capacity of 1,500 cc which provides enough capacity to run an uninterrupted steady-state flooding test for an average permeability core-sample. The bottles each have a floating piston inside which separates the pressurising hydraulic oil from the injection fluid (e.g. CO_2 and brine). Each pump is connected to the sample bottles and an hydraulic oil feed tank using a pair of electronically controlled pneumatic valves, which are opened or closed using air pressure. The utilisation of the electronic valves and the fact that the pumps can be operated in two synchronised pairs (Fig. 3.5) makes the pumps capable of injecting fluids non-stop for as long as required. The pressure, volume and flow-rate values can be set and recorded with accuracies of 2 psi, 0.05 cc and 0.05 cc/h respectively. All the injection fluids are passed through a 0.5 micron sintered stainless steel in-line filter element to remove any potential plugging material from the injection line prior to entry into the core-sample.

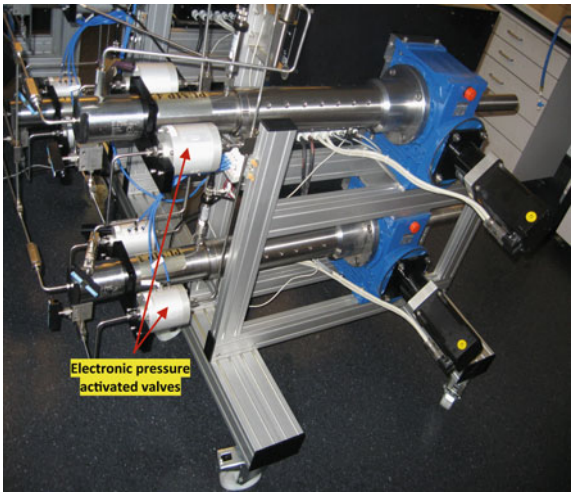

Fig. 3.5 The double synchronised injection pumps and their electronic pressure activated valves

3.2.2 The Core-Holder

The core-holder used during this research (Fig. 3.6) was one of Temco's HCH series standard biaxial core-holder range. Standard biaxial or hydrostatic type core-holders are defined as core-holders that have common radial and axial pressure applied to the core-sample. In other words, the same axial and radial confining pressure is applied through the annular space along the outer diameter of the core-sample and to the end of the core-sample using a floating end plug (Fig. 3.7). Two confining pressure ports are provided so that the annular space between the core-sample and the inner diameter of the core-holder body can be filled with overburden fluid using one of the ports while the air is easily expelled from the other. The outlet distribution plug is connected to a ¼″ tube, which through the bore located in the centre of the end cap, can slide back and forth as required. This allows the distribution plug to move inside the core-holder and remain in constant contact with the core-sample as the rock is compressed. Furthermore, this allows different lengths of core-samples to be tested in the same core-holder. The distribution plugs are provided with more than one inlet or outlet port to be able to connect the inlet or outlet pressure sensor to one port while the fluids are injected or produced from the other ports. In order to reduce the system dead volumes and improve the volume measurement accuracies, the volumes of all ports and flow lines have been kept to a minimum. The core-holder has an adjustable stand, so that the core-holder could be oriented in vertical or horizontal directions as required.

As can be seen in the cross-sectional view of the tip of the end distribution plugs in the left bottom corner of Fig. 3.7, a specially designed spider-web-type groove pattern is utilised. This is to make sure that the fluids, before entering or exiting the core-sample, were evenly distributed on the whole face of the core-sample.

Fig. 3.6 The Temco biaxial core-holder used during the core-flooding experiments

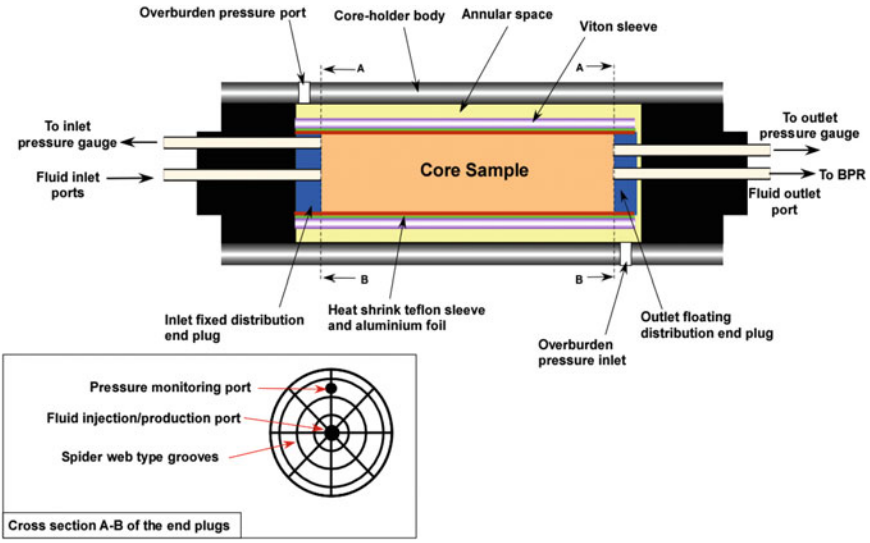

Fig. 3.7 Schematic cross-sectional illustration of the configuration of the core-holder assembly used during core-flooding experiments

This type of groove pattern is very effective in making the capillary inlet and outlet effects, which are commonly experienced during the displacement experiments, less pronounced. Again as can be seen in Fig. 3.7, for the core-flooding experiments conducted during this research, a special multilayer combination sleeve was used. This combination sleeve was necessary due to the tendency of CO_2 to diffuse and penetrate through most flexible rubber sleeves which firstly could cause the sleeve to lose its integrity and fail. Secondly, due to loss of CO_2 through diffusion, the

material balance calculations for each individual experiment, which was necessary to work out the residual saturations inside the core-sample, would not add up. This combination sleeve was made of three layers including one layer of heat-shrink Teflon sleeve, one layer of aluminium foil and one layer of conventional Viton sleeve. The heat-shrink Teflon sleeve had an extremely low permeability to CO_2, however, to make sure that the CO_2 would not escape to the overburden annular space, a layer of aluminium foil was also placed between the Teflon and the Viton sleeve.

The overburden fluid, which is of high quality hydraulic oil, is first injected using a hand-pump into an intermediate cylinder (Fig. 3.2) with a small nitrogen gas cushion on top and then the pressure is transferred from the bottom of the cylinder to the overburden pressure inlet of the core-holder. Due to the high compressibility of the gas, the gas cushion on top of the intermediate cylinder serves as a pulsation dampener to eliminate any abrupt change in the overburden pressure which could occur for instance due to any small temperature variation. All core-holder out-flow fluids are passed through a dome-type back-pressure regulator (BPR). The BPR keeps the pressure inside the sample constant and equal to reservoir in situ pore pressure and prevents back-flow of the produced fluids into the core-sample. The advantage of a dome-type BPR over other BPR types (e.g. diaphragm type) is that it can handle multiphase flow while regulating the pressure with very high precision. The pressure regulation inside the BPR is provided using nitrogen gas. Gas is recommended for this type of pressure regulation since it is highly compressible and as a result provides smooth pressure regulation. It is worth noting that, to prevent any potential pressure variations due to change in the room temperature, both the back pressure and the overburden pressure intermediate cylinders are placed inside a constant temperature convection air bath.

3.2.3 The Separation and Collection System

The separation and collection system comprises of a high pressure-high temperature 3 phase vertical separator (Fig. 3.8), three collection pumps (Fig. 3.9) and associated sensors. The core-sample out-flow fluids, after passing through the BPR, enter the separator. The separation occurs due to gravity inside the specially designed separator, which can operate at the same pressure and temperature as reservoir in situ conditions (i.e. P–T conditions inside the core sample). This is highly beneficial, especially for the material balance calculations, since there is no need to back-convert the produced volumes to reservoir conditions, which would be necessary if the fluids were being flushed into ambient conditions. Furthermore, for the experiments carried during this research, the high pressure inside the separator eliminated the evolution of the CO_2 already dissolved in the CO_2-saturated injection brine or the evaporation of the hot water coming out of the core-sample, both of which could cause serious errors during the material balance calculations.

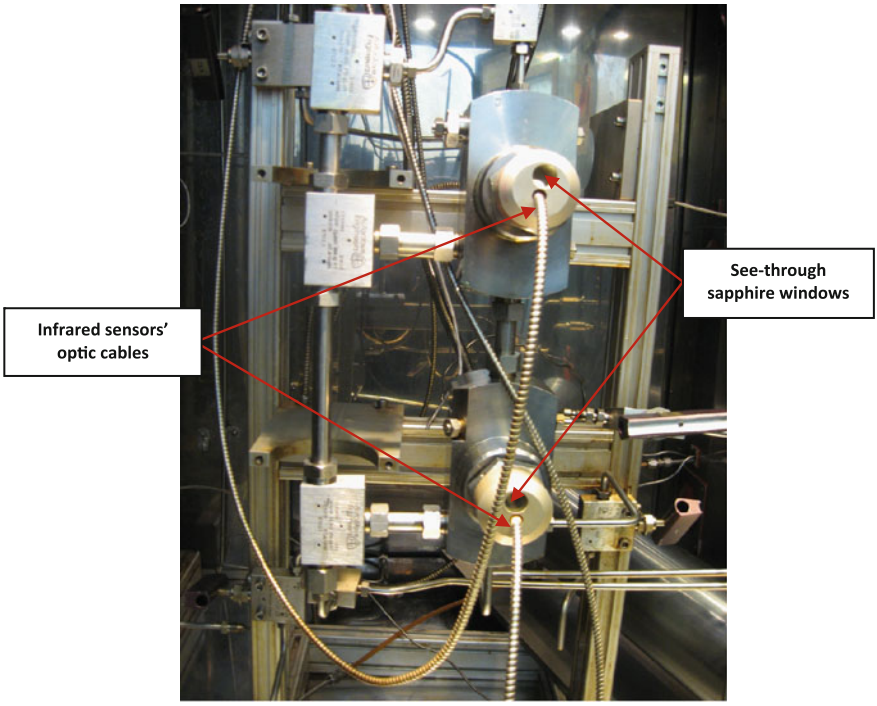

Fig. 3.8 The 3-phase high pressure-high temperature separator utilised during this research

For the separator to work properly, in addition to gas and brine, there needs to be a third phase crude oil present in it. This is due to the fact that the separator's infrared sensors, which detect and help to adjust the fluid levels inside the separator, operate using the fact that dark crude oil is not transparent to infrared light. Since before the commencement of any experiment the crude phase becomes fully saturated with the gas, its existence does not interfere with the displacement experiments in any way. For the experiments carried out during this research, the crude was chosen having very low asphaltene content and was a relatively light crude type to avoid any asphaltene precipitation occurring in the separator as it came in contact with CO_2.

There is one collection pump for each fluid phase present in the separator. In terms of the functionality, the collection pumps are identical to the injection pumps. During each flooding experiment, the gas collection pump can be operated under a constant pressure procedure. This is necessary to keep the separator pressure constant. The constant pressure is regulated using a PID controller module integrated into the pump's electronic interface. The controller parameters can be adjusted to collect appropriate amounts of gas when the gas is being produced from the sample while the pressure is kept constant and equal to the in situ reservoir pressure. When running a flooding experiment, the brine collection

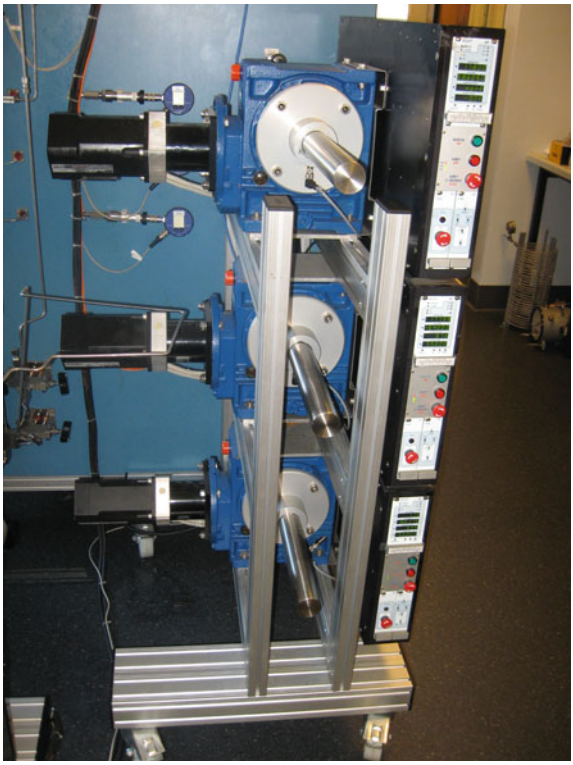

Fig. 3.9 Three collection pumps connected to the separator and their associated electronics

pump is controlled using another PID controller module, which is being fed by the output signals transmitted from the separator's level detecting infrared sensors. For instance, if brine is produced into the separator, the interface between the crude oil and the brine would rise inside the separator. The magnitude of this rise is detected by the infrared sensors and a command is sent to the pump's PID controller module to collect appropriate amounts of brine to keep the crude-brine interface steady and constant inside the separator. Similar to the gas collection pump, the PID controller parameters for the brine collection pump could be adjusted appropriately to make the PID controller's response proportional to the magnitude of the rise in the crude-brine interface detected by the corresponding infrared sensor.

3.2.4 The Data Logging and Monitoring System

All of the sensors and electronic interfaces of the apparatus are connected to two computers with appropriate data logging and monitoring software installed on both (Fig. 3.10). The whole system including the sensors, the PID controllers, the

Fig. 3.10 One of the two PCs connected to the apparatus for data-logging and monitoring purposes

injection and collection pumps and the pneumatic valves are monitored and controlled using these two computers. The data logging can be done with time-steps as short as 1 s.

3.3 The Material

3.3.1 Fluids

In total four different types of fluids were used during the various stages of the experimental work conducted. These fluids included dead brine (i.e. brine with no dissolved gas content), CO_2-saturated brine (i.e. brine saturated with CO_2 at the in situ reservoir P–T conditions), water-saturated CO_2 (i.e. supercritical CO_2 saturated with water vapour) and water-saturated methane. The CO_2 gas used was of a bottled high-purity grade (99.99%) carbon dioxide and the methane gas sample used contained 99% methane. The brine was prepared in the lab using demineralised water and appropriate amounts of analytical grade (99.95%) sodium chloride (NaCl). The required PVT properties (e.g. viscosities and mutual solubilities) of the fluids used under the desired reservoir conditions were calculated using various databases and literature resources reviewed in Chap. 2 (e.g. interactive online models provided by US National Institute of Standards and Technology [1] and the Zhenhao Duan Research Group [2]).

3.3.2 Core Samples

After shales with 46%, sandstones make up about 32% of all the sedimentary rocks, followed by carbonates with 22% [3]. Therefore, deep sandstone aquifers are considered abundant in many sedimentary basins all around the world and present a large storage capacity available for immediate CO_2 storage. The core samples used during this experimental work were all sandstone and were chosen from a number of varieties to cover a range of sandstone types present in such geological structures. The core samples could be divided into four different groups based on their origin, porosity and permeability ranges and the type and degree of their clay content.

The samples in Group 1 were those drilled in both horizontal and vertical directions from the whole-cores taken from Well CRC-1 drilled into the Naylor Field of CO_2-CRC's Otway Basin Project (OBP) back in 2007. OBP has been the first CCS demonstration project undertaken in Australia with the main aim of demonstrating that CO_2 can be safely captured, transported and stored underground under Australian conditions [4]. Before being subjected to CO_2 injection in March 2008, the Naylor Field was a small depleted gas reservoir in the onshore Otway Basin in central southern Victoria, Australia [5]. In this field the Waarre Formation was the main hydrocarbon reservoir [6]. The core samples tested here were drilled from Unit C of this formation. Unit C rocks are made up of interbedded sandstone and claystone [5] and the sandstones are generally quartz arenites, medium to coarse grained, fair to well sorted with characteristically high flow rates [6].

In cutting the samples, care was always taken to drill them from homogeneous sections of the whole-cores to avoid the undesirable artefacts during the flooding experiments caused by the localised small heterogeneities which may be present in the core samples. The core samples in Group 1 (Fig. 3.11) were of moderate to high permeability and moderate porosity values, which are typical characteristics of the Waarre C sandstone. This group of samples were identified by having the word CO_2CRC at the beginning of their names followed by the sample number and then the letter H or V at the end of their names as an indication of the sample direction being horizontal or vertical respectively (e.g. CO_2CRC-7-V).

The second group of samples (Fig. 3.12) were drilled from two separate quarried Berea Sandstone blocks purchased from Vermilion, Ohio in the United States. As requested from the supplier in the U.S., the two blocks were different from each other with respect to their absolute permeabilities. The Berea samples were characterised by clean, well-sorted and fine to medium grained sandstones with moderate to high permeability and moderate porosity values. The grains of the Berea sandstone consisted of predominantly quartz (85–90%) and feldspar (3–6%). The sand grains are cemented by quartz, dolomite (1–2%), clays (6–8%), and traces of iron sulphides. In a similar fashion to the samples in Group 1, these samples were identified by having the letters BS (standing for Berea Sandstone) at the beginning of their names followed by the sample number and then the letter H or V (horizontal or vertical) at the end of their names (e.g. BS-1-H).

Fig. 3.11 Two sandstone core-plugs drilled in horizontal direction from whole-cores taken from Waarre C formation in the Naylor Field

Fig. 3.12 Two Berea Sandstone core-plugs taken from quarried blocks

The rock samples in Group 3 (Fig. 3.13) were of Donnybrook Sandstone drilled from quarried blocks taken from the Donnybrook area in the South-west of Western Australia. These samples were of yellowish felspathic sandstone with a principal bonding of kaolin or halloysite and traces of iron oxide. As a general characteristic of the Donnybrook Sandstone, these samples were of low permeability and moderate porosity values. These samples were identified by the letters DB (standing for Donnybrook) at the beginning of their names followed by their sample number and then the letter H or V (vertical or horizontal) at the end of their names (e.g. DB-2-V).

The fourth group of samples (Fig. 3.14) included a few short glauconitic sandstone samples. These samples were drilled in both horizontal and vertical directions from the whole-cores taken from an Australian offshore gas reservoir. The samples in this group were of moderate permeability and porosity values. These core samples were identified by letters CL (standing for Core Laboratories who kindly provided us with these samples) at the beginning of their names followed by the sample number and letter H or V (horizontal or vertical) at the end of their names (e.g. CL-40-H).

Fig. 3.13 Two Donnybrook Sandstone core-plugs taken from quarried blocks

Fig. 3.14 Two glauconitic sandstone core-plugs drilled from whole-cores taken from an Australian gas reservoir-green dots are glauconite particles within the sandstone texture

3.4 Experimental Procedure

For all the experimental work carried out during this research the experiments followed procedures which were based on the various standard protocols that have been outlined in the literature. Apart from the core-flooding experiments which constituted the core of this research program, there was a variety of other experimental and preparation work carried out as well, which included:

- Cutting core-plugs out of the whole-cores taken from the wells or quarried blocks.
- Cleaning core-plugs of any possible hydrocarbon, salt and drilling fluid residues.
- Measuring porosity of the core-plugs.

- Aging the samples in synthetic formation brine to restore their original wettability.
- Running NMR tests on the brine saturated samples before and after each core-flooding test.
- Pre-saturating the brine with CO_2 before using it for the flooding experiments.

In the following section of this chapter, a detailed description is presented of the procedures followed during the above-mentioned experimental work.

3.4.1 Core-Plug Preparation and Preliminary Measurements

The core-holder of the core-flooding apparatus can accommodate core-samples with exact 1.5″ (38.1 mm) in diameter and up to 33 cm long. Therefore the core plugs were cut using a pedestal press drill with 1.5″ inner diameter coring bit. Since using fresh water and oil based fluids during coring operations may cause formation damage by causing clay swelling or sever contamination and potentially wettability alteration, all the coring operations were done either dry or using non-damaging brine. After the coring, the end faces of the core-samples were trimmed and smoothed to ensure a proper contact between the core-holder end plugs and the end faces of the core-samples to eliminate any capillary discontinuity. The core plugs were taken with the maximum length of 10 cm as this is the maximum length the porosity measurement instrument could accommodate. However, due to the limitation set by the diameter of the available whole-cores, many of the core-plugs had to be cut with the length in the range of 4–6 cm. In order to investigate the directional dependence of the displacement performance in the porous media, where possible, the core-plugs were cut in the vertical direction (i.e. perpendicular to the natural bedding) as well as in the horizontal direction (i.e. parallel to the natural bedding).

After cutting the core-plugs they were cleaned of any possible residual hydrocarbons and salts using warm toluene and methanol, respectively [7]. This was carried out using a Dean-Stark apparatus (Fig. 3.15). Depending on the permeability of the samples, the cleaning time varied from 15 to 48 h. During the cleaning process special care was always taken not to expose the samples to excessive heat which could be damaging to the samples. After cleaning the core-plugs, they were dried in a vented oven at 60°C for around 24 h or until stable weights were obtained, indicating that the samples were dry. The 60°C temperature was chosen to prevent the evaporation of any clay bound water which could cause damage to any clay minerals present in the samples [8]. After removing the samples from the oven they were cooled down inside a desiccator to room temperature prior to further analysis. Once the samples cooled down their dimensions (i.e. diameter and length) were measured using a caliper.

The AP-608 Automated Permeameter-Porosimeter from Coretest was used for porosity measurements. This apparatus is equipped with a hydrostatic core-holder

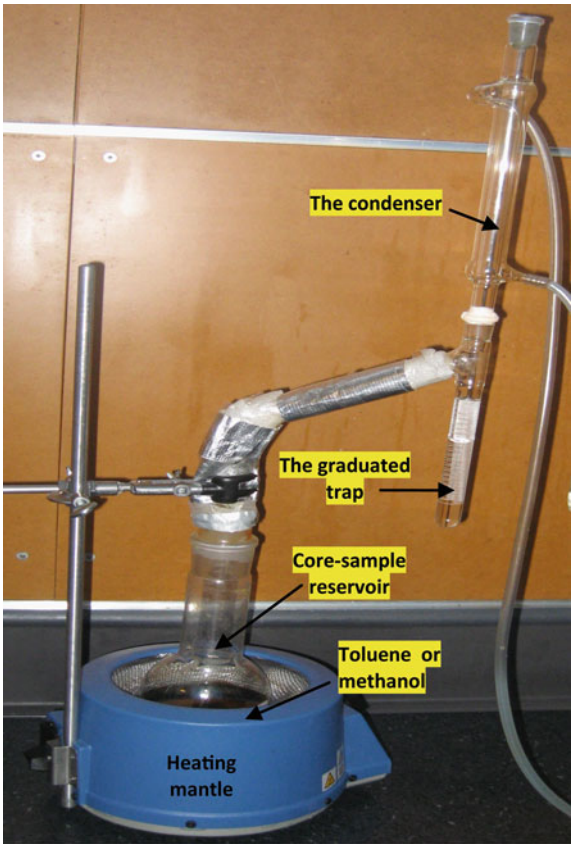

Fig. 3.15 The Dean-Stark apparatus

which can carry out porosity measurements at net effective pressures up to 9,500 psi. Using the AP-608 instruments the porosity of the samples is measured using a Boyle's law technique. Because of its high diffusivity and being non-toxic and non-damaging to the core samples, to measure porosity, low pressure (max 200 psi) helium gas was used as the pore fluid.

3.4.2 The Sample Restoration Process

As was discussed in Chap. 2, the displacement performance during core-flooding experiments is highly influenced by the wettability condition of the porous media. In addition, the results of the NMR analysis carried out on the core-samples before and after the displacement tests are also highly dependent on the wettability condition of the core-samples [9, 10]. Therefore, while the cleaned sandstone core-plugs are normally considered to be strongly water-wet [11, 12], in order to make

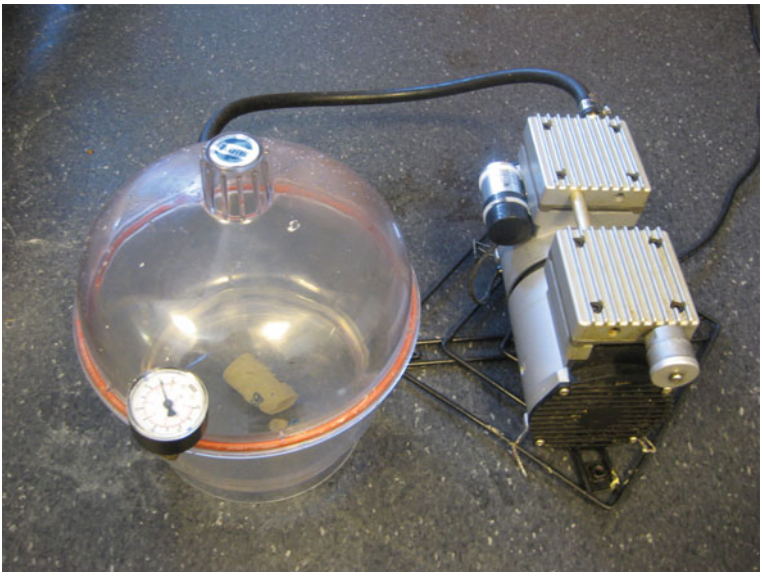

Fig. 3.16 A core-sample left in the desiccator under vacuum to be saturated by brine

sure that the samples were representative of the desired reservoir conditions, the samples' wetting tendencies, if ever changed during the sample handling procedures, needed to be restored to their originally water-wet condition. Therefore, once the porosity of the samples was determined, they were immersed in synthetic formation brine, made by dissolving NaCl in distilled water, inside a desiccator (Fig. 3.16). The samples were left immersed in brine under constant vacuum for a minimum of 2 weeks, which is in the range of time recommended in the literature [11–13], to establish adsorption equilibrium and restore the water-wetness of the core-samples. It is worth noting that during this time, the brine level inside the desiccator was constantly monitored and if the level dropped due to evaporation, appropriate volumes of distilled water were added to the solution. This long aging process was in addition to a second 48 h aging process which would be carried out later on individual samples, using de-aerated brine under the in situ reservoir P–T conditions on each individual core-sample before flooding them by CO_2-saturated brine and supercritical CO_2 consecutively.

3.4.3 NMR Measurements

Nuclear Magnetic Resonance refers to the response of atomic nuclei of hydrogen when it is immersed in a static magnetic field and exposed to a second oscillating one. Response of the NMR relaxation measurements can be used to extract useful

petrophysical information such as irreducible bulk volume (BVI), clay-bound water volume (CBW), and movable bulk volume (BVM). This allows defining effective porosity, total porosity, and permeability index [14].

Among others, the properties of the fluids contained in the pore space of a porous medium which influence the data obtained from the NMR measurements are longitudinal relaxation time (T1), transverse relaxation time (T2). T1 is a measure of how fast the protons in the fluid exposed to the external magnetic field relax longitudinally (relative to the axis of the static magnetic field). T2 is an indication of how fast the protons relax transversely (again relative to the axis of the static magnetic field) [14]. T2 relaxation time depends on many parameters such pore fluid type, mineralogy and pore sizes. Among these, when dealing with the same rock type and the same pore filling fluid, pore size is the most important parameter that controls T2 relaxation time. There is a direct relationship between pore size and T2. In other words, as pore size of a porous media increases it takes more time for hydrogen nuclei to relax thus T2 will increase. Whereas for rocks with small pore sizes T2 relaxation time shift toward smaller values.

NMR analysis tests were carried out on a number of the restored and fully brine-saturated core-plugs before and after each flooding experiment. All the NMR measurements were carried out using a Resonance Instruments Maran-Ultra 2 MHz bench-top spectrometer with a standard homogeneous field probe and an additional gradient coil set. The following principle objectives were pursued while running the NMR tests:

- *Sample relative pore-size distribution determination*: as mentioned earlier, the NMR T2 relaxation time depends on the pore-size distribution of the porous medium under investigation, therefore by analysing the T2 distribution from each NMR test, a clearer picture of the pore-size distribution of the core-sample under investigation can be drawn. This could be very useful while interpreting the results of the core-flooding tests.
- *Detection of any change in the pore-size distribution*: since NMR T2 relaxation time depends on the size and distribution of the pores, any possible change in the pore-size distribution of the core-samples may be detected by running NMR tests on the samples before and after being subjected to the cyclic flooding experiments. The changes in the pore-size distribution may occur through dissolution or precipitation of minerals inside the pore network of the core-sample during the flooding process, or possible change in the properties of the clay minerals (e.g. clay swelling and fine migration). The other potential cause of any change in the pore network of the sample, which could be detected using NMR results, could be irreversible or plastic deformation of the sample while under pressure.

The following steps were followed for each NMR test:

1. The restored core-plugs were left immersed in synthetic formation brine inside a desiccator under vacuum for, depending on the permeability of the samples, at least 72 h. The vacuum was necessary to accelerate the saturation process by sucking the trapped air out of the pore spaces of the samples and also to remove

the air which normally is pre-dissolved in the brine used for saturating the samples. The level of brine in the desiccator was monitored constantly and any drop in the brine level was compensated by adding appropriate volumes of distilled water to the desiccator.

2. After getting the core-samples saturated, they were removed one by one from the desiccator and weighed to determine the weight of the saturated sample. This was done as quickly as possible to prevent the evaporation of water from the pores of the sample exposed to the air.
3. The weighed samples were again immersed individually in the brine inside glass jars then capped and left inside a water bath to be heated to 35°C. This was necessary because the temperature inside the NMR machine's sample chamber was 35°C and to prevent any experimental error, the sample needed to be pre-heated to the same temperature.
4. After 3–4 h and once the samples' temperature equilibrated with the water inside the bath they were remove from the jar one at a time and tightly wrapped in clean plastic film. The plastic film wrap was necessary to prevent the evaporation of water from the sample pores during the experiment. Again, the wrapping was performed as quickly as possible to prevent the evaporation of water from the sample pores exposed to the air. Care also was taken not to leave any free water on the sample's surface as this could cause serious error during NMR measurements.
5. Then the sample was lowered into the NMR machine's sample chamber. It is worth noting that before running any NMR test the machine was first calibrated for the signal amplitude versus water content using a small jar containing 15 cc of water. The water sample used for calibration was doped with nickel chloride. This was necessary to reduce the water relaxation time and make it comparable to those of bounded water in the pore space of porous medium. A hard pulse CPMG (Carr–Purcell–Meiboom–Gill) sequence was used to generate the T2 relaxation spectrum on all the samples. CMPG-T2 is the most commonly implemented NMR measurement in the down-hole environment and is one of the easiest low-field methods to implement and to interpret [15].
6. At the conclusion of each NMR run, the DXP programme provided by Resonance Instruments as part of the MARAN2 spectrometer software was used to transform the echo decays to T2 spectra. This T2 distribution acquired from the NMR measurements can be used to estimate the size distribution of the brine-filled pores [15, 16], which constitute the full pore-size distribution spectra of the fully brine-saturated samples studied in this research.

3.4.4 Mutual Pre-Saturation of Brine and CO_2

Before proceeding further, the brine and CO_2 which were used during the main core-flooding experiments were required to become fully saturated with each other at the reservoir in situ P–T conditions. This was necessary for the following reasons:

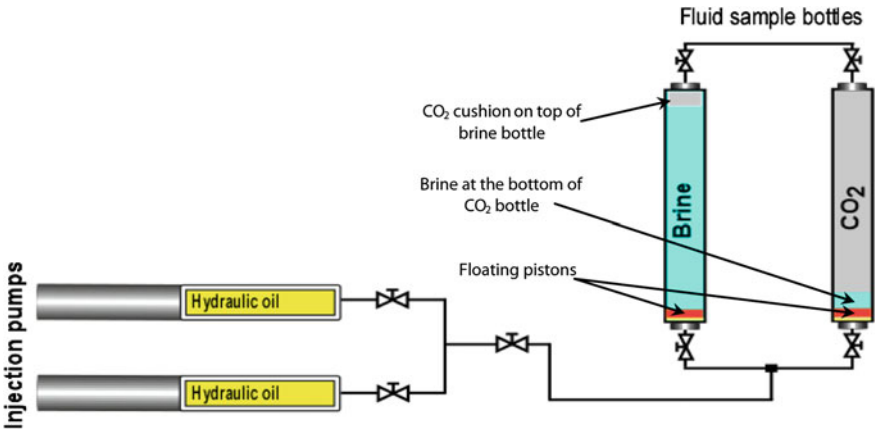

Fig. 3.17 Schematic diagram of the configuration used to bring CO_2 and brine in contact with each other

- The main objective of this research was to investigate the displacement performance of the CO_2-brine-rock system under an immiscible displacement procedure. Therefore, in order to avoid the CO_2 diffusion into the brine or the water evaporation into CO_2 and the formation of a miscible or partially miscible process, the brine and CO_2 were required to become mutually saturated with each other.
- If the mutual pre-saturation was ignored, continuous injection of the displacing phase close to the conclusion of each flooding experiment would cause excessive evaporation or dissolution of the displaced phase into the displacing phase and subsequently the residual saturation of the displaced phase (i.e. CO_2 or brine) would be reduced to unrealistically low values.
- During the CO_2 flooding of the brine saturated core-sample, if the water evaporation mentioned above takes place, depending on the degree of brine salinity, there would be salt residues left inside the pore space of the core-sample which could undesirably alter the displacement performance of the system specially close to the end of each flooding stage.

To avoid the above-mentioned complications, the brine and CO_2 were mutually saturated with each other prior to the start of the core-flooding tests. Below are the steps which outline the procedure followed to make sure that, as required, brine and CO_2 became fully saturated with each other:

1. Two out of the three fluid sample bottles were cleaned, vacuumed and filled, one with CO_2 and the other with de-aerated brine and they were brought to reservoir in situ P–T conditions.
2. After isolating the bottles from the outside, CO_2 was brought in contact with the brine by opening the relevant valves and using the lines connecting the two bottles together (Fig. 3.17).

3. While the two bottles were connected, using one of the injection pumps, about 200 cc of the brine was injected into the CO_2 bottle. After waiting for 10–15 min for the brine to settle at the bottom of the CO_2 bottle, about the same volume as the injected brine (i.e. 200 cc) CO_2 was injected into the brine bottle. Due to gravity, this volume of CO_2 would stay like a gas cushion on top of the brine bottle.
4. Then the system was left for about 5 days for the CO_2 cushion to diffuse into the brine and for the brine at the bottom of the CO_2 bottle to evaporate into the CO_2 phase. The convection mixing [17, 18] phenomenon was expected to enhance the diffusion of CO_2 into the brine in order to create a more homogenous mixture. During this time one of the injection pumps shown in Fig. 3.17 was left connected directly to the CO_2 bottle while operating under constant pressure (equal to reservoir pressure) procedure. During this process, the two bottles and connecting lines were inside a constant temperature (equal to reservoir temperature) convection oven. The CO_2 being dissolved into the brine could be sensed through monitoring the small changes in the volume of the pump which kept the pressure of the CO_2 bottle constant.
5. After the above-mentioned time, the CO_2 bottle was isolated by closing the valve on its top. Then a cylindrical stainless steel sample (D = 1.5″ L = 7 cm) which had a small bore axially drilled in its centre was loaded into the core-holder. Then all the lines and the bore in the centre of the stainless steel sample were vacuumed and then filled with dead formation brine and then pressurised to the desired reservoir pressure. Then the fluid inside the brine bottle was injected to displace the dead brine into the separator which was at the same pressure and temperature as reservoir conditions. After producing the dead brine inside the lines and steel sample and the cushion gas which was originally on top of the brine bottle, the CO_2 saturated brine would be produced into the separator. Once the brine production was detected, the CO_2 collection pump was set to operate a under constant pressure (equal to reservoir pressure) procedure. If the volume of the existing CO_2 inside the CO_2 collection pump kept decreasing, it was a sign that further CO_2 was being dissolved into the produced brine in the separator and the CO_2 and brine needed to be left in contact for a few more days. But if the volume of CO_2 inside the CO_2 collection pump did not change it was a sign that the brine was fully saturated with CO_2.

Steps 3, 4 and 5 were repeated until it was felt that the brine had become fully saturated with CO_2. It is worth noting that, during the flooding experiments, any produced CO_2 could be recycled back into its corresponding fluid sample through recycling lines shown in red in Fig. 3.2. The CO_2 phase inside the CO_2 bottle was expected to become saturated with water vapour soon after the 200 cc water was placed at the bottom of the bottle. It is worth noting that, the methane gas sample (i.e. CH_4), which was used during some of the core-flooding experiments, was also saturated with water vapour using a third bottle (Fig. 3.4) in the same fashion as CO_2.

3.4.5 The Core-Flooding Experiments

As mentioned before, the core-flooding experiments constituted the main part of this research. While the overall concept and procedure of a standard CO_2-brine core-flooding experiment remained the same, in order to achieve the previously outlined objectives of this research, several different sets of flooding experiments were carried out during this research. The difference between the various sets of experiments was only in small but important details- such as changing various rock or fluid parameters and investigating the consequent effects on the results. In this final part of the current chapter, first an overall discussion on the core-flooding experiments, addressing the technical issues and the uncertainties, different methodologies and interpretation techniques, is presented. Then the experimental procedure for a basic CO_2-brine flooding experiment is outlined and afterwards in the final sections of this chapter, other variants of this basic approach and how they helped to achieve the main objectives of this research are explained.

3.4.5.1 Technical Issues and Uncertainties

The results of the core-flooding experiments have become increasingly important in hydrocarbon reservoir studies especially in the reservoir modelling and simulation processes. This importance becomes more apparent knowing that, with the dramatic advances made in computing technology during the last two decades, the dynamic reservoir simulation has become the most appropriate method for accurate prediction of the dynamic behaviour of hydrocarbon reservoirs, natural gas storage sites and of course CO_2 geo-sequestration projects. Despite the experiences gained and the advances made in the measurement technology, much data measured today are still questionable and there are a number of uncertainties to be addressed before carrying out any experimental study. In order to design the most appropriate experimental procedure for any core-flooding study and fully understand and acknowledge the uncertainties involved, as explained below, it is necessary first to point out a series of facts which require special attention.

The core-samples used during core-flooding experiments need to be representative of the desired in situ reservoir rock conditions. This applies to both physical and chemical properties. The most suitable core-sample for core-flooding studies is the one chosen carefully from the right reservoir interval in the first place and secondly is preserved during the subsequent handling procedures so it would retain its representative properties. If the sample is not or cannot be preserved there are a number of processes which could help to restore its original condition [11, 12]. But a sample chosen from the wrong reservoir interval or for example with the degree of heterogeneity not representative of the actual overall reservoir quality, has to be discarded or replaced by a more representative sample. In addition to the rock samples, the fluid samples used during the experiments also need to be representative of the reservoir in situ fluids. These fluid samples could be taken from the

reservoir interval of the well using special sampling techniques or made in the lab by combining different elements (e.g. distilled water, salts, natural gas or CO_2, dead crude etc.) in the right proportions.

After acquiring representative rock and fluid samples and taking into account the reservoir rock and fluid characteristics, technical issues and the intended purpose of running the experiments, the most appropriate laboratory technique should be chosen. For instance, as will be explained in more details later, in order to measure relative permeabilities there are various different experimental methods to follow (e.g. steady-state, unsteady-state and centrifuge) [19–22], each with its own advantages and disadvantages. Furthermore, once a specific experimental method is chosen, towards getting the most, practically possible, accurate results, there are a number of experimental issues which need to be addressed. Some of these experimental issues are discussed below along with their practical remedies.

- *Gravity segregation*: gravity segregation is the stratification of the fluids, with different density values, flowing through a porous media due to the gravity and buoyancy forces. The gravity segregation is expected to be dominant in the medium to high permeability samples where the fluids used have high density contrast [23, 24]. In order to avoid gravity segregation or gravity override, when they are expected to occur and considered unfavourable, the core-holder containing the sample could be oriented vertically [25, 26] or the injection flow-rate could be increased. Equation 3.1 can be used to calculate the Bond Number which is a dimensionless number revealing the ratio of gravitational to capillary forces during a flooding experiment.

$$N_{Bo} = \frac{(\rho_1 - \rho_2).g.l^2}{\sigma} \tag{3.1}$$

Where: N_{BO} = Bond Number, *dimensionless*
ρ = fluid density, subscripts 1 and 2 refer to the displacing and displaced fluids respectively, kg/m^3
l = characteristic dimension of the porous medium pores, m
g = gravity acceleration constant, m/s^2
σ = interfacial tension between the two fluids, N/m

- *Capillary end effect*: as will be discussed later, the most commonly used method to carry out the flooding experiments is the unsteady-state or dynamic displacement method. The commonly used interpretation techniques for this method are based on the theoretical analysis of immiscible displacement due to Buckley and Leverett [27]. In their analysis, Buckley and Leverett [27] ignored the capillary pressure term which could cause the occurrence of the frequently experienced capillary end effect phenomenon [28, 29]. The capillary end effect refers to the saturation anomaly which occurs close to the outlet face of the core-sample subjected to the flooding procedure. If, for example, oil and water are flowing through a water-wet core-sample under steady-state conditions and the sample was initially saturated with water, then one can imagine that both fluids

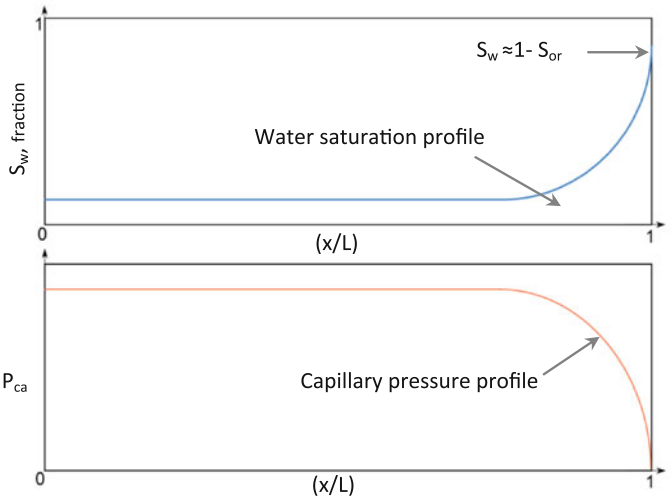

Fig. 3.18 Saturation and capillary pressure profiles along the core-sample length in the presence of the end effect, x = distance from the inlet and L = total length of the sample

immediately after reaching the outlet face of the core-sample would leave the sample at the same pressure. Therefore the capillary pressure inside the sample which is defined by Eq. 3.2 must be zero at the outlet since at the outlet $P_{oil} = P_{water}$.

$$P_{ca} = P_{oil} - P_{water} \tag{3.2}$$

- But since the capillary pressure is a direct function of the saturation, the wetting phase saturation at the outlet has to be equal to the saturation corresponding to zero capillary pressure (i.e. $(1 - S_{or})$). This causes the holdup of water and abrupt increase in water saturation close to the outlet face of the core-sample (Fig. 3.18). Rapoport and Leas [30] introduced a scaling coefficient (Eq. 3.3) for strongly wetted systems which could be adjusted by changing a number of experimental variables (e.g. flow-rate and sample length) to achieve stabilised flow conditions to which the theory formulated by Buckley and Leverett would be applicable.
- The variables of flow-rate and viscosity appearing in Eq. 3.3 can also be seen in Eq. 3.4 which is used to calculate the Capillary Number. The Capillary Number is a dimensionless number showing the relative magnitude of viscous to capillary forces during a flooding procedure.
- In addition to flow-rate and viscosity, length of the porous medium is also included in the scaling coefficient equation. The larger lengths help to reduce the significance of the error caused by the occurrence of the end effect by making

the length of that portion of the sample influenced by the end effect less pronounced compared to the total length of the sample.

$$Scaling\ coefficien\ t = L.u.\mu \tag{3.3}$$

Where: L = total length of the porous media, cm
u = superficial displacement velocity, cm/s
μ = viscosity of the wetting phase, cP

$$N_{ca} = \frac{\mu_1.u}{\sigma} \tag{3.4}$$

Where: N_{Ca} = capillary Number, *dimensionless*
μ_1 = viscosity of the displacing fluid, $Pa.s$
u = superficial displacement velocity, m/s
σ = interfacial tension between the two fluids, N/m

- Rapoport and Leas [30] suggested that in order to have stabilised flooding, the criteria set in Eq. 3.5 needs to be satisfied.

$$L.u.\mu \geq 1 - 5 \tag{3.5}$$

- After his experimental studies Haugen [31] concluded that the criterion set by Rapoport and Leas [30] was too strong when it comes to intermediately wetted systems. He suggested that a scaling coefficient of $L.u.\mu \geq 0.1$ was sufficient to achieve a stabilised flow.
- *Unstable displacement*: when a fluid displaces a more viscous one in a porous media, due to unfavourable mobility ratio (Eq. 3.6), the displacement front may become unstable resulting in viscous fingering instead of a piston-like displacement with a uniform sharp displacement front. As discussed above, flooding experiments need to be conducted at flow-rates that create a sufficiently high differential pressure across the core-sample required to secure a stabilized flow up to the breakthrough and an after breakthrough flow which is not affected by capillary effects. On the other hand, the flow-rate needs to be sufficiently low to avoid unstable displacement and viscous fingering. It is worth noting that the instability and viscous fingering discussed here is merely caused by an unfavourable mobility ratio or high displacement velocity and is different from the instability caused by the presence of severe heterogeneity (e.g. continuous high permeability streaks in a low permeability formation mass) within the porous media.

$$M = \frac{k_{r1}\mu_2}{k_{r2}\mu_1} \tag{3.6}$$

Where: M = end-point mobility ratio, *dimensionless*
μ_1 = viscosity of the displacing fluid, cP
μ_2 = viscosity of the displaced fluid, cP
k_{r1} = end-point relative permeability of the displacing fluid
k_{r2} = end-point relative permeability of the displaced fluid

- Similar to the scaling coefficient introduced by Rapoport and Leas [30] which is used to reduce the capillary pressure effect on the displacement, Peters and Flock [32] also proposed to use the Stability Number (Eq. 3.7) which can be used to adjust the injection flow-rate in order to avoid instability and viscous fingering during the flooding experiments. This stability number was obtained by extending the stability theory of Chuoke et al. [33].

$$N_s = \frac{(M-1).(u-u_c).\mu_1.d^2}{N_w.k_{r1}.\sigma} \tag{3.7}$$

Where: N_s = stability number, *dimensionless*
M = end-point mobility ratio, *dimensionless*
μ_1 = viscosity of the displacing fluid, $(Pa.s)$
u = Superficial velocity, (m/s)
u_c = critical superficial velocity that always insures stable displacement, (m/s)
d = core diameter, (m)
N_w = wettability constant, *dimensionless*
k_{r1} = end point relative permeability of the displacing fluid
σ = IFT, (N/m)

- The critical value of the stability number has been experimentally determined to be 13.56 [31, 32, 34].
- *Composite core-samples*: due to the size limitation imposed by the diameter or length of the whole-cores retrieved from the wells, the length of the laboratory core-plugs are normally short. As mentioned before, the capillary end effect is more pronounced in short core-plugs. Furthermore, the relative accuracy of the volume measurements, while using short samples, is low. To overcome these issues several short core-plugs are usually stacked together to form a long composite core and this longer sample is used during flooding experiments. The underlying assumption is that the individual core-plugs making up the longer composite core are similar both with regards to capillary pressure and relative permeability characteristics. In reality, however, different core-plugs often have different properties and as a result the ordering of the individual core-plugs influences the displacement performance of the composite core.
- Huppler [35] for the first time proposed an ordering criterion which was based on the absolute permeability of the individual core-plugs. He proposed to order

the core-plugs in such a way that the harmonic average permeability of all sections would be as close as possible to the overall average permeability of the composite core. Each section is defined as part of the composite core which could include one or several individual core-plugs. Huppler [35] also suggested putting those sections, which have the closest average permeability to the overall permeability, close to the outlet of the composite core. Apart from the criterion proposed by Huppler [35] it is normal practice within the industry that when constructing a composite core, the core-plugs are arranged in the order of increasing permeability towards the outlet of the core (ascending order) [36]. The argument behind utilising an ascending order is that with the increase in absolute permeability the capillary pressure decreases and therefore putting the high permeability samples at the end would reduce the severity of the above-discussed capillary end effect. Langaas et al. [36] have shown that this is not the case and in fact it is the ordering of the core-plugs in a descending order which helps to reduce the influence of the capillary end effect on displacement experiments.

- As discussed before, Darcy's Law (Eq. 2.2) could be used to describe the one-dimensional flow of two immiscible fluids in porous media. The Leverett J function [37], which is expressed by Eq. 3.8, relates the capillary pressures of different porous media of varying porosity and permeability but of the same lithology. In addition, Eq. 3.8 proposes that capillary pressure is inversely proportional to square root of the permeability of the porous media (Eq. 3.9).

$$J(S_w) = \frac{P_{ca}(S_w)}{\sigma . \cos\theta} \sqrt{\frac{k}{\phi}} \tag{3.8}$$

Where: $J(S_w)$ = Leverett J function
$P_{ca}(S_w)$ = capillary pressure
k = absolute permeability of the porous media
θ = the wettability angle
σ = IFT between the two fluids
ϕ = porosity of the porous media

$$P_{ca}(S_w) \propto J(S_w) \, . \, \sqrt{\frac{\phi}{k}} \tag{3.9}$$

It is also known that, as mentioned before, increasing the flow-rate would decrease the severity of the end effect. So it can be concluded that for a given injection flow-rate, decreasing the permeability increases the differential pressure across the sample and reduces the severity of the capillary end effect. This opposes the common belief that higher permeability core-plugs should be placed close to

the end of a composite core to reduce the severity of the end effect. As Langaas et al. [36] have discussed in their paper, the reason for the decrease in the capillary pressure effect with decrease in the absolute permeability is the fact that an increase in the capillary forces is proportional to $1/\sqrt{k}$ (Eq. 3.9) while an increase in viscous forces is proportional to $1/k$ (Eq. 2.2). Therefore, the ratio of capillary forces to viscous forces decreases with decrease in the sample permeability resulting in the decrease in the severity of the capillary end effect.
One other issue which needs to be addressed while using composite cores is establishing capillary continuity between the faces of the individual core-plugs. Polishing the end faces of the core-plugs would help to reduce the capillary discontinuity between them. In addition, in order to help improve the situation, different researchers have used different bridging material from kaolinite powder to diatomaceous earth and tissue papers [38–41]. It has been shown that by utilising these two techniques reasonable capillary continuity could be achieved between adjacent core-plugs in a composite core.

3.4.5.2 Methodologies and Interpretation Techniques

The core-flooding experiments which are conducted to measure relative permeabilities can be performed in the lab using three different methods, namely, steady-state, unsteady-sate or dynamic displacement and centrifuge. As will be explained in more detail later, among these three methods the unsteady-state is the one that theoretically mimics what in realty occurs during fluid displacement in an underground reservoir. Presented below is a description of each of these methods along with a discussion of their pros and cons.

- *The steady-state method*: in this method relative permeabilities can be measured directly. In other words, the saturations, flow-rates and pressure gradients are measured during the experiment and then Darcy's equation (Eq. 2.2) could be used directly to calculate the relative permeabilities for each fluid phase. This method involves the simultaneous injection of the two immiscible phases through the sample at a number of fixed metered fractional flows (Eqs. 3.10 and 3.11).

$$f_1 = \frac{q_1}{q_1 + q_2} \tag{3.10}$$

$$f_2 = \frac{q_2}{q_1 + q_2} \tag{3.11}$$

Where: f_1 = fractional flow of fluid 1
f_2 = fractional flow of fluid 2
q = injection flow-rate

- Generally, a steady-state experiment starts with the sample fully saturated with one of two fluids (e.g. the wetting phase in a drainage experiment) then in a series of consecutive steps, gradually the fraction flow of the other fluid is increased until the last step where only the latter fluid is injected. Each step is allowed to continue until the state-state conditions are reached (i.e. the inlet flow-rates are equal to the outlet flow-rates and the differential pressure across the sample is constant and stable). Using the steady-state method, the relative permeabilities could be measured for the entire moveable fluid saturation range. The estimation of saturation during the experiment can be done through various methods including the material balance technique, X-ray CT scanning method, NMR method, resistivity measurement etc.
- Various steady-state techniques used to measure relative permeabilities include the Penn-State method, the Hassler method, the single-sample dynamic method, the stationary fluid method, the Hafford method and the modified Penn-State method [22]. The main difference between these various methods is the way capillary equilibrium is established between fluids in order to reduce or eliminate the end effect.
- A list of the issues associated with the steady-state method includes:
  - Under steady-state conditions it is assumed that the saturation profile along the sample is uniform. This may not be a valid assumption if gravitational or capillary forces are dominant during displacement.
  - The steady-state procedure does not in reality represent the exact process which occurs in an underground reservoir. In other words, there is no actual flood process (i.e. displacement of one fluid by the other) involved and the saturation shock front observed during usual reservoir flooding procedure, does not form.
  - The steady-state conditions are time-consuming and costly to achieve. It could take up to several hours to several days to attain the desired equilibrium conditions at each saturation level.
  - Nevertheless, with the advances made in the technology and automation of many of the tasks involved, some of the above-mentioned problems have reduced.
  - *The unsteady-state* (*USS*) *method*: unlike stead-state this method is an indirect method of the relative permeability measurement. The Buckley-Leverett theory for linear displacement of immiscible and incompressible fluids is the basis of all the data analysis and interpretation techniques used for this method [42]. Because of the considerably less time required, this method is the most widely used, yet it is the one most prone to measurement and interpretation errors [19]. The USS or dynamic displacement method normally starts with the sample fully saturated with one fluid (e.g. the wetting phase in a drainage experiment). While only one fluid is flowing through the sample, the differential pressure across the sample is measured. This value is a key parameter while utilising various interpretation techniques to calculate the relative permeabilities. Then, the second displacing phase is injected

through the sample at an appropriate flow-rate to displace the first phase. During this time the production flow-rates of the two phases and the differential pressures across the sample is monitored and recorded against time and the injected volumes. The USS experiments are normally conducted at a constant injection flow-rate but under certain circumstances (e.g. when the fluids are considered to be highly compressible) a constant pressure procedure needs to be followed.

- There are various mathematical [43], graphical [44] and numerical history matching [45] techniques to calculate the relative permeability values from USS experiments. The majority of these interpretation techniques ignore the effect of capillary forces on the displacement. A list of issues associated with the USS method are:
  - The previously explained capillary end effect is commonly observed during USS experiments.
  - Viscous fingering and instabilities, gravity segregation and also channelling in heterogeneous samples could occur which are practically difficult to monitor and account for properly.
  - Unless the mobility of the displacing fluid is much higher than the in situ displaced fluids (i.e. $M \gg 1$(Eq. 3.6)), the time period between the breakthrough (BT) until the complete flood-out is very short and therefore relative permeabilities can only be calculated for a small range of moveable saturations.
  - Accurate measurement of the breakthrough (BT) time is vital for many interpretation techniques used to calculate the relative permeabilities. Therefore even a small mistake in detecting the BT time can render the results of the calculations not representative of the properties of the bulk of the sample used.
- A number of the above mentioned issues can be resolved by taking extra measures before and during a USS experiment. However, some of them are not avoidable (e.g. the short time between BT and complete flood-out).
- *The centrifuge method*: this method is an unsteady-state technique and similar to the USS method as an indirect method to measure the relative permeabilities. In the centrifuge method, small pre-saturated samples are held usually without confining pressure in centrifuge buckets and rotated at elevated angular speed. During the rotation, the sample in situ fluids are exposed to a known centrifugal force and the rate of liquid production is measured using calibrated graduated tubes. The relative permeabilities are then calculated using the test data through mathematical methods [46]. Usually the sample is surrounded by the displacing phase so any spontaneous imbibition occurs prior to the controlled centrifugation. The Hagoort's method [47] is the basis for all the analysis performed in the centrifuge method. There are a number of assumptions involved in the Hagoort's method [47] including negligible capillary effects, infinite incoming phase mobility, an instantaneous start-up, and constant gravitational effects in

the sample [20], which may not be justified in the actual experiments carried out in the lab. One major drawback of the centrifuge method is the fact that it only gives the relative permeabilities of the displaced phase. Nevertheless, it is claimed that the centrifuge method is not affected by the viscous fingering problem observed the during dynamic displacement method and it is the best method to simulate the gravity drainage process [42, 47].

It is worth noting that in addition to the above-described laboratory methods used to generate the relative permeabilities, there are various other techniques through which relative permeabilities can be calculated. Empirical techniques using the models presented in the literature, of which a comprehensive review is presented by Honarpour et al. [22], are useful sometimes to avoid the difficulties involved in the lab measurements. Using empirical techniques is not the best substitute for the lab measured data, but it is often used for extrapolation of the limited laboratory data. Relative permeabilities can also be calculated using the available production history of the reservoir and its fluid properties [22, 42]. Pressure transient testing is another potential method for calculating the in situ effective permeabilities provided that it is used in combination with accurate down-hole flow measurement techniques [42].

3.4.5.3 The Core-Flooding Procedure

A series of steps were followed in a basic unsteady-state CO_2-brine drainage core-flooding experiment in which brine was displaced by CO_2. This experiment represented the process which takes place when CO_2 is introduced into the subsurface storage aquifer for the first time. The steps outlined below were followed once the core-samples had been already cut and cleaned and then dried in the oven before their dimensions were measured as well as their porosity values. Finally, after having the core-samples saturated with de-aerated brine, NMR measurements were carried out on them and again, like before, left in the oven to dry out.

1. *Loading the core-sample into the biaxial core-holder*:

   1.1 The cleaned and dried core-sample was inserted into an adequate length of heat-shrink Teflon sleeve and then the sleeve was heated using a heating gun to shrink and grab the sample. Then the sample was wrapped in a layer of aluminium foil and the wrapped sample was inserted into a Viton sleeve while placed on the core-holder's inlet end plug (i.e. the fixed end plug) (Fig. 3.19). The sleeve dimensions are engineered to perfectly fit the outer diameter of the sample while leaving a small annular space between the outer diameter of the sleeve and the inner diameter of the core-holder.

   1.2 The assembly was inserted into the core-holder body and the inlet end cap was screwed into place. After ensuring the sample inside the combination sleeve was resting firmly on the fixed end plug the core-holder's outlet end plug (i.e. the adjustable floating end plug) was inserted into the other end of

Fig. 3.19 **a** composite core sample placed inside a heat-shrink sleeve and the fixed end plug is inserted into one end of the sleeve. **b** The core-sample (after being wrapped in the aluminium foil) together with the fixed end plug are inserted into a long Viton sleeve. **c** The fixed end plug inserted into the sleeve assembly containing the core-sample beside the adjustable floating end plug

the sleeve and then the end cap was tightened in place. The floating arrangement allows the end plug to adjust its position to the length of the core-sample and the core sample would fit perfectly between the two end plugs (Fig. 3.19).

1.3 The small annular space between the outer diameter of the Viton sleeve and the inner diameter of the core-holder body was filled slowly with high quality hydraulic oil using a hand-pump. The oil was injected into the annulus from the core-holder's lower overburden pressure port so that air would be expelled from the upper port (Fig. 3.7). Once the oil was seen coming out of the upper port, the annulus was full of hydraulic oil and the port was capped.

1.4 Using the hand-pump, the hydraulic oil injection was continued to raise the overburden pressure to the desired pressure. To make sure that the core-sample was fitted properly between the end-plugs, the inlet and outlet fluid ports of the core-holder were left open. If the fit was not proper, the overburden fluid would leak through and come out of the ports and easily detected. While increasing the overburden pressure gradually, care was taken not to increase the overburden pressure above the desired reservoir net effective pressure, otherwise the sample could be potentially deformed

or damaged and not being representative of the desired reservoir conditions anymore.

As mentioned before, there was a gas cushion injected on top of the overburden pressure cell (Fig. 3.2) to provide a stable and constant overburden pressure into the core-holder. It should be noted that during all the above and following steps, the temperature inside the oven, where the fluid bottles, separator, the core-holder and the collection pumps' reservoirs are located, was maintained at a constant desired reservoir temperature. Once the overburden pressure became stable and equal to reservoir net effective pressure the inlet and outlet fluid ports of the core holder were connected to their corresponding lines and the sample was ready to be evacuated of air. It is worth noting that on both sides of the core-holder there were two 3-Way- 2-Stem manifold valves installed which would allow access to either the core-holder or the rest of the injection lines while the other could be isolated.

2. *Evacuating the sample of air*:

   2.1 While the core-holder inlet and outlet were connected to their corresponding lines and isolated from the rest of the core-flooding rig, low pressure CO_2 gas was passed through the core-sample for 10–15 min to displace and replace the air trapped inside the pores of the sample. The CO_2 can be evacuated much more effectively from the sample under vacuum and remaining CO_2 gas, if any, can be dissolved readily in dead brine which would be injected into the sample later.
   2.2 After the CO_2 flush, the core-holder inlet and outlet valves were closed and then the core-holder assembly was connected to the vacuum line and the inlet valve was opened. The vacuum was maintained for 24 h. During this time, to monitor the vacuum process, pressure inside the sample was under constant observation.
   2.3 At the end of the vacuum period the inlet valve was closed and disconnected from the vacuum line.

3. *Saturating the sample with the dead brine*:

   3.1 After vacuuming the sample, a portable fluid sample bottle was cleaned, vacuumed and then filled with the de-aerated synthetic formation brine. Then it was connected to the inlet line of the core-holder and the inlet valve was opened letting the dead brine into the pre-evacuated sample and lines.
   3.2 The injection of the de-aerated brine was started in order to increase the sample pore pressure to the reservoir in situ pore pressure. Meanwhile, the overburden pressure was also raised at the same pace as the pore pressure to full reservoir in situ overburden pressure. This way both pore and overburden pressures would reach the full in situ values at the same time and the sample would never be exposed to pressures exceeding the reservoir in situ net effective pressure.

3.3 Once both pore and overburden pressures were equal to the desired in situ values, in order to have the sample fully saturated with brine, the pore fluid injection was left under the constant pressure procedure using one of the injection pumps for 48 h while the overburden pressure was monitored for any possible fluctuations and adjusted accordingly. The long 48 h saturation time under reservoir in situ P–T conditions was thought to be necessary to ensure that the sample became fully saturated with brine and any CO_2 or air left inside the small pores would be dissolved into the dead brine. Furthermore, on top of the previous minimum 2 weeks aging time inside the desiccator, this could serve as an additional aging period to establish adsorption equilibrium and restore the wettability of the sample, if changed, before the start of the flooding test.

4. *Displacing the dead brine with CO_2-saturated brine*:

4.1 After the 48 h saturation period, the core-holder outlet valve would be opened and the dead brine injection into the core-sample began with appropriate injection flow-rate, which depended on the sample permeability. This was to displace the saturating brine inside the sample which could have dissolved air or CO_2, if any, left inside the sample after evacuation. The fresh dead brine injection was continued for 3 sample pore-volumes (PV) or until stable differential pressure across the sample was achieved. This stabilised differential pressure could be used to calculate the sample permeability under in situ reservoir conditions. It is worth noting that, as it was mentioned before, the core-holder out-flow fluids were produced into the separator which operated at reservoir P–T conditions and the separator pressure was maintained constant by using the gas volume contained inside the gas collection pump. Therefore, as the dead brine was being produced into the separator the dissolution of CO_2 into the freshly produced brine was easily noticeable by monitoring the gas volume inside the gas collection pump.

4.2 After closing the corresponding valves, the core-holder and the lines were isolated from the dead brine injection bottle so it could be removed. After the disconnection of the dead brine bottle the sample pore pressure was monitored for any possible pressure drops, which could cause evolution of CO_2 during the subsequent injection of the CO_2-saturated brine. Any pressure drop is a sign of leakage in the lines or valves which needed to be fixed and then the pressure restored to reservoir pressure before proceeding further.

4.3 Through opening the related valves, the CO_2-saturated brine injection began into the core sample at constant flow-rate under the desired reservoir temperature, pore pressure and overburden pressure conditions. The CO_2-saturated brine injection continued until steady-state conditions were achieved. Here, the steady-state conditions mean no more dissolution of CO_2 into the brine as it was being produced into the separator, which was noticeable in the case of the dead brine production, and establishment of

the stable and constant differential pressure across the sample. Once steady-state conditions were reached the differential pressure across the sample was measured. This is an important parameter which could be used during the interpretation of the experimental data.

5. *Displacing the CO_2-saturated brine with supercritical CO_2 (drainage)*:

   5.1 After reaching the steady-state conditions, the core-sample was ready for the main drainage displacement process. After isolating the brine bottle from the injection line by closing the valve on its top, the volume readings of all the injection and collection pumps were recorded. These values together with the system dead volumes would be required later to work out the sample in situ saturations during and at the conclusion of the flooding experiment using a material balance technique.

   5.2 After, if necessary, adjusting the pressure inside the CO_2 bottle, the valve on top of the bottle was opened letting the CO_2 injection into the sample to begin. The CO_2 injection began at an appropriate constant flow-rate. The differential pressure across the sample was monitored to detect the CO_2 breakthrough time as soon as it happened. After breakthrough the CO_2 and brine production rates would change quickly and the value of the parameters inside the PID controller modules for the gas and brine collection pumps needed to be adjusted accordingly. Therefore, the detection of breakthrough time was vital for the stability of the fluid interfaces inside the separator. The CO_2 injection continued until the steady-state conditions were achieved. Here, the steady-state conditions mean no more brine production from the sample and having stable and constant differential pressure across the sample.

   5.3 Generally, once the steady-state conditions were reached, the sample would be subjected to a short period of so called "bump flow" which means abrupt increase in the injection flow-rate [21, 30, 48]. This was necessary to establish the end point relative permeabilities and verify the presence of any end effects induced by possible capillary pressure discontinuity, which is normally more pronounced in the case of high permeability samples. After the bump flow, in order to record the stabilised, and possibly reduced post-bump differential pressure across the sample, the flow-rate was restored to its pre-bump value.

During the above procedure certain parameters, which would be used during the interpretation and data analysis, needed to be recorded against time at adequate time steps. These parameters included core-holder inlet and outlet pressures, the brine and CO_2 production and/or injection volumes and flow-rates, breakthrough time, stabilised condition parameters (e.g. terminal flow-rate and differential pressure).

In order to achieve the objectives of this research, the basic flooding procedure described above was slightly modified and/or extended to several subsequent imbibition and drainage cycles. In the following section these variants of the basic flooding procedure are described:

As was discussed before, saturation history (i.e. hysteresis phenomenon) can have strong effects on multiphase behaviour of the porous media when subjected to the flooding process. In order to investigate the potential effects of the saturation history, flooding procedure followed for the above single stage drainage process was extended to several subsequent cyclic imbibition and drainage processes. The following steps were performed in addition to the steps involved in carrying out the basic flooding experiment described above. To show that these subsequent steps follow the above numbered procedure, the numbering starts from 6.

6. *Displacing the sample with the CO_2 saturated brine (imbibition)*:

   6.1 After the conclusion of the primary drainage stage the core-sample was ready for the first imbibition displacement process. After isolating the CO_2 bottle from the injection line and, if required, adjusting the pressure inside the brine bottle to the desired reservoir pressure, the volume readings of all the injection and collection pumps were recorded for the same reason stated previously in Item 5.1 (page xxx).

   6.2 By opening relevant valves, the injection of the CO_2-saturated brine into the sample began at a constant flow-rate. For the same reason stated in Item 5.2 (page xxx) the differential pressure across the sample was closely monitored to detect the brine breakthrough time as soon as it happened. The brine injection continued until the steady-state conditions were achieved. Like before, here the steady-state conditions mean no more CO_2 production from the sample and having stable and constant differential pressure across the sample.

   6.3 For the same reason stated for the primary drainage stage, once steady-state conditions were reached, the sample was subjected to a short period of bump flow. Since the viscosity of the displacing phase (brine) was much higher than the displaced phase (CO_2) conducting a "bump" flow was thought to be unnecessary.

Similar to the primary drainage stage, during the above steps, data logging was performed on all the parameters expected to be required during the subsequent data analysis and interpretation tasks.

After finishing the steps described under Items 5 (page xxx) and 6 (page xxx), the sample had undergone a drainage cycle followed by a subsequent imbibition cycle. In order to investigate further the effect of the cyclic CO_2-brine injection, the sample was subjected to a minimum of three more pairs of consecutive drainage and imbibition cycles. The steps involved in each drainage cycle were similar to those explained under Item 6 (page xxx) and likewise, the steps involved in each subsequent imbibition cycle were similar to those explained under Item 6 (page xxx).

At the conclusion of the experiment, the core-holder was depressurised and the sample was removed. As was mentioned before, in order to evaluate the possible changes in the properties of the sample caused by the cyclic flooding process, porosity and dimension measurements were performed on the oven-dried sample

and then NMR measurements were carried out after fully saturating the sample with de-aerated brine.

As was discussed previously, subsurface disposal of CO_2 is accompanied by a rise in the in situ reservoir pore pressure. As a result, the reservoir net effective pressure (Eq. 3.12) decreases. As discussed in the previous sections of this chapter, those rock properties considered dependant on the effective pressure are expected to be altered by this change in the in situ stress field. In order to investigate these alterations, either qualitatively or quantitatively or both, the experimental procedures explained under Items 55 (page xxx) to 6 (page xxx) were repeated again but this time under reduced overburden pressure.

$$P_{net\,effective} = P_{overburden} - P_{pore} \tag{3.12}$$

To be able to compare the results of these new experiments to the original experiments conducted under the full reservoir overburden pressure, after completing the required analysis on them, the same samples used during the previous tests were used again.

A third type of core-flooding experiment was designed to investigate the effect of the presence of a third phase residual saturation on the displacement performance during deep CO_2 disposal. In order to achieve this objective, an additional experimental stage was conducted before commencing the procedure explained under Item 5 (page xxx). After saturating the sample with the CO_2-saturated brine (the procedure explained under Item 4 on page xxx) the following procedure was followed to establish the residual methane saturation before commencing the usual cyclic CO_2-brine injection.

1. *Establishing the residual methane saturation*:

(a) After displacing the dead brine with the CO_2-saturated brine and reaching the steady-state conditions, the methane bottle pressure was, if required, adjusted to the full reservoir in situ pressure. Then, for the same reason stated before, all the volume readings of the injection and collection pumps were recorded.
(b) By opening the relevant valves, methane injection into the sample (drainage process) was started at a constant flow-rate. As discussed before, in order to detect the exact methane breakthrough time, which was vital for adjusting the PID controller parameters within the collection system, relevant experimental parameters were closely monitored. The methane injection was continued until desired steady-state conditions were achieved.

After completing this first drainage cycle, the sample was subjected to a subsequent imbibition process by injection of CO_2-saturated brine to displace the methane.

(c) After reaching the steady-state conditions at the end of the methane injection, the pressure inside bottle containing the CO_2-saturated brine was, if required, adjusted to full reservoir in situ pressure. Then all the volume readings of the injection and collection pumps were recorded.

(d) After isolating the gas bottle from the injection line, by opening the relevant valves, brine injection into the sample was started at constant flow-rate. Like before, in order to detect the exact brine breakthrough time, relevant experimental parameters were closely monitored. The injection of the CO_2-saturated brine was continued until the desired steady-state conditions were achieved.

For the rest of the experiment, the normal cyclic CO_2-brine injection procedures, which were explained under Items 5 (page xxx) and 6 (page xxx), were followed. Like before, all of the experimental parameters which would be used during data analysis and interpretations were recorded during all of the above described procedures.

It is worth noting that, in order to avoid extremely time consuming procedures, the previously prepared CO_2-saturated brine was again used to displace methane, not the brine, which would be ideally saturated with methane. Since the brine was fully saturated with CO_2 already it was assumed that under such conditions the solubility of the methane in the brine would be negligible.

References

1. NIST (2010) Thermophysical properties of fluid systems. http://webbook.nist.gov/chemistry/fluid/, US National Institute of Standards and Technology. Accessed 17 June 2010
2. Zhenhao Duan Research Group (2010) Interactive online models. http://www.geochem-model.org/models.htm, Institute of Geology and Geophysics, Chinese Academy of Sciences. Accessed 25 June 2010
3. Leet LD, Judson S (1971) Physical geology. Prentice-Hall, New Jersey
4. Sharma S, Cook P, Berly T, Lees M (2009) The CO_2CRC otway project: overcoming challenges from planning to execution of Australia's first CCS project. Energy Procedia 1:1965–1972
5. Knackstedt MA, Dance T, Kumar M, Averdunk H, Paterson L (2010) Enumerating permeability, surface areas, and residual capillary trapping of CO_2 in 3D: digital analysis of CO_2CRC otway project core, SPE 134625, SPE annual technical conference and exhibition, Society of Petroleum Engineers, Florence, Italy
6. Spencer L, Xu Q, LaPedalina F, Weir G (2006) Site characterization of the Otway Basin Storage Pilot in Australia. Proceeding of the 8th international conference on greenhouse gas control technologies, Trondheim, Norway
7. Gluyas J, Swarbrick R (2004) Petroleum geoscience. Blackwell Publishing, Oxford
8. Byrne M, Patey I (2004) Core sample preparation—an insight into new procedures. International symposium of the society of core analysts, Abu Dhabi, UAE
9. Chen J, Hirasaki GJ, Flaum M (2006) NMR wettability indices. Effect of OBM on wettability and NMR responses. J Pet Sci Eng 52:161–171
10. Fleury M, Deflandre F (2003) Quantitative evaluation of porous media wettability using NMR relaxometry. Magn Reson Imaging 21:385–387
11. Anderson WG (1986) Wettability literature survey–Part 1: rock/oil/brine interactions and the effects of core handling on wettability: SPE 13932. SPE J Pet Technol 38:1125–1144
12. Wendell DJ, Anderson WG, Meyers JD (1987) Restored-state core analysis for the hutton reservoir: SPE 14298. SPE Form Eval 2:509–517
13. Mungan N (1966) Certain wettability effects in laboratory waterfloods: SPE 1203. SPE J Pet Technol 18:247–252

14. Coates GR, Xiao L, Prammer MG (1999) NMR logging-principles and applications. Halliburton Energy Services, Houston
15. Clennell B, Raven M, Borysenko A, Sedev R, Dewhurst D (2006) Shale petrophysics: electrical, dielectric and nuclear magnetic resonance studies of mudrocks and clays. SPWLA 47th annual logging symposium, Society of Petrophysicists and Well Log Analysts, Veracruz, Mexico
16. Chen Q, Kinzelbach W, Ye C, Yue Y (2002) Variations of permeability and pore size distribution of porous media with pressure. J Environ Qual 31:500–505
17. Ennis-King J, Paterson L (2007) Coupling of geochemical reactions and convective mixing in the long-term geological storage of carbon dioxide. Int J Greenh Gas Control 1:86–93
18. Ennis-King J, Paterson L, Gale J, Kaya Y (2003) Rate of dissolution due to convective mixing in the underground storage of carbon dioxide. Greenhouse gas control technologies—6th international conference, Kyoto, Japan
19. Ali JK (1997) Developments in measurement and interpretation techniques in coreflood tests to determine relative permeabilities, SPE 39016. Latin American and Caribbean petroleum engineering conference, Society of Petroleum Engineers, Rio de Janeiro, Brazil
20. Boukadi FH, Bemani AS, Babadagli T (2005) Investigating uncertainties in relative permeability measurements. Energy Sources Part A: Recovery Util Environ Eff 27:719–728
21. Heaviside J, Black CJJ (1983) Fundamentals of relative permeability: experimental and theoretical considerations, SPE 12173. SPE annual technical conference and exhibition, Society of Petroleum Engineers of AIME, San Francisco, California
22. Honarpour M, Koederitz L, Harvey AH (1986) Relative permeability of petroleum reservoirs. CRC Press, Boca Raton
23. Craig FFJ, Sanderlin JL, Moore DW, Geffen TM (1957) A laboratory study of gravity segregation in frontal drives: SPE 676-G. Pet Trans AIME 210:275–282
24. Guo Y Nilsen V, Hovland F (1991) Gravity effect under steady-state and unsteady-state core flooding and criteria to avoid it. The second society of core analysts european core analysis symposium London, UK
25. Bed Jr BA, Nunes CS (1984) Velocity and gravity effects in relative permeability measurements. MSc theses, The Department of Petroleum Engineering Stanford University
26. Kinzel LD, Hill GA (1989) Experimental study of dispersion in a consolidated sandstone. Can J Chem Eng 67:39–44
27. Buckley SE, Leverett MC (1942) Mechanism of fluid displacement in sands: SPE 942107. Pet Trans AIME 146:107–116
28. Donnez P (2007) Essentials of reservoir engineering. Editions Technip, Paris
29. Huang DD, Honarpour MM (1998) Capillary end effects in coreflood calculations. J Pet Sci Eng 19:103–117
30. Rapoport LA, Leas WJ (1953) Properties of linear waterfloods: SPE 213-G. Pet Trans AIME 198:139–148
31. Haugen J (1990) Scaling criterion for relative permeability experiments on samples with intermediate wettability. Society of core analysts symposium, London, UK
32. Peters EJ, Flock DL (1981) The onset of instability during two-phase immiscible displacement in porous media: SPE 8371. SPE J 21:249–258
33. Chuoke RL, van Meurs P, van der Poel C (1959) The instability of slow, immiscible, viscous liquid-liquid displacements in permeable media: SPE 1141. Pet Trans AIME 216:188–194
34. Peters EJ, Khataniar S (1987) The effect of instability on relative permeability curves obtained by the dynamic-displacement method: SPE 14713. SPE Form Eval 2:469–474
35. Huppler JD (1969) Waterflood relative permeabilities in composite cores. J Pet Technol 21:539–540
36. Langaas K, Ekrann S, Ebeltoft E (1998) A criterion for ordering individuals in a composite core. J Pet Sci Eng 19:21–32
37. Leverett MC (1941) Capillary behavior in porous solids: SPE 941152. Pet Trans AIME 142:152–169

38. Abu-Khamsin SA, Ayub M, Al-Marhoun MA, Menouar H (1993) Waterflooding in a tarmat reservoir laboratory model. J Pet Sci Eng 9:251–261
39. Hinkley RE, Davis LA (1986) Capillary pressure discontinuities and end effects in homogeneous composite cores: effect of flow rate and wettability, SPE 15596. SPE annual technical conference and exhibition, Copyright 1986, Society of Petroleum Engineers, Inc, New Orleans, Louisiana
40. Øyno L, Uleberg K, Whitson CH (1995) Dry gas injection in fractured chalk reservoirs–An experimental approach. Society of Core Analysts Symposium, San Francisco, CA, USA
41. Zekri AY, Almehaideb RA (2006) Relative permeability measurements of composite cores: An experimental approach. Pet Sci Technol 24:717–736
42. Honarpour M, Mahmood SM (1988) Relative-permeability measurements: an overview: SPE 18565. SPE J Pet Technol 40:963–966
43. Johnson EF, Bossler DP, Naumann VO (1959) Calculation of relative permeability from displacement experiments. Pet Trans AIME 216:370–372
44. Jones SC, Roszelle WO (1978) Graphical techniques for determining relative permeability from displacement experiments: SPE 6045. SPE J Pet Technol 30:807–817
45. Archer JS, Wong SW (1973) Use of a reservoir simulator to interpret laboratory waterflood data: SPE 3551. SPE J 13:343–347
46. Van Spronsen E (1982) Three-phase relative permeability measurements using the centrifuge method, SPE 10688. SPE Enhanced oil recovery symposium, Copyright 1982, Society of Petroleum Engineers of AIME, Tulsa, Oklahoma
47. Hagoort J (1980) Oil recovery by gravity drainage: SPE 7424. SPE J 20:139–150
48. Bennion B, Bachu S (2008) Drainage and imbibition relative permeability relationships for supercritical CO_2/brine and H_2S/brine systems in intergranular sandstone, carbonate, shale, and anhydrite rocks: SPE 99326. SPE Reserv Eval Eng 11:487–496

Chapter 4
Experimental Results

4.1 Introduction

As discussed in, in order to achieve the objectives of this study various types of laboratory work were conducted during the course of development of this research program. The laboratory work carried out ranged from sample preparation and routine core analysis to core-flooding tests and NMR measurements. This chapter presents in details the results of the various experimental work performed.

This chapter starts with presenting some details regarding the P–T conditions of the tests conducted. This is followed by a presentation of the basic physical properties of the core samples used. The third part presents the results of the core-flooding experiments carried out and the chapter ends with an outline of the results of NMR measurements conducted on a number of the samples before and after they underwent the flooding procedures.

4.2 P–T Conditions for the Experiments

Table 4.1 lists the values of the in situ reservoir condition parameters used during the experiments which were carried out under high pressure and temperature. The pressure, temperature and salinity values used were the same as the in situ reservoir conditions of the Naylor Field of the Otway Basin Project (OBP). Unit C of the Waarre Formation in the Naylor Field, which has been chosen as the target for the first phase of CO_2 injection, is located at a depth of about 2,050 m. This is the depth where all the core samples tested came or assumed to have come from. The values of the pore pressure, temperature and salinity of the formation water were extracted from the CO2CRC's internal geology and reservoir engineering reports while the overburden pressure was calculated using Eq. 4.1 and an overburden pressure gradient of 1 psi/ft, as a typical average value suggested in the literature [1, 2].

A. Saeedi, *Experimental Study of Multiphase Flow in Porous Media during CO_2 Geo-Sequestration Processes*, Springer Theses, DOI: 10.1007/978-3-642-25041-5_4,

Table 4.1 Reservoir P–T conditions during the experiments (when applicable)

Reservoir parameter	Value
Pore pressure (psi)	2,580
Overburden pressure (psi)	6,725
Reservoir temperature (°C)	83
Formation water salinity (ppm NaCl)	20,000

Table 4.2 Characteristics of the core samples used for the experiments

Item no.	Group no.	Sample ID	Length (cm)	Diameter (cm)	Lithology	Porosity (%)	Permeability (mD)
1	1	CO2CRC-1-V	9.79	3.88	Sandstone	20.01	751.1
2	1	CO2CRC-2,3-H*	9.18	3.89	Sandstone	17.31	788.3
3	1	CO2CRC-7-V	9.17	3.88	Sandstone	21.35	1,899.6
4	1	CO2CRC-11,14-H*	8.23	3.88	Sandstone	22.03	3,409.8
5	1	CO2CRC-36-V	8.62	3.88	Sandstone	17.26	108.2
6	1	CO2CRC-39,42-H*	9.1	3.87	Sandstone	15.49	252.6
7	2	BS-1-H	8.42	3.72	Sandstone	17.97	234.6
8	2	BS-2-H	8.46	3.73	Sandstone	18.4	141.13
9	2	BS-3-V	8.35	3.73	Sandstone	18.64	194.4
11	3	DB-1-H	7.18	3.81	Sandstone	16.01	14
12	3	DB-2-V	7.04	3.8	Sandstone	16.19	12.2
13	4	CL-40,68-H*	9.8	3.84	Sandstone	14.42	123.5

* Composite core samples (i.e. the core sample is made up of two separate short core-plugs)

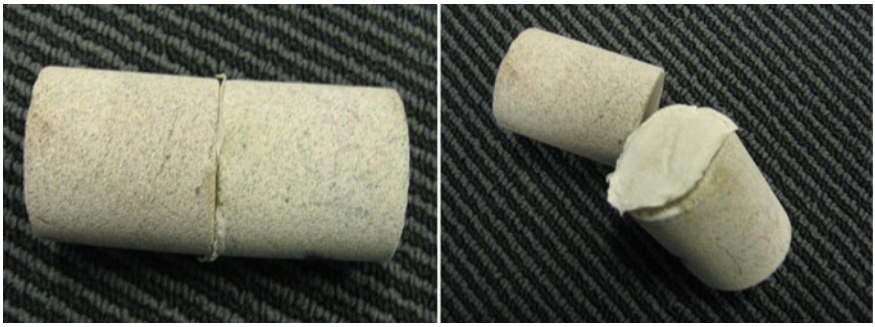

Fig. 4.1 A composite core sample after undergoing a core-flooding test and the two layers of the lint-free tissue paper between them

$$P_{overburden} = Gr_{overburden} \times Depth \tag{4.1}$$

Table 4.3 Summary of the cyclic CO_2-brine flooding tests conducted on various samples ($IFT_{CO2\text{-}brine} = 30$ dyne/cm, contact angle = 0)

Test no.	Sample name	Pore vol (cc)	k (mD)	Overburden pressure (psi)	Pore pressure (psi)	CO_2 inj. flow-rate (cc/hr)	Water inj. flow-rate (cc/hr)	Capillary number (Nc)	Rapoport scaling coefficient
1	CO2CRC-1-V	23.213	751.10	6,725	2,580	300	250	8.93E − 05	0.157
2	CO2CRC-2,3-H	18.859	788.30	6,725	2,580	300	250	8.88E − 05	0.147
3	CO2CRC-7-V	23.1	1,899.60	6,725	2,580	300	300	8.93E − 05	0.147
4	CO2CRC-11, 14-H	21.5	3,409.80	6,725	2,580	300	300	8.93E − 05	0.132
5	CO2CRC-36-V	17.564	108.22	6,725	2,580	250	200	7.44E − 05	0.115
6	CO2CRC-39, 42-H	16.49	252.60	6,725	2,580	250	200	7.48E − 05	0.122
7	BS-1-H	16.476	234.60	6,725	2,580	300	200	9.71E − 05	0.147
8	BS-2-H	17.27	151.1	3,500	2,580	300	200	9.66E − 05	0.147
9	BS-2-H	17.09	145.99	5,000	2,580	300	200	9.66E − 05	0.147
10	BS-2-H	16.975	141.13	6,725	2,580	300	200	9.66E − 05	0.147
11	BS-2-H	16.975	141.13	6,725	2,580	120	100	3.86E − 05	0.059
12	BS-3-V	17.002	194.36	6,725	2,580	300	200	9.66E − 05	0.145
13	DB-1-H	13.135	14.00	6,725	2,580	150	100	4.63E − 05	0.060
14	DB-1-H	13.135	14.00	6,725	2,580	200	150	6.17E − 05	0.080
15	DB-2-V	12.894	12.20	6,725	2,580	150	100	4.65E − 05	0.059
16	CL-40,68-H	16.725	123.50	6,725	2,580	300	200	9.11E − 05	0.161

Table 4.4 End-point brine saturation at the end of each injection cycle during the cyclic CO_2-brine injection experiments

Test no.	Sample name	End-point brine saturation (%)						
		1st Drain.	*1st Imb.*	*2nd Drain.*	*2nd Imb.*	*3rd Drain.*	*3rd Imb.*	*4th Drain.*
1	CO2CRC-1-V	44.7	82.2	46.1	82.2	45.6	82.5	44.6
2	CO2CRC-2,3-H	50.1	80.4	51.2	80.3	50.8	80.7	51.1
3	CO2CRC-7-V	46.9	90.6	46.4	91.2	45.8	90.2	46.3
4	CO2CRC-11,14-H	52.4	91.0	52.3	88.8	51.2	90.3	50.2
5	CO2CRC-36-V	50.8	79.1	51.5	78.9	52.2	79.0	50.4
6	CO2CRC-39,42-H	54.6	80.2	–	–	–	–	–
7	BS-1-H	44.9	78.5	44.7	79.0	44.1	78.8	44.8
8	BS-2-H	49.5	85.2	48.9	85.3	48.5	84.3	48.2
9	BS-2-H	47.0	82.0	47.4	83.1	47.3	82.5	47.2
10	BS-2-H	44.8	80.6	44.0	80.4	44.4	81.1	44.9
11	BS-2-H	49.5	81.4	49.4	81.3	49.4	81.3	49.3
12	BS-3-V	45.8	76.5	45.1	76.4	45.4	76.7	45.6
13	DB-1-H	60.5	73.2	58.4	71.4	57.7	72.2	57.9
14	DB-1-H	59.0	73.8	–	–	–	–	–
15	DB-2-V	64.6	71.8	–	–	–	–	–
16	CL-40,68-H	51.9	78.1	48.2	78.7	48.4	79.2	49.2

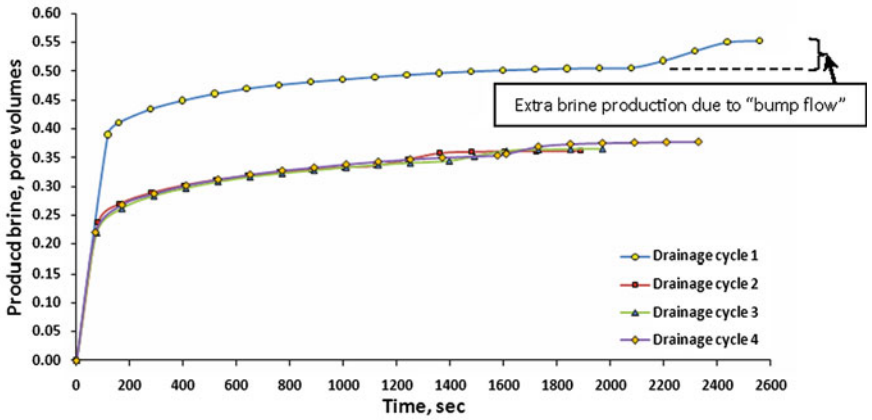

Fig. 4.2 Brine production versus time for the four drainage cycles conducted in test number 1 on sample CO2CRC-1-V (k = 751.1 mD, Ø = 20.01%)

Where: $P_{overburden} =$ overburden pressure, psi

$Gr_{overburden} =$ overburden pressure gradient, $\frac{psi}{ft}$

$Depth =$ total vertical depth (TVD), ft

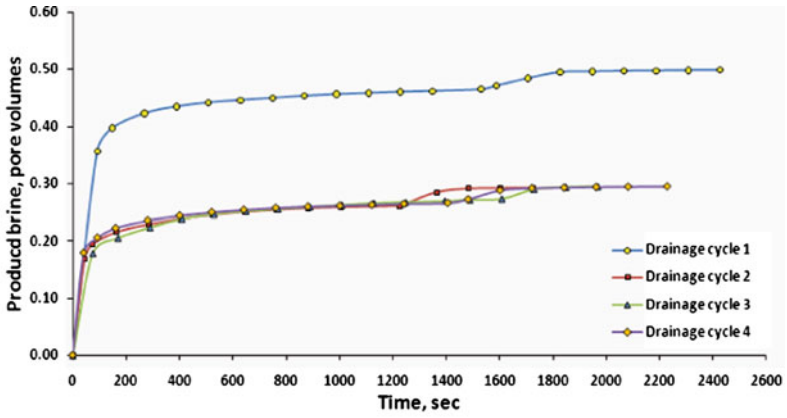

Fig. 4.3 Brine production versus time for the four drainage cycles conducted in test number 2 on sample CO2CRC-2,3-H (k = 788.3 mD, Ø = 17.31%)

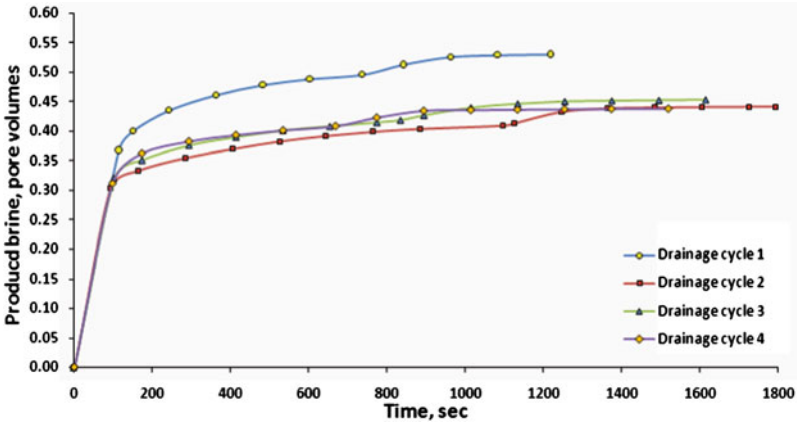

Fig. 4.4 Brine production versus time for the four drainage cycles conducted in test number 3 on sample CO2CRC-7-V (k = 1,899.6 mD, Ø = 21.35%)

4.3 Core Sample Properties

A total of 13 core samples (either one single piece or composite) were used during the experimental work carried out (Table 4.2). It is worth noting that the number of samples tested was more than 20 and the 13 samples listed here were those using which quality experimental data were generated. As listed in Table 4.2 the core samples used were all sandstone and, with slight variations, all of conventional 1.5″ (38.1 mm) diameter but with varying lengths. Detailed descriptions about various samples groups were presented previously in Chap. 3. The permeability values reported in Table 4.2 were those measured under full in situ

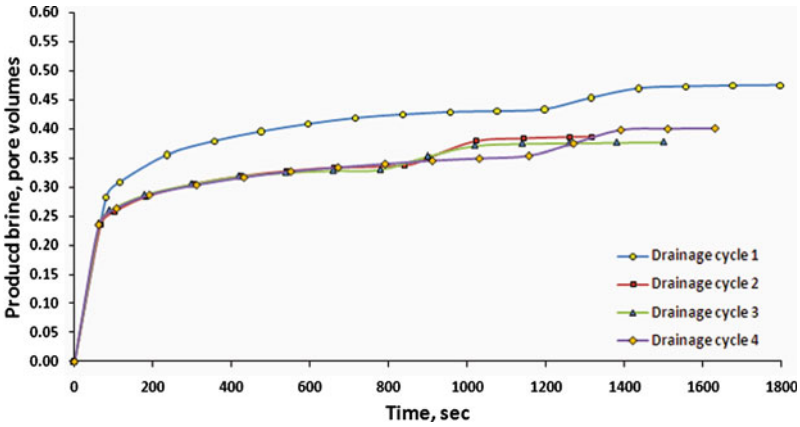

Fig. 4.5 Brine production versus time for the four drainage cycles conducted in test number 4 on sample CO2CRC-11,14-H (k = 3,409.8 mD, Ø = 22.03%)

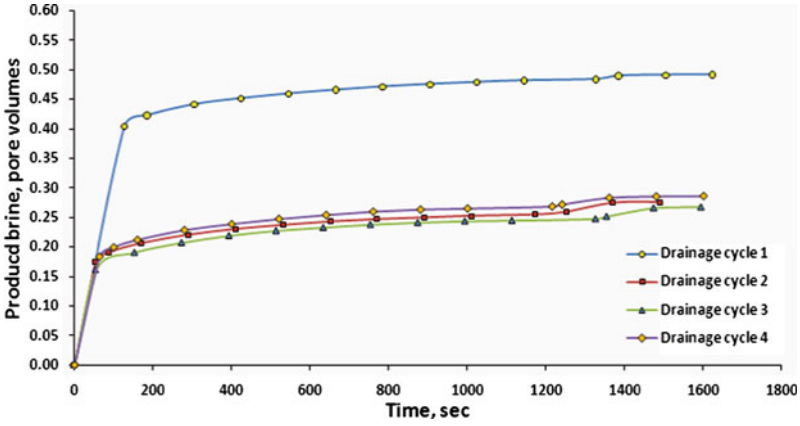

Fig. 4.6 Brine production versus time for the four drainage cycles conducted in test number 5 on sample CO2CRC-36-V (k = 108.2 mD, Ø = 17.26%)

reservoir P–T conditions using brine and porosities values were measured under full in situ net effective pressure using a helium porosimeter.

4.3.1 Composite Cores

As reported in Table 4.2, some of the samples tested were composite core samples each made up of two short core-plugs (Fig. 4.1). In constructing the composite core samples, all the guidelines and procedures described in Chap. 3 were

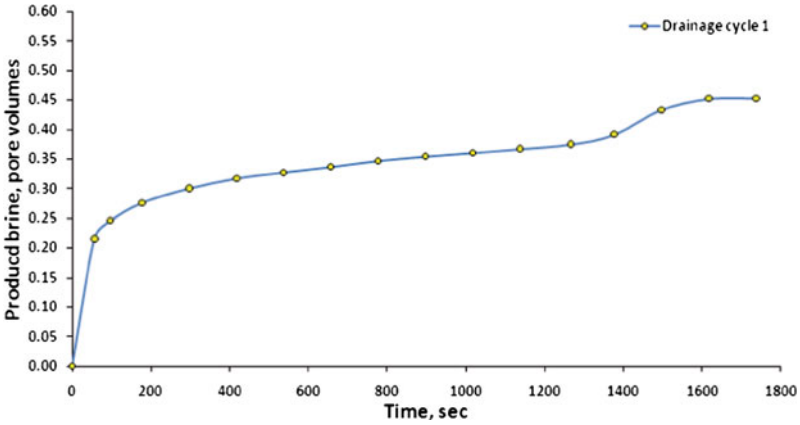

Fig. 4.7 Brine production versus time for the first drainage cycle conducted in test number 6 on sample CO2CRC-39,42-H (k = 252.6 mD, Ø = 15.49%)

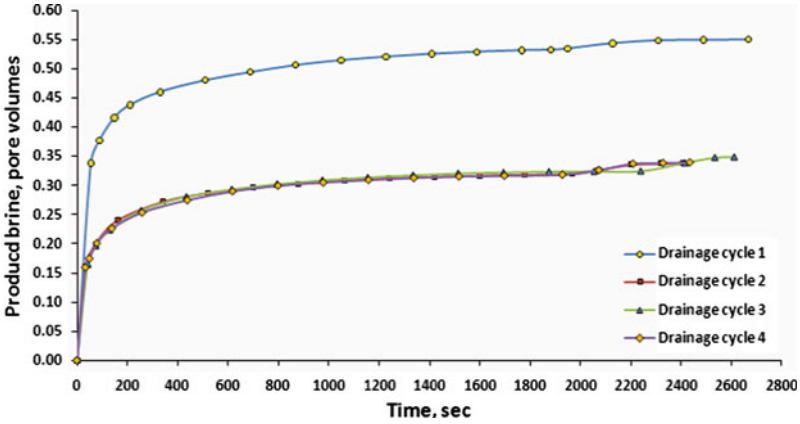

Fig. 4.8 Brine production versus time for the four drainage cycles conducted in test number 7 on sample BS-1-H (k = 234.6 mD, Ø = 17.97%)

followed. For instance, to reduce the pressure and saturation disturbances between the two core-plugs, their end-faces were polished and then two layers of a lint-free tissue paper were placed between the two adjacent end-faces (Fig. 4.1). The reason for choosing the tissue paper among the various bridging material mentioned in the literature [3–6] is that it is strongly water wet and thus would establish an adequate capillary bridge between the core-plugs for the purpose of flooding experiments conducted during this research. The paper used was of lint-free type to prevent the potential release of paper fines into the pore space of the sample and potentially causing damage to the sample during the flooding experiments.

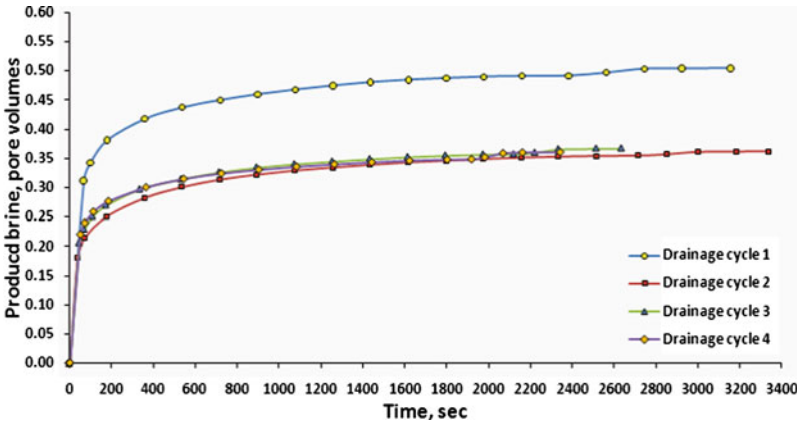

Fig. 4.9 Brine production versus time for the four drainage cycles conducted in test number 8 on sample BS-2-H (k = 151.1 mD, Ø = 18.4%, Confining P = 3,500 psi)

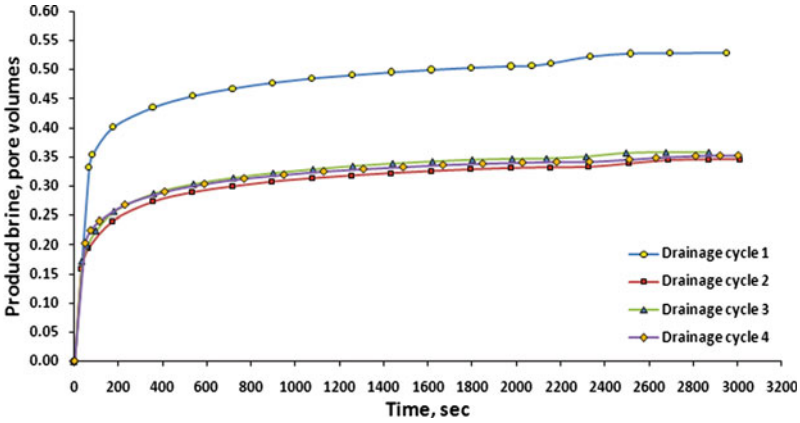

Fig. 4.10 Brine production versus time for the four drainage cycles conducted in test number 9 on sample BS-2-H (k = 145.9 mD, Ø = 18.51%, Confining P = 5,000 psi)

4.4 Results of Core-Flooding Experiments

More than 35 sets of cyclic core-flooding experiments were conducted during the laboratory work carried out, out of which 20 experiments generated quality data to be presented here. Based on the research objectives pursued, the core-flooding experiments can be divided into the following four main categories:

- Category 1: those experiments run in order to investigate the effect of cyclic injection of brine and CO_2 on the multiphase flow behaviour during CO_2 sequestration in the porous medium.

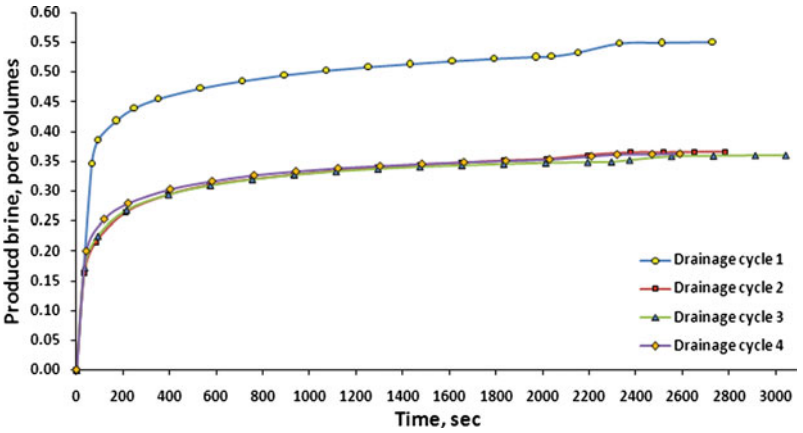

Fig. 4.11 Brine production versus time for the four drainage cycles conducted in test number 10 on sample BS-2-H (k = 141.13 mD, Ø = 18.4%, Confining P = 6,725 psi CO_2 inj. Flow-rate = 300 cc/hr)

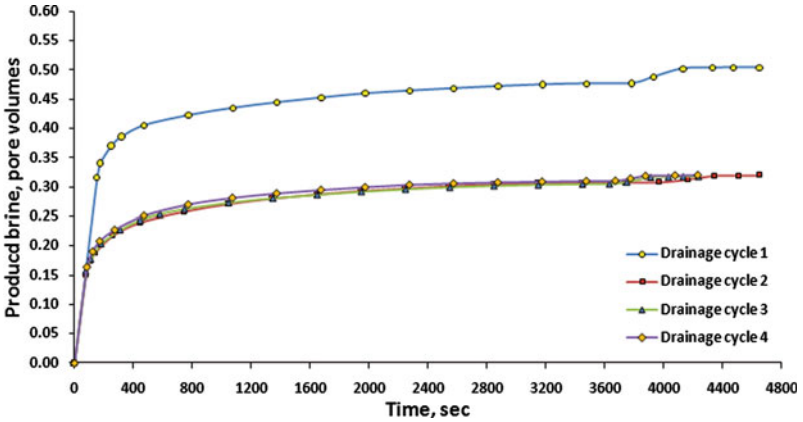

Fig. 4.12 Brine production versus time for the four drainage cycles conducted in test number 11 on sample BS-2-H (k = 141.13 mD, Ø = 18.4%, Confining P = 6,725 psi, CO_2 inj. Flow-rate = 120 cc/hr)

- Category 2: those flooding experiments carried out in order to evaluate the change in the multiphase flow characteristics of the porous medium with change in the flow direction (horizontal versus vertical) during underground CO_2 disposal.
- Category 3: those experiments conducted in order to evaluate the effect of increase in the reservoir pore pressure and subsequent reduction in the net effective pressure applied to the pores space on the multiphase flow behaviour during underground CO_2 disposal.

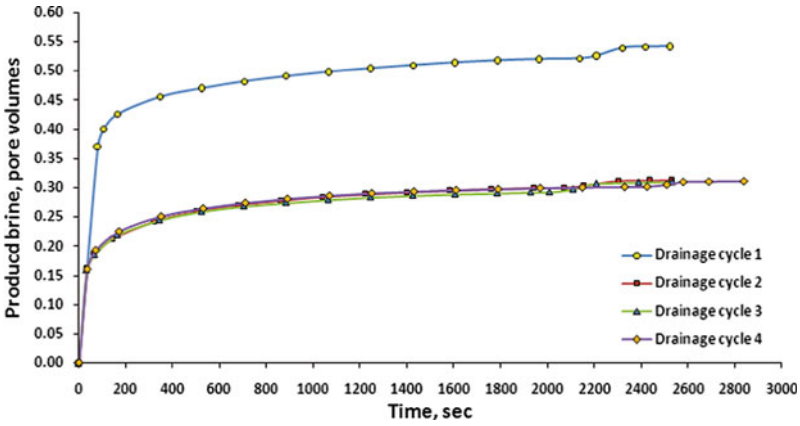

Fig. 4.13 Brine production versus time for the four drainage cycles conducted in test number 12 on sample BS-3-V (k = 194.4 mD, Ø = 18.64%)

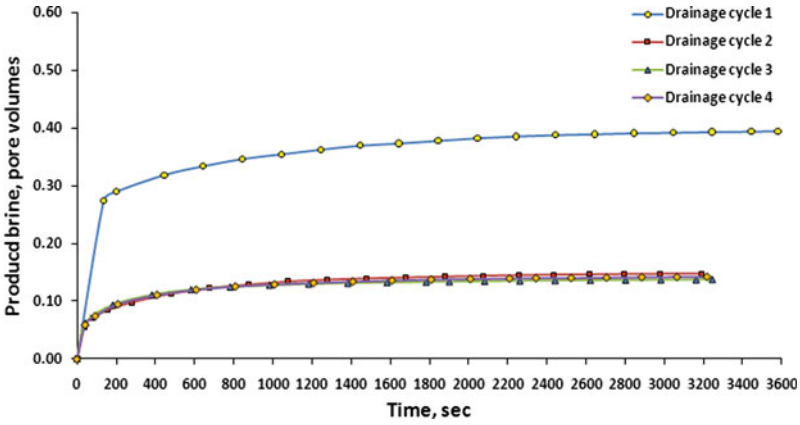

Fig. 4.14 Brine production versus time for the four drainage cycles conducted in test number 13 on sample DB-1-H (k = 14 mD, Ø = 16.01%, CO_2 inj. flow-rate = 150 cc/hr)

- Category 4: those core-flooding tests conducted in order to understand the effects that the existence of residual methane (representing natural gas) saturation may have on the multiphase flow behaviour during deep CO_2 injection into depleted gas reservoirs for sequestration purposes.

In addition to these main objectives investigated by running the core-flooding experiments, by conducting other complementary experimental work, the following items were also investigated:

- Potential change in the pore-network of the porous medium after being subjected to CO_2-brine injection.

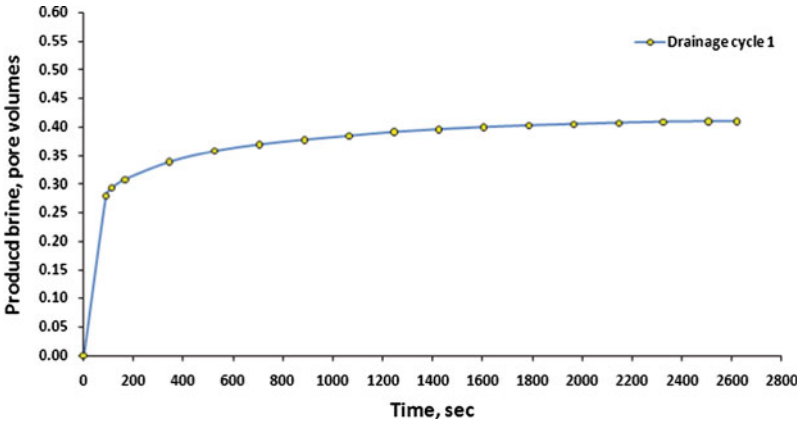

Fig. 4.15 Brine production versus time for the first drainage cycle conducted in test number 14 on sample DB-1-H (k = 14 mD, Ø = 16.01%, CO_2 inj. flow-rate = 200 cc/hr)

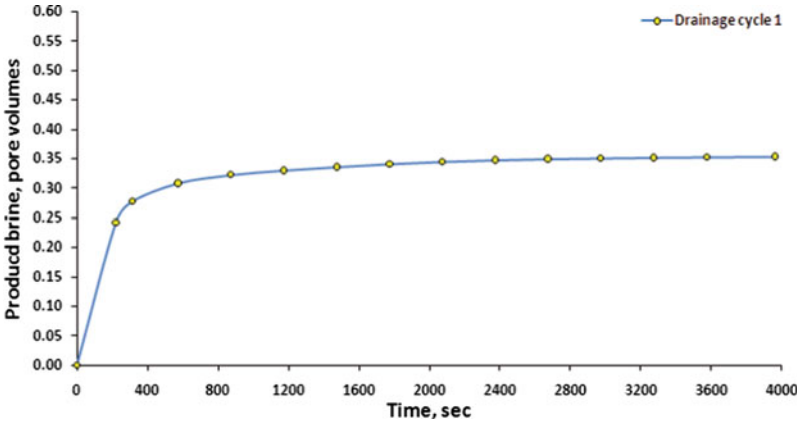

Fig. 4.16 Brine production versus time for the first drainage cycle conducted in test number 15 on sample DB-2-V (k = 12.2 mD, Ø = 16.19%)

- Potential change in the physical properties (e.g. porosity, etc.) of the porous medium after undergoing cyclic CO_2-brine injection.

These last two items were investigated through carrying out NMR analysis and porosity/pore volume measurements on a number of the core samples tested before and after the flooding experiments. The results of these complementary experimental works will be presented in separate sections in the second half of this chapter.

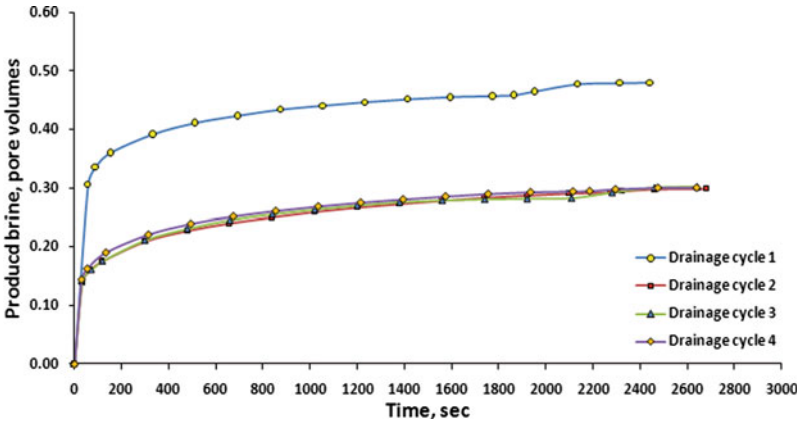

Fig. 4.17 Brine production versus time for the four drainage cycles conducted in test number 16 on sample CL40,68-H (k = 123.5 mD, Ø = 14.42%)

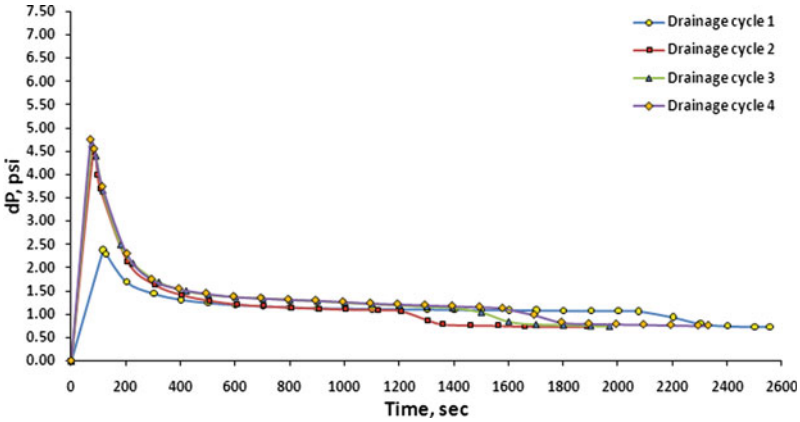

Fig. 4.18 Differential pressure across the sample versus time for the four drainage cycles conducted in test number 1 on sample CO2CRC-1-V (k = 751.1 mD, Ø = 20.01%)

4.4.1 Cyclic CO_2-Brine Injection

In total, 16 experiments were conducted with the specific focus of investigating the effect of cyclic CO_2-brine injection on the multiphase flow behaviour of the rock-fluids system during underground CO_2 disposal. These experiments were run on samples with varying porosity and permeability values chosen from all four sample groups described in the previous section of this chapter. All the experiments were carried out using the core-flooding apparatus described in Chap. 3 and according to the experimental procedure outlined in the same chapter. As described previously,

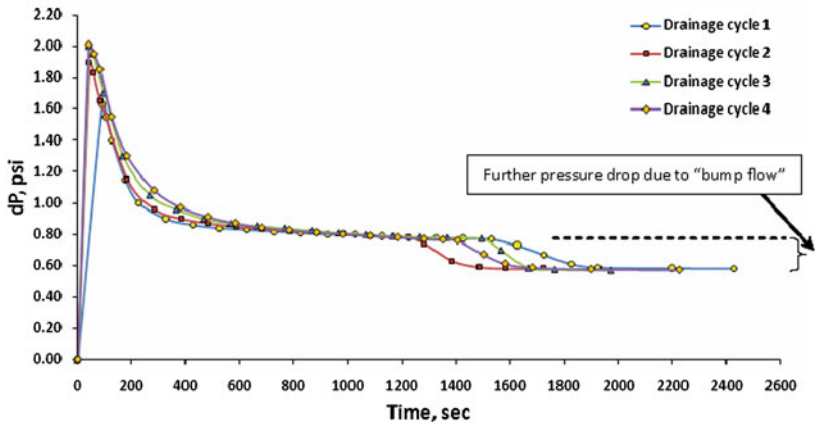

Fig. 4.19 Differential pressure across the sample versus time for the four drainage cycles conducted in test number 2 on sample CO2CRC-2,3-H (k = 788.3 mD, Ø = 17.31%)

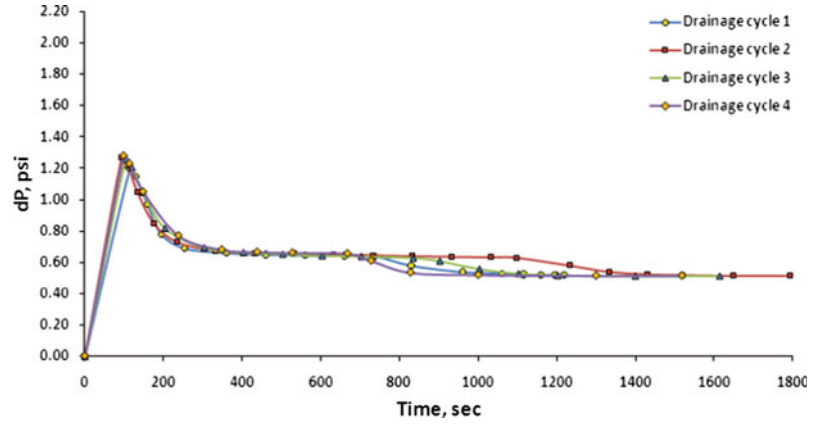

Fig. 4.20 Differential pressure across the sample versus time for the four drainage cycles conducted in test number 3 on sample CO2CRC-7-V (k = 1,899.6 mD, Ø = 21.35%)

these cyclic injections were performed by conducting consecutive drainage and imbibition floods on each core sample tested. Due to the viscosity and density contrast between supercritical CO_2 and brine, any long time-lag between the end of one injection cycle and the start of the next could distort the stabilised and uniform saturation profile achieved at the end of the first cycle. Therefore, for each sample, as many injection cycles as possible were performed non-stop in one day only. The number of injection cycles performed on each individual sample may vary as it was dependant mainly on the absolute permeability of the sample as being the main rock property dictating the required time to reach stabilised steady-state conditions,

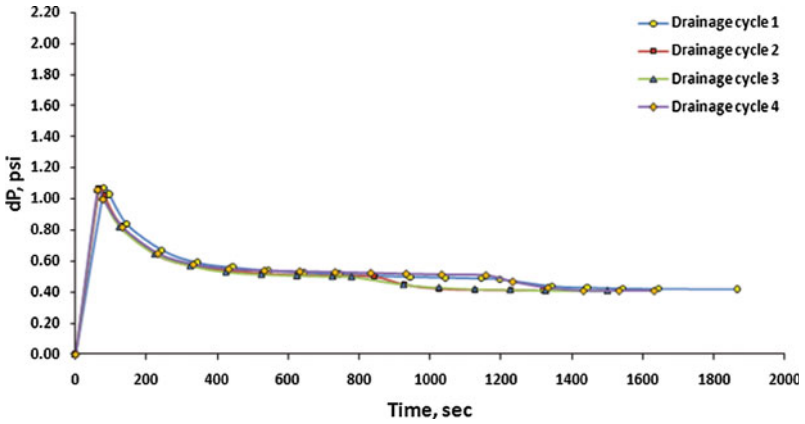

Fig. 4.21 Differential pressure across the sample versus time for the four drainage cycles conducted in test number 4 on sample CO2CRC-11,14-H (k = 3,409.8 mD, Ø = 22.03%)

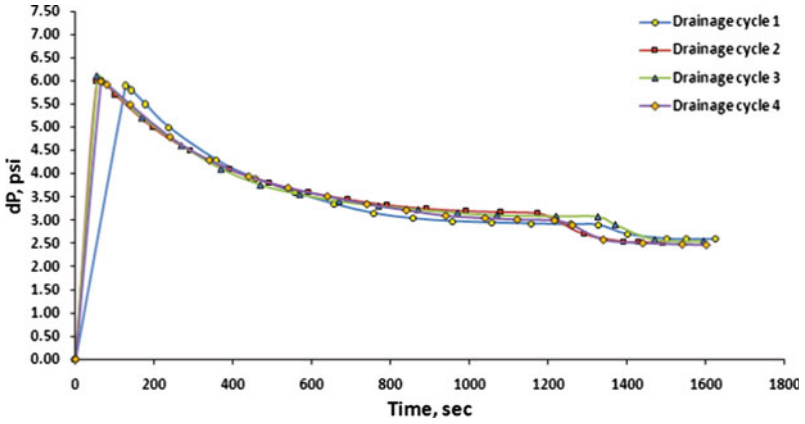

Fig. 4.22 Differential pressure across the sample versus time for the four drainage cycles conducted in test number 5 on sample CO2CRC-36-V (k = 108.2 mD, Ø = 17.26%)

which would signal the conclusion of each injection cycle. During each injection cycle on average about 12 pore volumes of CO_2 or brine were passed through the core sample before stabilised conditions (i.e. no more production of the displaced phase and stable pressure drop across the sample) were reached. As discussed in the previous chapter, in order to eliminate the effect of gravity segregation (underrun or override of the injected fluids) within the sample tested while undergoing the core-flooding experiments, the core-holder containing the sample was placed vertically and injection was performed from base to the top.

In addition to providing some general information about each experiment conducted and the end-point brine saturations for each injection cycle,

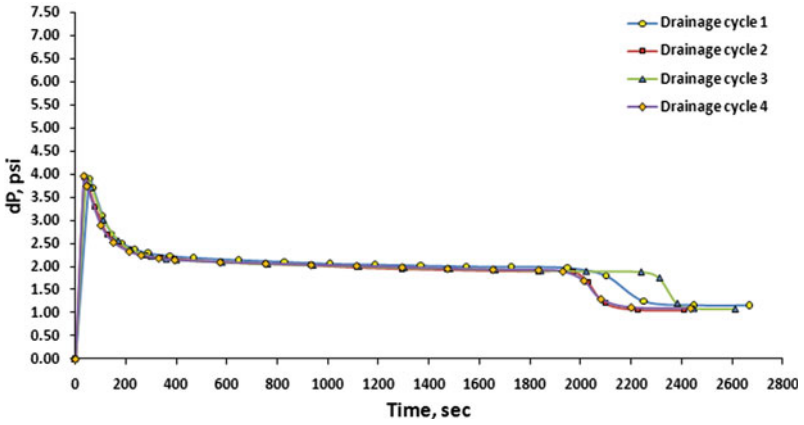

Fig. 4.23 Differential pressure across the sample versus time for the four drainage cycles conducted in test number 7 on sample BS-1-H (k = 234.6 mD, Ø = 17.97%)

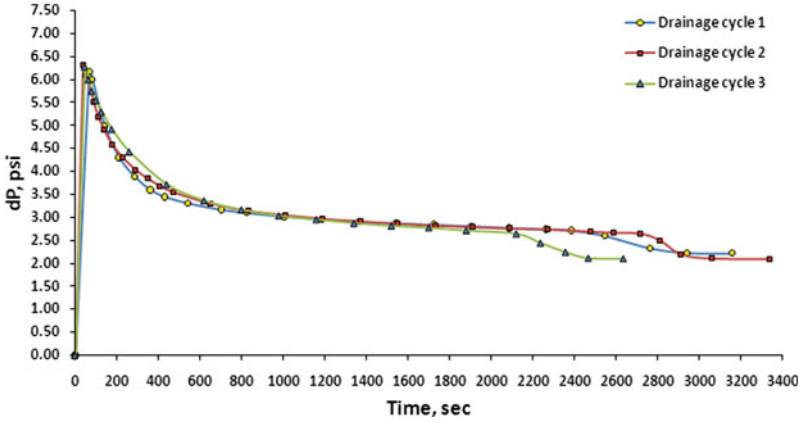

Fig. 4.24 Differential pressure across the sample versus time for the first three drainage cycles conducted in test number 8 on sample BS-2-H (k = 151.1 mD, Ø = 18.4%, Confining P = 3,500 psi)

the following section of this chapter presents the results of the brine production and differential pressure across the sample, all versus time. The brine production and differential pressure profiles are provided for each individual injection cycle performed on each sample. The brine production profiles presented are for the drainage cycles only. Due to the fact that supercritical CO_2 has a much lower viscosity than brine, the cycles involving the displacement of CO_2 by brine (imbibition) were of highly favourable mobility ratios (M) [i.e. (M) $<<$ 1] and as a result only very small amounts of CO_2 were produced after the brine breakthrough (BT). As will be shown later for two experiments, the trend of any possible change

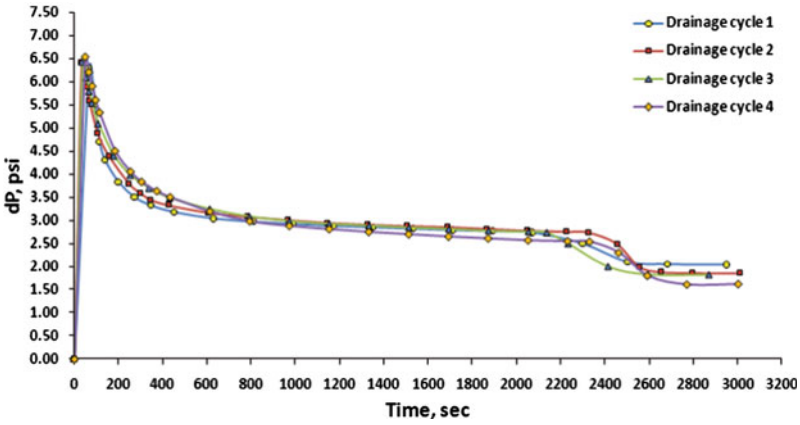

Fig. 4.25 Differential pressure across the sample versus time for the four drainage cycles conducted in test number 9 on sample BS-2-H (k = 145.9 mD, Ø = 18.51%, Confining P = 5,000 psi)

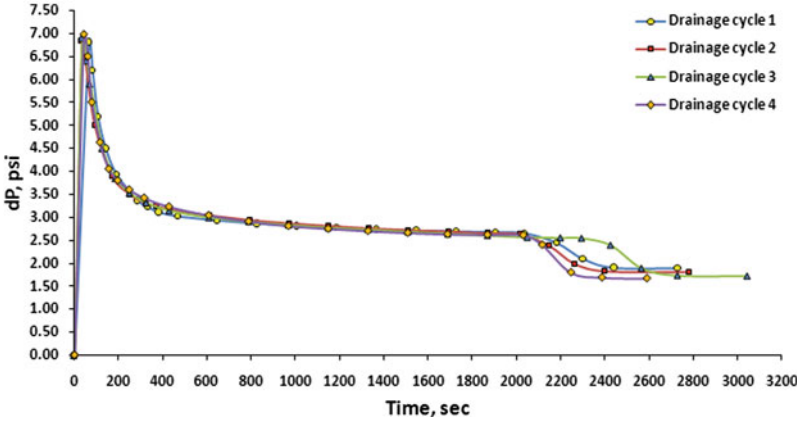

Fig. 4.26 Differential pressure across the sample versus time for the four drainage cycles conducted in test number 10 on sample BS-2-H (k = 141.13 mD, Ø = 18.4%, Confining P = 6,725 psi CO_2 inj. Flow-rate = 300 cc/hr)

in the pressure profiles of the consecutive imbibition cycles was similar to that of consecutive drainage cycles for the same experiment. Therefore, except for those two experiments, presenting the differential pressure profiles for the drainage cycles only was considered adequate in achieving the objectives perused. It is worth noting that the actual raw experimental data were recorded for every second using the monitoring/controlling software of the core-flooding apparatus. However, the graphs presented here show the data which were fitted to the raw data with approximately 1–3 min time intervals between two successive data points.

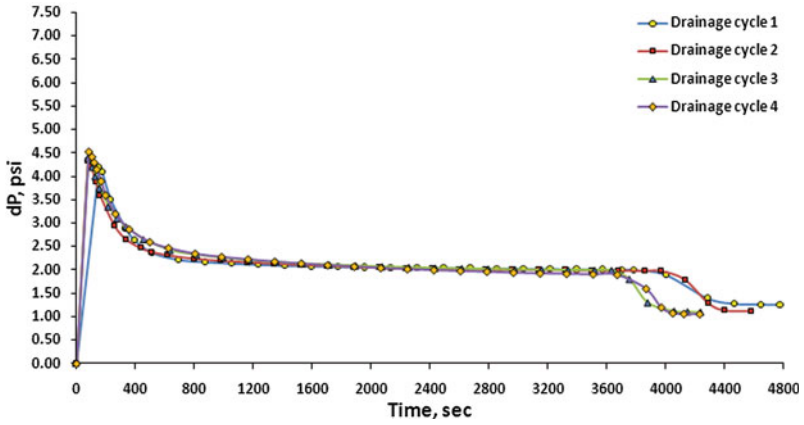

Fig. 4.27 Differential pressure across the sample versus time for the four drainage cycles conducted in test number 11 on sample BS-2-H (k = 141.13 mD, Ø = 18.4%, Confining P = 6725 psi, CO_2 inj. Flow-rate = 120 cc/hr)

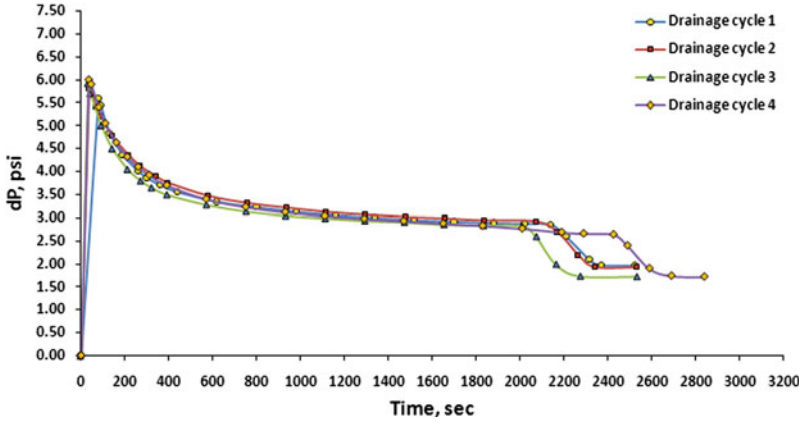

Fig. 4.28 Differential pressure across the sample versus time for the four drainage cycles conducted in test number 12 on sample BS-3-V (k = 194.4 mD, Ø = 18.64%)

The size of the time intervals depended on the total duration of each experiment (i.e. the longer the total duration of the experiment, the longer the time intervals between the data points of the fitted data).

Listed in Table 4.3 are the values of a number of important sample and experimental condition parameters. As can be seen from this table, a few experiments also were run under varying injection flow-rates or under overburden pressures different from that of the reservoir in situ overburden pressure. These experiments were to investigate the effect of change in the flow-rate or in situ net effective stress on the multiphase flow characteristics during the cyclic CO_2-brine

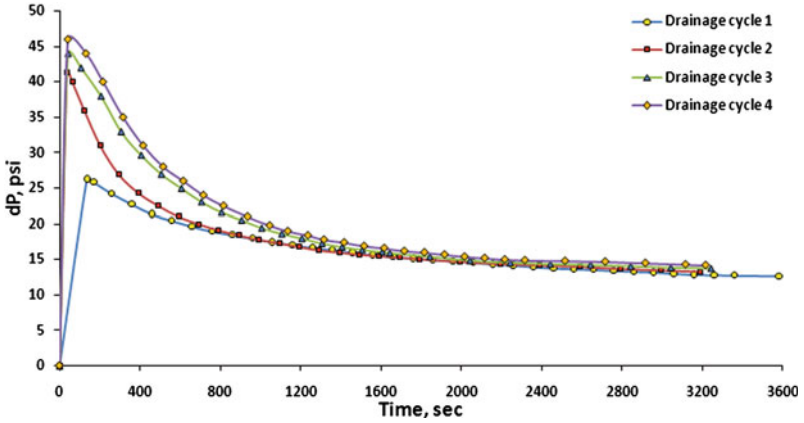

Fig. 4.29 Differential pressure across the sample versus time for the four drainage cycles conducted in test number 13 on sample DB-1-H (k = 14 mD, Ø = 16.01%, CO_2 inj. flow-rate = 150 cc/hr)

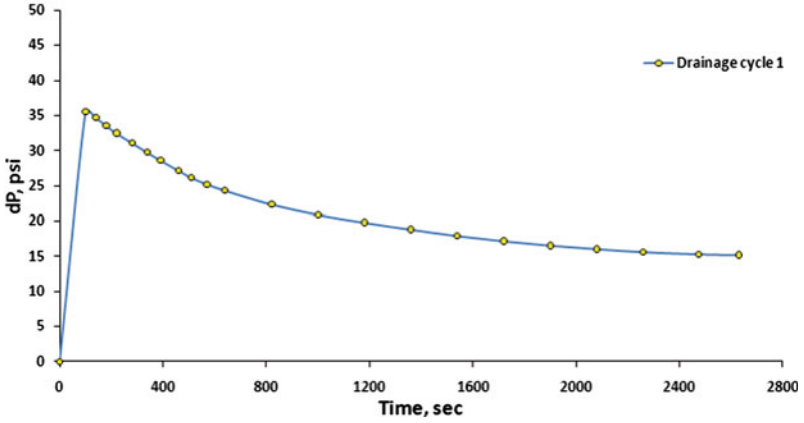

Fig. 4.30 Differential pressure across the sample versus time for the first drainage cycle conducted in test number 14 on sample DB-1-H (k = 14 mD, Ø = 16.01%, CO_2 inj. flow-rate = 200 cc/hr)

injection. To achieve the other objective of this research, which was investigating the possible directional dependence of the multiphase flow behaviour during geological CO_2 storage, a number of the samples were drilled from the same reservoir interval or quarried block in both horizontal and vertical directions.

Table 4.4 lists the end-point brine saturations obtained at the end of the injection cycles performed during all 16 cyclic CO_2-brine flooding experiments conducted on various samples. As can be seen from the table, for three experiments the end-point brine saturations are reported for the first drainage and first

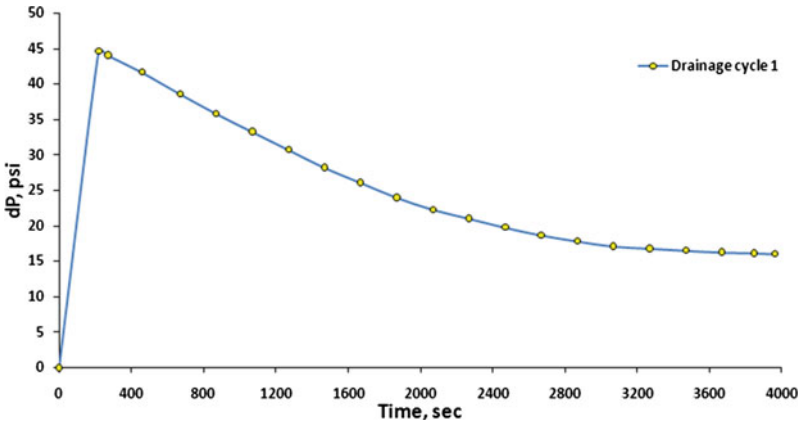

Fig. 4.31 Differential pressure across the sample versus time for the first drainage cycle conducted in test number 15 on sample DB-2-V (k = 12.2 mD, Ø = 16.19%)

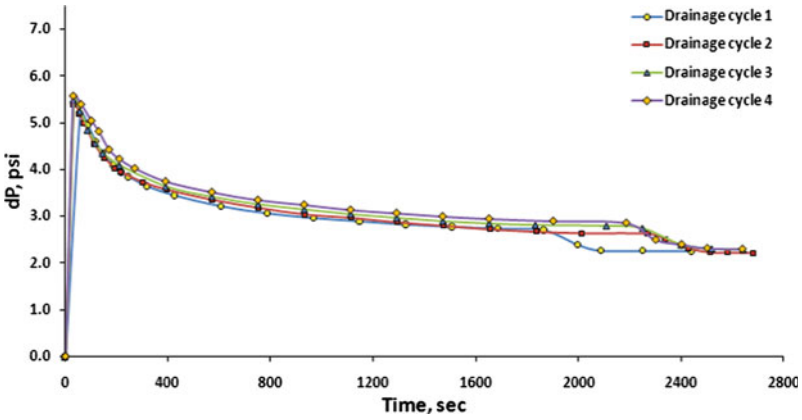

Fig. 4.32 Differential pressure across the sample versus time for the four drainage cycles conducted in test number 16 on sample CL-40,68-H (k = 123.5 mD, Ø = 14.42%)

imbibition cycles only. This is because either a hardware failure occurred during the experiment or the recorded brine production data for the rest of the cycles were not of reliable quality to be analysed and reported here.

Figures 4.2, 4.3, 4.4, 4.5, 4.6, 4.7, 4.8, 4.9, 4.10, 4.11, 4.12, 4.13, 4.14, 4.15, 4.16, and 4.17 are the brine production profiles observed at the outlet face of each sample tested. One figure is presented for each sample tested showing the brine productions versus time for all the drainage cycles performed on that sample. As discussed in Chap. 3, a short period of so called "bump flow" was carried out at the conclusion of each cycle. This was necessary, especially in the moderate to high permeability samples, to establish true end-point saturations and remove any

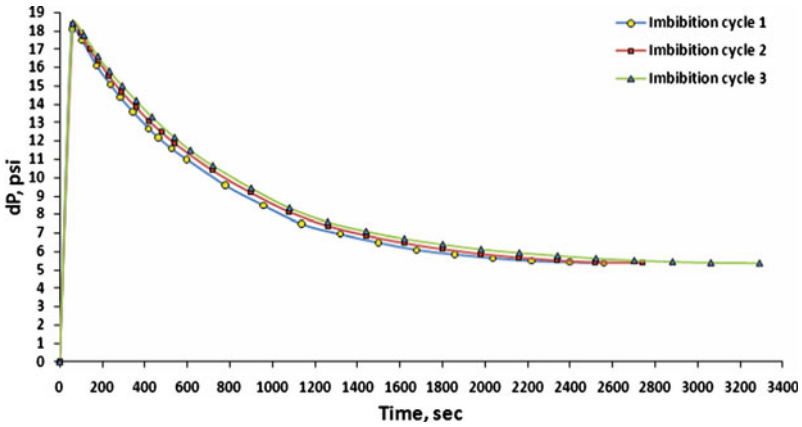

Fig. 4.33 Differential pressure across the sample versus time for the three imbibition cycles conducted in test number 5 on sample CO2CRC-36-V (k = 108.2 mD, Ø = 17.26%)

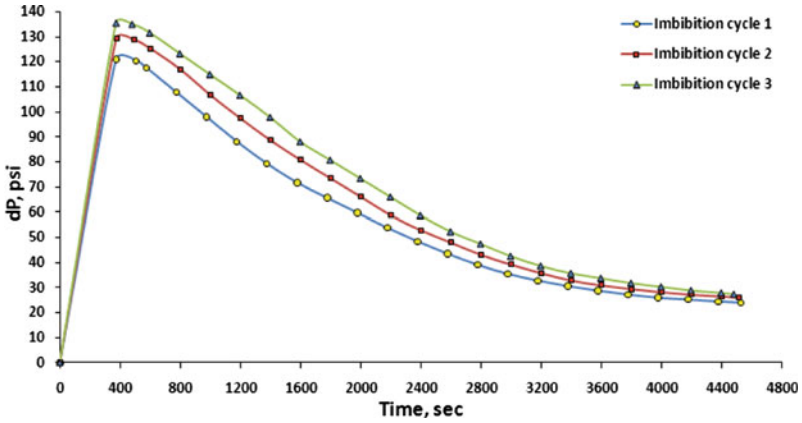

Fig. 4.34 Differential pressure across the sample versus time for the three imbibition cycles conducted in test number 13 on sample DB-1-H (k = 14 mD, Ø = 16.01%, CO_2 inj. flow-rate = 150 cc/hr)

potential anomalous brine hold-up, which may have been created at the outlet of the sample due to the well-characterised capillary end effect phenomenon. As can be seen in the graphs plotted, for the majority of the experiments conducted, abrupt increase in brine production close to the end of each injection cycle due to the "bump flow", confirmed the existence of such saturation anomalies.

Figures 4.18, 4.19, 4.20, 4.21, 4.22, 4.23, 4.24, 4.25, 4.26, 4.27, 4.28, 4.29, 4.30, 4.31 and 4.32 are the differential pressures across the sample versus time for all the experiments whose brine production profiles were reported earlier. In addition to the drainage cycles, the differential pressure profiles during imbibition

Table 4.5 Summary of the cyclic CO_2-brine flooding tests conducted on various samples with initial residual methane saturation ($IFT_{CH4\text{-}brine} = 45$ dyne/cm, contact angle = 0)

Test no.	Sample name	Pore vol (cc)	k (mD)	Overburden pressure (psi)	Pore pressure (psi)	CH_4 inj. flow-rate (cc/hr)	CO_2 inj. flow-rate (cc/hr)	Water inj. flow-rate (cc/hr)	Capillary number for CH_4 flood
17	CO2CRC-2,3-H	18.859	788.3	6,725	2,580	300	300	200	2.65E - 06
18	BS-1-H	16.476	234.6	6,725	2,580	300	300	200	2.90E - 06
19	BS-2-H	16.975	141.1	6,725	2,580	300	300	200	2.88E - 06
20	BS-3-V	17.002	194.4	6,725	2,580	300	300	200	2.88E - 06

Table 4.6 End-point brine saturation values at the end of each injection cycle during the cyclic CO_2-brine injection experiments with initial residual methane saturation

Test no.	Sample name	End-point brine saturation (%)						
		1st Drain., CH_4	*1st Imb.*	*2nd Drain., CO_2*	*2nd Imb.*	*3rd Drain., CO_2*	*3rd Imb.*	*4th Drain., CO_2*
17	CO2CRC-2,3-H	35.0	71.3	49.5	77.0	49.0	79.8	51.8
18	BS-1-H	29.4	68.0	38.0	70.5	40.1	76.5	43.4
19	BS-2-H	35	67.6	37.1	73.9	40.6	76.3	43.4
20	BS-3-V	29.1	67.6	34.7	72.1	38.5	75.1	43.1

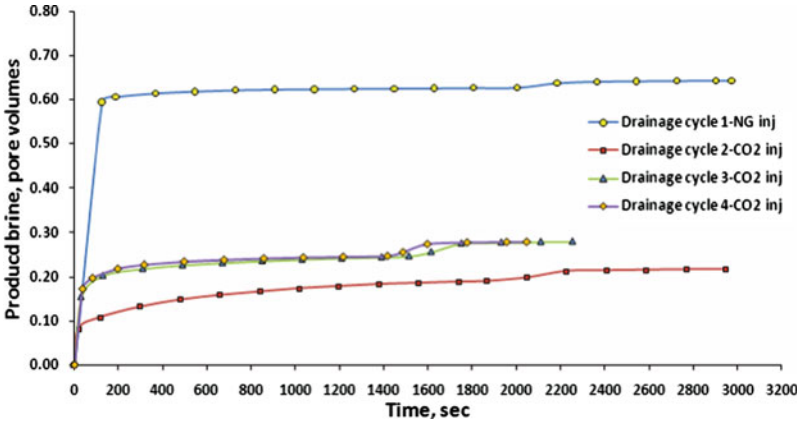

Fig. 4.35 Brine production versus time for the four drainage cycles conducted in test number 17 on sample CO2CRC-2,3-H (k = 788.3 mD, Ø = 17.31%)

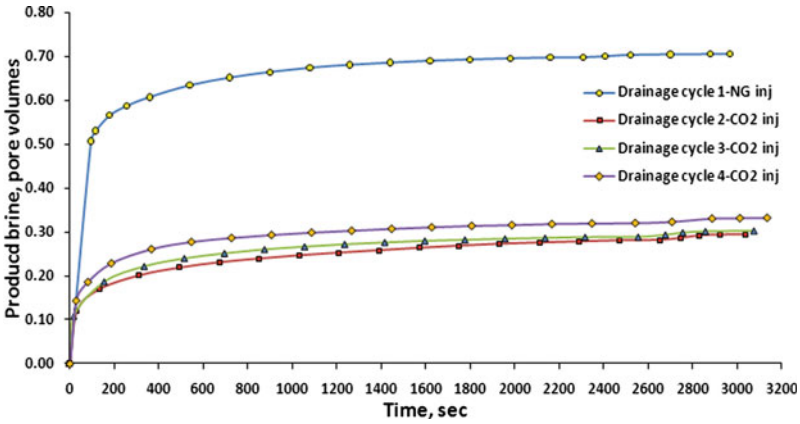

Fig. 4.36 Brine production versus time for the four drainage cycles conducted in test number 18 on sample BS-1-H (k = 234.6 mD, Ø = 17.97%)

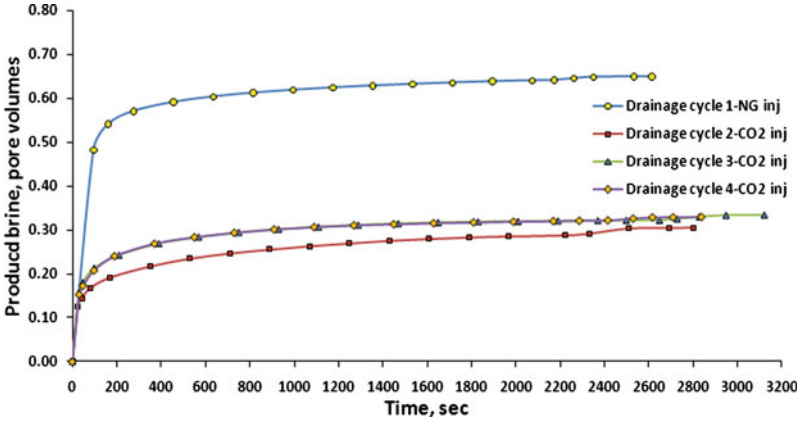

Fig. 4.37 Brine production versus time for the four drainage cycles conducted in test number 19 on sample BS-2-H (k = 141.13 mD, Ø = 18.4%, Confining P = 6725 psi)

cycles are also presented for the two samples of CO2CRC-36-V and DB-1-H in Figs. 4.33 and 4.34 for comparison purposes. The differential pressure data for all the drainage or imbibition cycles are displayed for each sample in one single graph. The majority of the differential pressure profiles for the drainage cycles show a sudden, steep decline close to their conclusion. These abrupt declines were due to the removal of the anomalous brine saturation, caused mainly by the capillary end effect, through conducting the previously described "bump flow".

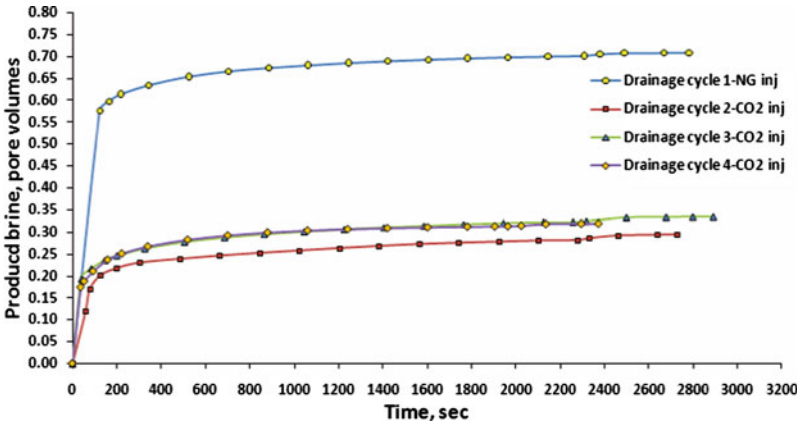

Fig. 4.38 Brine production versus time for the four drainage cycles conducted in test number 20 on sample BS-3-V (k = 194.4 mD, Ø = 18.64%)

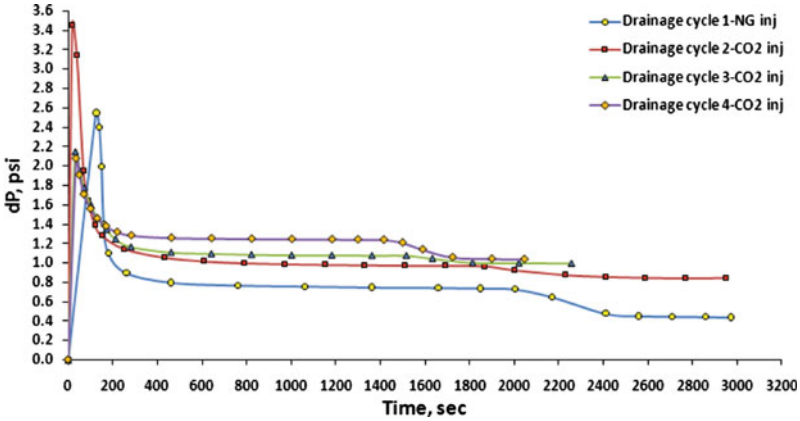

Fig. 4.39 Differential pressure across the sample versus time for the four drainage cycles conducted in test number 17 on sample CO2CRC-2,3-H (k = 788.3 mD, Ø = 17.31%)

4.4.2 Cyclic CO_2-Brine Injection—Effect of Residual Natural Gas Saturation

As discussed previously, one main objective of this research was to investigate the potential effects that the existence of residual natural gas (represented here by methane) saturation may have on the multiphase flow behaviour during geological CO_2 sequestration. In order to achieve this goal, the same procedure followed for the cyclic CO_2-brine flooding experiments was repeated again with the only

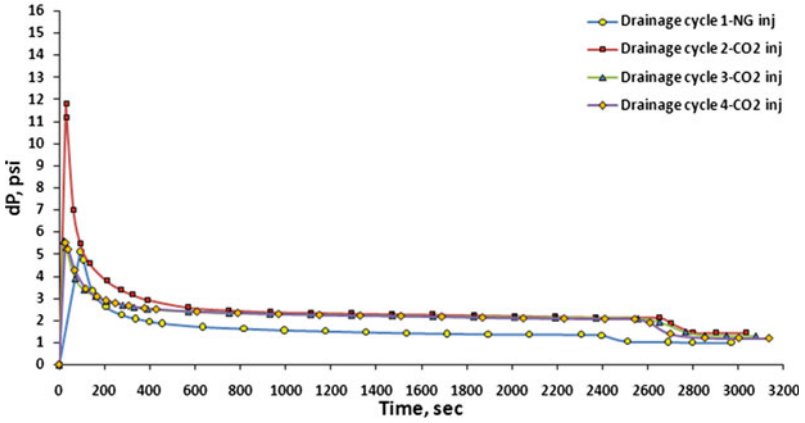

Fig. 4.40 Differential pressure across the sample versus time for the four drainage cycles conducted in test number 18 on sample BS-1-H (k = 234.6 mD, Ø = 17.97%)

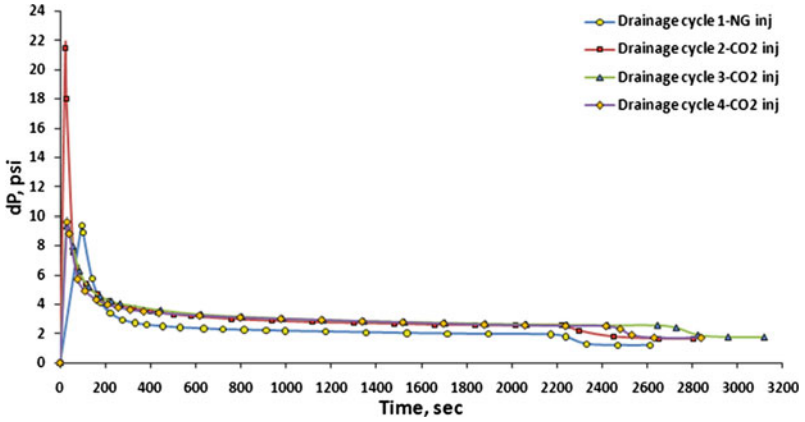

Fig. 4.41 Differential pressure across the sample versus time for the four drainage cycles conducted in test number 19 on sample BS-2-H (k = 141.13 mD, Ø = 18.4%, Confining P = 6,725 psi)

difference being the use of methane (representing natural gas here) as the displacing phase during the first drainage cycle instead of CO_2.

In total seven experiments conducted out of which, after performing quality checks, four experiments were chosen whose results are presented here. The samples were chosen from among those used during the previous stage of experimental work. Presented in Table 4.5 are the values of a number of important parameters regarding the samples tested and the experimental conditions under which the tests were run.

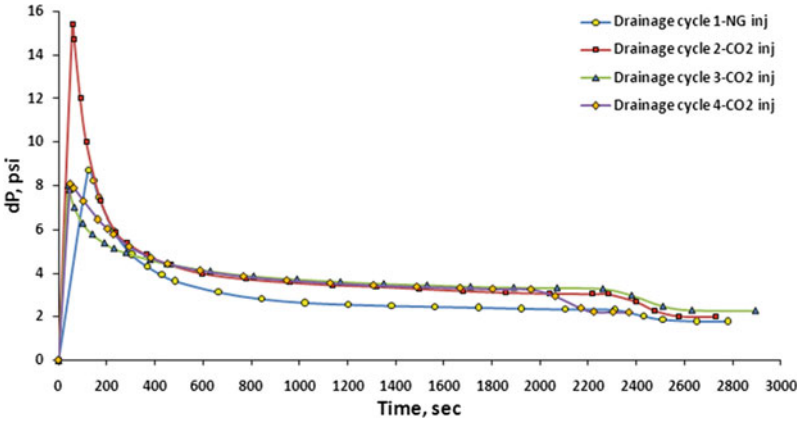

Fig. 4.42 Differential pressure across the sample versus time for the four drainage cycles conducted in test number 20 on sample BS-3-V (k = 194.4 mD, Ø = 18.64%)

Table 4.7 NMR aqcuision parameters used during the the NMR measurements

Parameter name	Abbreviation	Value
90 degree pulse (μs)	P90	27.6
180 degree pulse (μs)	P180	55.2
Probe dead time (μs)	DEAD1	70
Receiver dead time (μs)	DEAD2	20
Spectrometer frequency (MHz)	SF	1.921
Offset from SF (Hz)	O1	−18,636.1
Filter width (Hz)	FW	100,000
Dwell time (μs)	DW	1
Sweep width (Hz)	SW	1,000,000
Points per echo (points)	SI	3
Number of echoes	NECH	12,000
Number of scans	NS	256
Receiver gain (%)	RG	64
Relaxation delay (μs)	RD	15,000,000
90–180 degree pulse gap (μs)	TAU	240
90 degree pulse phase list (rec: 0213)	PH1	213
Receiver phase list (rec: 0213)	PH2	213
180 Degree pulse phase list (rec: 1122)	PH3	1,122

Table 4.6 lists all the end-point brine saturations measured at the end of all the drainage and imbibition floods performed on the four samples tested. As indicated in the table, the first column of the saturation data, corresponding to the first drainage flood, shows the end-point saturations achieved through injecting CH_4 to displace the brine. The rest of the drainage cycles were carried out using CO_2.

Plotted in Figs. 4.35, 4.36, 4.37, and 4.38 are the brine productions versus time for all the drainage cycles performed on the samples tested during this stage of the

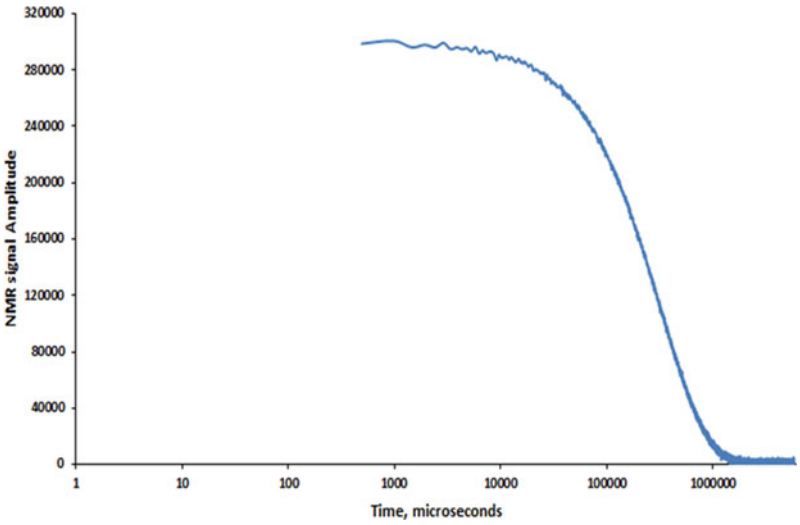

Fig. 4.43 The decay of spin-echo train for the 15 ml NiCl solution sample

experimental work. Here again any abrupt increase in the produced brine close to the end of each cycle was due to the removal of the brine holdup, caused by mainly the capillary end effect, through conducting the "bump flow".

The differential pressure profiles displayed in Figs. 4.39, 4.40, 4.41, and 4.42 correspond to the brine production profiles reported in Figs. 4.35, 4.36, 4.37, and 4.38 respectively.

4.5 Results of NMR Measurements

As mentioned in Chap. 3, a Resonance Instruments Maran-Ultra 2 MHz bench-top spectrometer was used to carry out the NMR measurements. The NMR tests were conducted on most of the samples used during the core-flooding tests. For a number of these samples NMR measurements were carried out twice, once before and once again after they underwent the cyclic flooding experiments. As mentioned previously, a hard pulse CPMG sequence was used to generate the T2 relaxation spectrum on the samples tested. The acquisition parameters applied to the NMR tests are listed in Table 4.7. Since the majority of the samples analysed were of moderate to high porosity and permeability ranges, this combination of parameters was considered adequate to generate T2 distribution data representative of the pore-size distribution of the samples. As can be seen from Table 4.7, the number of scans (NS) was set to 256, which would help to generate high quality data by achieving high signal-to-noise ratios. A 15 second relaxation delay (RD) also guarantees full polarisation for accurate measurements.

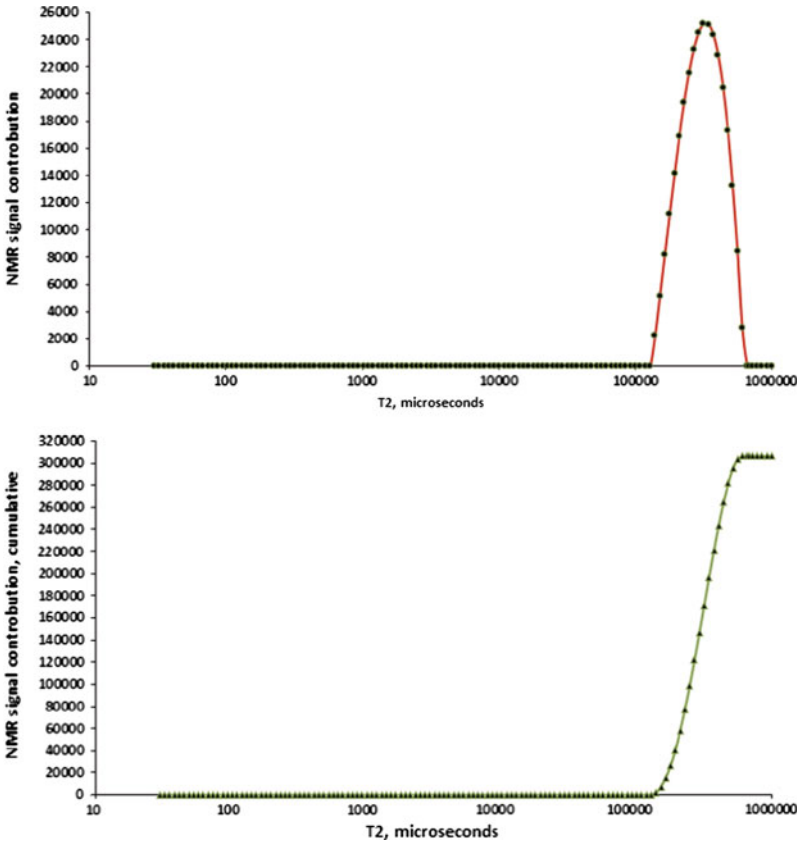

Fig. 4.44 NMR T2 distribution for the 15 ml NiCl solution sample: incremental T2 distribution (*top*) and cumulative T2 distribution (*bottom*)

Figure 4.43 shows the decay of the spin-echo trains for an NMR test (CPMG sequence) conducted on a 15 ml NiCl solution sample. The initial amplitude (or cumulative T2 distribution) recorded here for this known volume of water can be used later in conjunction with the initial amplitude (or cumulative T2 distribution) recorded for those samples tested afterwards to evaluate their NMR porosity. Figure 4.44 shows the incremental and cumulative T2 relaxation time distributions for the 15 ml NiCl solution.

The above-mentioned water sample was used also, as required on several occasions, to calibrate the NMR instrument using the Free Induction Decay (FID) acquisition sequence. Since conducting the NMR measurements was not part of the original research plan and the decision to run them was made relatively late, for a few samples (e.g. Sample CO2CRC-36-V) the NMR measurements were done only after they had already undergone several sets of cyclic injections and consequently their original NMR data are not known.

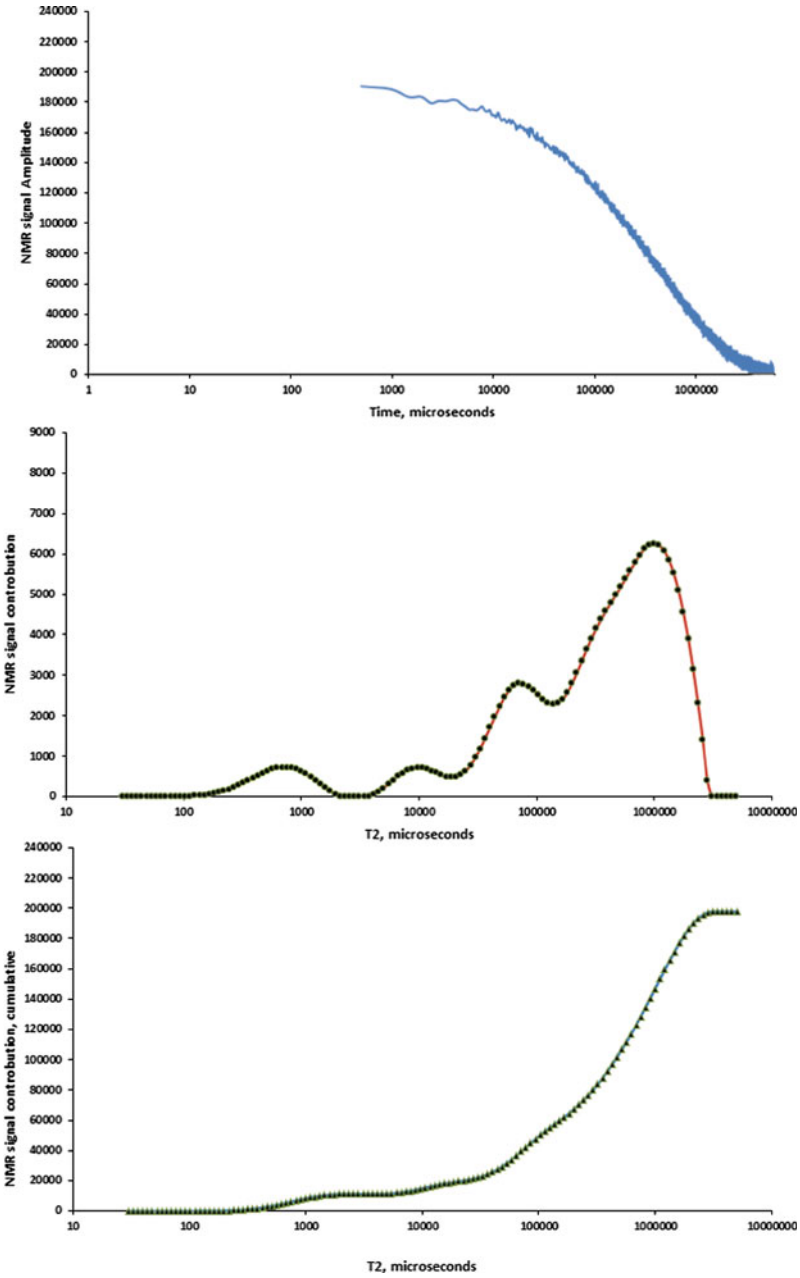

Fig. 4.45 NMR results for sample CO2CRC-2-H: raw spin-echo decay (*top*), incremental T2 distribution (*middle*) and cumulative T2 distribution (*bottom*)

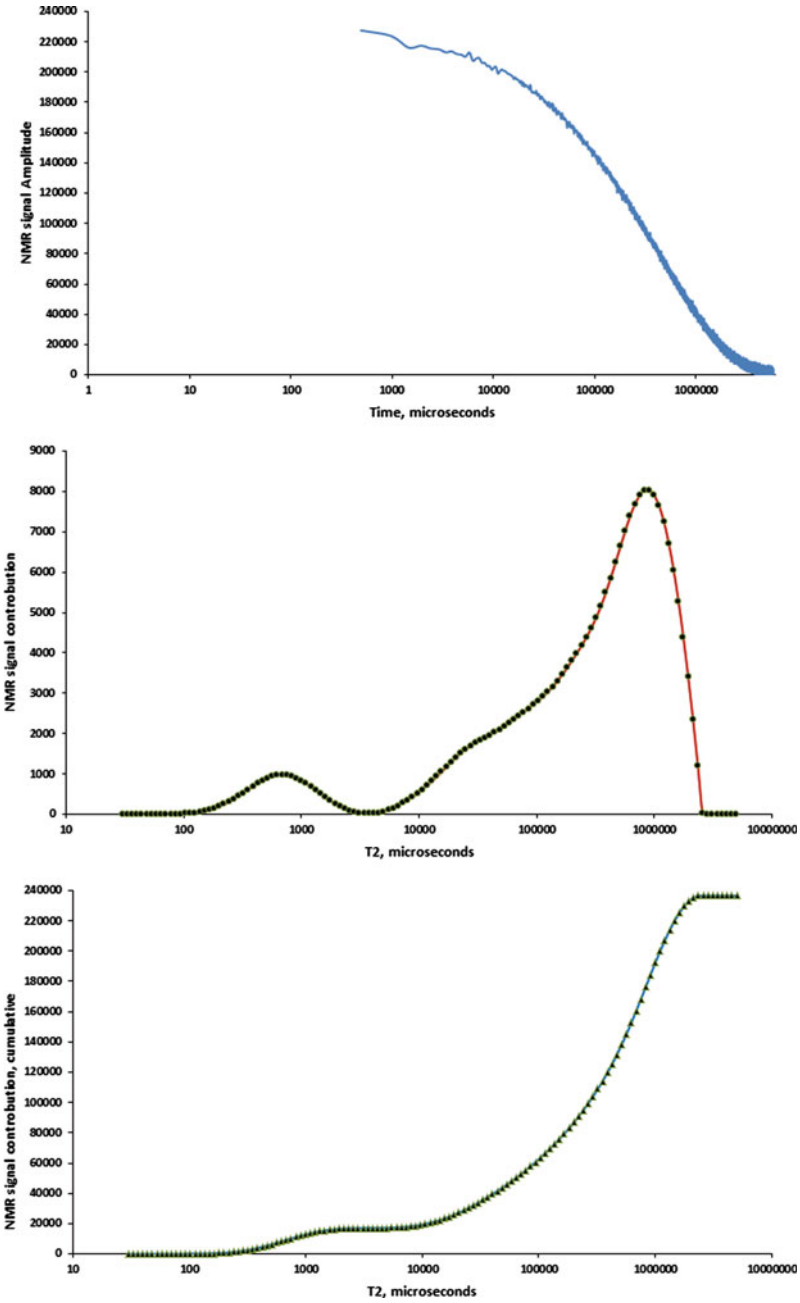

Fig. 4.46 NMR results for sample CO2CRC-3-H: raw spin-echo decay (*top*), incremental T2 distribution (*middle*) and cumulative T2 distribution (*bottom*)

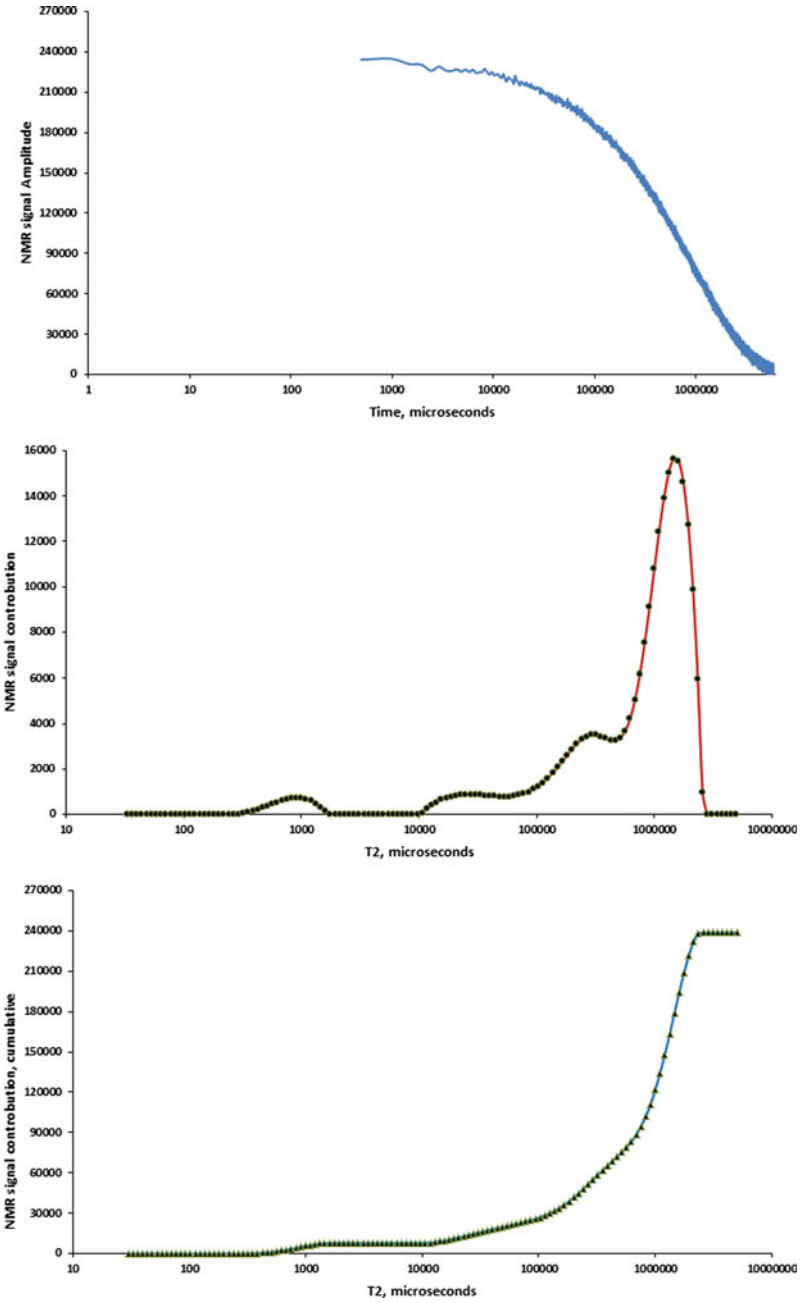

Fig. 4.47 NMR results for sample CO2CRC-11-H: raw spin-echo decay (*top*), incremental T2 distribution (*middle*) and cumulative T2 distribution (*bottom*)

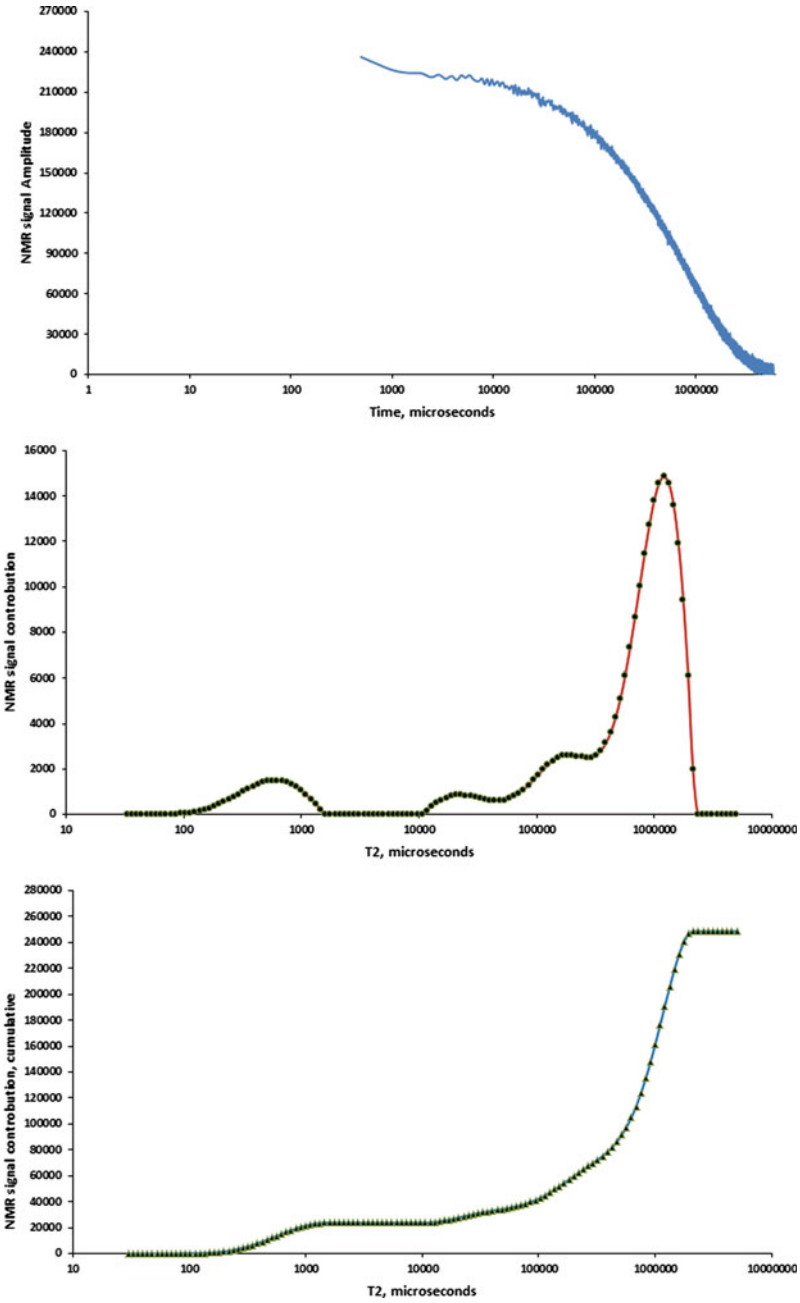

Fig. 4.48 NMR results for sample CO2CRC-14-H: raw spin-echo decay (*top*), incremental T2 distribution (*middle*) and cumulative T2 distribution (*bottom*)

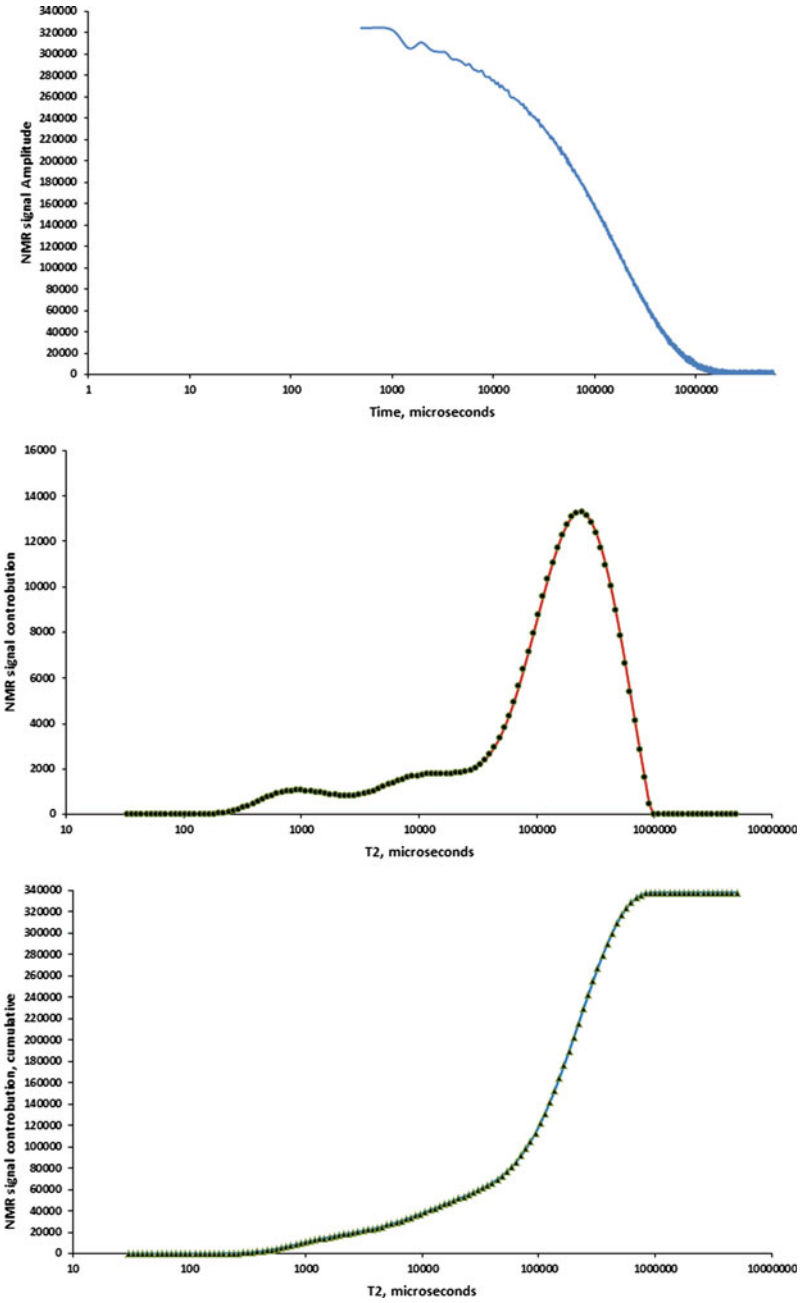

Fig. 4.49 NMR results for sample BS-1-H: raw spin-echo decay (*top*), incremental T2 distribution (*middle*) and cumulative T2 distribution (*bottom*)

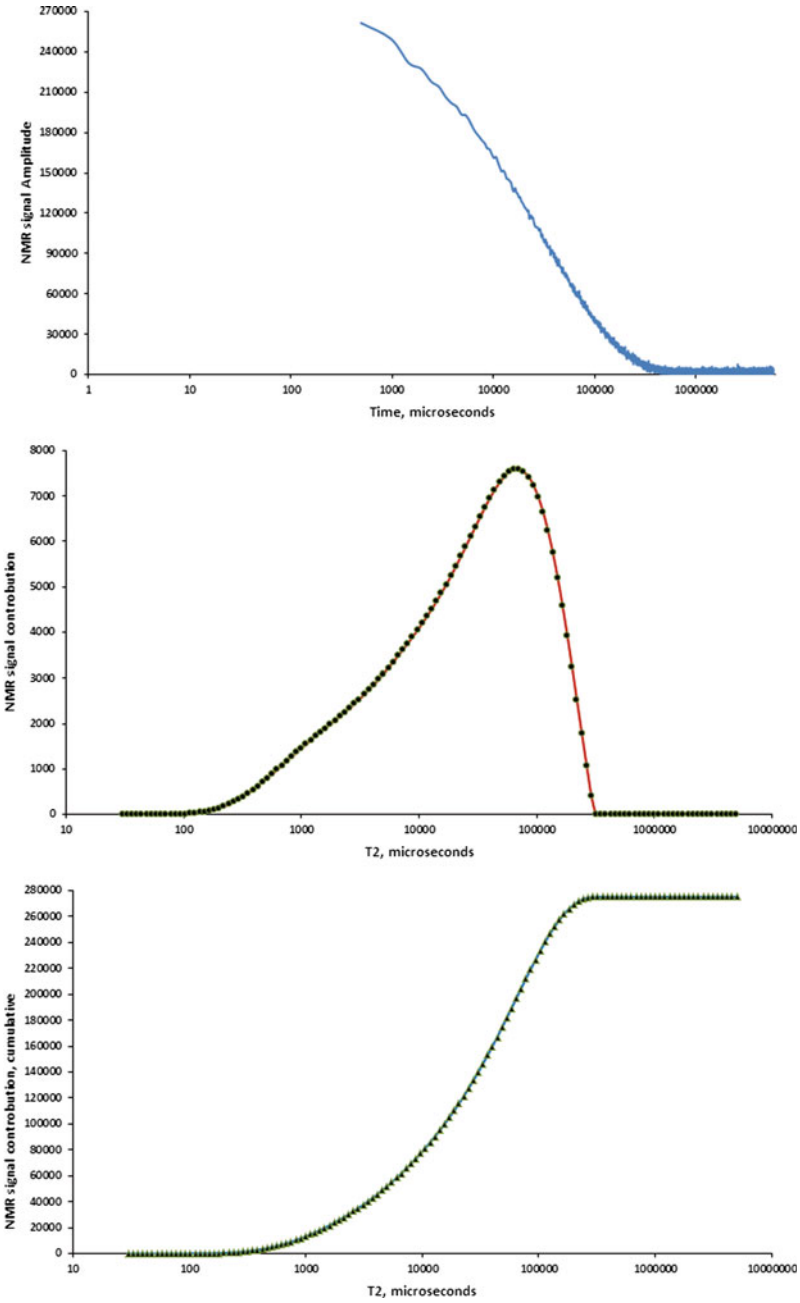

Fig. 4.50 NMR results for sample DB-1-H: raw spin-echo decay (*top*), incremental T2 distribution (*middle*) and cumulative T2 distribution (*bottom*)

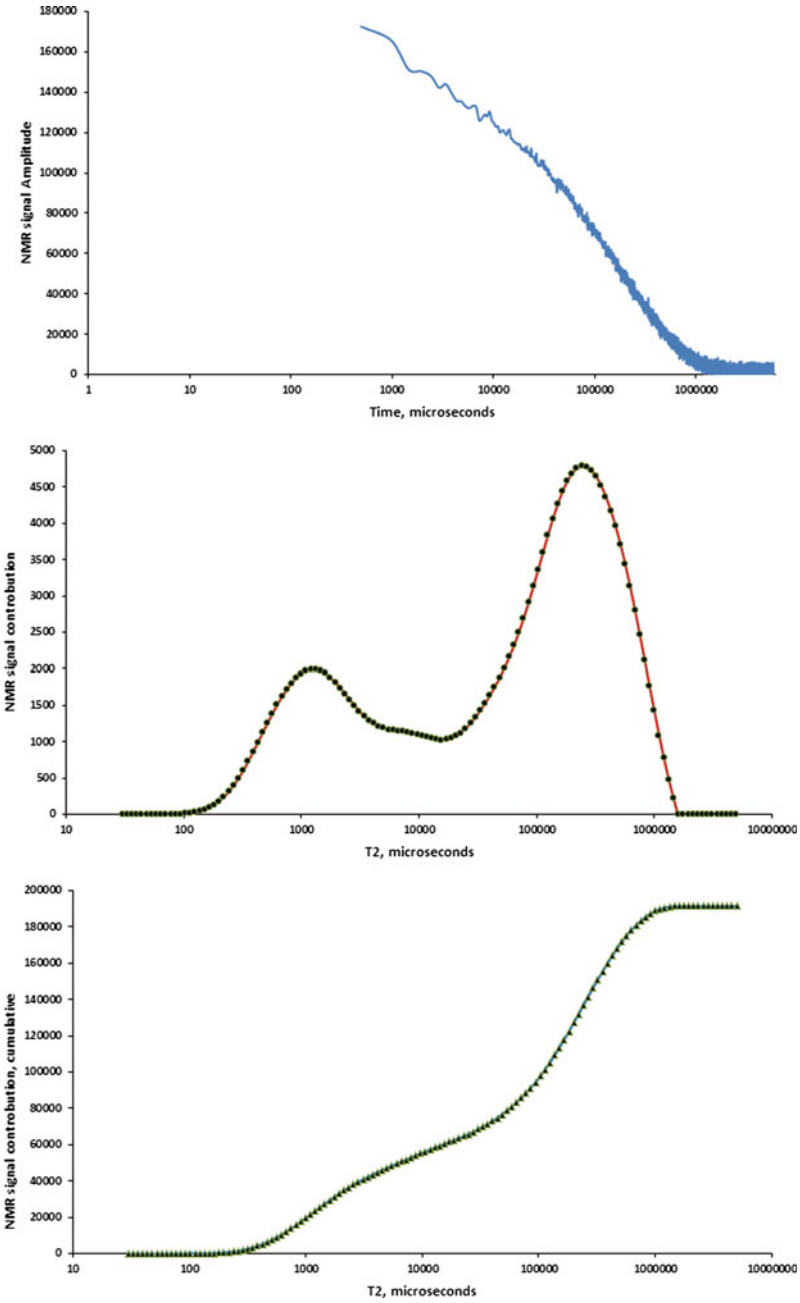

Fig. 4.51 NMR results for sample CL-40-H: raw spin-echo decay (*top*), incremental T2 distribution (*middle*) and cumulative T2 distribution (*bottom*)

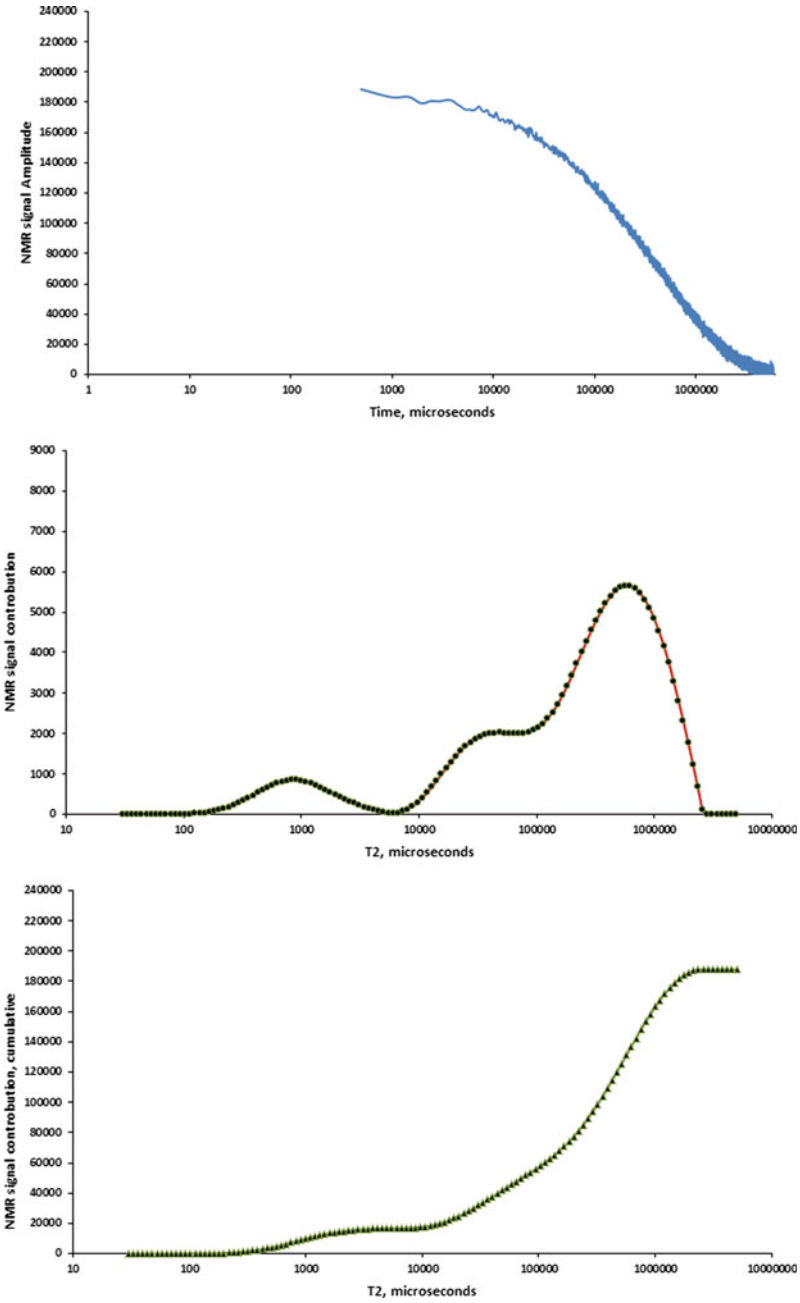

Fig. 4.52 NMR results for sample CO2CRC-2-H after flooding: raw spin-echo decay (*top*), incremental T2 distribution (*middle*) and cumulative T2 distribution (*bottom*)

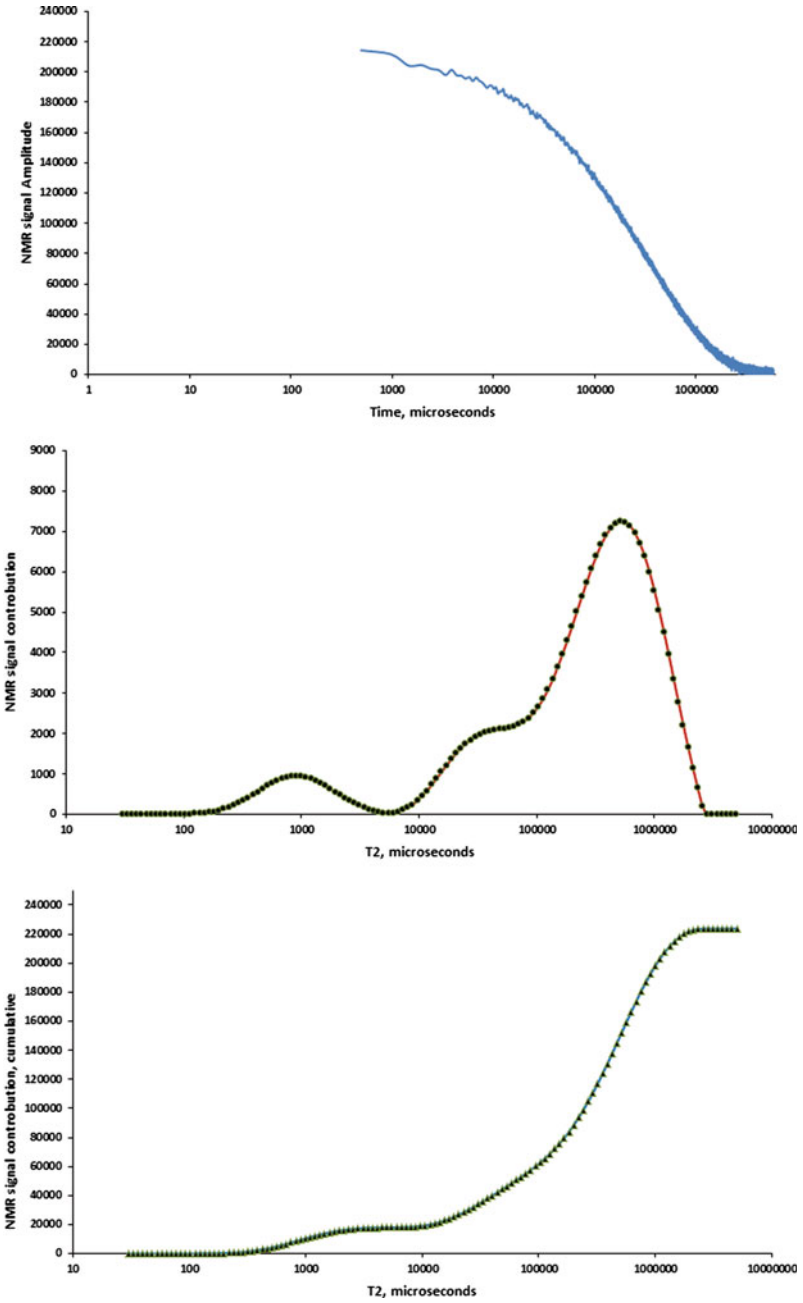

Fig. 4.53 NMR results for sample CO2CRC-3-H after flooding: raw spin-echo decay (*top*), incremental T2 distribution (*middle*) and cumulative T2 distribution (*bottom*)

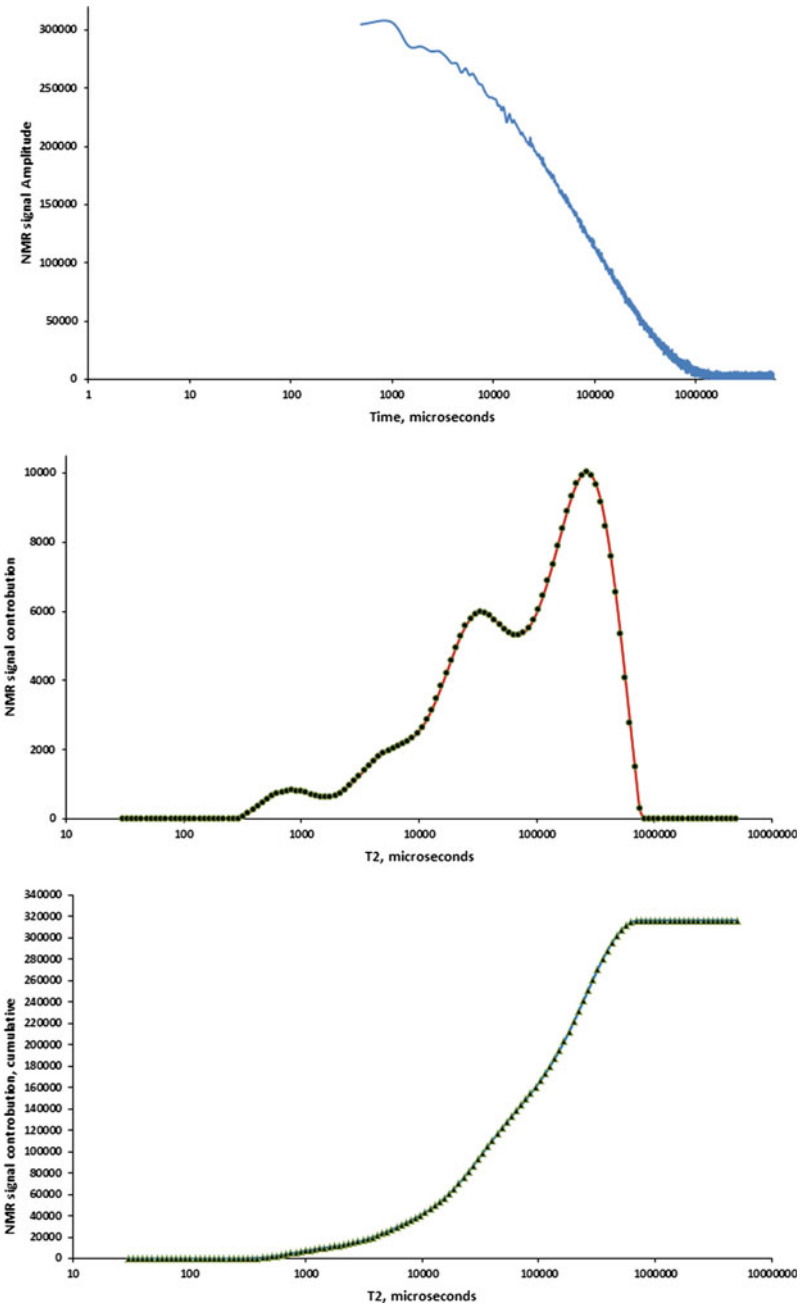

Fig. 4.54 NMR results for sample CO2CRC-36-V after flooding: raw spin-echo decay (*top*), incremental T2 distribution (*middle*) and cumulative T2 distribution (*bottom*)

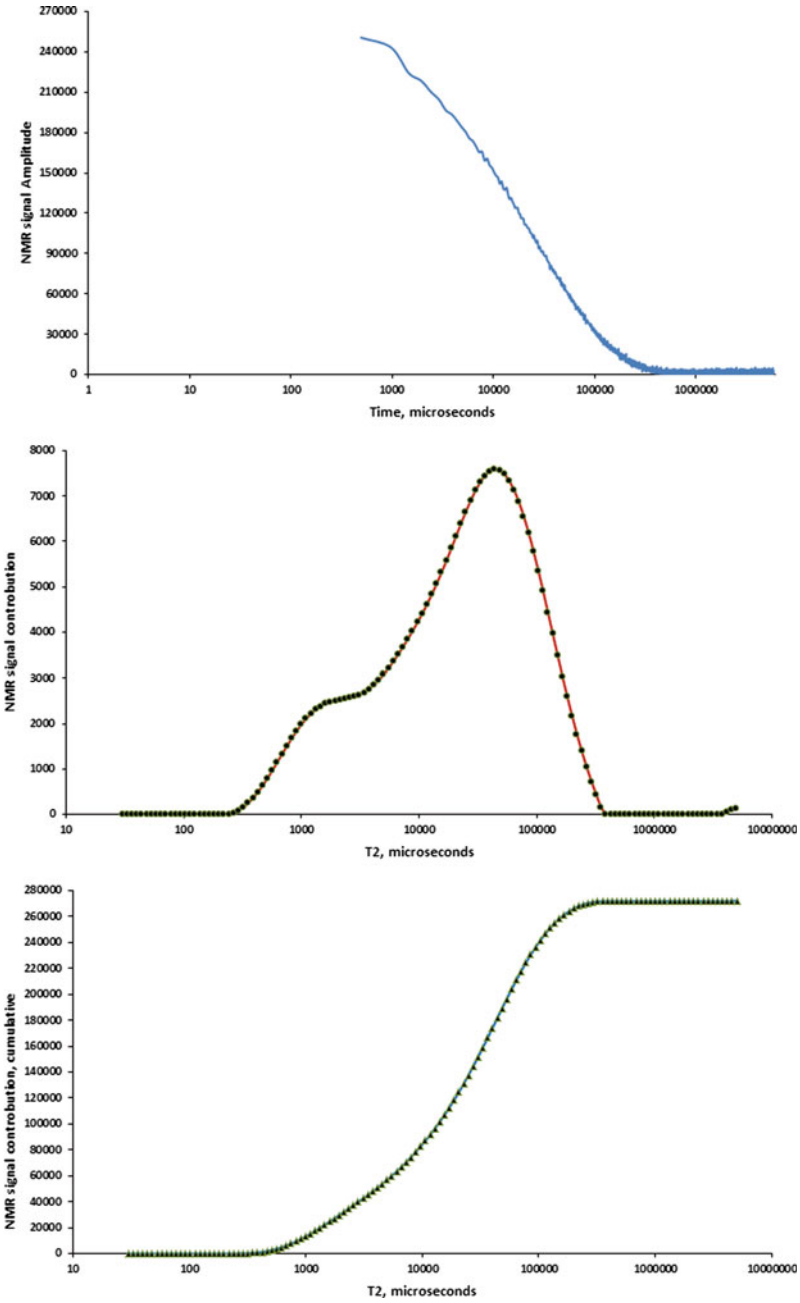

Fig. 4.55 NMR results for sample DB-1-H after flooding: raw spin-echo decay (*top*), incremental T2 distribution (*middle*) and cumulative T2 distribution (*bottom*)

Table 4.8 Porosity values for a number of the core samples after performing the flooding experiments on them

No.	Group no.	Sample ID	Length (cm)	Diameter (cm)	Porosity (%)
2	1	CO2CRC-2,3-H*	9.14	3.88	17.18
4	1	CO2CRC-11,14-H*	8.17	3.87	21.84
5	1	CO2CRC-36-V	8.57	3.86	17.1
7	2	BS-1-H	8.42	3.72	17.85
13	4	CL-40,68-H*	9.77	3.83	14.33

* Composite core samples

Table 4.9 Increase in the concentration of a number of chemical element in a mixture of several brine samples after being injected through a few samples

Chemical species	Unit	Amount of increase after the test
Bicarbonate as $CaCO_3$	mg/l	480
Calcium- filterable	mg/l	123
Carbonate as $CaCO_3$	mg/l	<1
Magnesium- filterable	mg/l	37
Potassium- filterable	mg/l	1
Silica as Si	mg/l	2.7

The first part of the NMR results is presented in Figs. 4.45, 4.46, 4.47, 4.48, 4.49, 4.50, and 4.51 in the form of raw spin-echo decay and both incremental and cumulative T2 distributions for each sample tested. These figures show the NMR results for the tests conducted on the samples before they went through the core-flooding experiments.

As indicated before in Table 4.2, some of the samples used were composite samples including Sample CO2CRC-2,3-H. As can be seen from the results plotted in Figs. 4.45 and 4.46, for the purpose of NMR measurements, the short core-plugs making up this composite core were tested individually. In this manner, not only each sample can be examined on its own for any change in its NMR response after undergoing the cyclic injections, but also any possible effect of the distance to injection point on the way these potential changes may occur can be investigated.

Figures 4.52, 4.53, 4.54, and 4.55 show the results of the NMR tests conducted on a number of samples after being subjected to the cyclic flooding experiments. These results are also plotted as raw spin-echo decay and both incremental and cumulative T2 distributions for each sample tested.

4.6 Results of Other Complementary Measurements

After carrying out the cyclic flooding tests, a second set of porosity measurements was conducted on a number of the core samples. Two chemical composition analyses were also performed on two samples of the brine used during the

core-flooding experiments. One of the brine samples was taken from the original brine before being injected through the core samples and the other sample was a mixture of several brine samples taken from the produced brine on the outlet side of a few samples including two Berea and two of the cores taken from the CO2CRC's Naylor Field. These complementary analysis and measurements were conducted in order to better understand the effects that the coupled supercritical CO_2 and brine flow may have on the petrophysical characteristics of the core samples. Table 4.8 presents the dimension and porosity measurements conducted on a number of core samples after the completion of the core-flooding experiments.

Table 4.9 has been constructed using the results of the two brine chemical composition analyses mentioned earlier. The third column of this table shows the amount of increase in the concentration of a few chemical species, which could potentially have originated from the possible chemical reactions between the rock and the fluids during the flooding experiments.

References

1. Lyons WC, Plisga GJ (2005) Standard handbook of petroleum and natural gas engineering, 2nd edn. Gulf Professional Publishing Elsevier, Burlington
2. Tiab D, Donaldson EC (2004) Petrophysics. Gulf Professional Publishing–Elsevier, Burlington
3. Abu-Khamsin SA, Ayub M, Al-Marhoun MA, Menouar H (1993) Water flooding in a tarmat reservoir laboratory model. J Pet Sci Eng 9:51–261
4. Hinkley RE, Davis LA (1986) Capillary pressure discontinuities and end effects in homogeneous composite cores: effect of flow rate and wettability. SPE 15596, SPE annual technical conference and exhibition, Copyright 1986, Society of petroleum engineers, Inc., New Orleans, Louisiana
5. Øyno L, Uleberg K, Whitson CH (1995) Dry gas injection in fractured chalk reservoirs—an experimental approach. Society of core analysts symposium, San Francisco, CA, USA
6. Zekri AY, Almehaideb RA (2006) Relative permeability measurements of composite cores—an experimental approach. Pet Sci Technol 24:717–736

Chapter 5
Interpretation, Analysis and Discussion

5.1 Introduction

Apart from the basic routine core analysis, 20 cyclic core-flooding experiments and 11 NMR measurements were conducted on a total of 13 sandstone core samples during the experimental work carried out throughout this research. In addition, two chemical composition analyses were also done on the brine samples taken during the flooding tests. The results obtained through running the above-mentioned experiments were presented in details in the previous chapter. This chapter, however, is dedicated to the interpretation, analyses and discussion of those results, to find out how they help achieving the research objectives outlined earlier.

This chapter starts with a short analysis of the relationship between the porosity and permeability of the samples. Then, using the experimental results obtained, the effects of a number of factors on the multiphase flow characteristics of the rock-fluids system during underground CO_2 disposal will be analysed and discussed. As mentioned previously, all the experimental work carried out were designed while keeping in mind the common goal of achieve the research objectives. Here again, all the analyses and discussions are organised in a way that would help achieving the same goal. It is worth noting that for a number of factors investigated during this research and the obtained results, to the best of the author's knowledge, there were no similar or analogous studies done to date, the results of which are available in the literature. Therefore, during the related analyses and discussions no reference can be made to any published literature for comparison purposes.

A. Saeedi, *Experimental Study of Multiphase Flow in Porous Media during CO_2 Geo-Sequestration Processes*, Springer Theses, DOI: 10.1007/978-3-642-25041-5_5,

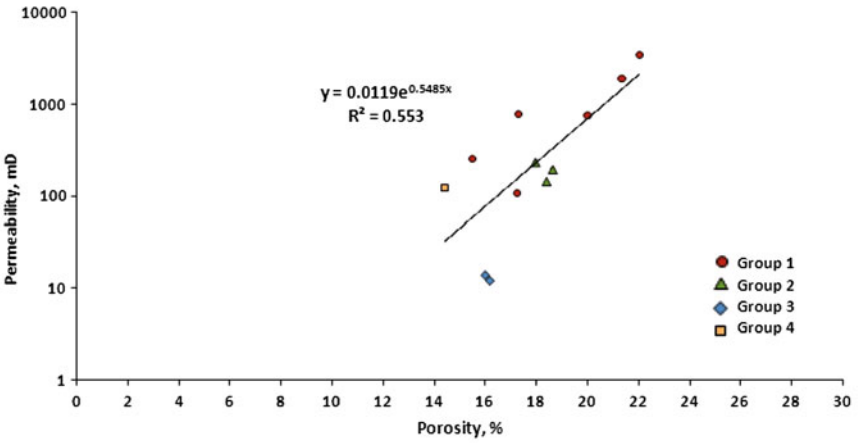

Fig. 5.1 Porosity–permeability relationship for various samples within different groups

5.2 Porosity–Permeability Relationship of Samples

As discussed previously in Chap. 4, the core samples used during the experiments were all sandstone and based on their origin, porosity and permeability values and the type and degree of their clay content, were divided into four groups (Table 4.2). Presented in Fig. 5.1 is a cross-plot showing the typical relationship between the porosity and permeability values of the core samples. Despite the fact that there may not be a valid universal relationship defined between the porosity and permeability of a porous medium [1, 2], it is apparent from the figure below and as generally one may expect, the lowest porosities belong to the lowest permeable samples and the highest ones belong to the samples which have the highest permeabilities.

5.3 Effects of Cyclic CO_2-Brine Flooding

As briefly discussed in Chap. 2, cyclic or alternating CO_2-brine flooding may be experienced by parts of the porous medium, in one way or another, during many CO_2 geo-sequestration processes. This flooding pattern is more frequently observed during seasonal or intermittent injection or where CO_2 is injected in alternative cycles with water in an attempt to obtain a better lateral dispersion of CO_2 and/or control the mobility and impede the fast upward evolution of the CO_2 plume or enhance the permanent sequestration of CO_2 in form of the trapped residual phase. The CO_2-brine core-flooding experiments carried out by other researchers to date do not extend beyond two injection cycles, including a primary

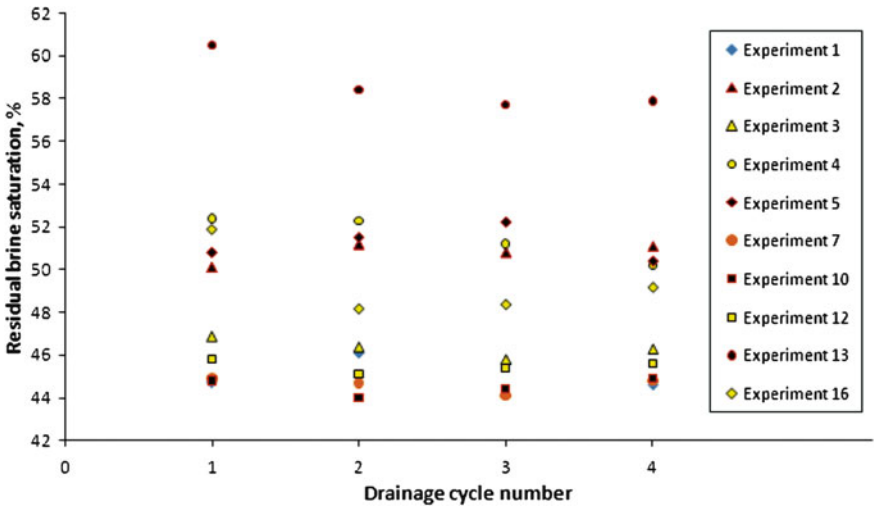

Fig. 5.2 Residual brine saturation data obtained at the end of all drainage cycles

drainage flood followed by a subsequent imbibition flood. The results presented in Sect. 4.4.1 of Chap. 4 in the form of brine production and differential pressure profiles, however, were for various core samples subjected to extra extended cyclic CO_2-brine injections of up to seven injection cycles. During the following discussions, using the experimental results achieved, the potential effects of such cyclic flooding on the multiphase flow characteristics of the rock-fluids system during subsurface CO_2 storage will be analysed and discussed.

5.3.1 Effects on the Saturation Profiles

5.3.1.1 Drainage Cycles

Figure 5.2 shows the end-point residual brine saturation data for the total of four drainage floods performed on various samples. With regards to the effect of the cyclic injection on the production profiles or the end point saturations, as can be seen from Fig. 5.2, apart from a number of slight variations, there is no significant or consistent trend apparent among the data. The saturation data for experiments number 6, 8, 9, 11, 14 and 15 are not included in this plot. Experiments number 8, 9, 11 and 14 were run for sensitivity analysis only, and their experimental conditions (e.g. net effective stress or injection flow-rate) were different from the rest of the experiments and experiments 6 and 15 only produced quality saturation data during their first drainage floods. As stated above, it seems that the saturation data from one cycle to the other were not affected by the cyclic flooding process;

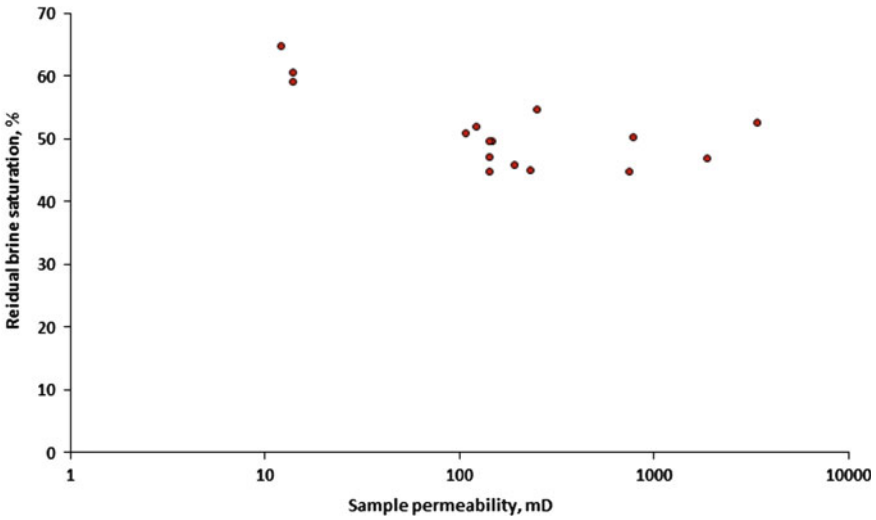

Fig. 5.3 Residual brine saturation values at the end of the first drainage cycle for all 16 experiments conducted

however, there are a number of points, which need to be discussed about the saturation data for each individual drainage flood. A number of the following discussions are presented on the saturation data for the first drainage flood only but since all drainage floods produced fairly similar results, they can be extended to the rest of three drainage floods.

If the end-point saturation data presented in Table 4.4 are analysed closely it can be seen that the residual brine saturations achieved at the end of the primary drainage floods are abnormally high across the whole range of the samples tested. These abnormal residual saturations become more apparent when they are compared to those resulted from using the CH_4-brine fluid system (Table 4.6) for a number of samples tested for a second time using this fluid system. For the samples tested using both CO_2-brine and CH_4-brine fluid systems, residual brine saturations at the end of the drainage floods are on average about 15% higher when CO_2 displaced the brine ($S_{wr,ave} = 46.4\%$) compared to when CH_4 displaced the same brine ($S_{wr,ave} = 32.1\%$) under the same P–T conditions. These abnormal trends are also evident among the limited experimental data available in the literature [3–7]. Furthermore, if the end-point residual saturations are plotted versus sample permeability (Fig. 5.3), it can be seen that the residual brine saturations do not show the expected inverse linear relationship with permeability, especially for the moderate to high permeability samples.

The most likely reason behind the abnormal trends observed among the saturation data obtained from the drainage floods lay within the forces (i.e. capillary and viscous) which may dominate the displacements and the possible interplay between these forces. The drainage floods conducted here were suffering from

Table 5.1 Comparison between CO_2 and CH_4 viscosity and IFT (when in contact with brine) under the experimental conditions applied

Fluid	Viscosity (cP)	IFT (mN/m)
CO_2	0.039	30
CH_4	0.017	45
Brine	0.36	–

Table 5.2 Comparison of the displacement efficiency indicators between the two cases of CO_2 displacing the brine and CH_4 displacing the brine

Test no.	Sample ID	CO_2 injection	CH_4 injection	Pore volume brine produced up to BT (fraction)	End point residual brine saturation (%)
2	CO2CRC-2,3-H	x		0.356	50.1
17			x	0.595	35
7	BS-1-H	x		0.338	44.9
18			x	0.507	29.4
10	BS-2-H	x		0.347	44.8
19			x	0.482	35
12	BS-3-V	x		0.371	45.8
20			x	0.576	29.1

highly unstable displacement fronts promoted by high mobility ratio. In addition, low IFT between the supercritical CO_2 and brine under experimental conditions applied, further intensified the instability of the displacement front. Generally, as also pointed out by McDougall et al. [8], during an immiscible drainage displacement dominated by high viscosity ratio ($M \gg 1$), reduction in the IFT renders the displacement front less stable worsening the viscous fingering which would eventually result in early breakthrough of the less viscous non-wetting fluid. The early breakthrough coupled with high viscosity contrast not only reduces the recovery of the displaced wetting phase at breakthrough but also decreases the final achievable recovery factor. In fact, for those samples tested using both fluid systems, if the results of the experiments conducted using CH_4-brine fluid pair is compared to those of the CO_2-brine system, the effect of change in IFT and how it may help to improve the displacement efficiency becomes more apparent.

As can be seen from Table 5.1, under the P–T conditions applied during the experiments, the IFT of the CH_4-brine system is about 30% greater than that of the CO_2-brine system. Furthermore, the viscosity ratio of the CH_4-brine fluid pair is nearly 130% greater than that of the CO_2-brine fluid system. Based on the difference between the viscosity ratios one may tend to conclude that the sweep efficiency during the displacement of brine by CO_2 would be higher than when CH_4 displaces the brine. However, the experimental results proved otherwise. As can be seen from the data presented in Table 5.2, the sweep efficiency indicators (e.g. the volume of brine produced up to the less viscous non-wetting phase breakthrough (BT) and the end-point residual brine saturation) are signalling a more uniform and efficient displacement occurred during the displacement of brine

by CH_4. The only parameter which could have helped the CH_4-brine system to achieve this is the fluid system's IFT. One more evidence which could be presented in support of a more uniform displacement during the displacement of brine by CH_4, as apparent from the brine production profiles presented previously in Chap. 4 for the two fluid systems, is the considerably less incremental brine produced close to the end of the CH_4 injections due to the "bump flows" compared to that of the CO_2 injection floods. It should be noted that in order to eliminate any effect of variation in flow-rate on the displacements, for each sample the injection flow-rates for both CH_4 and CO_2 floods were the same. The observed effect of IFT on the sweep efficiency during such drainage floods as those conducted here can also be seen in the experimental results published by Bennion and Bachu [4]. The results published by the authors show that displacement of brine by H_2S (lower IFT) resulted in higher residual brine saturations compared to displacement of brine by CO_2 (higher IFT) under the same experimental conditions.

It is worth noting that, since the sandstone samples used were all considered to be strongly water-wet, without any wettability alterations, for both CO_2 and CH_4 displacements, the contact angles are assumed to be zero. However, if wettability alteration due to CO_2 contact with the porous medium [9] is also considered to occur, the difference in contact angle (θ) between the CO_2-brine and CH_4-brine systems could also influence the displacement.

It should be noted that the effect of change in IFT on the sweep efficiency during a drainage process would be most felt if the displacement suffers from a high mobility ratio. Otherwise, if the mobility ratio is less than one, in such processes, lowering or increasing the IFT is not expected to cause any considerable changes to residual wetting phase saturation.

As indicated earlier, Fig. 5.3 shows the end-point brine saturations obtained at the end of the first drainage floods performed on various samples. For the same reasons stated earlier, the saturation data for Experiment No. 8, 9, 11 and 14 are not included in the plot. As mentioned earlier and can be seen in the figure, the residual brine saturations for a number of the samples do not fit well into the expected trend of being inversely proportional to the permeability of the samples. Even, considering the saturation data for the highest permeability samples, one may expect that for sufficiently high permeabilities the trend may level off or even become opposed to the expectations. Apart from the occurrence of non-uniform displacement under the influence of low IFT and high mobility ratio, other possible causes of such behaviour could be unstable displacement caused by excessively high displacement velocities [10] or gravity segregation [11, 12].

Unstable displacement may be excluded from the likely causes as it was investigated by flow-rate sensitivity analysis. Experiment 11 is a repeat of Experiment 10 carried out afterwards, through the normal cyclic flooding procedure explained elsewhere, while decreasing the CO_2 injection flow-rate from 300 to 120 cc/hr and brine injection flow-rate from 200 to 100 cc/hr. Both of these experiments were conducted on Sample BS-2-H, which was a sample with a moderate permeability. As can be seen in the saturation data presented in Table 5.3, for the first drainage cycle, not only this change did not improve the

Table 5.3 The results of flow-rate sensitivity analysis performed on two samples

Test no.	Sample ID	k (mD)	CO_2 Flow-rate (cc/hr)	Pore volume brine produced before BT (fraction)	End point residual brine saturation (%)
10	BS-2-H	141.1	300	0.347	44.8
11	BS-2-H	141.1	120	0.316	49.5
13	DB-1-H	14	150	0.274	60.5
14	DB-1-H	14	200	0.280	59.0

sweep efficiency, which could have done through promoting presumably more stable displacement, but also reduced the brine recovery both at CO_2 breakthrough (BT) and at the end of the drainage cycles. The reduced brine recovery occurred because the coupled effect of high mobility ratio and low IFT became more pronounced in the case of low injection flow-rate, which in turn reduced the brine recovery by promoting a more non-uniform displacement. The same sensitivity analysis was performed once again on a low permeability sample (Sample DB-1-H). Here the CO_2 injection flow-rate was increased to 200 cc/hr from an original value of 150 cc/hr and brine injection was increased from 100 to 150 cc/hr. The higher flow-rate once again did not promote unstable displacement and even slightly improved the sweep efficiency. Here the difference between the end point residual brine saturations achieved for the two scenarios was negligible because, as confirmed previously in the case of 150 cc/hr CO_2 injection, through conducting the "bump flow", the displacements were fairly uniform with minimum capillary interferences. The highly non-uniform and rate dependence of displacement of brine by CO_2 was also confirmed through core-flooding simulations carried out by Shi et al. [13].

The effect of gravity segregation was systematically removed from the experiments by placing the samples vertically inside the core-holder and performing the injections from base to the top. Therefore, the abnormal trend present among the saturation data measured for the samples with the higher permeabilities can only be attributed to the non-uniform displacement caused by the coupled effects of high mobility ratio, promoted by high viscosity contrast between the displaced and displacing fluids, and the low IFT. This argument is also supported by the relatively small Capillary Numbers (N_{ca}) (Eq. 3.4) and Rapoport Scaling Coefficients (Eq. 3.3) [14] calculated for each experiment and listed in Table 4.3.

If the saturation data reported in Table 4.4 are analysed further, it can be seen that there are a few samples for which some of the highest residual brine saturations were obtained. A list of these samples is presented in Table 5.4. Apart from the already presented discussion on the reasons of occurrence of such high residual brine saturations, using their physical characteristics or the results of further complementary analysis, in the following section of this chapter other reasons which could have possibly contributed to such abnormally high residual saturations will be examined.

Table 5.4 Samples with the highest end point residual brine saturations

Test no.	Sample ID	k (mD)	End point residual brine saturation (%)
2	CO2CRC-2,3-H	788.30	50.1
4	CO2CRC-11,14-H	3,409.80	52.4
6	CO2CRC-39,42-H	252.60	54.6
5	CO2CRC-36-V	108.22	50.8
13	DB-1-H	14.00	60.5
16	CL-40,68-H	123.50	51.9

Sample CO2CRC-11,14-H had one of the highest residual brine saturations but it was also the most permeable among all the samples, so most likely, its flooding process was severely influenced by combined effects of high mobility ratio and low IFT, resulting in such a high residual saturation value. Two other samples with the highest obtained residual brine saturations are DB-1-H and DB-2-V but, unlike CO2CRC-11,14-H, these two samples have the lowest permeabilities among all the samples. Low permeabilities, to some extent, help to explain their high residual saturations. Moreover, the incremental NMR T2 distribution data presented in Fig. 4.50 for Sample DB-1-H, which represents the relative pore size distribution within this sample, confirms that its pore size distribution contains a large proportion of small micro-sized pores as well as larger pores. Although such data is not available for DB-2-V but since it was cut from the same quarried block and adjacent to DB-1-H, it should have the same characteristics. During the CO_2 flooding of these samples, the brine present in small pores may not be displaced as the high mobility ratio discourages the CO_2 from invading them once it establishes its path through the larger pores [15]. There is still a possible reason for why sample DB-2-V has a higher residual brine saturation compared to DB-1-H, which will be explained later.

CO2CRC-2,3-H and CO2CRC-39,42-H were the next two samples with high residual brine saturations. If the high residual brine saturations in these samples are to be attributed to the coupled effects of high mobility ratio and low IFT, their residual saturations should be comparable to Samples CO2CRC-1-V and BS-1-H respectively, as these latter samples have permeabilities and dimensions close to the samples in question, and there was also no heterogeneities apparent in any of the samples, to which the high residual saturations could be attributed. The NMR T2 distributions presented in Figs. 4.45 and 4.46 for the two core-plugs included in Sample CO2CRC-2,3-H also show that at least this sample has relatively large pores and the overall shape of its relative pore size distribution is similar to that of the Berea samples. The main shared features between CO2CRC-2,3-H and CO2CRC-39,42-H are the fact that both of them are composite samples, each made up of two short samples and both are highly permeable and made of medium to coarse grained sandstones. Despite the fact that their end faces were polished and a few layers of lint-free tissue paper were inserted between them, most likely, there were two separate saturation anomalies present in each of these two composite samples during the flooding experiments. One close to their sample's outlet

as expected and another possibly at the joint between the two short core-plugs included in each sample. This type of saturation anomaly specific to composite cores has been also reported by other researchers [16]. Since the core-plugs making up these composite samples were made of relatively moderate to coarse grained sandstones, most likely, the polishing and insertion of tissue paper did not help to form a suitable capillary bridge between them and therefore the capillary discontinuity between the short plugs was not totally eliminated.

The last two samples to be discussed from Table 5.4 with regards to their high residual saturations are CO2CRC-36-V and CL-40,68-H. Both of these samples were of moderate permeability values, so the high residual brine saturations may be ascribed to the combined effects of high mobility ratio and low IFT, but the residual saturation levels for these samples were higher than those obtained for other samples of similar permeabilities and dimensions. One possible explanation for such behaviour lies within the NMR T2 distributions of these samples showing their relative pore size distributions. Figures 4.51 and 4.54 show that both of these samples have relatively high proportions of small pore sizes which could contribute to high residual saturations. It is worth noting that part of the small pore sizes picked up by the NMR test for Sample CL-40,68-H could belong to the relatively high glauconite content of this sample. Sample CL-40,68-H was a composite sample but since this sample, unlike the samples reviewed previously, was not made of coarse grained sand and perfect polished and smooth end faces were achieved with them, the existence of a saturation anomaly at the joint between the two core-plugs was excluded from the possible causes of its high residual brine saturation. The small pore sizes present in Sample CO2CRC-36-V were partly due to a narrow streak of fine grained sand diagonally cutting through the cross-section of the sample. The core-scale heterogeneity caused by the streak could also have played a part in its high residual brine saturation.

Generally, Berea Sandstone samples, had some of the lowest residual saturations, which could be attributed to their high degree of homogeneity coupled with their moderate permeability. The NMR T2 data generated for one of them (Fig. 4.49) also confirms that these samples benefited from a fairly homogeneous unimodal pore size distribution.

5.3.1.2 Imbibition Cycles

The end-point residual CO_2 saturations obtained at the end of all three imbibition floods conducted on all the samples are presented in Fig. 5.4. Similar to the brine residual saturations discussed before, apart from a number of slight variations, there is no significant trend present among the data plotted in Fig. 5.4, which can possibly be used to support any possible effect of the cyclic flooding on the saturation profiles. However, if the saturation data resulted from the first imbibition floods performed on various samples are analysed alone, there seems to be an excellent correlation between the residual CO_2 saturations and the permeability of the samples (Fig. 5.5). As one may expect, the residual saturation decreases with

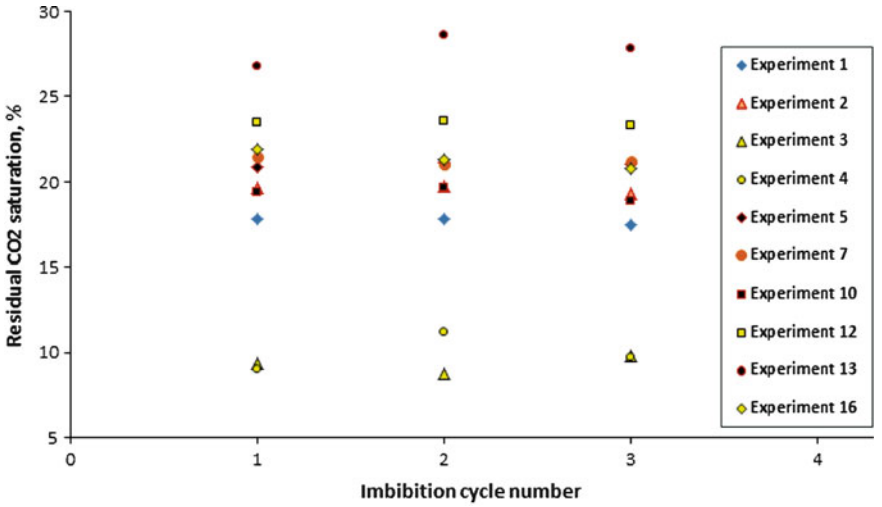

Fig. 5.4 End-point residual CO_2 saturations for all the imbibition cycles performed on various samples

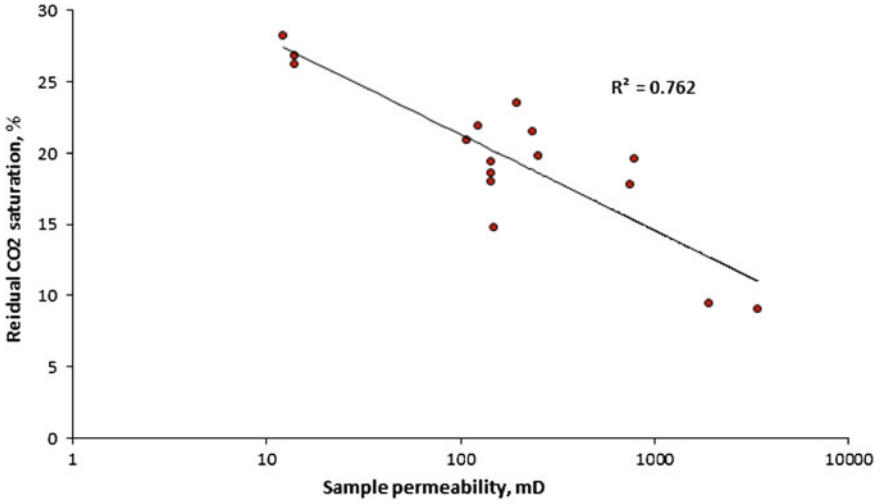

Fig. 5.5 Residual CO_2 saturtion versus sample permeability

increase in the sample permeability. Unlike the trend found among the residual brine saturations, the trend found here remains consistent across the whole range of permeability values. This can be interpreted as a sign that displacement during the imbibition floods was a uniform displacement without any major capillary interference. This is expected since considering the large contrast between the

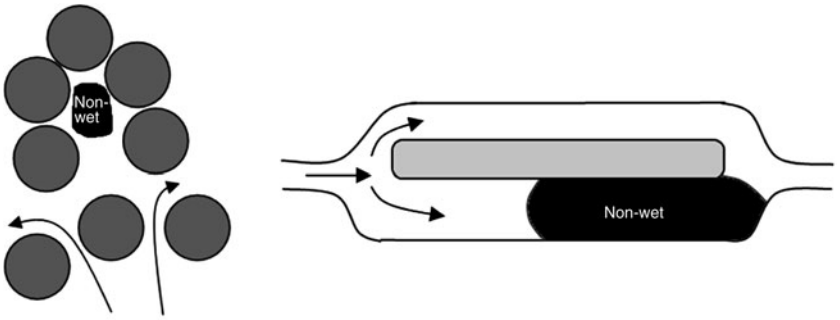

Fig. 5.6 The pore doublet (*right*) and dead-end (*left*) trapping models (after [17])

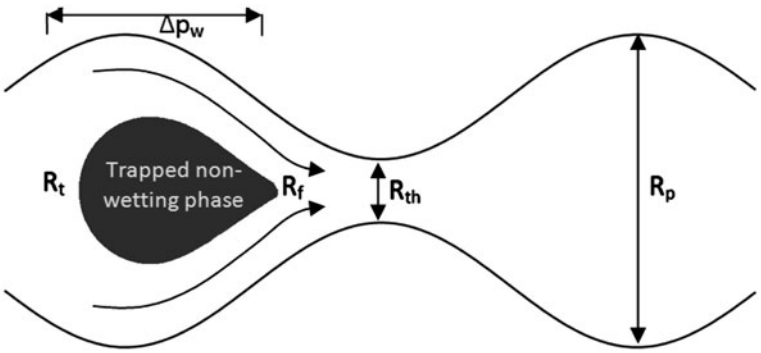

Fig. 5.7 The snap-off trapping model

viscosities of brine and CO_2 under the experimental conditions applied here, the displacement of CO_2 by brine benefits from a very low mobility ratio resulting in near perfect piston-like displacement type.

With brine being the wetting phase and CO_2 the non-wetting phase, the residual trapping of CO_2 in the pore space would occur as a result of pore scale capillary forces [17, 18]. Generally there are three trapping models which could be used to describe how the trapping of the non-wetting phase occurs. These three possible trapping models namely pore-doublet, dead-end and snap-off models [19, 17], are shown schematically in Figs. 5.6 and 5.7. The pore-doublet model is more frequently seen in poorly sorted rocks or in rocks with a dual-porosity network [17], while the severity of residual trapping caused by snap-off depends mainly on the aspect ratio of the pore to pore throat sizes. Because of the high contrast between the viscosities of brine and CO_2, which influences the mobility ratios during both drainage and imbibition, CO_2 normally does not tend to displace the brine located in smaller pores or the dead-ends to give rise to the possibility of residual trapping of CO_2 by the dead-end trapping mechanism during a subsequent imbibition flood.

Also, since the samples used during this research were mostly well sorted sandstones, the possibility of having residual saturation due to pore doublet was low. Therefore snap-off, which is normally known to be responsible for 80% of the trapped non-wetting phase in porous media, can be declared as the main trapping mechanism during the experiments conducted here.

As evident from the residual saturation data obtained at the end of the imbibition floods conducted during the cyclic CO_2-brine injections (Table 4.4), one important feature of such displacement processes is their relatively low residual CO_2 saturation levels compared to those obtained when other common gases are displaced by brine. As will be shown later, while conducting the core-flooding experiments on the same samples, replacing the CO_2 by CH_4, yielded considerably higher residual gas saturations. The most likely reason for this behaviour is explained in the next a few pages using the snap-off trapping model which is depicted in Fig. 5.7.

Figure 5.7 shows how a ganglion of the non-wetting phase may be trapped as residual saturation during an imbibition displacement process. If P_w and $P_{nw,up}$ are defined as the pressures within the wetting and non-wetting phases at the upstream point of the ganglion, the relationship between these two pressures and the capillary pressure (P_{ca}) can be defined by Eq. 5.1.

$$P_{ca} = P_{nw} - P_w \tag{5.1}$$

Then replacing P_{ca} with appropriate terms and rearranging the equation results in the following equation.

$$P_{nw,up} = P_w - \frac{2\sigma \cos\theta}{R_t} \tag{5.2}$$

Where: σ = interfacial tension between the wetting and non-wetting phases
R_t= radius of the large upstream part of the ganglion
θ = contact angle

Similar relationship can be written between the pressures downstream of the ganglion:

$$P_{nw,down} = P_w - \Delta p_w - \frac{2\sigma \cos\theta}{R_f} \tag{5.3}$$

Where: $P_{nw,down}$ = pressure in the non-wetting phase downstream of the ganglion
R_f= radius of the small downstream part of the ganglion
Δp_w = pressure drop in the wetting phase across the ganglion length

It is clear that the trapped non-wetting ganglion can move through the pore throat constriction if only $P_{nw,down} < P_{nw,up}$, which means:

$$\Delta p_w > 2\sigma \cos\theta \left(\frac{1}{R_f} - \frac{1}{R_t}\right) \tag{5.4}$$

As can be seen from Fig. 5.7, with a good approximation R_f and R_t could be replaced by R_{th}(radius of the pore throat) and R_p(radius of the pore body) respectively. This results in Eq. 5.5.

$$\Delta p_w > 2\sigma \cos\theta \left(\frac{1}{R_p} - \frac{1}{R_{th}}\right) \tag{5.5}$$

What Eq. 5.5 means is that the possibility of the ganglion being trapped depends not only on the aspect ratio of the pore channel but also on the IFT (σ) between the wetting and non-wetting phases. In other words, as one main objective during many EOR processes, if during an imbibition process all flood conditions (e.g. pressure, temperature, etc.) remain the same, a reduction in the IFT would result in lower residual saturation of the non-wetting phase. Therefore, for the case of CO_2 and brine, due to the low IFT between the two phases, we can expect to have low trapped residual CO_2 saturations. This is exactly what the residual saturation data resulting from the imbibition cycles showed during this experimental work. The already low amount of trapped residual CO_2 could reduce further when it is coupled with abnormally high residual brine saturations, which is likely to result, due to high mobility ratio and low IFT, during the displacement of brine by the injected CO_2. Since less brine is displaced during a drainage flood, less CO_2 would be available to be potentially trapped as a residual phase during a subsequent imbibition process. This is in agreement with the "Land" trapping model [20], which relates the trapped residual non-wetting phase during an imbibition process to the maximum non-wetting phase saturation achieved at the end of the preceding drainage cycle.

5.3.1.3 Some Practical Implications

Based on the experimental results obtained the cyclic flooding pattern is not expected to influence the saturation profiles achieved during CO_2 geo-sequestration processes, however, the discussions presented on the displacement efficiency during such processes can have important implications for any planned CO_2 geological storage project.

Normally, when it comes to storing CO_2 in geological media, one big concern among the members of the public as well as the technical community is whether the injected CO_2 would stay where it is injected to, at least over reasonable times scale (e.g. geological time) if not for perpetuity. Any potential leakage could

eventually lead to CO_2 reaching the surface and not only being released to the atmosphere again undermining the whole purpose of CO_2 geo-sequestration but also could possibly contaminate the vital potable water aquifers along the way.

Overall, as discussed in details in Chap. 2, the injected CO_2 can be permanently trapped in the subsurface geological structures through four different trapping mechanisms of structural trapping, solubility trapping, capillary residual trapping, and mineral trapping [3, 21–25]. Among the four potential trapping mechanisms capillary residual trapping and mineral trapping are considered the safest and any CO_2 trapped through these two mechanisms can be considered to have been trapped permanently over any time scale. As also pointed out before, the mineral trapping process is very slow and is expected to take hundreds if not thousands of years from the onset of the CO_2 injection to reach its full trapping potential. Furthermore, many underground reservoirs have low mineralisation potential. Also, since the mineralisation process is extremely slow, generally, there needs to be an extensive sealing layer in place to keep the solute and the formation minerals in contact for long enough time so the chemical reactions would start to work. The entrapment of CO_2 through capillary residual trapping, however, is fast, can occur in any type of geological formation and there is no need for a sealing layer to make it happen. Furthermore, under desired conditions, the amount of trapped CO_2 through capillary residual trapping could be considerable. Therefore, it can be concluded that CO_2 entrapment in the form of the residual saturation within the pores of the host formation is the most desirable among all four possible active trapping mechanisms.

While capillary residual trapping has considerable potential to help all CO_2 geo-sequestration processes achieving their common objective, the experimental results obtained during this research show that first of all the levels of residually trapped non-wetting phase is significantly less when brine displaces CO_2 compared to when for example brine displaces CH_4. Secondly, the significance of the residual capillary trapping in real life operations is dependent on many factors. Among others, two factors which found considerably influencing this process were formation permeability and injection flow-rate. As expected, the higher the permeability, eventually, the less going to be the amount of CO_2 trapped in the form of residual saturation. Low CO_2 injection flow-rate could have similar impact on the residually trapped CO_2 volumes as the high formation permeability. It should be noted that the injection velocities during the experimental work carried out here were all several orders of magnitude higher than those achievable during the real life in situ fluid displacements. Therefore, the residual saturations obtained here could be considered too optimistic compared to the overall residual saturation levels realistically achievable over the entire storage medium in real life.

While CO_2 sequestration in high permeability geological media may seem attractive as they benefit from high injectivity, the fact that the capacity of such formations to trap CO_2 in the form of the desired residual saturation is low, could make them less favourable for CO_2 geo-sequestration, especially when CO_2 is going to be injected in the absence of a comprehensive seal to trap the large volume of free CO_2 migrating upwards. However, the undesirable low injectivity

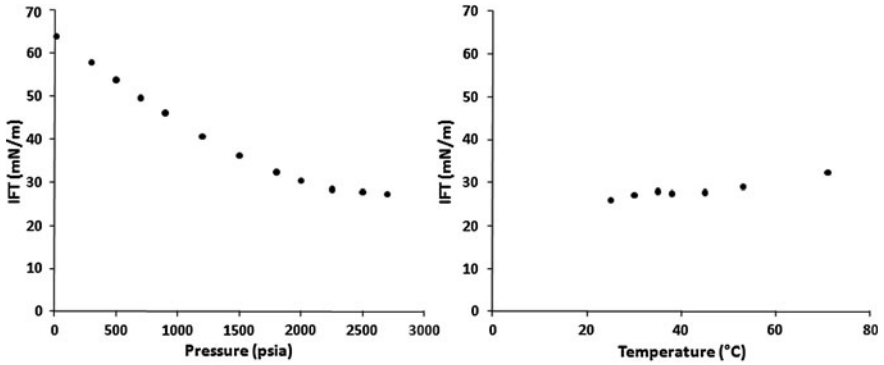

Fig. 5.8 Effect of pressure and temperture on the IFT of the water–CO_2 system (data taken from [32])

during injection into low permeability reservoirs, demands a thorough screening process to establish a range of formation permeability which while offers acceptable levels of CO_2 injectivity, on the other hand, provides adequate volumes of residually trapped CO_2.

Density contrast (gravity forces), viscosity ratio (viscous forces) and IFT (capillary forces) are the three main fluid property related factors which could have considerable impact on the performance of any immiscible displacement in porous media. Generally, as the experimental data obtained during this research also demonstrated, due to very low viscosity ratio the displacement of CO_2 by the wetting brine phase, during majority of the CO_2 geo-sequestration processes, is expected to be of piston-like type benefiting from a stable front which would result in a uniform displacement. On the other hand, during the CO_2 injection stage, as discussed earlier, due to high viscosity ratio and low IFT, displacement front is highly unstable resulting in highly non-uniform displacement of wetting phase brine by CO_2. The in situ pressure and temperature, which are mainly dependant on the depth at which the storage medium is located, are the two main parameters which control the fluid properties. Based on the available data and models in the literature [26–30] the densities and viscosities of the fluids and fluid mixtures involved during the CO_2 geo-sequestration process increase with increase in pressure while temperature has the inverse effect. Again based on the published data in the literature [31–33] the IFT of the CO_2-brine system decreases with increase in pressure but increases with increase in temperature (Fig. 5.8). However, as can be seen from Fig. 5.8, the available experimental data show that the effect of pressure on IFT is much stronger than that of temperature.

The experimental results obtained here, when the displacement efficiency of the CO_2-brine system is compared to that of the CH_4-brine system, clearly, indicated that during a drainage process dominated by high viscosity ratio ($M \gg 1$), any alteration to the IFT has significantly higher impact on the displacement performance than any change to the viscosity ratio as long as the viscosity ratio remains

high ($M \gg 1$). Also, any change to the IFT of the system can considerably alter the significance of the snap-off model to trap the non-wetting CO_2 when it is being displaced by brine (imbibition). Therefore, when taking into account the earlier presented review of the effect of pressure and temperature on fluid properties, it can be concluded that the deeper the target storage medium is, overall, the lower going to be the IFT of the system which eventually may lead to lower levels of capillary residual trapping of the injected CO_2. For example, using the data plotted in Fig. 5.8 and considering an average hydrostatic pressure gradient of 0.435 psi/ft (fresh water), an increase of 2,300 ft (701 m) in depth from 3,415 ft ($P = 1{,}500$ psia) to 5,715 ft ($P = 2{,}500$ psia) causes a decrease of almost 30% in IFT of the CO_2-brine system. As the experimental results showed, a 30% reduction in IFT from the CH_4-brine system to CO_2-brine system decreased the volumes of the capillary trapped non-wetting phase by an average of 10%. It is worth noting that increase in the depth could decrease the density contrast between the in situ brine and the injected supercritical CO_2 and reduce the intensity of the buoyancy forces acting on the injected CO_2 to push it upwards. Therefore, there may not be a solid conclusion drawn on whether injecting CO_2 into deeper formations would make it less safe than the shallower formations to trap large volumes of CO_2. It is worth mentioning that, when it comes to the depth requirement of a CO_2 storage medium it has already been established that the injection should be performed deep enough for the CO_2 to exist in the dense supercritical state.

5.3.2 Effects on the Differential Pressure Profiles

Despite the fact that for the case of cyclic CO_2-brine injection, there could not be found any significant relationship between the saturation data from one cycle to the next, the data obtained for the differential pressure across the sample show moderate to strong dependence on the cyclic flooding pattern. As mentioned in the previous chapter and will be discussed in more detail later, apart from a slight difference between them, the pressure data obtained during both drainage and imbibition cycles show similar trends. Therefore, unlike the saturation data, the two collections of pressure data generated (one for drainage and another for imbibition) will be analysed and discussed together. One important point which needs to be mentioned with regards to the reported pressure data is that any data with a value less than 2 psi is outside the accuracy of the pressure sensors used. Therefore, for the high permeability samples (e.g. CO2CRC-2,3-H) part of the measured differential pressure profiles fall outside the accuracy of the pressure transducers but for the moderate permeability samples, apart from the low end-point pressures, the reported differential pressure profiles for the individual injection cycles were reliable in terms of accuracy.

The normalised differential pressures across the sample at a point in time just before CO_2 breakthrough (BT) for drainage floods performed on various samples are plotted in Fig. 5.9. The differential pressure values for each sample are

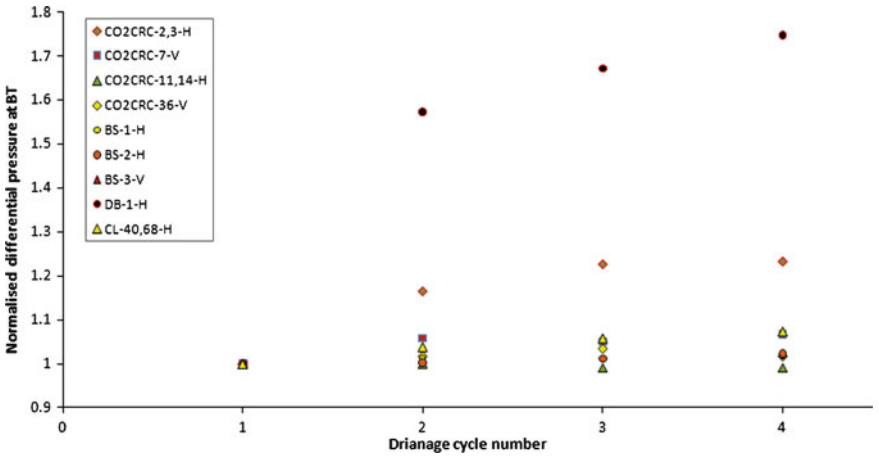

Fig. 5.9 Normalised differential pressures across the samples at a time just before CO_2 breakthrough (BT) for the drainage cycles

normalised by dividing them by the differential pressure for the first cycle for that sample. As can be seen from the graph, there seems to be a moderate trend present among the data. The apparent general trend shows increase in the differential pressure from the first cycle to the last. This increase, however, seems to tend to level off with increasing the number of cycles. A large portion of the data plotted in Fig. 5.9 are for moderate to high permeability samples and as evident from the graph, despite the existence of a reasonable trend among the data for these samples, they also suffer from a number of uncorrelated fluctuations. As already pointed out, the main reason for this behaviour is the fact that the differential pressure values (either the absolute values or their relative differences from one cycle to the next) for these samples were very small and the accuracy issue explained earlier dominated some of the measured data. One other possible cause of any uncorrelated fluctuation, as discussed in detail previously, could be non-uniform displacement of brine caused by high mobility ratio and low IFT.

For the majority of the samples tested, the moderate trend observed among the data reported in Fig. 5.9 starts to diminish after CO_2 breakthrough as each drainage cycle approaches its completion. This is demonstrated by plotting those data in Fig. 5.10 for the end of the drainage cycles. As can be seen from this graph, except for a few samples, including Sample DB-1-H, which is the lowest permeable sample, the rest of the data do not show any significant trend, which could be used to relate the change in the differential pressure profiles from one cycle to the next to the cyclic injection pattern. The likely cause of deviation from the original observed trend could be the fact that, first of all, towards the conclusion of each drainage cycle, the magnitude of the differential pressures become smaller and smaller until they stabilise and this makes the accuracy of the measured data worse towards the end of each cycle. Secondly, the recorded data after the CO_2

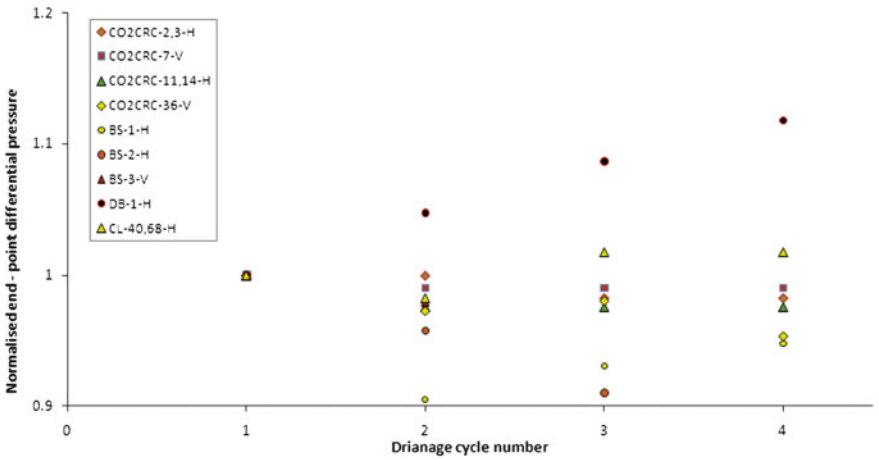

Fig. 5.10 Normalised end-point differential pressures across the samples at the end of the drainage cycles

breakthrough are strongly affected by non-uniform capillary dominated displacement. If the after breakthrough data could be corrected for the negative effects of these influencing factors, very likely, they would also show trends similar to those observed among the data for before CO_2 breakthrough.

A similar trend to the one observed among the differential pressure data for the drainage cycles can also be seen among the data reported in Figs. 4.33 and 4.34 for the imbibition cycles performed on two samples. The trend which exists among the imbibition data however, is persistent for almost all the data after brine breakthrough. This could be attributed to the fact that, unlike the drainage cycles, imbibition floods do not suffer from negative impacts of unfavourable mobility ratio and low IFT. Therefore, the imbibition displacements are fairly uniform all over. The viscosity of the displacing phase is also more than 10 times higher, which makes the differential pressure during the imbibition cycles to be larger in magnitude and less prone to measurement in-accuracies. The other parameter, which confirms the existence of a uniform displacement during the imbibition cycles, is the brine breakthrough time which, unlike the slightly fluctuating breakthrough times for the drainage cycles, remains almost the same from one imbibition cycle to the next for each sample tested. During the following discussion I have tried to find the most likely causes of the trends observed among the differential pressure data and see how these trends could be related to the cyclic flooding pattern.

Based on the data and discussions presented here the general conclusion could be that with each consecutive injection cycle the pressure drop within the porous medium increases, however, it tends to level off gradually. As explained in Chap. 2, one possible cause of such behaviour could be any formation damage which may occur inside the pore space due to the migration of fines, which could fully or

partially plug or bridge the pore-throats. These fines are expected to be mainly dislodged clay particles within the samples or tiny particles inside the injection fluids pumped into the core samples. As described in the experimental procedure in Chap. 3, the possibility of the presence of any particle in the injection fluids was eliminated by using a 0.5 micron sintered stainless steel high pressure in-line filter. With regards to clay particles, the majority of the samples used were of fairly clean sand (e.g. Berea Sandstone and the samples from the Naylor Field). The type of clay in Sample CL-40,68-H, which contained high clay content, was glauconite. Generally, glauconite, because of its relatively large particle sizes, does not tend to produce such fines that can be released into the pore space and cause formation damage. The only samples which could be prone to fines migration were DB-1-H and DB-2-V, which contained kaolinite. Although, overall, existing evidences show that for majority of the samples damage to the samples due to fines migration may not be the main cause of the observed trend among the pressure data but it also may not be totally excluded from the equation at least for Samples DB-1-H and DB-2-V.

The other possible cause of the observed trend among the differential pressure data could be the potential reactions between the slightly acidic brine (saturated with CO_2) and a number of minerals inside the pore space of the samples (Eqs. 2.4–2.8). These minerals include mainly calcite and dolomite, which exist in a number of samples mainly as the cement bounding the grains together and also making up a small fraction of the matrix. Based on the literature review presented at the end of Chap. 2, the net effect of the possible dissolution and precipitation of these minerals could change the samples properties and even the strength of the samples to withstand the reservoir's in situ net effective pressure. Using the results of the brine composition analyses (Table 4.9), it can be confirmed that mineral dissolution occurred during the experiments conducted. They even showed that silica, which constitutes most of the grains in the sandstone samples, could be affected. The occurrence of mineral precipitation could only be confirmed using appropriate techniques- such as SEM (Scanning Electron Microscopy). This type of analysis was not performed as part of this research but based on the available reports in the literature (reviewed in Chap. 2), the material dissolved in brine can subsequently precipitate in various forms and cause another type of formation damage. As a conclusion, based on the analyses performed and the information presented in the literature, occurrence of mineral precipitation could possibly have occurred during the experiments, which may have caused damage to the sample pore space and subsequent changes in the differential pressure profiles from one cycle to the next.

One more likely cause of change in the differential pressure profiles could be gradual physical compaction (creep) of the core samples during the extended cyclic floodings. This could occur in both high and low permeability samples but its relative impact is most felt by low porosity and permeability samples [34, 35], which, in most cases, would originally have the narrowest pore channels. Based on the dimension and porosity measurements performed on a number of the samples after they underwent the cyclic floodings (Table 4.8), it was confirmed that indeed

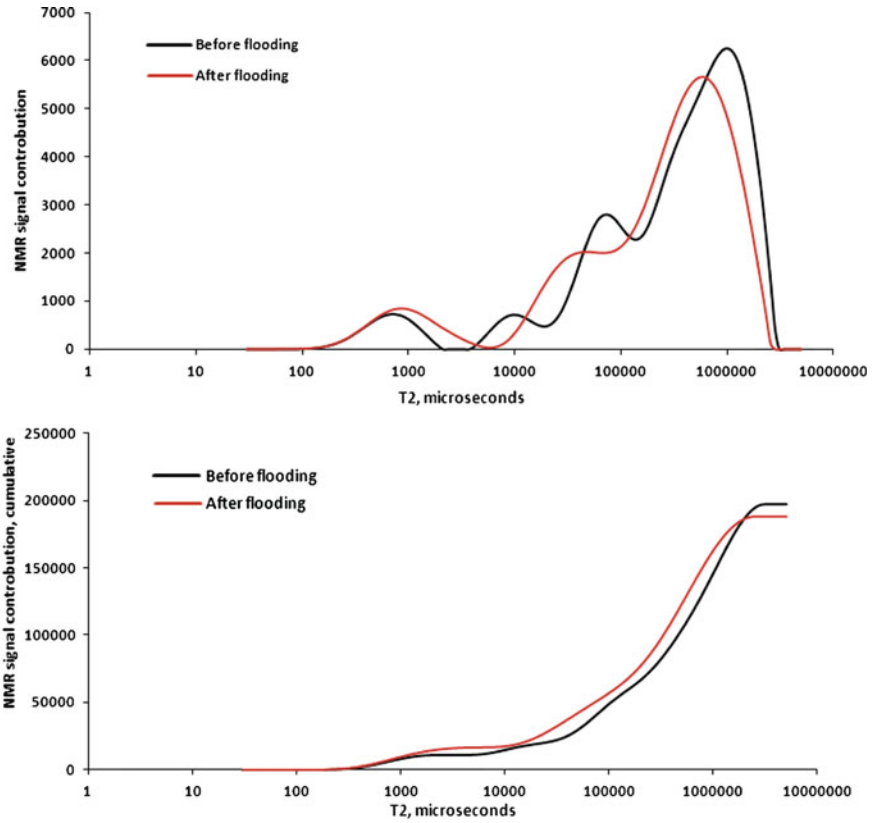

Fig. 5.11 Change in the incremental (*top*) and cumulative (*bottom*) T2 distribution of Sample CO2CRC-2-H after undergoing cyclic CO_2-brine injection

core samples, to some degree, had undergone irreversible plastic compaction. Furthermore, using the results of the NMR measurements conducted on a number of the samples before and after the flooding experiments, a slight reduction in the total pore volume of the samples was detected. Figures 5.11 and 5.12 are the incremental and cumulative T2 distribution for Samples CO2CRC-2-H and CO2CRC-3-H, which were stacked together to make up composite sample CO2CRC-2,3-H. Figure 5.13 also presents the same data for Sample DB-1-H. As can be seen from these graphs, overall, all of the incremental T2 distributions, representing the relative pore size distribution of the samples, are shifted to the left, towards smaller pore sizes. The cumulative total T2, which is a measure of the total pore volume of each sample, shows a reduction for all three samples after subjecting them to the cyclic injections (Figs. 5.11 and 5.12). Since some of the samples had calcite or dolomite or both within their cement, the already discussed mineral dissolution, which was confirmed to have occurred during the injection

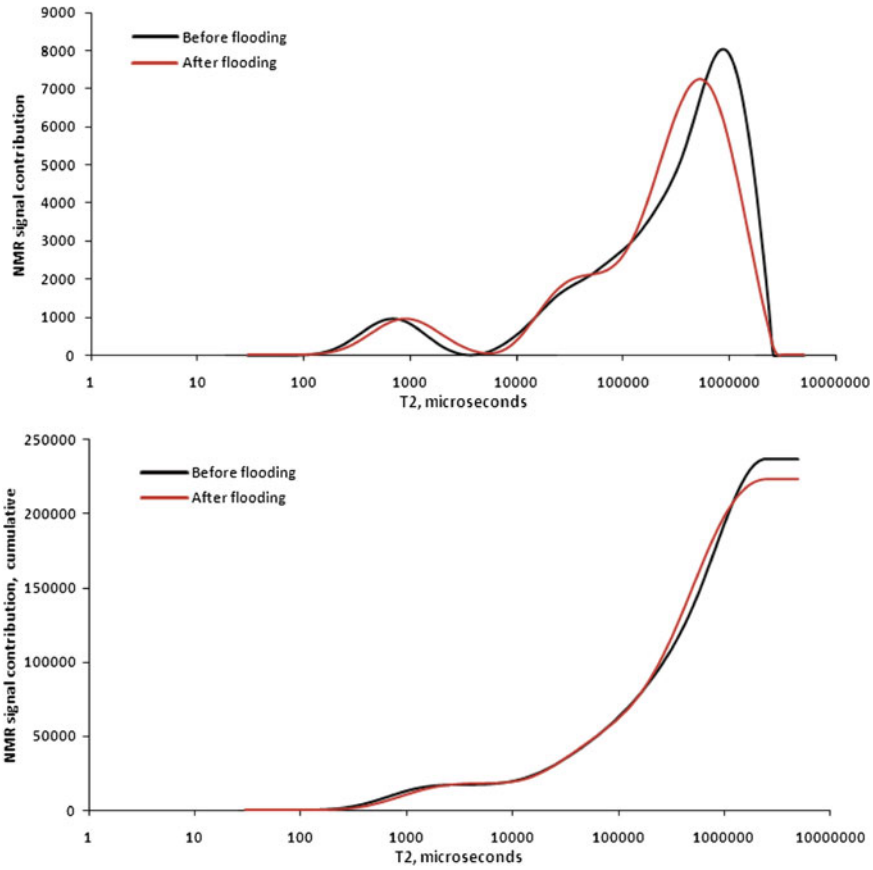

Fig. 5.12 Change in the incremental (*top*) and cumulative (*bottom*) T2 distribution of Sample CO2CRC-3-H after undergoing cyclic CO_2-brine injection

cycles, could have enhanced this plastic deformation of the samples by weakening the bond between the grains.

The last likely cause of the observed trend among the differential pressure data, at least for the first two drainage cycles, could be the saturation history or capillary hysteresis [24, 36, 37]. During the first drainage cycle CO_2 displaces only brine and there is no non-wetting phase (CO_2) saturation present in the pores, however, during a subsequent drainage cycle, there would be a non-wetting phase saturation left behind from a preceding imbibition cycle. As discussed before, since during an imbibition cycle, the trapped residual non-wetting phase saturation normally, due to the dominant snap-off mechanism, is left behind in pore bodies in the form of blobs and ganglia, it can put sever restriction on the flow of the wetting phase during a subsequent drainage cycle when it is being displaced by the non-wetting phase and this can create larger differential pressures across the porous medium.

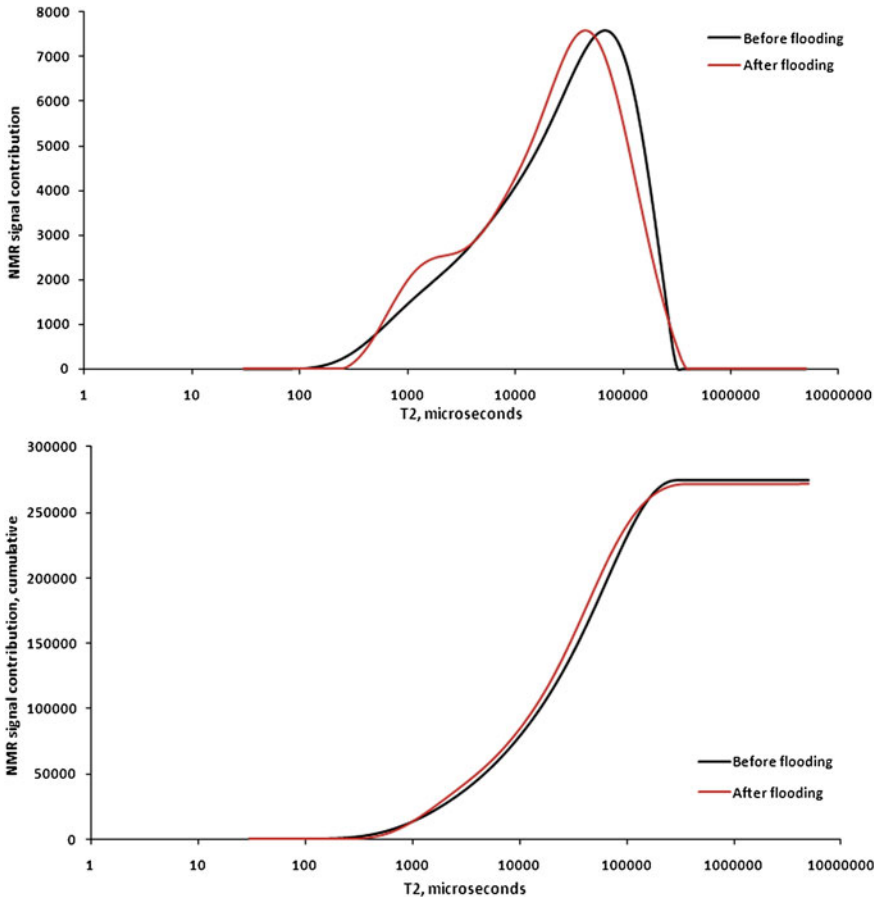

Fig. 5.13 Change in the incremental (*top*) and cumulative (*bottom*) T2 distribution of Sample DB-1-H after undergoing cyclic CO_2-brine injection

For majority of the samples, as evident from the relatively large jump in the differential pressure from the first drainage cycle to the second one, the effect of saturation history is mostly pronounced in the first two drainage cycles. After the second drainage, both saturation and differential pressure data do not show appreciable changes from one cycle to the other, therefore, the impact of the saturation history, would be minimal on the subsequent drainage cycles.

The observed trend among the differential pressure data (increase at the beginning followed by gradual stabilisation) is a characteristic of all four main possible causes discussed (i.e. fines migration, mineral dissolution/precipitation, plastic compaction and saturation history). However, as pointed out earlier, fines migration could be reasonably ruled out as the main cause for this behaviour for the majority of the experiments. The existing experimental evidences show that

plastic compaction, possibly enhanced by dissolution of the cements bounding the sandstone grains together, and the hysteresis effect have been the most influencing factors.

Sample CO2CRC-2-H was placed upstream of Sample CO2CRC-3-H within the composite sample including both. The NMR analysis was performed on these two short core-plugs separately with the hope of finding any effect of flow direction on the possible changes which may occur in the samples, but overall, the detected changes, at least with respect to their magnitude, are almost the same for both and there were no significant differences found between the two which could be possibly related to the direction of the fluid flow.

If the plotted pressure drop profiles in Figs. 4.18–4.34 are studied more closely, it can be seen that, for many of the samples tested, the pressure profiles become slightly less concave from the first injection cycle towards the last one. A less concave pressure profile is commonly a characteristic of low permeability core samples. Therefore, observing such behaviour supports the possibility of reduction in the pore and pore-throat sizes, which was confirmed to be the case by the results of the NMR measurements.

As a conclusion to this section, one may predict that the pressure drop within a porous medium subjected to the cyclic flooding of CO_2 and brine to increase gradually as further injection cycles are performed. Although, this increase is expected to level off after finite number of injection cycles. The results obtained here, apart from other various parts of the reservoir which may undergo cyclic flooding, have special application to the area around the wellbore. Any damage to this part of the reservoir due to any of the mechanisms discussed earlier (i.e. fines migration, dissolution and subsequent precipitation of minerals, pore-space compaction enhanced by dissolution of the cement and weakening of the rock, hysteresis effect, etc.) would eventually result in the reduction, or in extreme cases, loss of injectivity. It is worth noting that any damage caused by pore-space compaction could become less significant as the reservoir pore pressure increases with further CO_2 injection reducing the net effective pressure applied to the storage medium. It needs to be mentioned that the cyclic injection of CO_2 and brine may not always cause damage to the formation. Under favourable conditions the opposite could be possible too. However, among the possible interactions between the fluids and the rock, the only one which may cause enhancement to the formation is mineral dissolution.

5.4 Effects of Flow Direction

It is well known that both horizontal and vertical displacements would occur during various stages of CO_2 geological storage. For instance, during initial CO_2 injection the flow would be mainly in the horizontal direction but later on and during the eventual evolution of the CO_2 plume towards the top of the storage medium, vertical flow also enters the equation. It was also discussed in Chap. 2

Table 5.5 Effect of flow direction on the end-point residual saturations

Test no.	Sample name	Pore vol (cc)	k (mD)	End-point residual saturation (%)	
				1st *Drain.*	1st *Imb.*
3	CO2CRC-7-V	23.1	1,899.6	46.9	9.4
4	CO2CRC-11,14-H	21.5	3,409.8	52.4	9.0
5	CO2CRC-36-V	17.564	108.22	50.8	20.9
6	CO2CRC-39,42-H	16.49	252.6	54.6	19.8
12	BS-3-V	17.002	194.36	45.8	23.5
7	BS-1-H	16.476	234.6	44.9	21.5
15	DB-2-V	12.894	12.2	64.6	28.2
13	DB-1-H	13.135	14	60.5	26.8

how the displacement direction can influence the multiphase flow behaviour during such operations. Therefore, as mentioned previously, in order to have a better understanding of the horizontal versus vertical multiphase flow applicable to CO_2 geo-sequestration, for a few of the sandstone groups tested, samples were drilled in both horizontal and vertical directions. For each group of samples, in order to eliminate any spatial variations in the properties of the samples, which, apart from the direction, could influence the results, fairly homogeneous vertical and horizontal samples were drilled as close as possible to each other. Table 5.5 shows the experiments run on a number of horizontal and their corresponding vertical samples. From the second row to the bottom of the table, in each pair of rows, first is a vertical sample then its corresponding horizontal sample.

It is apparent from the data presented in Table 5.5, that the end-point residual CO_2 saturations are consistently higher for the less permeable vertical samples, which is consistent with the expectations but contrary to the residual oil saturations obtained by Crotti and Rosbaco [38] in horizontal versus vertical direction tests using an oil–water system. However, it needs to be mentioned that, in the experiments conducted by Crotti and Rosbaco [38], the initial residual water saturation to oil had been, surprisingly, the same in all directions.

As discussed before in Chap. 2, in the vertical direction, even in homogenous samples, the pore channels can be more tortuous and the number of pore-throats per unit of area in the vertical direction also could be less than the corresponding horizontal direction. These features could lead to a higher possibility for CO_2 entrapment by the snap-off mechanism, which, as mentioned before, is expected to be the dominant mechanism in trapping the non-wetting CO_2 phase. The entrapment of CO_2 in the vertical direction could improve even more if the porous media becomes more heterogeneous in the vertical direction, which is the case in many situations.

A consistent trend, similar to that observed among the residual CO_2 saturations, cannot be seen among the residual brine saturations for the first drainage cycle conducted on the first two pairs of samples listed in Table 5.5. For both pairs, the residual brine saturations in the horizontal samples are higher, which is contrary to the expectations. As discussed previously, this anomalous residual brine saturation

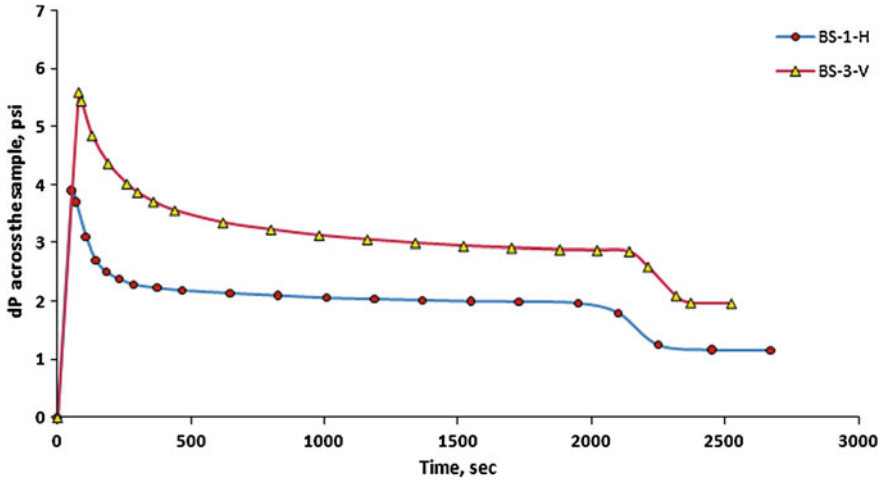

Fig. 5.14 Differential pressures across the sample versus time during the first drainage floods for Samples BS-1-H and BS-3-V

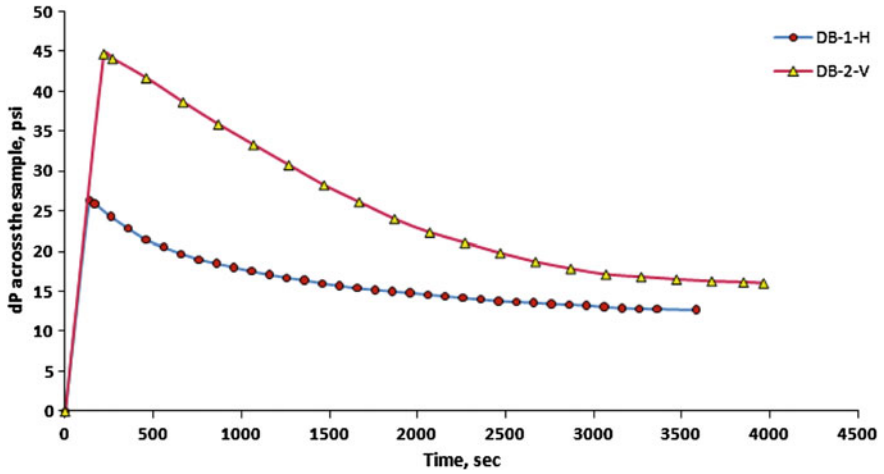

Fig. 5.15 Differential pressures across the sample versus time during the first drainage floods for Samples DB-1-H and DB-2-V

could be possibly attributed to the non-uniform brine displacement in these samples caused by the highly mobile CO_2 and low IFT. This reasoning becomes more likely when knowing that both of the horizontal samples in question were the highest permeable samples among all and both were composite cores. Since both were constructed using short core-plugs made of moderate to coarse grained sandstones, the tissue papers insert into their joints, potentially, failed to establish an adequate capillary bridge. The last two sample pairs listed in the table, however,

show lower residual brine saturation in the horizontal direction, which could be attributed to higher permeability in this direction coupled with other pore network features such as less tortuous pore channels and more pore openings in this direction.

Figures 5.14 and 5.15 are the differential pressure profiles for the first drainage floods performed on two sample pairs of BS-1-H and BS-3-V and DB-1-H and DB-2-H, respectively. As evident in the graphs plotted, the vertical samples show greater differential pressures and less concave curves compared to those for the horizontal samples. Both of these are features commonly seen in less permeable samples and confirm the discussion presented above regarding the size and number of the pore-throats in the vertical direction. It should be noted that the difference between the magnitudes of the differential pressures for each pair is not necessarily proportional to the difference between their absolute permeabilities. This is another indication that the horizontal samples are different from the vertical ones not only with regards to their absolute permeability values but also with respect to other features related to pores and pore channels even in a homogeneous porous medium like Berea Sandstone.

As the main conclusion to the discussion presented here, in order to have realistic estimates of the amount of CO_2 which could be trapped as residual saturation and how the CO_2 plume would spread and evolve, applying the data generated in the lab using horizontal samples only would not be adequate. This becomes especially important if the storage medium lacks a comprehensive seal to prevent the evolution of CO_2 into upper layers. Since CO_2 would eventually move upwards, the vertical flow, not only can improve the entrapment by increasing the amount of CO_2 which could be trapped as residual saturation, but also it would enhance the sequestration of CO_2 by other means such as dissolution in the formation brine and in-mineral trapping by postponing the evolution of the CO_2 plume towards the upper layers.

5.5 Effects of Change in Reservoir Stress Field

Due to the fact that, unless it is done as a means of EOR, during CO_2 injection into underground structures for sequestration purposes, there is no fluid withdrawal involved, reservoir pressure is expected to rise over time. The main focus of the literature and research carried out to date on the subject of CO_2 geo-sequestration has been mainly on the effect of this increase in the reservoir pore pressure on the integrity of the seal. However, since pores and pore channels are known to be sensitive to the net effective pressure applied to the porous medium [39], one may also expect that such changes in pressure may influence the multiphase flow characteristics of the fluids-rock system. The possibility of occurrence of such changes and their potential consequences would make the application of the results obtained for full in situ reservoir pressures, to predictions done for the entire life of a CO_2 sequestration project, questionable. In order to verify the occurrence of such

Table 5.6 Sample properties, experimental conditions and residual saturations obtained during stress sensitivity analysis performed on Sample BS-2-H

Test no.	Sample ID	Pore vol (cc)	k (mD)	Overburden pressure (psi)	Pore pressure (psi)	Pore volumes of brine produced before BT during 1st drainage flood	End-point residual saturation (%)	
							1st *Drain.*	1st *Imb.*
8	BS-2-H	17.27	150.1	3,500	2,580	0.312	49.5	14.8
9	BS-2-H	17.09	145.99	5,000	2,580	0.333	47	18
10	BS-2-H	16.975	141.13	6,725	2,580	0.347	44.8	19.4

changes and if they happen, have a better understanding of the effects they may have during CO_2-brine flooding processes, three cyclic flooding experiments were conducted on sample BS-2-H each with a different net effective pressure. During the experiments, the pore pressure was kept constant and in order to change the net effective pressure the confining pressure applied to the sample was varied. The experiments were conducted with the lowest net effective pressure first and the one with highest net effective pressure last. In between the experiments the sample was not removed from the core-holder but the experimental procedure outlined before, was followed for all three experiments in exactly the same order to make sure that everything remained the same except the effective pressure. Table 5.6 shows how overburden pressure was changed from one test to the next while keeping the pore pressure constant.

As can be seen from Table 5.6, variation in the net effective pressure changed the sample's pore volume and permeability as expected. The change in the pore volume versus the effective pressure was measured through routine core analysis performed previously. Furthermore, as plotted in the two graphs shown in Fig. 5.16, the resulting data also revealed how both CO_2 and brine end-point residual saturations can change with change in the reservoir stress field. As evident among the data, residual brine saturation decreased by increase in the net effective pressure on the sample while residual CO_2 saturation increased.

The changes in the brine residual saturations could be attributed mainly to the fact that the sample undergoes further compaction due to the higher net effective pressures applied. Both pore and pore-throats are expected to shrink in size with increase in the net effective pressure. That is why the absolute permeability of the sample is reduced under higher confining pressures. These changes can alter the displacement performance of the CO_2 floods by making the displacement more efficient through increasing the pore-throat capillary entry pressure for the invading non-wetting CO_2 phase, making the displacement front more stable, which as discussed in detail previously, and as can be seen from Table 5.6, increases the amount of brine produced before CO_2 breakthrough. More efficient displacement of brine during the experiment with the highest net effective pressure was verified by reducing the effective pressure to a very low value after the experiment reached stabilised conditions. This reduction in the net effective

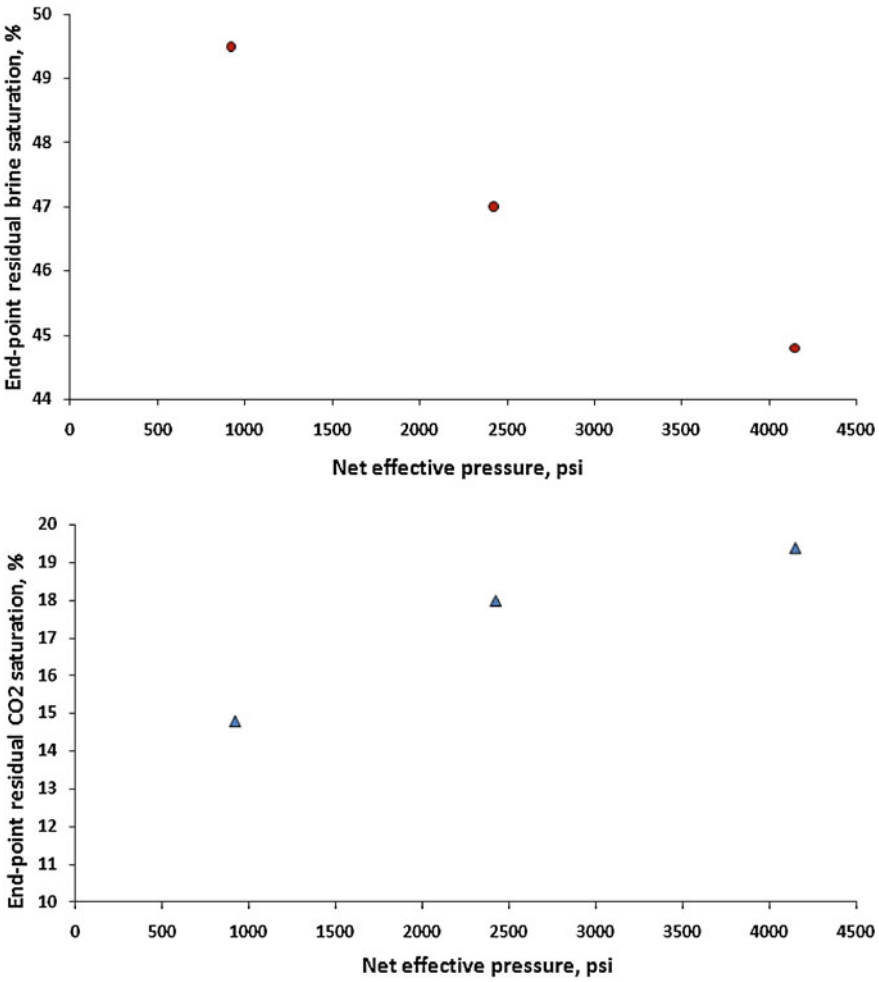

Fig. 5.16 End-point residual saturations from experiments conducted on sample BS-2-H under varying net effective pressures

pressure failed to cause any further brine production, which could have happened if, presumably, brine recovery under higher effective pressure was less efficient.

It is worth noting that reduction in pore and pore-throat sizes could lead to better displacement if the sample's pore network is fairly homogeneous (i.e. has a unimodal pore size distribution). Otherwise, any excessive compaction could make the small pores inaccessible to CO_2 which in turn would lead to higher residual brine saturations. The other factor which could have played a part in decreasing the residual brine saturations could possibly be a change in the sample's pore volume and pore network, due to the coupled effect of mineral dissolution and precipitation, as the cyclic injections proceeded from one experiment to the next.

The observed increases in the CO_2 residual saturations with increase in the net effective pressure, however, seem to have been more influenced by changes occurred to the pore and pore-throat sizes due to mechanical compaction of the sample. These possible changes could potentially intensify the snap-off mechanism towards trapping more CO_2 as residual phase. Also again here, based on the Land trapping model [20], it can be said that more efficient brine displacement during drainage under high net effective pressures could have led to more CO_2 entrapment during the subsequent imbibition.

Based on the discussion presented, it can be concluded that the residual CO_2 saturation is expected to increase with increase in the net effective pressure on the porous medium. The results obtained here could have potential effects on the expected amount of CO_2, which could be sequestered in the form of trapped residual saturation over time. In other words, the results show that over time as the net effective pressure applied to the reservoir decreases, the capacity of the reservoir to trap CO_2 as a residual phase would decrease, which in principle could lead to mobilisation of some of the already trapped CO_2. This is something which would be undesirable under any circumstances. It is worth noting that during the experiments conducted here, pore pressure remained the same from one test to another. Apart from the expected physical change in the porous medium, any change in the properties of the fluids with pressure could also influence the displacement results. With increase in pore pressure, IFT of the CO_2-brine system is expected to decrease but CO_2 viscosity and density both increase. Increase in viscosity and density of CO_2 could improve the displacement by promoting more uniform displacements but the reduction in IFT could result in drop in CO_2 entrapment due to the dominant snap-off trapping mechanism.

5.6 Effects of Residual Natural Gas Saturation

The advantages and disadvantages of using depleted or active hydrocarbon reservoirs as potential candidates for CO_2- geo-sequestration were pointed out previously (Table 1.2). But the potential effects of the existence of residual hydrocarbon, especially natural gas (represented by CH_4 here), on the multiphase flow occurring during CO_2 geo-sequestration have not been well studied. As mentioned previously, the only available data on this topic in the literature are the results of researches conducted on the potential usage of CO_2 for enhanced hydrocarbon recovery purposes. As mentioned earlier, in an attempt to investigate such effects, as part of the experimental work carried out in this research, a number of specially designed cyclic flooding experiments, similar to the previously discussed cyclic CO_2-brine injections, were conducted but this time the first drainage flood was performed using CH_4 instead of CO_2.

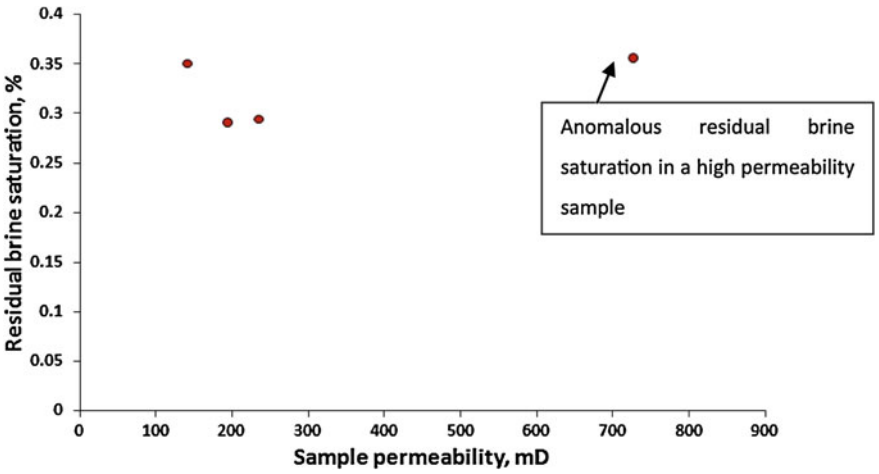

Fig. 5.17 Residual brine saturations for the primary drainage cycles conducted on various samples

5.6.1 Effects on the Saturation Profiles

Versus sample permeability Figs. 5.17 and 5.18 show the residual brine and residual CH_4 saturations obtained at the ends of the first drainage and first imbibition floods, respectively, for a number of samples tested during this part of the experimental work. As can be seen here again the residual brine saturation in a high permeability sample is abnormally high, which could be interpreted as a sign of non-uniform displacement dominated by a high mobility ratio. As discussed earlier, since the IFT of the CH_4-brine is higher, the previously discussed negative effect of IFT on the displacement efficiency is believed to be less pronounced here compared to the CO_2-brine flooding experiments. If the data plotted in Figs. 5.17 and 5.18 are compared to those obtained for normal CO_2-brine flooding experiments, although the trends observed here are similar to those identified for the case of CO_2-brine, there is a distinctive difference between the two. As pointed out before, the magnitudes of residual non-wetting phase saturations reported here are considerably higher than those measured for the CO_2-brine system, while residual brine saturations are much lower than those obtained for the CO_2-brine system. As discussed previously, this can be explained using the differences in mobility ratios and IFT values between the two cases.

The higher residual non-wetting phase saturations for the CH_4 injection experiments (Fig. 5.18), compared to those of the CO_2 floods (Fig. 5.5), could be attributed to the higher IFT values between CH_4 and brine. The same reasoning used to show why residual CO_2 saturation was relatively low (using Eqs. 5.1–5.5) could be used here again to show why residual CH_4 saturations are higher compared to those of CO_2.

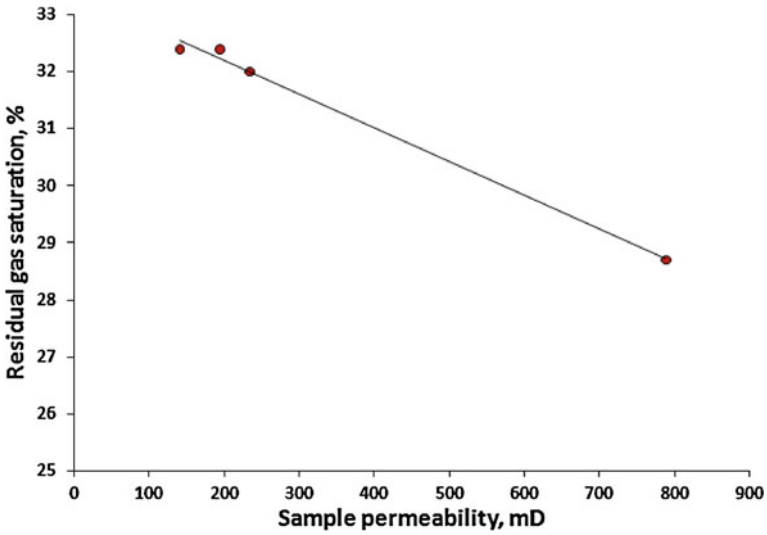

Fig. 5.18 Residual gas saturation for the primary imbibition cycles conducted on various samples

The most important result of the experiments conducted in this part of the research is revealed when the changes in the residual saturations, once the samples were subjected to the normal cyclic CO_2-brine flooding after the first CH_4 injection, are examined. Figure 5.19 shows the normalised residual brine (top) and residual non-wetting phase (bottom) saturations versus the drainage and imbibition cycle numbers, respectively. For each sample tested, the residual brine and non-wetting phase saturations were normalised by dividing them by the residual brine or CH_4 saturations obtained at the end of the first drainage or imbibition cycles, respectively. As evident from the graphs, there are strong and consistent trends present among the data plotted. The end-point residual brine saturations were increased from the lower values obtained for the CH_4 injections as the successive drainage floods were performed using CO_2. For each sample, the residual brine saturation resulting from the last drainage flood is very close to that of the CO_2 drainage floods performed previously on the same sample during the normal cyclic CO_2-brine injections. For each sample, the slope of the line connecting the residual brine data points resulting from the CH_4 injection and its subsequent CO_2 injection is highest for the most permeable sample, and is lowest for the least permeable sample among all. As the sample permeability decreases the samples show a more gradual increase in the end-point brine saturation as the cyclic CO_2 injections proceeded. For sample BS-3-V, the gradual increase in the residual brine saturations could also be attributed to the fact that this sample is a vertical sample and multiphase interferences are expected to be more pronounced in this sample compared to other horizontal samples tested here. This sample also showed

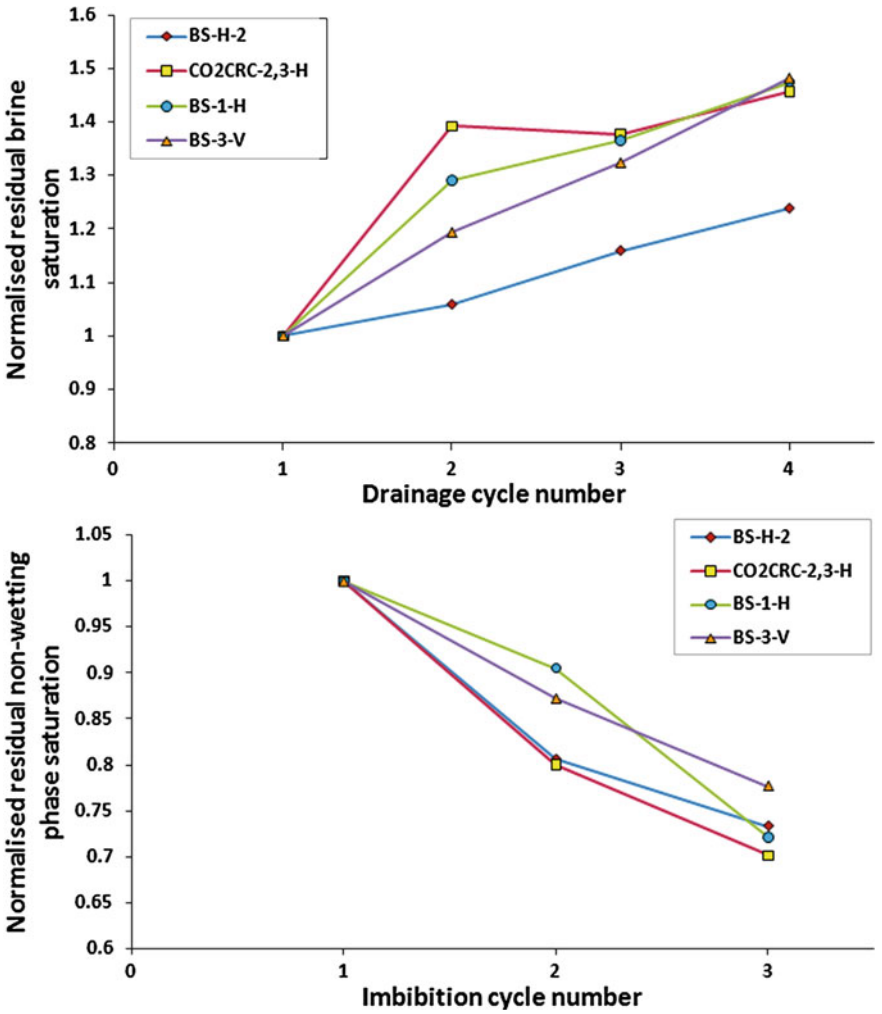

Fig. 5.19 Normalised end-point residual brine (*top*) and non-wetting phase (*bottom*) saturations versus injection cycle numbers for each sample

slightly higher residual gas saturation compared to its corresponding horizontal sample (i.e. sample BS-1-H).

As can be seen from the bottom graph in Fig. 5.19, again strong trends exist among the residual non-wetting phase saturation as the cyclic CO_2-brine injections followed the original CH_4 flooding. Here again, for each sample, the final obtained residual non-wetting phase saturation is close to that obtained at the end of the previously discussed imbibition flood performed on the same sample during the normal cyclic CO_2-brine floodings. For each sample, the consistency between the slope of the line connecting the first two data points and permeability of the

samples is not as great as that of the residual brine saturations, but still the effect of sample permeability can be seen for some of the experiments. Like before, compared with other samples, the vertical sample shows one of the most gradual decreases in the non-wetting phase residual saturation among all the samples tested.

The experimental results published by Seo [40] and Seo and Mamora [41] on displacement performance during the core-flooding experiments conducted to displace methane saturated samples by CO_2, could be used to discuss and explain the observed trends among the residual saturations reported here. As mentioned earlier in Chap. 2, the authors reported that displacement of methane by CO_2 was very efficient resulting in methane recovery factors ranging from 62 to 87% at CO_2 breakthrough (Table 2.13) and CO_2-in-methane dispersion coefficients as low as 0.01 cm^2/min. For instance, their test number 29, whose experimental conditions (P = 2,700 psi and T = 80°C) were the closest to the P–T conditions of the experiments conducted during this research (P = 2,580 psi and T = 83°C), resulted in a recovery factor of 82% at CO_2 breakthrough and a dispersion coefficient of only 0.07 cm^2/min. It needs to be noted that the injection flow-rates used by Seo [40] and Seo and Mamora [41] were much lower than those used here and because only the residual gas by-passed during the first imbibition flood was available to be displaced by the subsequent CO_2 injections, the recovery efficiencies achieved by Seo [40] and Seo and Mamora [41] may have not been possible to obtain during the experiments conducted here. However, the effect of higher permeable sandstone samples used here, compared to low permeability carbonate samples used by Seo [40] Seo and Mamora [41], should not be over looked.

By combining the experimental results obtained by Seo [40] and Seo and Mamora [41] and the observed trends in the residual saturations during the experiments conducted here, it may be concluded that:

- First of all, during each experiment, with each CO_2 injection (drainage) part of the trapped CH_4 was displaced and recovered by CO_2 while, due to the coupled effects of mobility ratio and lower IFT for the CO_2-brine system, supercritical CO_2 was unable to displace the brine to values lower than those achieved by CH_4. That is why during the second drainage flood (first CO_2 injection) the volume of the displaced brine is considerably less than that of other drainage floods performed before and after it (Figs. 4.35–4.38).
- Secondly, due to the lower IFT between CO_2 and brine, compared to that of CH_4-brine system, as more CH_4 is recovered and subsequently the CO_2 concentration is increased, the residual non-wetting phase at the end of each consecutive imbibition would decrease.

Taking into account the total 25–30 pore volumes of CO_2 injected during the three CO_2 injections performed for each experiment, it could be reasonably assumed that no more or negligible amounts of CH_4 would be left inside each sample after undergoing the third and last CO_2 injection flood. The fact that, based on the data plotted in the top graph in Fig. 5.19, most of the higher permeability

samples reached stable saturation values (close to those of normal CO_2-brine system) much faster than the lower permeability ones, the slope of the line connecting the first two data points for each experiment could represent the CH_4 recovery efficiency for each sample, meaning the higher the permeability, the higher the recovery efficiency. From the bottom graph, however, except for one or two samples, a similar conclusion cannot be drawn.

The above experimental results can have a considerable impact on the idea of storing CO_2 in depleted natural gas reservoirs. Based on the trends apparent within the results obtained, once CO_2 is injected into a depleted natural gas (represented by CH_4 here) reservoir, it will displace and replace the majority of the natural gas trapped as a residual phase, but, this necessarily does not mean that the replacing CO_2 will remain trapped in the form of a residual non-wetting phase in the same way as the original trapped natural gas did. In other words, injecting CO_2 into such storage reservoirs would not add any value to the process of CO_2 sequestration in terms of the magnitude of the desired trapped residual CO_2 saturations. As the results of the experiments revealed, over time the excess CO_2, with a permeability dependant rate, would be displaced by brine and eventually the trapped residual CO_2 saturations would be, more or less, the same as a normal CO_2-brine system. Over the long term, the above described phenomenon would potentially add to the amount of CO_2 which would exist in a porous medium as a free and movable phase (compared to the amounts during the initial stages of the process) rather than reducing it and this could pose a risk to any sequestration process implemented in such systems by putting more strain on any existing seal or cap-rock caused by, possibly unexpectedly, large amounts of free CO_2 phase beneath it.

5.6.2 Effects on the Differential Pressure Profiles

As could be seen from the data plotted in Figs. 4.39–4.42, the differential pressure data resulting from the experiments also show trends, which are overall, different from those observed during the normal cyclic CO_2-brine injections. The top graph included in Fig. 5.20 shows, for each sample, the normalised differential pressures across the sample at a moment in time just before the non-wetting phase (either CH_4 or CO_2) breakthrough (BT). For each sample, the differential pressure was normalised by dividing it by the differential pressure value measured just before breakthrough time of the first drainage flood performed using CH_4. As evident from the graph, there is a consistent trend present among the data for all the samples tested. Relative to the CH_4 flooding cycle, the observed differential pressure for each sample increased rapidly in the second drainage flood (first CO_2 injection) but afterwards the differential pressure dropped again and eventually became stabilised. For each sample, the differential pressures obtained during the last drainage flood are close to those observed for the normal CO_2-brine system.

For each sample tested, the bottom graph in Fig. 5.20 shows the normalised differential pressures across the sample measured at the conclusion of each

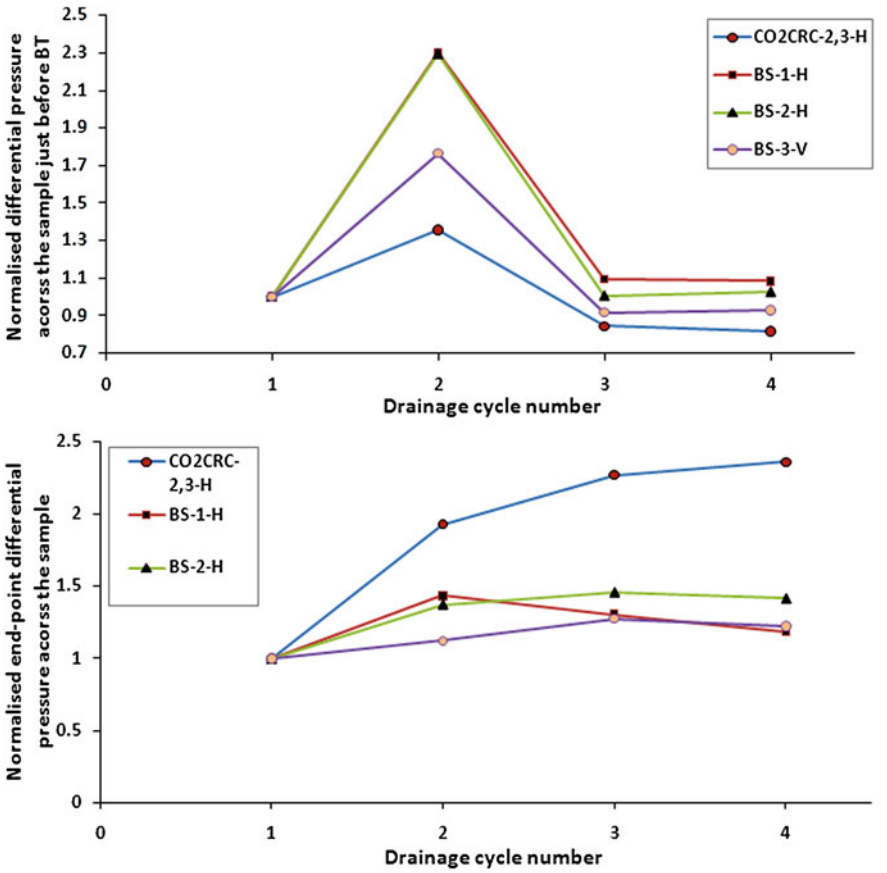

Fig. 5.20 Normalised differential pressures across the sample just before non-wetting phase breakthrough (BT) (*top*) and at the conclusion of each drainage cycle (*bottom*) versus drainage cycle numbers for each sample

drainage flood conducted on that sample, against the drainage cycle numbers. Here again, for each sample, the differential pressure was normalised by dividing it by the end-point differential pressure measured at the conclusion of the CH_4 injection cycle. The trend observed among the plotted data closely resembles that present among the differential pressure data obtained for the normal cyclic CO_2-brine injections. It is necessary to point out again that some of the pressure data obtained at this stage were also affected by the pressure measurement accuracy issue pointed out previously.

Among the data plotted for differential pressures just before the non-wetting phase breakthrough, there is a big jump from the first drainage flood (CH_4 injection) to the second one (first CO_2 injection). This is also clearly evident from the pressure profiles shown in Figs. 4.39–4.42. The most likely cause of such

behaviour could be the effect of the already explained saturation history. This jump was also seen among the differential pressure data for the normal cyclic CO_2-brine injections. However, it is much larger and more magnified here due to the higher residual CH_4 saturations left behind during the first imbibition flood conducted between the first two drainage floods. It is worth noting that other factors- such as the complexities associated with, somewhat, three-phase (CH_4, CO_2 and brine) versus two-phase flow, could have had impact on differential pressure profiles, especially with regards to the first CO_2 injection, during which the remaining CH_4 saturation is the highest among all.

When comparing the differential pressure profiles obtained during the normal cyclic CO_2-brine injections to those resulting from the CH_4-CO_2-brine flooding pattern for each sample, one can predict that low injectivity would be an issue during the early stages of any CO_2 storage into a depleted natural gas reservoir. However, over time the injectivity may improve and approach that expected from a saline aquifer with the same formation rock properties as the natural gas reservoir.

5.7 Relative Permeability Data

This last section of this chapter presents the relative permeability data generated for a number of core-flooding experiments. Using the experimental results (i.e. injection, production and differential pressure data recorded during the unsteady-state core-flooding experiments) the relative permeabilities were calculated using a numerical regression and history matching technique [3, 42, 43]. Sendra software from Weatherford Petroleum Consultants, which is based upon a two-phase, 1D black-oil simulation model together with an automated history matching routine, was used to reconcile time and spatially dependent experimental data and generate the relative permeabilities. Since the samples used during this research were fairly homogeneous, this method was expected to produce results representative of the actual flooding experiment run in the lab.

As discussed previously, most of the CO_2 injection floods were concluded with a period of "bump flow". The data used to generate the relative permeability curves were those for before the start of the "bump flow". The extra brine production after conducting the "bump flow" further increased the end-point relative permeability of CO_2. Plotted in Figs. 5.21 and 5.22, against absolute permeability of the samples, are the brine and CO_2 end-point relative permeabilities, respectively. The end-point brine relative permeabilities are for the end of the primary imbibition flood and those for the CO_2 phase are for the end of the primary drainage flood. It is worth noting that the CO_2 end-point relative permeabilities are those measured after conducting the "bump flow" to remove any potential end effects. As can be seen from the plotted data, both sets of data show reasonable correlations with the absolute permeability of the samples, but there is a much stronger correlation among the brine end-point relative permeabilities. The first

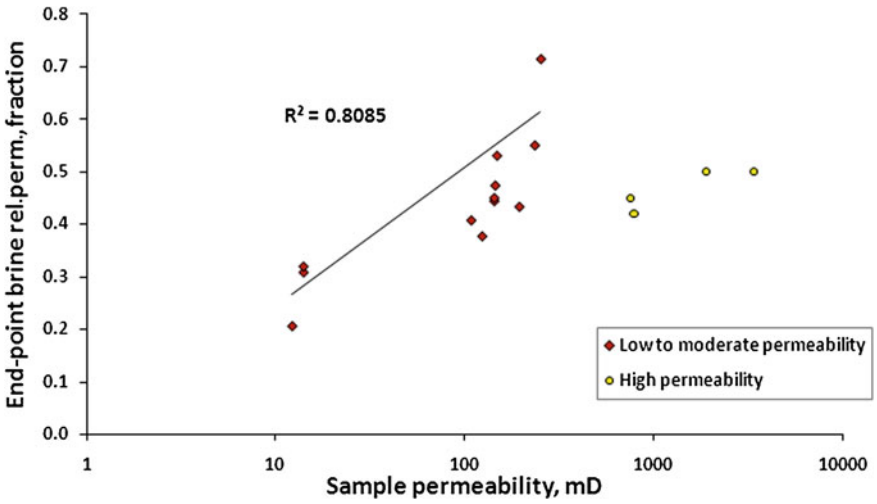

Fig. 5.21 End-point relative permeabilities of brine versus absolute permeability of the samples

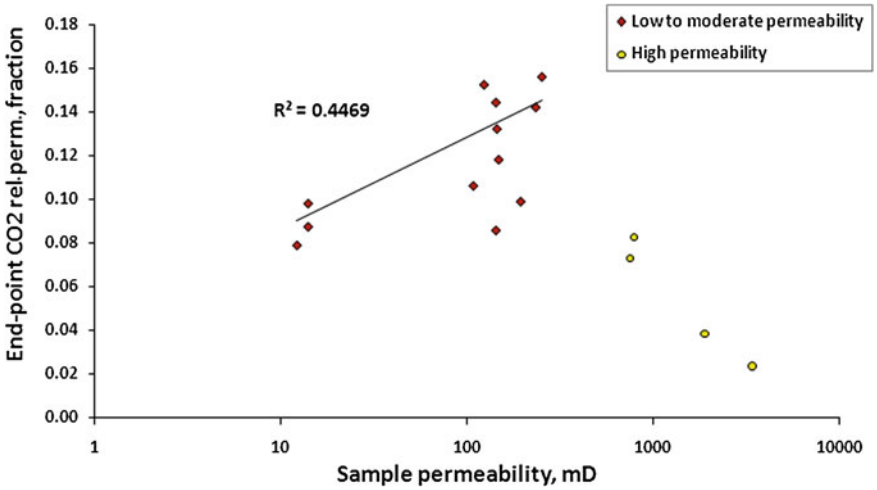

Fig. 5.22 Post-bump end-point relative permeabilities of CO_2 versus absolute permeability of the samples

likely reason for the weaker correlation among CO_2 end-points is that the drainage relative permeabilities are strongly affected by the non-uniform displacement and capillary end-effect phenomenon. The second reason could be the fact that close to the conclusion of the drainage floods, because of the low CO_2 viscosity, the differential pressure values would be very small and the measurement accuracy

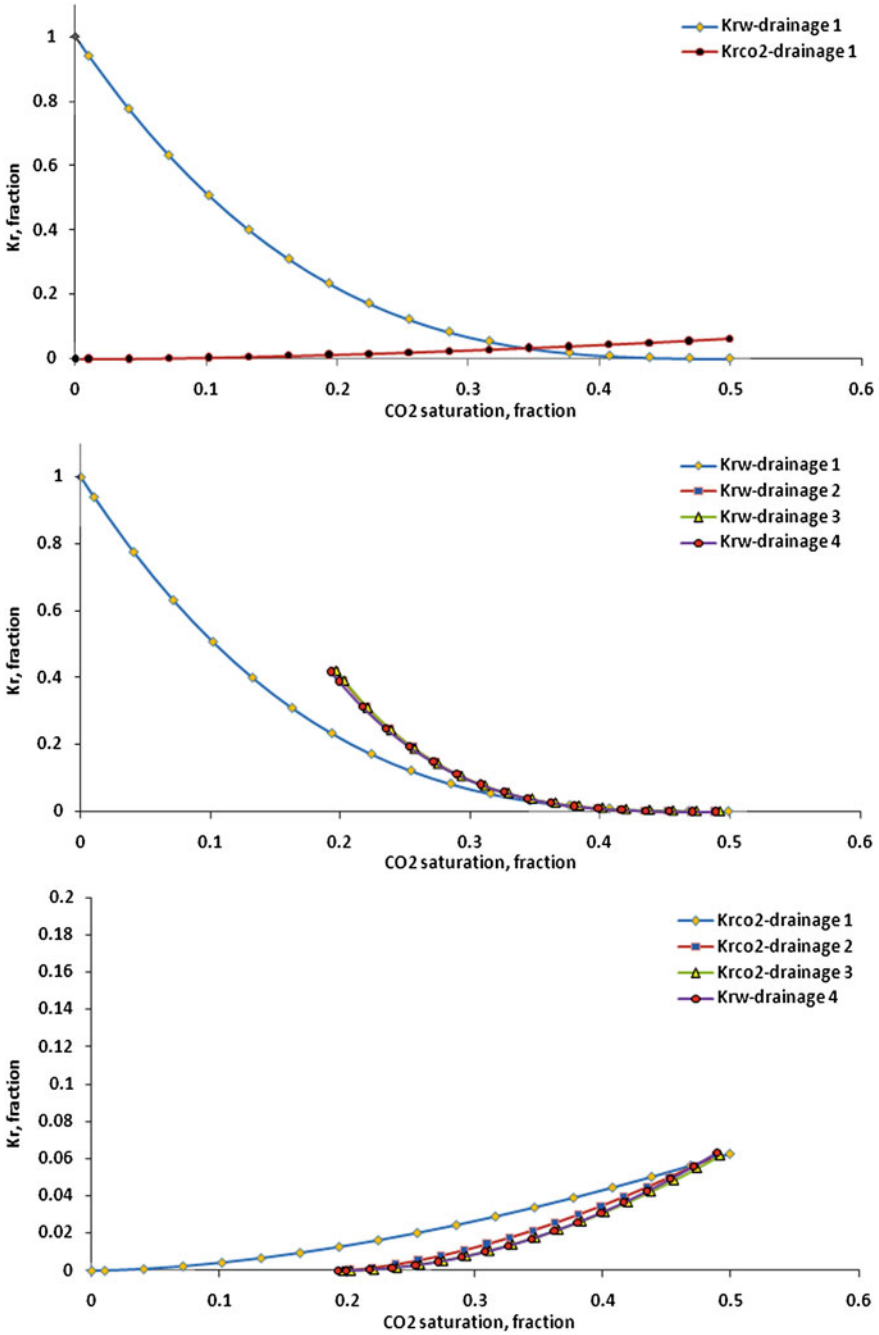

Fig. 5.23 Relative permeability data for sample CO2CRC-2,3-H during the cyclic drainage cycles conducted on this sample

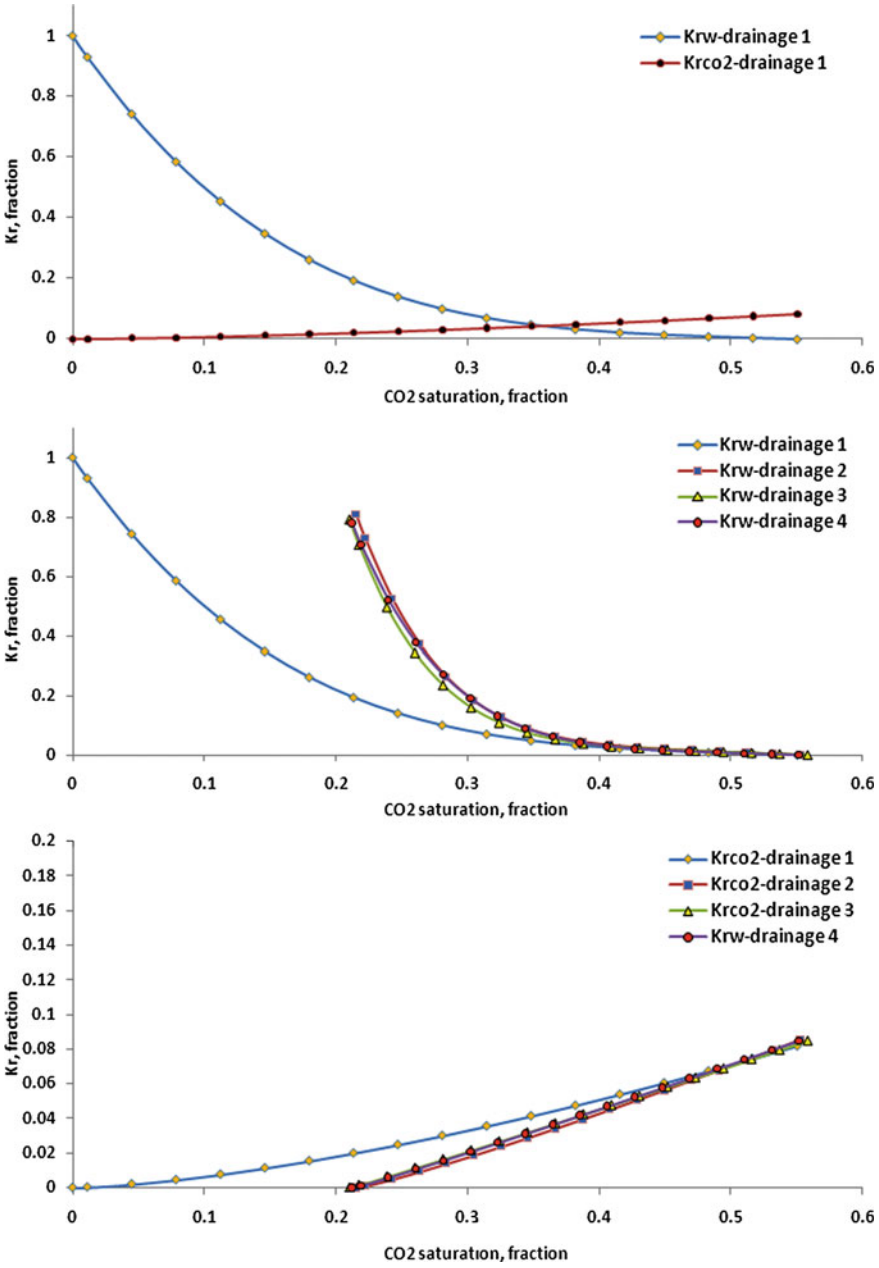

Fig. 5.24 Relative permeability data for sample BS-1-H during the cyclic drainage cycles conducted on this sample

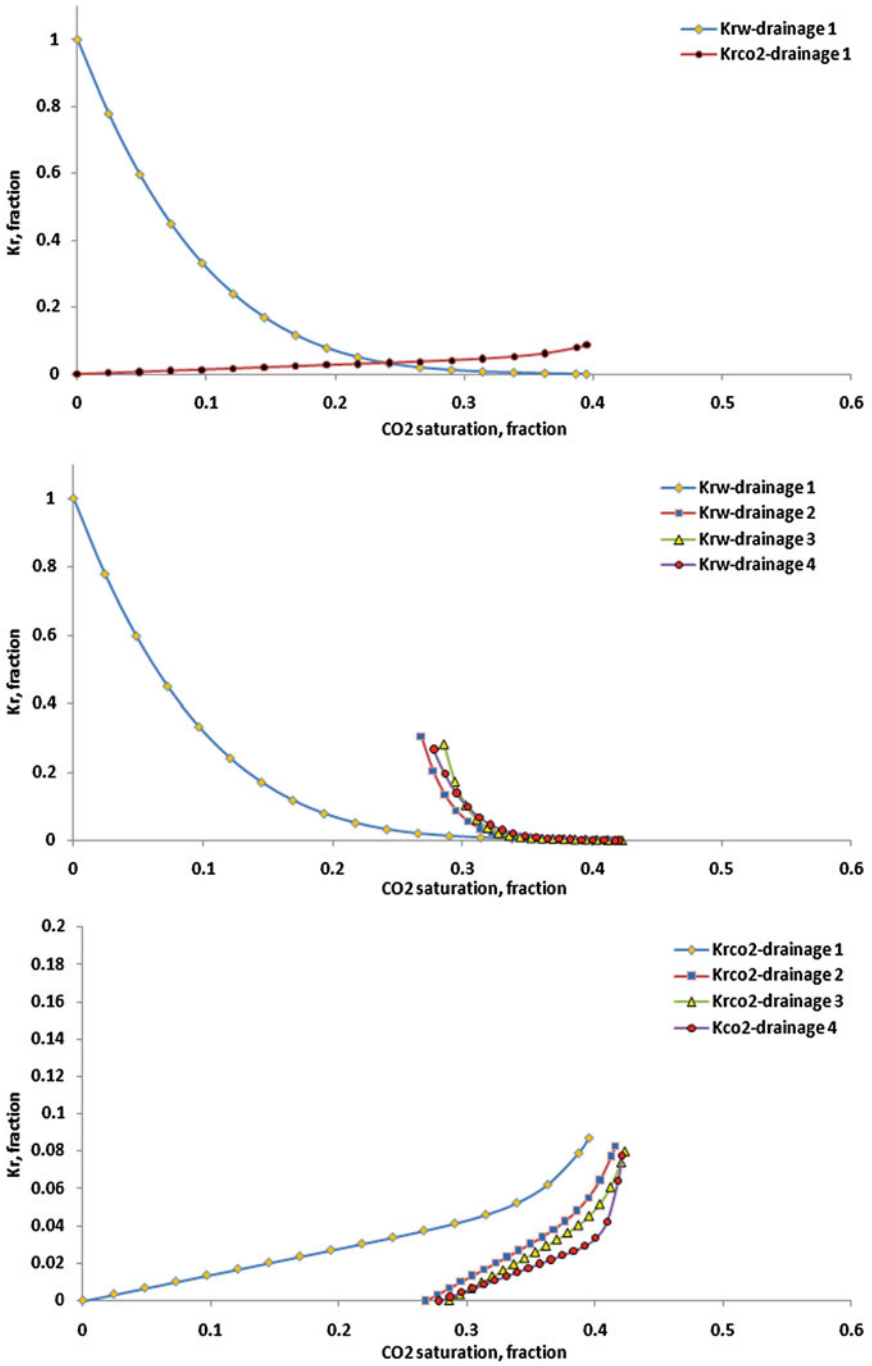

Fig. 5.25 Relative permeability data for sample DB-1-H during the cyclic drainage cycles conducted on this sample

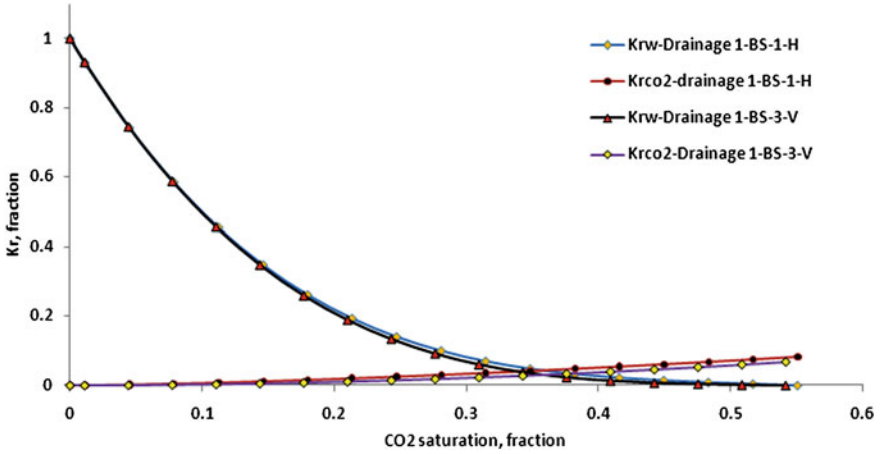

Fig. 5.26 Comparison between relative permeability curves of the first drainage cycle generated for sample BS-1-H and its corresponding vertical sample (BS-3-V)

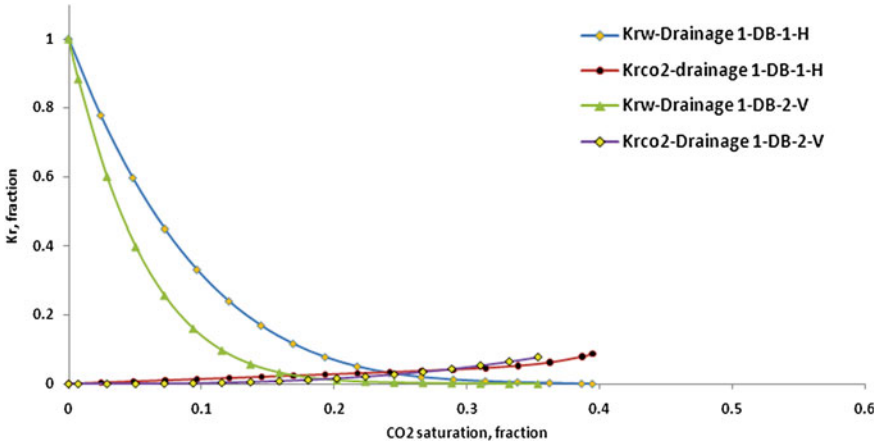

Fig. 5.27 Comparison between relative permeability curves of the first drainage cycle generated for sample DB-1-H and its corresponding vertical sample (DB-2-V)

issue mentioned before could influence the measurements. In fact, as presented in Figs. 5.21 and 5.22, with a different symbol and in a different colour, the end-point relative permeabilities for the highest permeable samples, even for the brine phase, are well off the main trend present among the data, and that is because the pressure data measured for these samples are strongly affected by the accuracy limitation of the pressure sensors. Therefore, overall, the relative permeabilities generated for higher permeability samples close to the conclusion of the drainage floods, are affected by some degree of uncertainty. This is due to the fact that, the differential

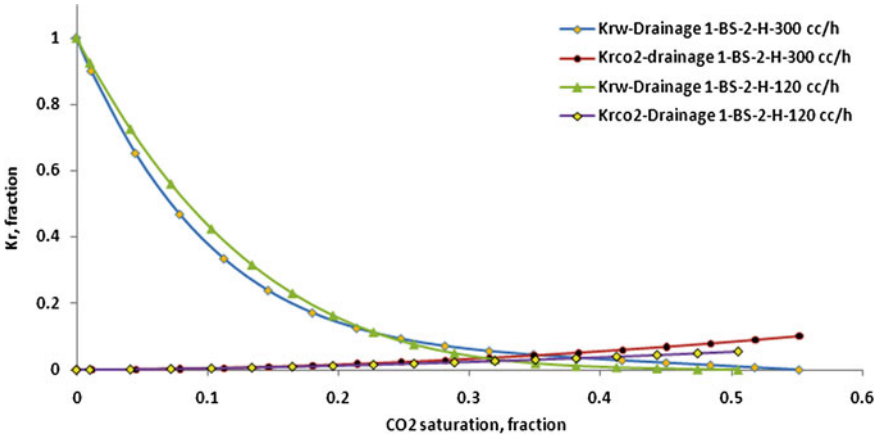

Fig. 5.28 Comparison between relative permeability curves of the first drainage cycle generated for Sample BS-1-H

pressures during this portion of these experiments are very small and, therefore, are highly affected by the measurement inaccuracies. This uncertainty would make that part of the relative permeability curves less reliable.

Figure 5.23 shows the relative permeability data generated for sample CO2CRC-2,3-H through the discussed history matching technique using the core-flooding data measured in the lab. As can be seen from this figure, despite the fact that sample CO2CRC-2,3-H was highly permeable, CO_2 end-point relative permeability was very low. This discrepancy could be attributed to the combined effects of the uncertainties in the differential pressure measurements, and the non-uniform displacements experienced during the drainage floods. As can be seen from Fig. 5.23, the relative permeability curves for both brine and CO_2 phases do not change considerably from one drainage cycle to the next. The slight variations observed in the curves are due to the previously reported small fluctuations in the brine production and differential pressure profiles among the four drainage floods. Similar trends and fluctuations observed for sample CO2CRC-2,3-H again can be seen in Fig. 5.24, which shows the relative permeability curves generated for sample BS-1-H. But the relative permeability data calculated for sample DB-1-H, which are presented in Fig. 5.25, show some extent of dependence on the cyclic flooding pattern. This is similar to the trend previously observed among the differential pressure data for this sample. A full discussion on the likely causes of existence of such trend was presented in earlier sections of this chapter.

Figure 5.26 shows a comparison between the relative permeability curves calculated for the two samples of BS-1-H and BS-3-V. As mentioned previously, these two samples were drilled from the same Berea Sandstone block, one in the horizontal and the other in the vertical direction. As can be seen, the relative permeability curves for the vertical sample are slightly more concave than the horizontal one, which confirms that, as may be expected, the multiphase

interference effect is greater when the fluids flowing in the vertical direction. This could be the main reason for the slightly higher residual brine saturation and slightly lower CO_2 end-point relative permeability for the vertical sample. In fact, as evident from Fig. 5.27, the higher multiphase interference effect during the floods performed on vertical samples, is confirmed to be more pronounced in the case of low permeability Donnybrook samples.

Figure 5.28 shows two sets of relative permeability curves generated for sample BS-1-H. One set is for a CO_2 injection flow-rate of 300 cc/hr and the other for a CO_2 injection flow-rate of 120 cc/hr. The effect of injection flow-rate clearly can be seen from the plotted data. While, it is difficult to explain the way the brine relative permeability curve has changed with changing flow-rate, the CO_2 relative permeability curves show that CO_2 would benefit from a higher overall and end-point relative permeabilities during the higher injection flow-rate. This is not unexpected, since during higher CO_2 injection flow-rate, brine would be displaced more efficiently and therefore its interferences with CO_2 would be less.

At the end, it is again necessary to point out that, except for two low permeability samples (i.e. DB-1-H and DB-2-V) during the core-flooding experiments conducted on many of the samples, unavoidably, the displacement of brine by CO_2 was highly non-uniform. The flow-rate sensitivity analyses and "bump flows" all confirmed the occurrence of such conditions. Therefore, the relative permeability curves derived for those higher permeability samples may not be totally reliable of being representative of the ideally uniform displacements described by the Buckley-Leverett theory.

References

1. Bernabé Y, Mok U, Evans B (2003) Permeability-porosity relationships in rocks subjected to various evolution processes. Pure Appl Geophys 160:937–960
2. Tiab D, Donaldson EC (2004) Petrophysics: Burlington, Massachusetts. Gulf Professional Publishing, Elsevier
3. Bennion B, Bachu S (2005) Relative permeability characteristics for supercritical CO2 displacing water in a veriety of potential sequestration zones in the Western Canada sedimentary basin. SPE 95547, The SPE annual technical conference and exhibition, Dallas, Texas, USA, Society of Petroleum Engineers
4. Bennion B, and Bachu S (2006c) Supercritical CO2 and H2S-brine drainage and imbibition relative permeability relationships for intergranular sandstone and carbonate formations. SPE 99326, SPE Europec/EAGE Annual Conference and Exhibition, Vienna, Austria, Society of Petroleum Engineers
5. Bennion B, Bachu S (2007) Permeability and relative permeability measurements at reservoir conditions for CO2-water systems in ultra low permeability confining caprocks. SPE 106995, EUROPEC/EAGE Conference and Exhibition, London, U.K., Society of Petroleum Engineers
6. Bennion B, Bachu S (2010) Drainage and imbibition CO2/brine relative permeability curves at reservoir conditions for carbonate formations. SPE 134028 SPE Annual Technical Conference and Exhibition, Florence, Italy, Society of Petroleum Engineers

7. Perrin J-C, Krause M, Kuo C-W, Miljkovic L, Charoba E, Benson SM (2009) Core-scale experimental study of relative permeability properties of CO_2 and brine in reservoir rocks. Energy Procedia 1:3515–3522
8. McDougall SR, Salino PA, Sorbie KS (1997) The effect of interfacial tension upon gas-oil relative permeability measurements: interpretation using pore-scale models. SPE Annual technical conference and exhibition, San Antonio, Texas
9. Chiquet P, Broseta D, Thibeau S (2007) Wettability alteration of caprock minerals by carbon dioxide. Geofluids 7:112–122
10. Peters EJ, Flock DL (1981) The onset of instability during two-phase immiscible displacement in porous media. SPE J 21:249–258 SPE 8371
11. Craig FFJ, Sanderlin JL, Moore DW, Geffen TM (1957) A laboratory study of gravity segregation in frontal drives. Pet Trans AIME 210:275–282 SPE 676-G
12. Guo Y, Nilsen V, Hovland F (1991) Gravity effect under steady-state and unsteady-state core flooding and criteria to avoid it. The Second Society of Core Analysts European Core Analysis Symposium London, UK
13. Shi J-Q, Xue Z, Durucan S (2010) Supercritical CO2 core flooding and imbibition in Tako sandstone–Influence of sub-core scale heterogeneity. Int J Greenhouse Gas Control 5(1):75–87
14. Rapoport LA, Leas WJ (1953) Properties of linear waterfloods. Pet Trans AIME 198:139–148 SPE 213-G
15. Espinoza DN, Santamarina JC (2010) Water-CO_2-mineral systems: Interfacial tension, contact angle, and diffusion-Implications to CO_2 geological storage. Water Resour Res 46:07537
16. Hinkley RE, Davis LA (1986) Capillary pressure discontinuities and end effects in homogeneous composite cores: effect of flow rate and wettability. SPE 15596, SPE Annual Technical Conference and Exhibition, New Orleans, Louisiana, 1986 Copyright 1986, Society of Petroleum Engineers, Inc
17. Holtz MH (2002) Residual gas saturation to aquifer influx: a calculation method for 3-D computer reservoir model construction. SPE 75502, SPE Gas Technology Symposium, Calgary, Alberta, Canada, Society of Petroleum Engineers
18. Jerauld GR, Salter SJ (1990) The effect of pore-structure on hysteresis in relative permeability and capillary pressure: pore-level modeling. Transp Porous Med 5:103–151
19. Dullien FAL (1992) Porous media: fluid transport and pore structure. Academic Press, New York
20. Land CS (1968) Calculation of imbibition relative permeability for two- and three-phase flow from rock properties. SPE J 8:149–156 SPE 1942
21. Baines SJ, Worden RH (2004) Geological storage of carbon dioxide: special publications. Geol Soc London 233:1–6
22. Ennis-King J, Paterson L, Gale J, KayaY (2003) Rate of dissolution due to convective mixing in the underground storage of carbon dioxide. Greenhouse Gas Control Technologies-6th International Conference, Kyoto, Japan
23. Hangx SJT (2009) Geological storage of CO2: mechanical and chemical effects on host and seal formations: PhD theses, Utrecht University, Utrecht, The Netherlands
24. Juanes R, Spiteri EJ Orr Jr FM, Blunt MJ (2006) Impact of relative permeability hysteresis on geological CO_2 storage Water Resources Research, 42
25. Kumar A, Ozah R, Noh M, Pope GA, Bryant S, Sepehrnoori K, Lake LW (2005) Reservoir simulation of CO_2 storage in deep saline aquifers. SPE J 10:336–348 SPE 89343
26. FC I (1967) A formaulation of the thermophysic properties of ordinary water substance. International Formulation Committee Secretariat, Düsseldorf
27. NIST (2010) Thermophysical properties of fluid systems. http://webbook.nist.gov/chemistry/fluid/, US National Institute of Standards and Technology (accessed 17/6/2010)
28. Span R, Wagner W (1996) A new equation of state for carbon dioxide covering the fluid region from triple-point temperature to 1100 K at pressures up to 800 MPa. J Phys Chem Ref Data 25:1509–1597

29. Wagner W, Pruss A (2002) The IAPWS formulation 1995 for the thermodynamic properties of ordinary water substance for general and scientific use. J Phys Chem Ref Data 31:387–535
30. Zhenhao Duan Research Group (2010) Interactive Online Models. http://www.geochem-model.org/models.htm, Institute of Geology and Geophysics, Chinese Academy of Sciences (Accessed 25/6/2010)
31. Bennion B, Bachu S (2008a) A correlation of the interfacial tension between supercritical phase CO2 and equilibrium brines as a function of salinity, temperature and pressure. SPE 114479, SPE Annual Technical Conference and Exhibition, Denver, Colorado, USA, Society of Petroleum Engineers
32. Chun B-S, Wilkinson GT (1995) Interfacial tension in high-pressure carbon dioxide mixtures. Ind Eng Chem Res 34:4371–4377
33. Hebach A, Oberhof A, Dahmen N, Kögel A, Ederer H, Dinjus E (2002) Interfacial tension at elevated pressures measurements and correlations in the water + carbon dioxide system. J Chem Eng Data 47:1540–1546
34. Hall HN (1953) Compressibility of reservoir rocks. Pet Trans AIME 198:309–311 SPE953309
35. Unalmiser S, Swalwell TJ (1993) A quick technique to define compressibility characteristics of hydrocarbon reservoir. SPE 25912, Low Permeability Reservoirs Symposium, Denver, Colorado, Society of Petroleum Engineers
36. Bennion B, Thomas FB Bietz RF (1996) The effect of trapped critical fluid saturations on reservoir permeability and conformance. Hycal Energy Research Laboratories Ltd., Hycal Energy Research Laboratories Ltd
37. Larsen JA, Skauge A (1995) Comparing hysteresis models for relative permeability in WAG studies, 1995 SCA Conference, Paper number 9506
38. Crotti MA, Rosbaco JA (1998) Relative permeability curves: the influence of flow direction and heterogeneities. Dependence of end point saturations on displacement mechanisms. SPE 39657, SPE/DOE Improved Oil Recovery Symposium, Tulsa, Oklahoma, Society of Petroleum Engineers
39. Chierici GL, Ciucci GM Long G, Eva F (1967) Effect of the overburden pressure on some petrophysical parameters of reservoir rocks. 7th World Petroleum Congress, Mexico City, Mexico, World Petroleum Congress
40. Seo JG (2004) Experimental and simulation studies of sequestration of supercritical carbon dioxide in depleted gas reservoirs: PhD theses, Texas A&M University, Texas, p 132
41. Seo JG, Mamora DD (2003) Experimental and simulation studies of sequestration of supercritical carbon dioxide in depleted gas reservoirs, SPE 81200, SPE 81200, SPE/EPA/DOE Exploration and Production Environmental Conference, San Antonio, Texas, Society of Petroleum Engineers
42. Archer JS, Wong SW (1973) Use of a reservoir simulator to interpret laboratory waterflood data. SPE J 13:343–347 SPE 3551
43. Sigmund PM, McCaffery FG (1979) An improved unsteady-state procedure for determining the relative-permeability characteristics of heterogeneous porous media. SPE J 19:15–28 SPE 6720

Chapter 6
Summary, Conclusions and Recommendations

6.1 Summary

A range of variable factors are expected to influence multiphase flow during CO_2 geological sequestration. In order to, qualitatively and quantitatively, investigate the effects of a number of these factors, a range of specially designed core-flooding experiments (complemented by some other minor laboratory work) was carried out. The investigated factors which were expected to have moderate to strong effect on the multiphase flow characteristics of the rock-fluids system during subsurface CO_2 disposal included: cyclic CO_2-brine flooding, flow direction (horizontal versus vertical), change in the reservoir net effective pressure and existence of residual natural gas (represented by CH_4 here) saturation.

Presented in Chap. 2 was a detailed review and discussion on the models and experimental data available on thermophysical properties of pure fluids and fluid mixtures expected to be encountered during CO_2 geo-sequestration. Furthermore, discussed in this chapter were theoretical overviews of the factors which were expected to influence multiphase flow during such processes. The majority of the factors discussed were those experimentally examined during this research. Chapter 2 concluded with an extensive revision of experimental data available in the literature with a specific application to underground CO_2 storage.

Chapter 3 provided a detailed description of the experimental equipment and materials used during the experimental work. In addition, this chapter presented detailed overviews of the experimental procedures which were based on the conventional and widely accepted standard protocols outlined in the literature, but at the same time were specially designed in order to achieve the objectives set out for this research program.

The results of the various experiments conducted were included in Chap. 4, while full analyses, interpretation and discussion of these results were presented in Chap. 5. Since the injectivity and storage capacity, at least from the storage side point of view, are the two mostly discussed topics when it comes to

A. Saeedi, *Experimental Study of Multiphase Flow in Porous Media during CO_2 Geo-Sequestration Processes*, Springer Theses, DOI: 10.1007/978-3-642-25041-5_6,

geo-sequestration of CO_2, the main focus of the analyses and discussions in this chapter was on evaluating the effects that the examined factors could potentially have on these two important issues.

6.2 Conclusions

The main conclusions arising from the experiments and subsequent analyses and discussions are summarised as follows:

1. General displacement of brine by CO_2 or vice versa:

- Overall, the residual brine saturations are abnormally high during displacement of wetting brine phase by non-wetting CO_2 phase. These abnormally high end-point residual brine saturations, specifically in moderate to high permeability porous media, could be attributed to the combined effects of the high mobility ratios and low IFT values dominating such drainage processes. This type of displacement is strongly flow-rate dependant.
- Unlike imbibition displacements conducted during EOR processes, during the displacement of the wetting brine phase by a low viscosity non-wetting phase (e.g. CO_2, natural gas, etc.) (a drainage process dominated by high mobility ratio) a reduction in the IFT value makes the displacement process less effective in terms of brine sweep efficiency.
- Overall, the residual CO_2 saturations during displacement of CO_2 by brine are relatively low. The low residual trapped CO_2 levels could be attributed to the low IFT values of the CO_2-brine system, which reduce the significance of the snap-off trapping mechanism as the main active capillary trapping mechanism during CO_2 geo-sequestration.
- The residual CO_2 trapping in high permeability porous media is expected to be low for two main reasons. First, the displacement of CO_2 by brine in such formations is very efficient. Second, based on the Land trapping model, low achievable maximum CO_2 saturations during a drainage flood in such porous media subsequently results in low levels of trapped CO_2 during a subsequent imbibition flood.
- Therefore, while CO_2 injectivity is expected to be favourable and very high in highly permeable formations, the extremely low levels of CO_2 entrapment in the form of the desired residual saturation may make them less favourable for CO_2 storage purposes especially in a system lacking a comprehensive seal.
- Due to the dependency of IFT of the CO_2-brine system on pressure and temperature which in turn depend on the depth of a storage medium (overall, IFT is expected to decrease with increase in depth), injecting CO_2 into deep formations may reduce the significance of the desired residual trapping mechanism towards entrapment of the injected CO_2.

To the best knowledge of the author, to date, presented in this theses is the most comprehensive discussion on the displacement efficiency and the general trends

expected to be present among the residual wetting and non-wetting phase saturations during CO_2 geo-sequestration, backed by experimental results.

2. Cyclic CO_2-brine flooding:

- Overall, in low permeability samples, while the end-point saturations (for both drainage and imbibition) are expected to remain steady during a cyclic/alternating flooding pattern, pressure profiles and as a result the end-point relative permeabilities may show moderate to strong dependence on the cyclic/alternating injection pattern. However, any observed trend would weaken as the permeability of the porous medium increases.
- In low permeability samples and samples susceptible to formation damage (e.g. fines migration, mineral dissolution/precipitation, etc.) the injectivity, (represented during the experiments by the differential pressure across the samples) may decrease as the cyclic CO_2-brine injection proceeds. However, it is likely that the extent of any reduction in the injectivity would stabilise after several injection cycles.
- During an extended cyclic CO_2-brine flooding of a porous medium, it is expected that the storage medium to undergo some degree of irreversible plastic deformation. One likely cause of such deformation is the dissolution of some minerals present in the cement bounding the rock grains together. Dissolution of the cement would weaken this bound and intensify the plastic compaction of the porous medium. Although, increase in the reservoir pore pressure could slow down the compaction process by reducing the net effective pressure applied to the storage medium.
- Due to the passage of excessive volumes of the injection fluids through the part of a reservoir adjacent to the wellbore, this area is the most susceptible to any possible formation damage due to fines migration, mineral dissolution and subsequent pore compaction. This can reduce the injectivity considerably over time.

To the author's best knowledge, such results as those described here on the effect of the cyclic CO_2-brine flooding on the multiphase flow characteristics of the rock-fluids system during CO_2-geosequestrtion especially for more than two consecutive injection cycles have not been produced in the literature to date.

3. Flow direction (Horizontal versus vertical):

- The flow direction influences the multiphase flow behaviour of the CO_2 and brine through a porous medium. Multiphase Interferences are highest in the vertical direction leading to higher residual saturations and higher pressure drops in this direction.
- The extent of the flow direction influence, however, depends on the relative pore size distribution and overall absolute permeability of the porous medium. A lower permeability porous medium with a multimodal pore size distribution character would be expected to exhibit the strongest directional dependence multiphase flow behaviour when subjected to CO_2-brine injection.

- Therefore, vertical flow, which is expected to occur during CO_2-geosequestration, would be beneficial by causing higher levels of CO_2 entrapment as residual saturation and impeding the undesirable upward flow of CO_2 and evolution of the CO_2 plume.

To the best knowledge of the author, there has been no experimental data produced in the literature to date on the effect of flow direction on the multiphase flow during underground CO_2 storage and the results achieved and the data generated here are the first of their kind.

4. Change in the reservoir stress field:

- The reservoir stress field is expected to change over time during the long term underground CO_2 disposal. This change occurs through an increase in pore pressure causing a reduction in the net effective pressure applied to the reservoir. Even when ignoring any change in the properties of the fluids caused by any increase in reservoir pore pressure, the change in the net effective pressure is expected to change the multiphase flow characteristics of the rock-fluids system by physically altering the pore network of the porous medium.
- A decrease in the reservoir net effective pressure is likely to decrease the maximum achievable CO_2 saturation and the subsequent trapped residual CO_2.
- Therefore, it could be the case that over time, with reduction in net effective pressure, some of the already trapped CO_2, in the form of residual saturation may become mobile again.
- Furthermore, if the effects of an increase in the pore pressure of the storage medium on fluid properties are considered, the density and viscosity of the CO_2 phase would increase promoting a more uniform displacement of brine by CO_2, but at the same time the fluid system's IFT would drop which could lead to a further reduction in the amount of CO_2 entrapment by the dominant snap-off trapping mechanism.

To the best knowledge of the author, such experimental results as those presented here on the effect of any change in the net effective pressure applied to the storage medium on the multiphase flow behaviour pertaining to the CO_2 geosequestration have not been produced in the literature to date.

5. Existence of residual natural gas saturation:

- The presence of residual natural gas saturation, which is expected to be the case in depleted natural gas reservoirs used as CO_2 storage sites, considerably influences the multiphase flow behaviour during cyclic CO_2-brine flooding.
- Much of the originally trapped residual natural gas would be displaced and replaced by the invading CO_2 phase. It would be expected that after 2–3 cycles of CO_2-brine injections, no more natural gas would remain trapped in the pores of the storage medium.
- With respect to CO_2 residual entrapment, replacement of natural gas by CO_2 may increase the amount of the capillary trapped CO_2 initially but this CO_2

becomes mobile easily with further brine flooding. Eventually, the volume of the trapped residual CO_2 is expected to be lowered to the same levels as those of injection of CO_2 into underground aquifers.
- The rate of replacement of residual natural gas by CO_2 during a cyclic CO_2-brine flooding process is a function of the permeability of the target porous medium. That is, the rate would be higher in a higher permeability medium.
- The presence of residual natural gas saturation, in the short term, would decrease the CO_2 injectivity considerably. However, the situation would improve as more natural gas is recovered and the saturation of the replacing CO_2 is gradually decreased by each subsequent flooding cycle.
- The rate of improvement in injectivity is expected to be higher in a high permeability porous media.

To the author's best knowledge, there has been no experimental data produced or a theoretical discussion presented in the literature to date on the potential effects of the residual natural gas on the multiphase flow during cyclic CO_2-brine injection during CO_2 geo-sequestration processes.

6. Relative permeabilities:

- Relative permeabilities during displacement of brine by highly mobile CO_2 in moderate to high permeability porous media are highly influenced by non-uniform displacement expected to occur during such displacement processes.
- The effect of the non-uniform displacement on relative permeabilities is especially pronounced for the CO_2 phase, resulting in highly suppressed CO_2 relative permeabilities. However, higher flooding rates would help to improve the situation.
- Cyclic CO_2-brine injection is not expected to change the relative permeabilities of the two phases over time in high permeability porous media. However, in low permeability media or those susceptible to formation damage (e.g. fines migration, mineral dissolution/precipitation and subsequent pore compaction, etc.) some degree of change is expected to occur in the relative permeabilities as the flooding cycles proceed.
- Flow of CO_2 and brine in the vertical direction is characterised by more concave relative permeability curves compared to flow in the horizontal direction, confirming a more pronounced multiphase interferences effect in this direction.

The relative permeability data available in the literature to date are for maximum two successive injection cycles (a primary drainage followed by a subsequent imbibition flood) while the relative permeability generated here cover a further three more drainage floods. Furthermore, the effects of a range of parameters on the relative permeability functions of the CO_2-brine system have been experimentally studied during this research for the first time.

6.3 Recommendations

A few of the factors whose influence on the multiphase flow during the geo-sequestration of CO_2 disposal examined during this research deserve further investigation as follows:

- The samples tested during this study covered a wide range of permeabilities but none of them fell in the range of 20–100 mD. Since CO_2-brine multiphase displacement in samples within this permeability range is expected to be more uniform, further investigation on any sample within this permeability range could improve the results achieved here.
- When investigating the effect of change in the reservoir stress field on the multiphase flow characteristics during subsurface CO_2 disposal, in order to eliminate the effects of other variable factors, apart from the change in net effective pressure, and draw a more solid conclusion, a new sample needs to be used with every value of the net effective pressure. However, the samples need to be as close as possible to each other in terms of physical properties and homogeneity. Furthermore, in order to investigate the effects of change in properties of the fluids as well, the change in reservoir stress field needs to be applied by increasing the pore pressure rather than reducing the overburden pressure.
- A number of other experimental instruments (e.g. X-ray CT, and further analysis e.g. SEM, thin-section studies, etc.) could help to enhance the understanding of the reactions and processes which may occur during the core-flooding experiments.
- The samples used during this research were all sandstone. Considering the potentially higher degree of interaction between the carbonate samples and the fluids involved, tests using carbonate samples could potentially yield more interesting results.

The effect of residual crude oil on multiphase flow during cyclic CO_2-brine flooding could add new insight to any future research in this area.

Index

A. Saeedi, *Experimental Study of Multiphase Flow in Porous Media during CO_2 Geo-Sequestration Processes*, Springer Theses, DOI: 10.1007/978-3-642-25041-5,